Development of Chiral Phosphoric Acids Catalyzed Site-selective Transformations and Synthesis and Applications of Immobilized CPAs towards Single-pot Functionalization of Monosaccharides

by

Sibin Wang

A dissertation submitted in partial fulfillment
of the requirements for the degree of
Doctor of Philosophy
(Chemistry)
in the University of Michigan
2021

Doctoral Committee:

Associate Professor Pavel Nagorny, Chair
Professor John Montgomery
Professor Nouri Neamati
Professor John P. Wolfe

Sibin Wang

sibinw@umich.edu

ORCID iD: 0000-0002-4062-1560

Dedication

To my dearest family.

Acknowledgements

First and foremost, I would love to thank my advisor Pavel Nagorny. Pavel, thank you very much for having me in your lab. Before I joined, I did not have any background in organic chemistry synthesis, but you still believed in me and trusted my abilities to achieve high and to be successful. I am grateful to have been one of your students. You are not only knowledgeable in organocatalysis and carbohydrates, but also supportive to my growth and development as a scientist. When I am in doubt, you are always encouraging and selfless offering me various potential solutions, opportunities and advise. Because of you, I knew whenever I needed assistance in research or outside of lab, I could always turn to you for help. Thank you for the endless support and countless opportunities you provided to me over the past five years. Thank you for giving me space and room to make mistakes and to learn from them. Thank you!

I am also grateful to have Professor John Montgomery, Professor John Wolfe and Professor Nouri Neamati in my committee. Thank you for sharing with me your expert knowledge in organocatalysis and carbohydrate chemistry. Thank you for offering all the precious suggestions, advice, and improvement to allow me to grow and to be better.

I would also love to thank my undergraduate advisor Professor Kimberley Frederick, who is always caring, understanding and supportive to me. It was one of my greatest honors to do research with Professor Frederick nine years ago. Her guidance and training has encouraged me to pursue higher to be not only a first-generation college student, but also a first-generation graduate student.

I am also gratifying for all the collaborators that I have been working with. I am grateful to my mentor Dr. Alonso Argüelles, who is the best mentor I could ever ask for when I joined Dr. Nagorny's lab. He is not only passionate about science, but also patient and detail oriented. His dedication to research has always motivated to be someone like him. In addition, I cherish the collaboration with Dr.Tay Rosenthal and Miyuki Hotta for the initial optimization of regioselective epoxide ring opening in chapter 2. I am also grateful to Dr. Jeonghyo Lee. I am fortunate to have collaborated with Dr. Jeonghyo Lee on two different projects. Dr. Lee has contributed initial studies in chapter 3. I also enjoyed my mentoring and working with Hao Guo in developing immobilized chiral phosphoric acids and studying computational mechanism, performed by Oleksii Zhelavskyi. Furthermore, I am grateful to have other collaborations with Dr. Iaroslav Khomutnyk and Dr. Hem Khatri for their valuable knowledge in synthesis, mechanism, and lab techniques. I also appreciate the time we spent together in lab including but not limited to Zachary Fejedelem, Nicolas Diaz, Nolan Carney, Sungjin Kim, Ryan Rutkoski, Natasha Perry, Zhongzheng Li and Qingqin Huang.

Moreover, my graduate school would have been significantly different without my friends: Weixuan Nie, Yanming Wang, Ryan Dodson, Michael W. Wolfe, Dr. Shuo Guo, Dr. Yinfu Lin, Mo Chen, Yishu Xu. Thank you for all the funny and memorable moments. My experience in Michigan would have been very different without you.

Last, but not least, thank you to my family. Thank you for their unconditional understanding, support, and love while pursuing my Ph.D degree. Thank you for offering the possibly best they could ever offer to allow me to explore myself. And thank you for all the love to me when I feel low. Without them, I would not be me today. All of the accomplishments and

achievements I have made would not have been possible without my family support. Thank you from the bottom of my heart!

Table of Contents

List of Tables

List of Figures

List of Schemes

List of Abbreviations

μg	microgram
μmol	micromole
6-dEB	6-deoxy-erythronolide B
Å	angstrom
Ac	acetyl
Aq	aqueous
Ar	aryl
atm	atmosphere (unit)
BINOL	1,1'-bi-2-naphthol
Bn	benzyl
Boc	tert-butyloxycarbonyl
BOM	benzyloxymethyl
BRSM	based on recovered starting material
Bu	butyl
Bz	benzoyl
Calcd	calculated
Cat.	catalyst
CPA	chiral phosphoric acid
Cy	cyclohexyl
d	days
DBNE	*N*,*N*-dibutylnorephedrine
DBU	1,8-diazabicyclo[5.4.0]undec-7-ene

DCE	1,2-dichloroethane
DCM	dichloromethane
DFT	density functional theory
DMAP	4-dimethylaminopyridine
DMF	dimethylformamide
d.r.	diastereomeric ratio
E1cb	elimination unimolecular conjugate base
ee	enantiomeric excess
equiv.	equivalent
Et	ethyl
EtOAc	ethyl acetate
FDA	Food and Drug Administration
g	gram
h	hours
Hex	hexanes
HPLC	high-performance liquid chromatography
HRMS	high resolution mass spectrometry
HSQC	heteronuclear single quantum correlation
Hz	hertz
i-Pr	isopropyl
IR	infrared
J	coupling constant
kcal	kilocalorie
M	molar
Me	methyl
MeCN	acetonitrile

mg	milligram
min	minutes
mL	milliliters
mmol	millimoles
MS	molecular sieves
MW	molecular weight
NIH	National Institute of Health
NBS	*N*-bromosuccinimide
NMR	nuclear magnetic resonance
n-BuLi	*n*-butyl lithium
Nu	nucleophile
o/n	overnight
PG	protecting group
Ph	phenyl
PhMe	toluene
PMB	para-methoxybenzyl
PPA	polyphosphoric acid
ppm	parts per million
Pr	propyl
R	alkyl group (generic)
rac	racemic
Rf	retention factor
r.r.	regioisomeric ratio
rt	room temperature
S_N1	unimolecular nucleophilic substitution
S_N2	bimolecular nucleophilic substitution

SPAN	spiro-2,2’-bichroman
SPINOL	1,1’-spirobiindane-7,7’-diol
t	time
TBAF	tetrabutylammonium fluoride
TBDPS	*t*-butyldiphenylsilyl
TBS	*t*-butyldimethylsilyl
t-Bu	*t*-butyl
TES	triethylsilyl
Tf	trifluoromethanesulfonyl
TFA	trifluoroacetic acid
TfOH	trifluoromethanesulfonic acid
THF	tetrahydrofuran
TLC	thin layer chromatography
Ts	*p*-toluenesulfonyl
UV	ultraviolet

Abstract

Site-selective transformations are of great importance in natural products synthesis and modification of pharmaceutical compounds. Although traditionally site-selectivity has been accomplished by exploring the enharent substrate reactivity with achiral reagents or catalysts or by relying on enzymatic reactions, a variety of recent examples suggest that chiral catalysts may provide effective means for achieving alternative modes of selectivity. Chiral phosphoric acids (CPAs) represent a particularly promissing subclass of chiral catalysts, and these catalysts have demonstrated significant potential in controlling regioselectivity of various natural products. This dissertation focuses on exploring the potential of CPAs to accomplish regioselective intramolecular epoxide ring openings, single-pot functionalization of monosaccharides via CPA-catalyzed regioselective acetalization of *trans*-1,2-diols, and synthesis and applications of immobilized CPAs to achieve reusing and recycling of catalysts in the single-pot functionalization of monosaccharides.

Chapter 1 provides an introduction to CPA catalysis and an overview of recent studies on chiral catalysts to achieve site-selective functionalization of polyol-based natural products. In addition, this chapter overviews the current state-of-the-art in using CPAs as the catalysts for the stereoselective and site-selective functionalization of natural products and other complex chiral molecules.

Chapter 2 describes the development of CPA-controlled regiodivergent cycloisomerization of natural antibiotic mupirocin methyl ester. Mupirocin is an epoxide-containing natural polyol

that is known to undergo unselective intramolecular epoxide cyclization leading to the mixture of regioisomeric products. We have developed a CPA-controlled methods for both *endo*- and *exo*-selective modes of cyclizations, forming either *exo*-product in 3:1 r.r. or *endo*-product in 18:1 r.r. Chapter 1 also describes the experimental and computational mechanistic studies focused on understanding the origins of regiocontrol. These studies suggest that both cyclizations happen through concerted and highly synchronous pathways strongly depending on the nature of the hydrogen bond network formed between the substrate and the catalyst.

Chapter 3 describes the development of regioselective CPA-catalyzed acetal protection of saccharide-based diols and triols and its application to the one-pot regioselective synthesis of differentially protected monosaccharides. This chapter also illustrates synthesis, characterization and development of immobilized on polystyrene matrix (*R*)-Ad-TRIP CPA, which could be recycled by filtration. This immobilized catalyst features high catalytic activity (0.5-0.1 mol% on 1-5 g scale) and can be reused multiple times without erosion in yields or selectivities. These features allowed to achieve gram scale one pot syntheses of several different *D*-glucose derivatives with the same batch of the recycled polymeric catalyst.

Chapter 4 provides the summary of the studies described in this dissertation. It also discusses the impact of this work and potential future studies using immobilized CPAs in continuous flow.

Chapter 1

Overview of Chiral Phosphoric Acids in the Synthesis and Functionalization of Natural Products

1.1. Introduction to chiral phosphoric acids (CPA) catalysis

Since the original reports by Akiyama[1] and Terada[2], CPAs have become one of the most important organocatalysts in asymmetric synthesis. According to Wheelers' report published on January 8, 2018, there have been increasing number of papers on CPA-catalyzed reactions, which open up a new route that have been previously reported as inaccessible enantioselective synthetic routes (Figure 1.1).[3]

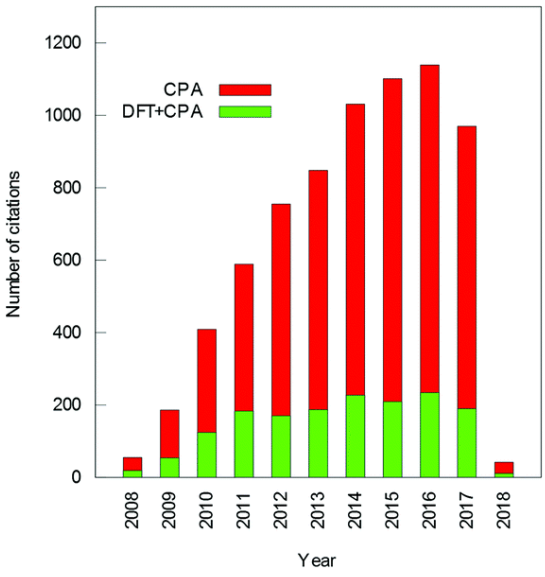

Figure 1.1 Growth in the number of papers on CPA-catalysed reactions

The wide and broad interest to CPA catalysis is due to the versatile structural features and modes of activations observed for CPAs.[4] There are many types of CPAs that have been developed to date, and one of the major differences comes from the nature of the chiral backbone, to which hydrogen phosphate functionality is attached. Perhaps, the most abundant and well investigated subgroup of CPAs are the catalysts containing BINOL backbone (Figure 1.2). According to Rueping's report, such CPAs typically contain a rigid BINOL-based core with substituents at the 3,3'-positions, which are essential for providing a chiral environment. These 3 and the 3' positions could be easily modified, which provides great means to fine-tune the selectivity of the catalyst. This chiral environment imposed by these substituents impacts the 3D-interactions between the catalyst and substrate and results in asymmetric induction that leads to the formation of a specific stereoisomer. The intermolecular interactions between the substrate and the CPA catalyst often arise due to the presence substrate interactions with the Brønsted acidic proton and phosphoryl oxygen, which could potentially act as either hydrogen bond donor or hydrogen bond acceptor. Even though its catalytic reactivity depends on the reaction system, many studies have shown the advantages of this two-point binding mode of activation in catalyst procedures.[4] Furthermore, the catalyst acidity and reactivity could be further adjusted via the electronic effects on the hydrogen phosphate moiety through the substituents at the BINOL backbone. These key structural features described above allow CPAs to be general and effective catalysts for a variety of applications.

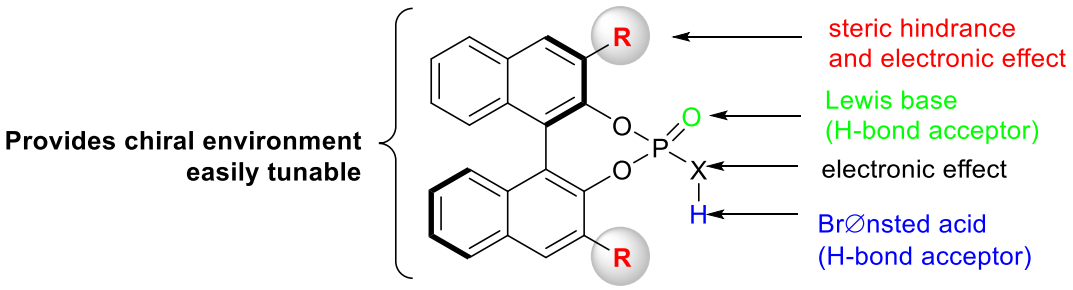

Figure 1.2. Features of CPAs and derivatives.

In their seminal exploration of CPAs as the catalysts, Terada and co-worker demonstrated the significance of substituents at the 3,3'-positions for controlling the enantioselectivity (Scheme 1.1)[2]. When Boc-protected imine **1-1a** was reacted with a di-ketone **1-1b**, Akiyama and co-workers observed that the substituents at the 3,3'-positions made a significant impact on the resultant enantioselectivity for the formation of product **1-1c**. When no substituent at the 3,3'-positions (cat **1-1A**) were present, **1-1c** was obtained in only 12% ee. However, after increasing the size and bulkiness of the substituents at the 3,3'-positions of CPAs **1-1A-D**, the enantioselectivity dramatically increased, and product **1-1c** was obtained in 95% ee when catalyst **1-1D** was used. Even though, the origin of enantioselectivity was not fully understood at the time of this report, later studies implied that the enantioselectivity results from either matched or mismatched chiral environment created by the CPAs.[4] With the small 3,3'-substituents such as H- in **1-1A**, the energy difference steric interactions is too small to differentiate between the *re*- or *si*-faces of the imine, which leads to poor selectivity. However, with the increased of bulkiness of the 3,3'-substituents, only *re*-face of **1-1a** is accessed by nucleophile **1-1b** (as the 3,3'-aryl substituents now block the *si*-face), which results in significantly higher enantioselectivity for the formation of **1-1c**.

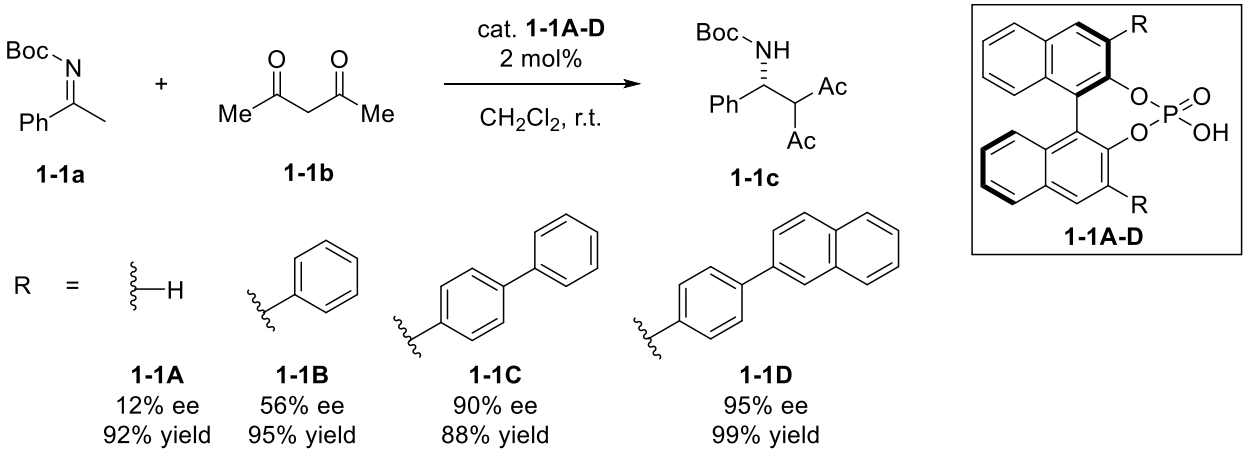

Scheme 1.1 Effect of 3,3'-substituents of CPA catalysts on the enantioselectivity for Mannich-type reactions.

Another key feature of CPAs is their acidity. Both computational and experimental studies have showed the acidity of CPAs could be controlled either by the substitution on the backbones or the substitution of the phosphorus oxygen (Figure 1.3A).[5] In their studies toward the enantioselective protonation reaction, Yamamoto and co-workers found that the acidity of CPAs plays a key role in catalyzing the asymmetric protonation of silyl enol ethers (Figure 1.3B).[6] When catalyst **1-2A** was used, there is little to no reactions, even with a prolonged reaction time. However, when a more acidic thiophosphoric acid **1-2B** was used, trace amounts of the desired product **1-2b** were obtained. Further evaluation of an even more acidic phosphoramide catalyst **1-2C** allowed to raise the yield to 97% and 78% ee of **1-2b**. The authors hypothesized that the reaction undergoes two-step sequence. The initial step involves the protonation of the enol ether with the CPA forming chiral ion pair **1-2c**. The protonation step was proposed to be both rate-limiting and enantiodifferentiating. This step was followed by desilylation with phenol to yield ketone **1-2b** and regenerate the CPA catalyst.

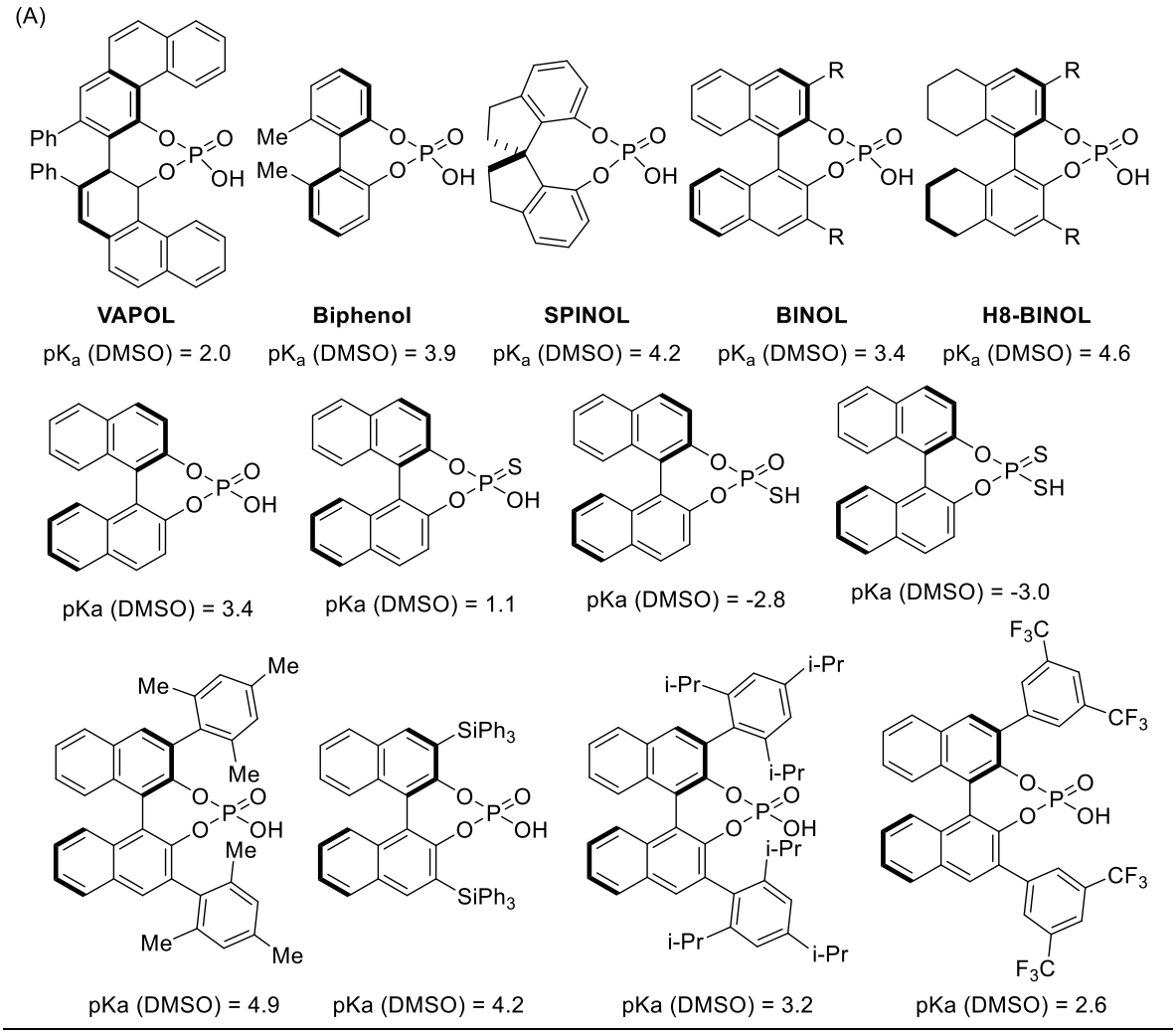

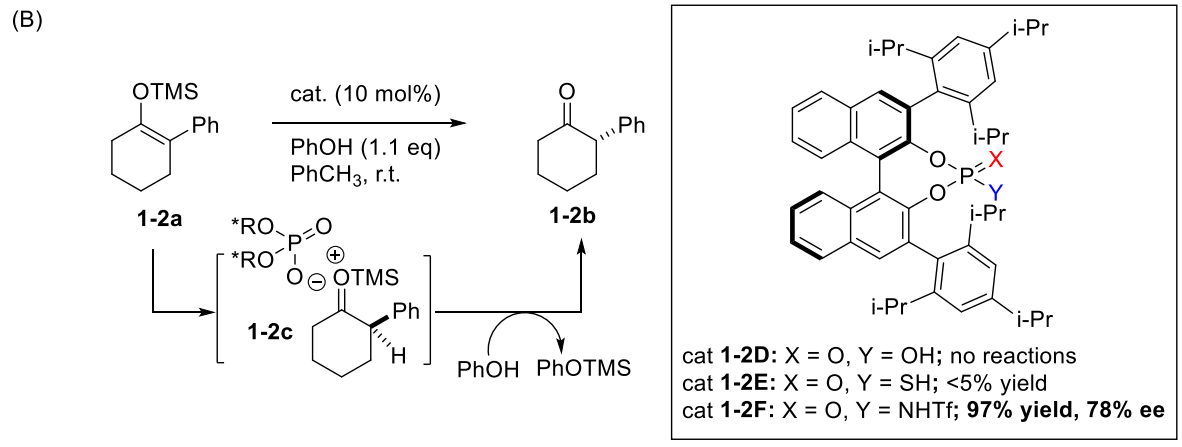

Figure 1.3 (A) Acidity of selected chiral phosphoric acids. (B) The application of acidity to control reactivity and selectivity.

In these prior examples CPAs were used as the bifunctional catalysts, in which hydrogen phosphate moiety acts as both a Brønsted acid and a Lewis base. In addition to these modes of activation involving a proton transfer step, there is a wide spectrum of the related transformations, in which CPAs may serve as bifunctional hydrogen bond donors and acceptors.[4] This ability to catalyze the reactions through multiple modes of activation is of particular significance as it allows to use CPA catalysis to promote multistep transformations. In their studies of the enantioselective N-H functionalization of indoles with α, β-unsaturated γ-lactams, the Huang group discovered that CPAs could protonate lactam **1-3a**, forming *N*-acyliminium/chiral phosphate ion pair **1-3d** (Scheme 1.2).[7] The *N*-acyliminium cation, phosphate anion and the N-H moiety of indole **1-3b** are interconnected through a network of hydrogen bonds and assume specific orientation in space that has minimized non-bonding interactions between the substrates and CPA backbone. This rigid complex undergoes a more favored reaction pathway that involves indole attack from the more accessible *Re*-face of the *N*-acyliminium ion to provide **1-3c** in good levels of enantiocontrol. Huang and co-workers have also demonstrated that the selectivity of this transformation is dependent on the acidity of CPAs. With less acidic CPA, such as **1-3A**, they were able to get 87% ee; however, higher ee value (up to 90%) was obtained with a more acidic CPA **1-3B.** They hypothesized that this is due to the formation of a stronger hydrogen bond network resulting in the tighter and more rigid intermediate **1-3d**.

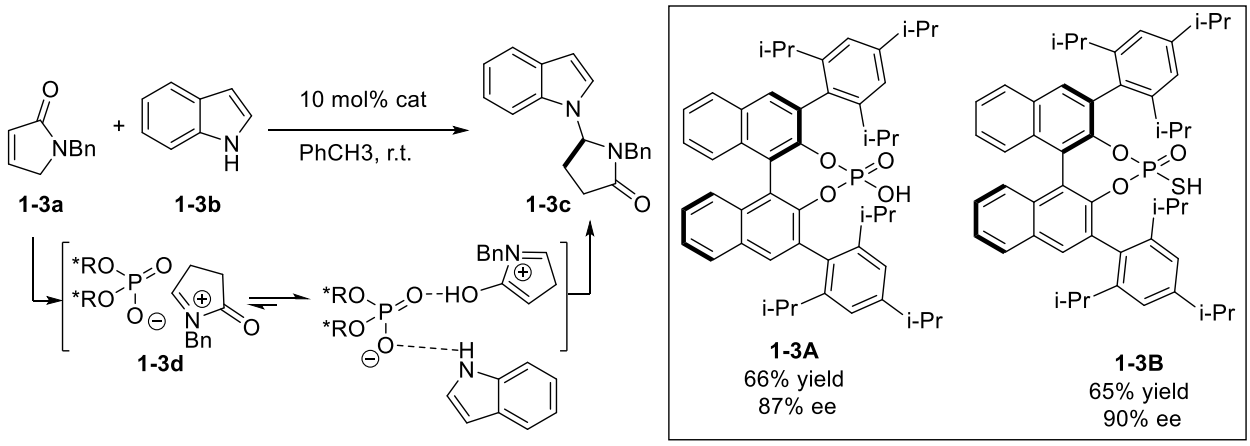

Scheme 1.2 Effects of phosphoryl atom in enantioselectivity

With a better understanding of CPAs and its roles in controlling enantioselectivity, scientists have also focused on the application of CPAs to other transformations, such as site-selective functionalization of natural products. The overview of chiral catalyst-controlled stereodifferentiating reactions, and the use of CPA catalysis to accomplish stereodifferentiating reactions in complex settings are provided in the subsequent sections of this Chapter.

1.2. The use of Chiral Catalysis for Achieving Stereodifferentiating Functionalization of Polyol-based Natural Products

The early examples of using the chiral catalysts to achieve stereodifferentiation reactions involved the studies of site-selective functionalization of polyol-based natural products. Such polyol-based natural products contain at multiple hydroxyl groups, which could serve as handles for the introduction of other functional groups such as alkenes, alkynes, halides, nitriles, sulfonates, azides, amines, esters, lactones, amides, and lactams. These modifications may lead to the significant enhancement of the biological and therapeutic properties of these natural products, and the ability to install these various functional groups into different parts of the molecules are key to medicinal chemistry studies (Figure 1.4).[8–13] Unfortunately, the presence of multiple

reaction centers in these complex molecules often significantly hinders medicinal chemist's ability to conduct SAR studies, and more direct methods for the natural product functionalization have received great attention in the recent years.[14]

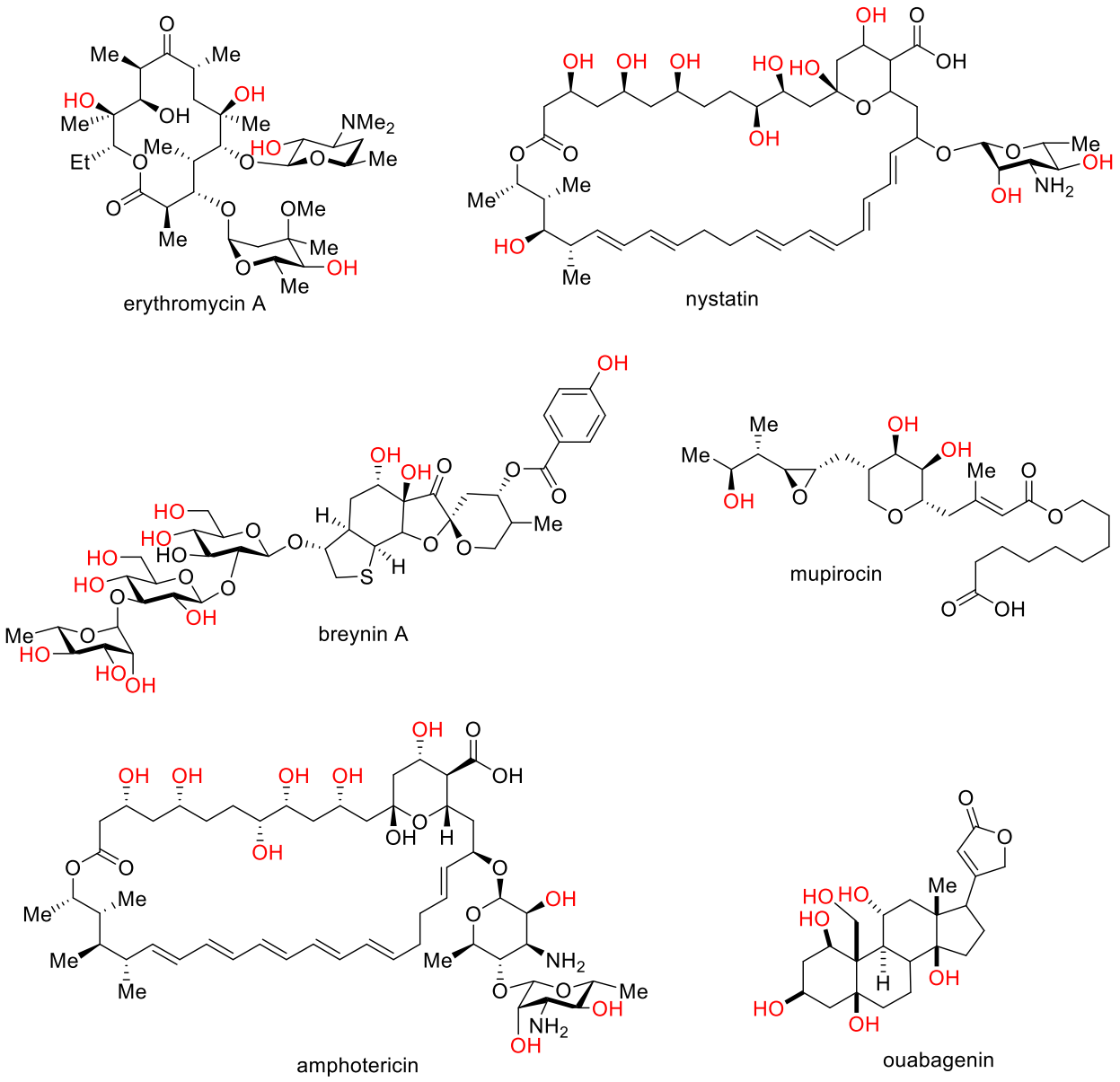

Figure 1.4 Examples of polyol-containing drugs and natural products.

The selective functionalization of a hydroxyl group in complex polyols represents a long-standing challenge as the hydroxyl groups often exhibit very similar reactivity profiles, in

particular, if they are placed into similar stereoelectronic environments. Such hydroxyl groups react competitively, and hard-to-separate mixtures of various regioisomeric products are formed. The use of chiral catalysts that recognize the local steric environment might significantly improve the selectivity in such cases and render one of the hydroxyl groups more reactive in comparison to the other. This situation is reflected by a diagram in Figure 1.5A that describes a hypothetical reaction where polyol A is converted to either product B or C. If the hydroxyl groups in A have similar reactivities, both pathways would have indistinguishably close activation energy barriers ($\Delta G_B^{\ddagger}$ and $\Delta G_C^{\ddagger} \sim \Delta G^{\ddagger}$) leading to the transition state B (TS_B) or transition state C (TS_C). Due to the close in energy TS_B and TS_C, equal quantities of the products B and C would be obtained. In a hypothetical scenario when a chiral catalyst may recognize the local environment around each of the hydroxyl moieties, one of the energy barriers could be lowered. Thus, in the case depicted in Figure 1.5A, the catalyst is preferably interacting with the hydroxyl group leading to formation of C, and the activation energy TS_C is lowered by $\Delta\Delta G^{\ddagger}$ as the result of this. Due to the lower activation energy, product C could be observed as the major product, and a regioselective formation of C over D could be now performed under the catalytic conditions. In order for a regioselective functionalization to be considered as a "highly selective" reaction, a ratio with greater than 40:1 should be accomplished, which requires a $\Delta\Delta G^{\ddagger}$ greater than 2.50 kcal/mol.[15]

It is important to note that the use of chiral catalysts may not only help to differentiate the chiral hydroxyl groups with similar reactivity, but also result in the selective functionalization of a less reactive hydroxyl. This, however, is a significantly more challenging to achieve scenario that is highly dependent on the initial difference between the energy barriers for the competitive processes. This situation is reflected in Figure 1.5B that describes a hypothetical reaction of polyol D resulting in products E or F. As the result of the higher activation energy barrier leading to E,

product F would be the major product under the standard reaction conditions. However, if the chiral catalyst could significantly reduce the activation energy barrier of the transition state TS_E, in such a way that it is now lower in energy then TS_F, product F would be formed preferentially. Therefore, the situations when the use of the chiral catalyst leads to switch in the reaction selectivity are possible in the cases when $\Delta\Delta G^{\ddagger}$ values are small enough for the catalyst to be able to overcome these barriers. It should be noted that the described above scenarios are applicable to both the cases leading to two different regioisomers and diastereomers since both types of transformations might be affected by the matched and mismatched interactions of the chiral catalyst and the reaction center(s).

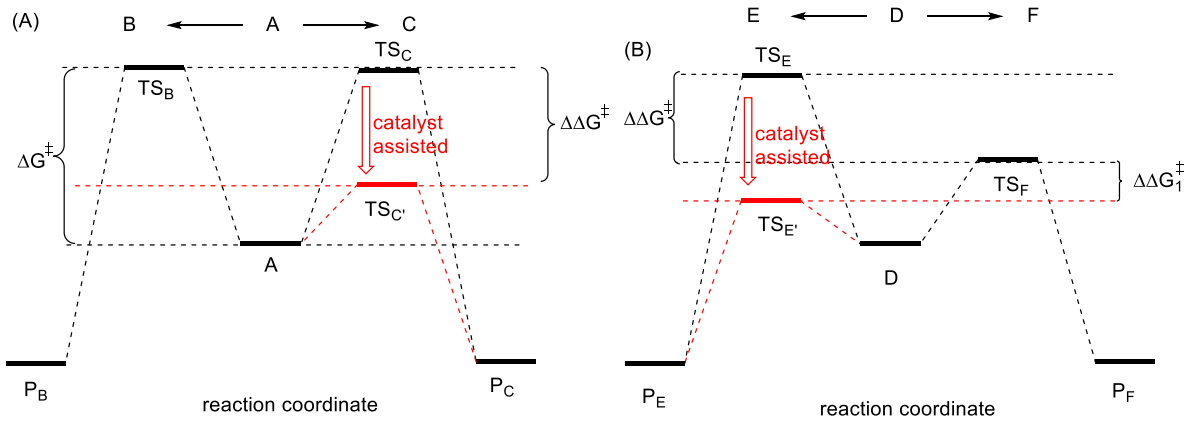

Figure 1.5 Energy diagrams of catalytic selective synthesis of (A) equal activation energy (B) different activation energy. TS = transition state.

The outlined above principles of the catalyst-controlled stereodifferentiation leading to selective pathways has many precedents in nature. Nature uses an array of biomolecular catalysts termed “enzymes” to control a variety of enantio-, diastereo- and regioselective transformations that are essential to the lifecycle of the living organism. The enzyme-based regioselective and diastereoselective functionalization of polyol-based natural products is also well-precedented, in particular in the context of the glycosylation reactions. For example, enzymes α-1,2-

mannosyltransferase Kre2p/Mnt1p[16] and glycosyltransferase DesVII/DesVIII[17] are known to accomplish a regio- and diastereoselective glycosylation of natural polyketides that possess multiple hydroxyl groups. These steps are key in the assembly of 12- and 14-membered glycosylated macrolide antibiotics. While incredibly effective in very complex settings, these enzymatic methods are often limited by the narrow substrate scopes and enzyme accessibility, which often creates a significant barrier for carrying the SAR studies on natural products.[9,18–20]

Due to the aforementioned limitations of the enzymatic methods, scientists have focused on developing other synthetic approaches that emulate enzymes and allow to achieve diastereoselective and regioselective functionalization of polyols as well as other types of natural products. A variety of synthetic strategies for the site selective modification of polyols have been based on the ability to selectively instal various protecting groups[21–23] as many protection methods allow to differentiate the hydroxyl groups based on often subtle differences in sterics and electronics around the reaction centers. Even though the selective installation of protecting groups represents one of the most reliable strategies for the regioselective functionalization of natural polyols developed to date, such strategies have significant limitations. One of such limitations comes from the lack of regiocontrol in cases when the reaction centers in the molecule have similar reactivity. In addition, a scenario when the easy-to-achieve selectivity does not lead to the desired simplification of the synthetic route are also quite common. Finally, due to their complexity many natural products are unstable to typical deprotection conditions and achieving a removal of the protecting group at the end of the synthesis may represent a formidable challenge. These factors prompted chemists to search for the alternative methods that help to minimize protecting group manipulations and functionalize alcohols in a more direct manner. Many of such studies have been focused on exploring chiral catalysts as enzyme surrogates, and a brief overview of the pioneering

work on exploring chiral catalysts for the site-selective functionalization of natural products is provided below.

The first examples of the catalysts-controlled regioselective functionalization of polyol-based natural products were reported by the Miller group.[19] These reports rely on the earlier work by the Miller group that explored the use of peptide-based nucleophilic organocatalysts for the enantioselective acylation and phosphorylation reactions.[14,19,24,25] A library of such catalysts could be readily synthesized using solid phase techniques, and the variation of amino acids in the peptide backbone helps to identify the optimal for catalysis sequence.

These concepts were subsequently applied to achieve site selective functionalization of antibiotic erythromycin A (**Scheme 1.3**). The control experiments using achiral catalyst *N*-methylimidazole (NMI) indicated that erythromycin A (**1-4A**) is preferentially acylated at the C2'-hydroxyl group of *L*-desosamine moiety to form **1.4b** as the major product. The authors hypothesized that this selectivity was likely due to the neighboring vicinal tertiary amine moiety that activates the C2'-hydroxyl group and makes it a better nucleophile. Furthermore, it was noticed that using 2 equivalents of the acylating reagent led to the selective acylation of the more reactive hydroxyl groups at the C2'- and C4''-positions. It was also realized that the C2' acetate group could be selectively cleaved during the work up procedure by using MeOH work up, leading to the monoacylated product **1-4c** containing acetate group at the C4''-position. The exploration of chiral peptide-based catalysts indicated that the C11-position of the macrolactone could be acylated in preference to the C2'- and C4''-hydroxyls. However, the initial reaction suffered from low conversion, and only 20% of the desired C11 acylated product (**1-4d**) was produced, despite prolonged reaction times. The subsequent optimization of the catalysts, solvents, and concentration, led to the discovery of catalyst **1-4B**, which provided 5:1 ratio (r.r.) of the

monoacylated products **1-4d** and **1-4b**. Even though the precise origins of regioselectivity for this catalytic reaction were not investigated, this study demonstrates that chiral catalysts may function as enzymes and their use may overturn the inherent reactivity profile of the natural products.

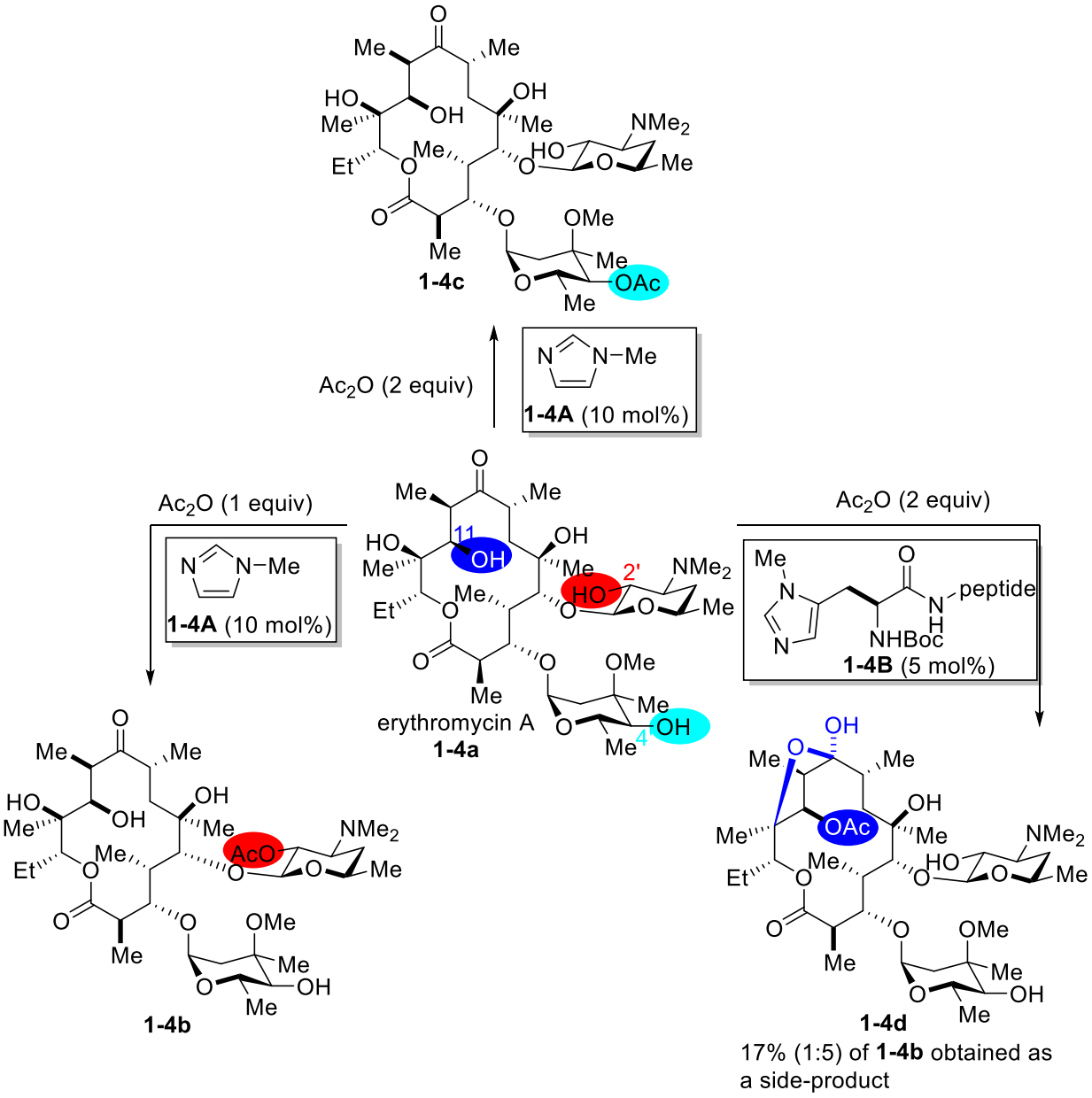

Scheme 1.3 Acylation of erythromycin A via NMI-based catalysts.

Following their initial work of using small peptide-based catalysts in controlling the regioselective functionalization of erythromycin A, the Miller group has also showed the power

and potential of using peptide-based catalysts in vancomycin (**1-5a**) esterification studies. In these studies Miller and coworkers observed that a selective protection of the two secondary hydroxyl groups (G_6-OH and G_4-OH) or a benzylic hydroxyl group (Z_6-OH) could be accomplished using the partially protected with Alloc/allyl groups vancomycin derivative **1-5a** (Scheme 1.4).[26] Initially, when no catalyst was used, no reaction was observed. Similarly, the reaction catalyzed by NMI, provided less than 5% of products, and recovery of the starting material. The subsequent screening and optimization of the catalysts resulted in identifying catalyst **1-5A** that promoted the acylation of the less reactive secondary G_4-OH leading to **1-5b** in 83% yield. The minor product **1-5b** resulting from the acylation of the primary G_6-OH was also isolated **1-5a** in 17% (entry 1). A completely different regioselectivity was observed with catalyst **1-5B**, which directed the acylation of the benzylic Z_6 position providing derivative **1-5d** in 94% along with the minor product **1-5b** (6% yield). Finally, catalyst **1-5C** that targets the primary G_6-OH group of **1-5a** leading to **1-5b** (% yield) along with 14% of **1-5c** was also identified. It is noteworthy that the key structural features in **1-5C** significantly differed from the key features in **1-5A** and **1-5B**. Earlier work by the Miller group suggested that **1-5C** binds to the ligand binding pocket of **1-5a** through a series of hydrogen bonds with the backbone amides; however, it was unclear if the same binding mode was operational with catalysts **1-5A** and **1-5B**.

This work further highlights the potential of using chiral catalysts for accomplishing regiodivergent functionalization of complex natural products and demonstrates the utility of this chemistry for the medicinal chemistry studies. The use of asymmetric catalysis allowed to achieve expedited access to nine new analogs of vancomycin, and their subsequent evaluation helped to identify a derivative with a superior to vancomycin antibacterial profile.

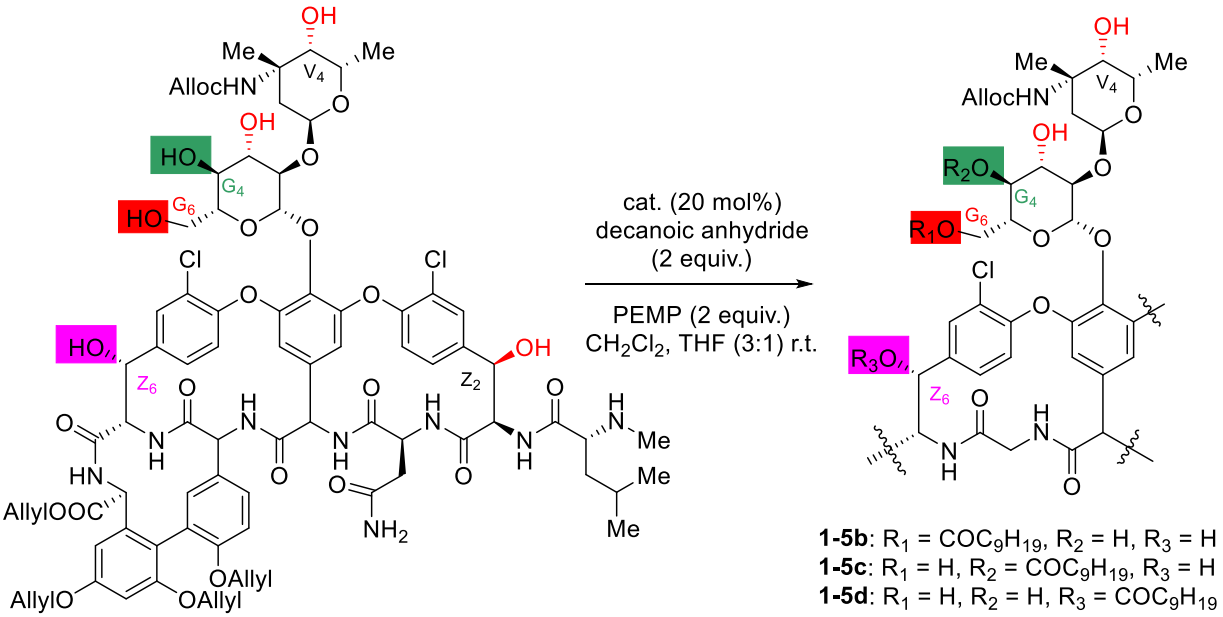

entry	cat.	conv. (%)	1-5b	:	1-5c	:	1-5d
1	none	no reaction	NA	:	NA	:	NA
2	NMI	<5	<5	:	<5	:	<5
3	**1-5A**	87	17	:	83	:	NA
4	**1-5B**	94	NA	:	6	:	94
5	**1-5C**	99	86	:	14	:	NA

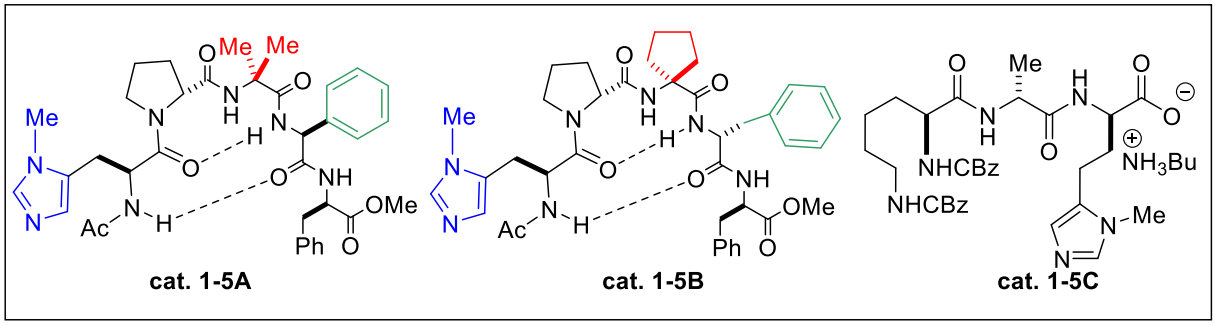

Scheme 1.4 Peptide catalyzed functionalization of vancomycin.

Following the aforementioned studies by the Miller group, Kawabata and coworkers has investigated chiral DMAP catalysts for the site-selective acylation of natural product lanatoside C (**Scheme 1.5**).[27] Lanatoside C is a glycosylated cardiac glycoside that contains nine hydroxyl groups. It is a glycosylated derivative of a more common cardenolide digoxin, and the only

difference in structures of these two natural products is in the extra *D*-glucose subunit in lanatoside C. The primary C_6-OH group of the terminal *D*-glucose is the most reactive hydroxyl in lanatoside C. The previous studies by the Kawabata group identified DMAP-based chiral amide catalysts that enable selective acylation of the C_4- rather than the C_6-position of the simple *D*-glucose derivatives. These prior results suggested that the use of chiral DMAP catalysts such as **1-6A** may also result in the C4’’’’-derivatization of lanatoside C.[28] Indeed, when DMAP was used as the catalyst in DMF, selective acylation of the C6’’’’-hydroxyl of lanatoside C was observed; however, this selectivity was overturned when DMAP was used in $CHCl_3$/THF (9:1) as the solvent (Scheme 1.5A). This later transformation provided product **1-6a** resulting from the selective acylation of the $C_{3''''}$- position (97:3 r.r.) along with the minor product of $C_{4''''}$-OH acylation **1-6b**. As anticipated, the use of the modified chiral DMAP-based catalyst **1-6B** resulted in the selective acylation of the $C_{4''''}$-position, and **1-6b** was obtained as the major product in 90:10 r.r. Kawabata and co-workers hypothesized that this regioselectivity was due to the specific arrangement of the hydrogen bonds between the catalysts and the $C_{3''''}$, $C_{4''''}$ and $C_{6''''}$ hydroxyls of the substrate. Consistent with this proposal, they carried a control experiment in an aprotic solvent (e.g. DMF) that disrupts hydrogen bonds and breaks the intramolecular interactions between the catalyst and substrates. Under these conditions, acylation with **1-6B** provided the C6’’’’-derivative as the major product, and these results were similar to what was previously observed for the achiral catalyst (e.g. DMAP) in DMF. These studies provided regiodivergent routes to various derivatives of lanatoside C and resulted in 9 different derivatives of this natural product. In addition to the aforementioned studies, the Kawabata group have highlighted the utility of the chiral DMAP-based catalysts for the site-selective acylation for 10-diacetylbaccatin III (Scheme 1.5B). The control experiments with DMAP suggested that, the C_7-OH and C_{10}-OH

postions of **1-6d** are the most reactive ones, and 38:62 r.r. of **1-6e:1-6f** was obtained. However, the formation of the C_7-acylation product could be significantly enhanced to 93:7 rr using catalyst **1-6B**.

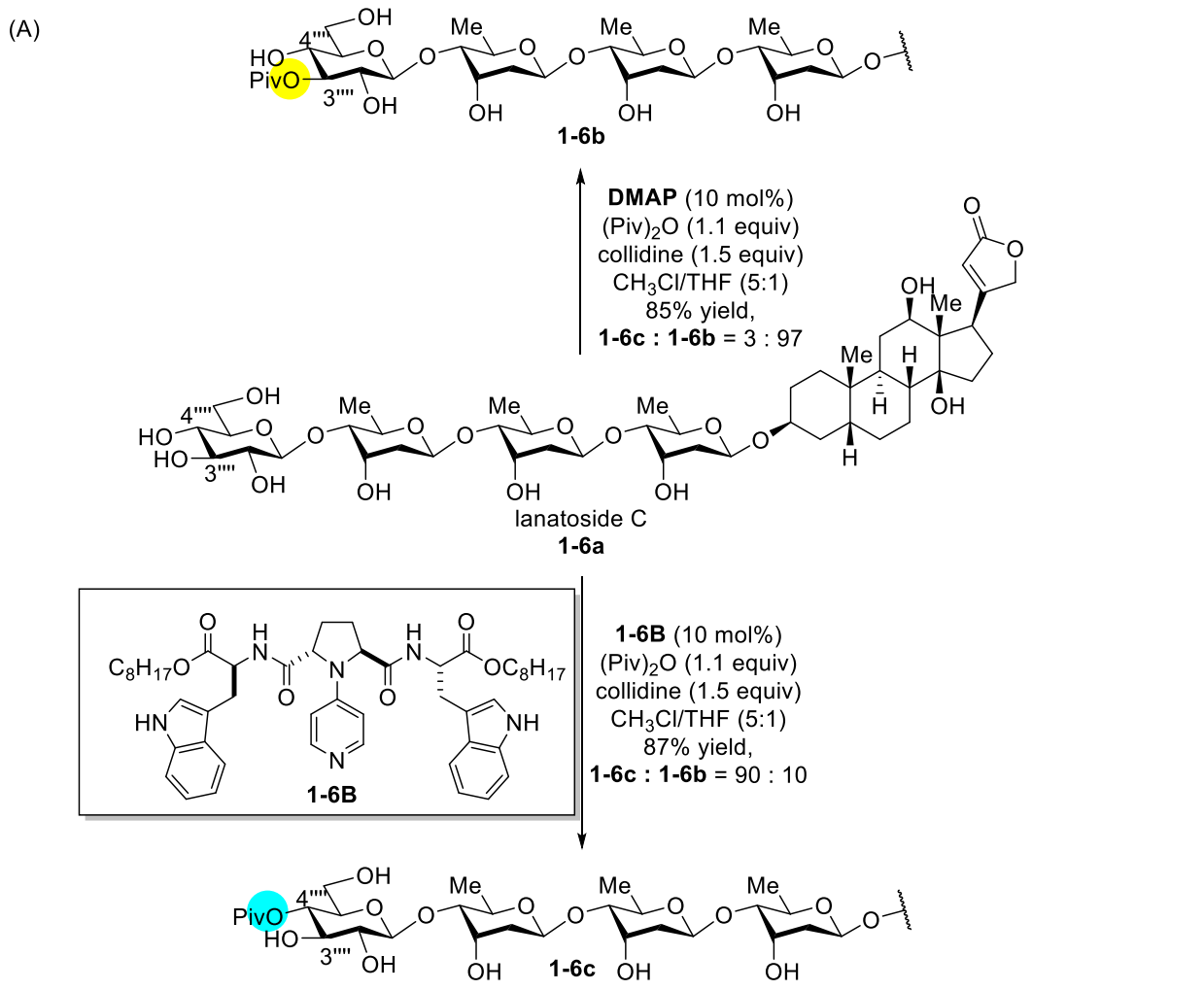

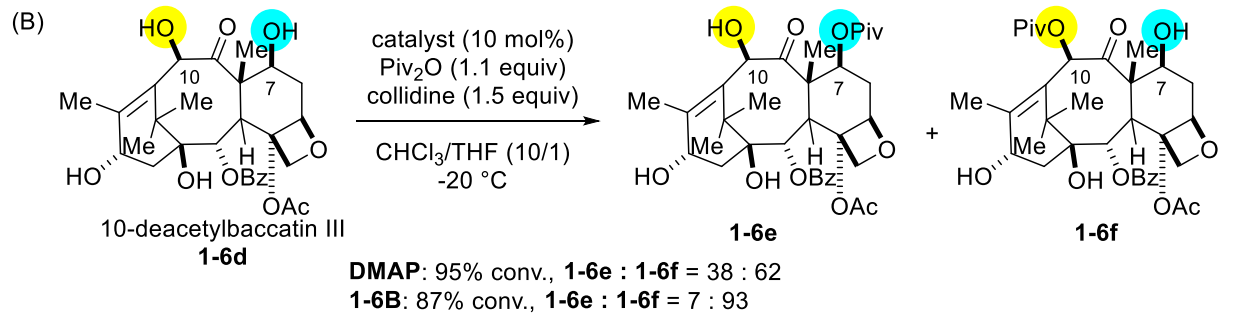

Scheme 1.5 peptide-based catalysts catalyzed regioselective acylation of (A) lanatoside C and (B) 10-diacetylbaccatin III.

In addition to the aforementioned work, similar methods based on using peptide catalysts to control site-selective acylation of apoptolidin[24] and 10-deacetylbaccatin III[29] have also been accomplished (Scheme 1.6). In their studies of site-selective acylation of apoptolidin (**1-7a**), Wender and co-workers utilized catalyst **1-7A** to acylate the C_2'- instead of the C_3'-position of the sugar. The reaction was performed at low-conversions to terminates the reactions before the competing di-acylation occurs. In the control experiment whith DMAP, acylation at the C_2'-position (**1-7b**) and C_3'-position (**1-7c**) happened to produce 1:1 of products **1-7b** and **1-7c** in ~50% conversion. However, after switching to peptide-based catalyst **1-7A**, a more selective formation of the diastereomer **1-7b** was noted in 4:1 d.r. and 50% conversion.

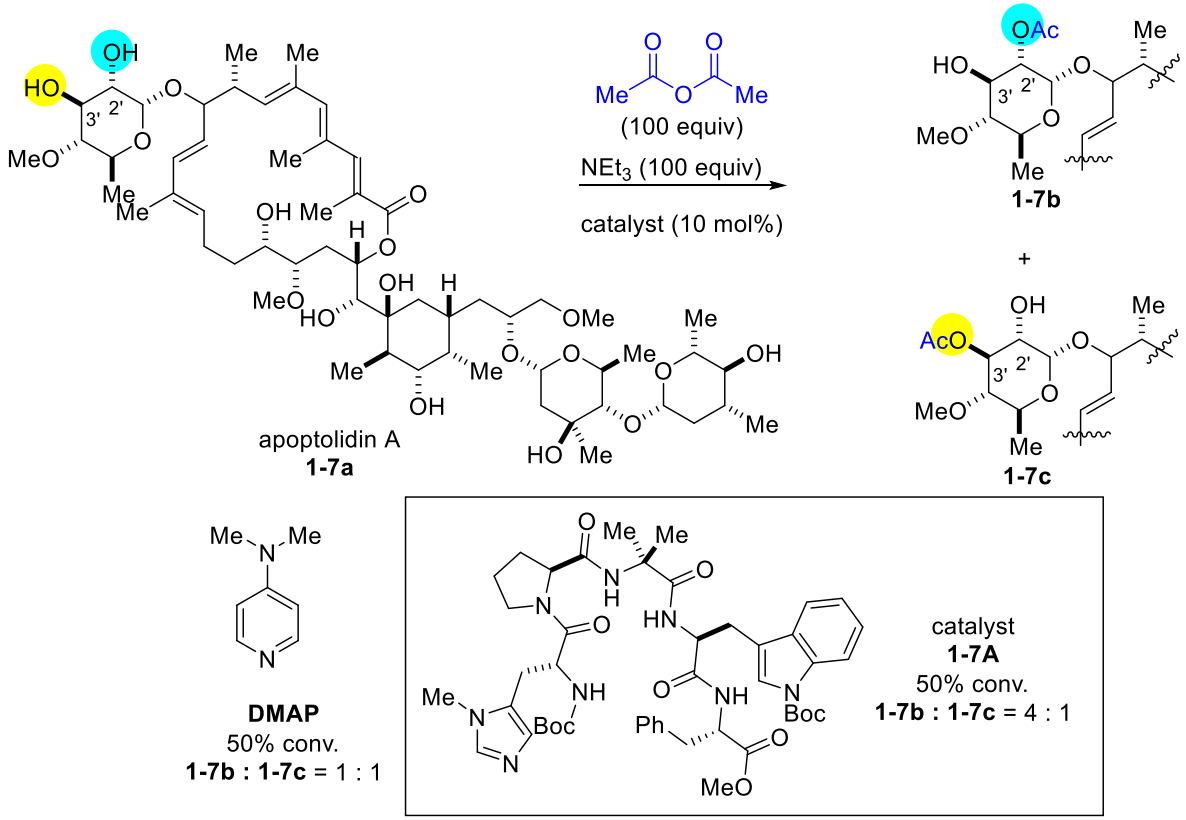

Scheme 1.6 Selective acylation via peptide-based catalysts of apoptolidin.

1.3. Overview of stereodifferentiating CPA-catalyzed reactions in the synthesis of natural products and natural product derivatives.

The aforementioned methodologies relying on using chiral catalysts for controlling the coure of regioselective functionalization of polyol-based natural products have inspired a variety of subsequent studies focused on exploring other types of electrophiles in the context of selective functionalization of natural products. With this regard, CPAs represent a great system to explore because of the highly tunable backbone, bifunctional nature of the hydrogen phosphate active site, and multiple modes of activation, by which they may promote the reaction with an electrophile. Due to these reasons, CPAs have been explored for the site-selective and stereoselective synthesis of natural products and their derivatives, and this subsection provides an overview of this work.

In 2012, the Nagorny group demonstrated that CPAs could control the stereochemistry of intramolecular glycosylation of *D*-glucal derivatives leading to more-challenging to access nonthermodynamic spiroketals.[30] These results suggested the possibility of carrying stereodifferention acetalization reactions in other, more complex, settings, and the Nagorny group pursuited several applications of these concepts.[31–33] Thus, in 2017, Nagorny and coworkers described the application of CPAs for the stereodivergent desymmetrizative glycosylation of protected 2-deoxystreptamine **1-8b** leading to the synthesis of aminoglycosides iso-neamine and iso-kanamycin B derivatives (Scheme 1.7).[34] This transformation involved the use of glycosyl donor **1-8a** that represents a *D*-mannose-derived trichloroacetimidate carrying a PMB protection at the $C_{2'}$- and $C_{6'}$-positions. The 2-deoxystreptamine **1-8b** is an achiral meso-derivative; however, its glycosylation at either C_4- or C_6-positions would lead to the loss of symmetry and formation of two diastereomeric products **1-8c** and **1-8d**. While the use of achiral catalysts led to the formation of the complex mixture of products, the use of (*R*)-catalysts as the catalysts favored the formation

of **1-8c**, while the (*S*)-CPA catalysts preferentially produced diastereomeric **1-8d**. The subsequent optimization of the CPA catalyst helped to identify **(*S*)-1-8A** as the optimal catalyst that resulted in the formation of the glycosylated product **1-8d** in 74% yield and 86:14 d.r. Similarly, the use of catalytic **(*R*)-1-8A** led to the product **1-8c** in 51% yield and 67:33 d.r.. The resultant glycosylated products were subsequently elaborated to the protected iso-neamine and iso-kanamycin B derivatives, and the synthesis of **1-8d** was carried on the gram scale. It is noteworthy that while nature utilizes enzymes to produce aminoglycosides equivalent to **1-8c**, there are no enzymatic processes that would provide access to the diastereomeric product **1-8d**. Therefore, not only this chemistry highlights the utility of CPAs for controlling the fundamentally important processes such as glycosylation reactions, but also demonstrates the power of asymmetric catalysis for accessing the derivatives that are not readily available through the enzymatic synthesis.

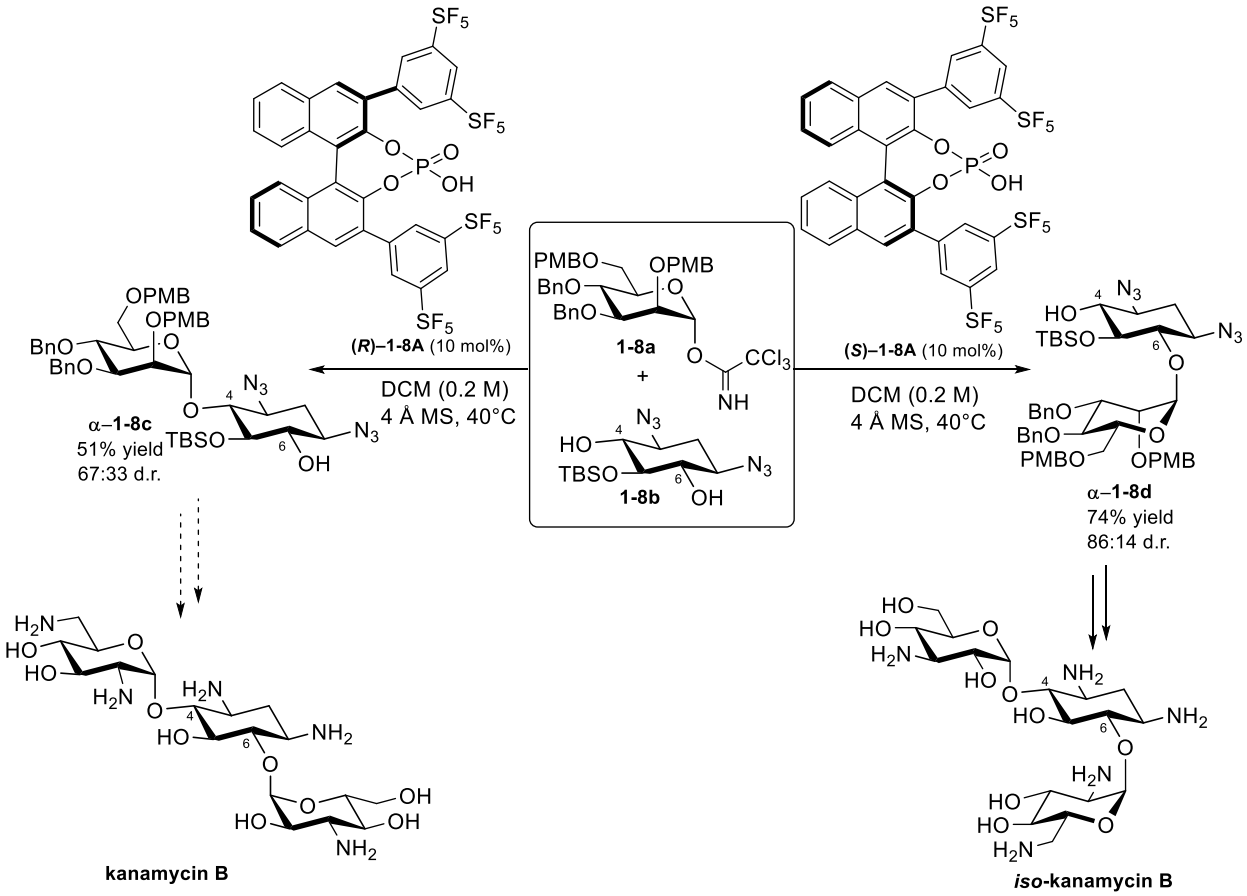

Scheme 1.7 Application of desymmetrizative glycosylation to synthesis of aminoglycosides.

In 2017, the Nagorny group described the application of chiral phosphoric acids (CPAs) for controling the regioselectivity of glycosylation of macrolactone polyols 6-deoxy-erythronolide B (6-dEB) and modified oleandomycin **(Scheme 1.8**).[35] 6-dEB is a biogenic precursor to erythromycins, and this biosynthetic pathway requires C_5-glycosylation with *L*-desosamine in order for 6-dEB oxidation into erythromycins by P450 enzymes. At the same time, it was discovered that 6-dEB was not a good substrate for the enzymatic glycosylations as low yields and the formation of the regioisomeric glycosides was observed. Similarly, the evaluation of the standard achiral catalysts resulted in mixtures of C_5-, C_3-, and *bis*-glycosylated products in moderate to low yields.

It was discovered that with (*S*)-BINOL-based CPAs the formation of the C_5-glycoside **1-9c** was enhanced, and that with the catalyst **1-9A** glycosylation occurred almost exclusively at the C_5-position in 98% yield and with 99:1 r.r. After extensive catalyst screening, the authors identified (*S*)-SPINOL-based CPA **1-9B** as the catalyst that was able to overcome the inherent selectivity preferences and selectively glycosylated the C_3-hydroxyl group of 6-dEB to provide the mono-glycosylated product **1-9b** in 82% yield and 73:27 r.r. These studies, however, did not lead to the catalyst that would favor the glycosylation of the C_{11}-hydroxyl group that would lead to product **1-9d**. However, it was circumvented by developing a catalyst free approach that takes advantage of the traceless protecting group. It was discovered that both the C_3- and C_5- hydroxyl groups could be temporarily protected as a cyclic boronic acid ester intermediate, **1-9e**, which could then be glycosylated at the remaining C_{11}-position followed by the removal of the cyclic boronic acid ester upon work up. This one-pot three operation protocol results in the regioselective glycosylation at the C_{11}-position leading to product **1-9d**, in 62% yield and 99:1 r.r. These studies represent the

first example of chiral catalyst-controlled regioselective glycosylation of complex polyol-based natural products, and describe the strategies for the selective synthesis of all three possible regioisomers of 6-dEB.

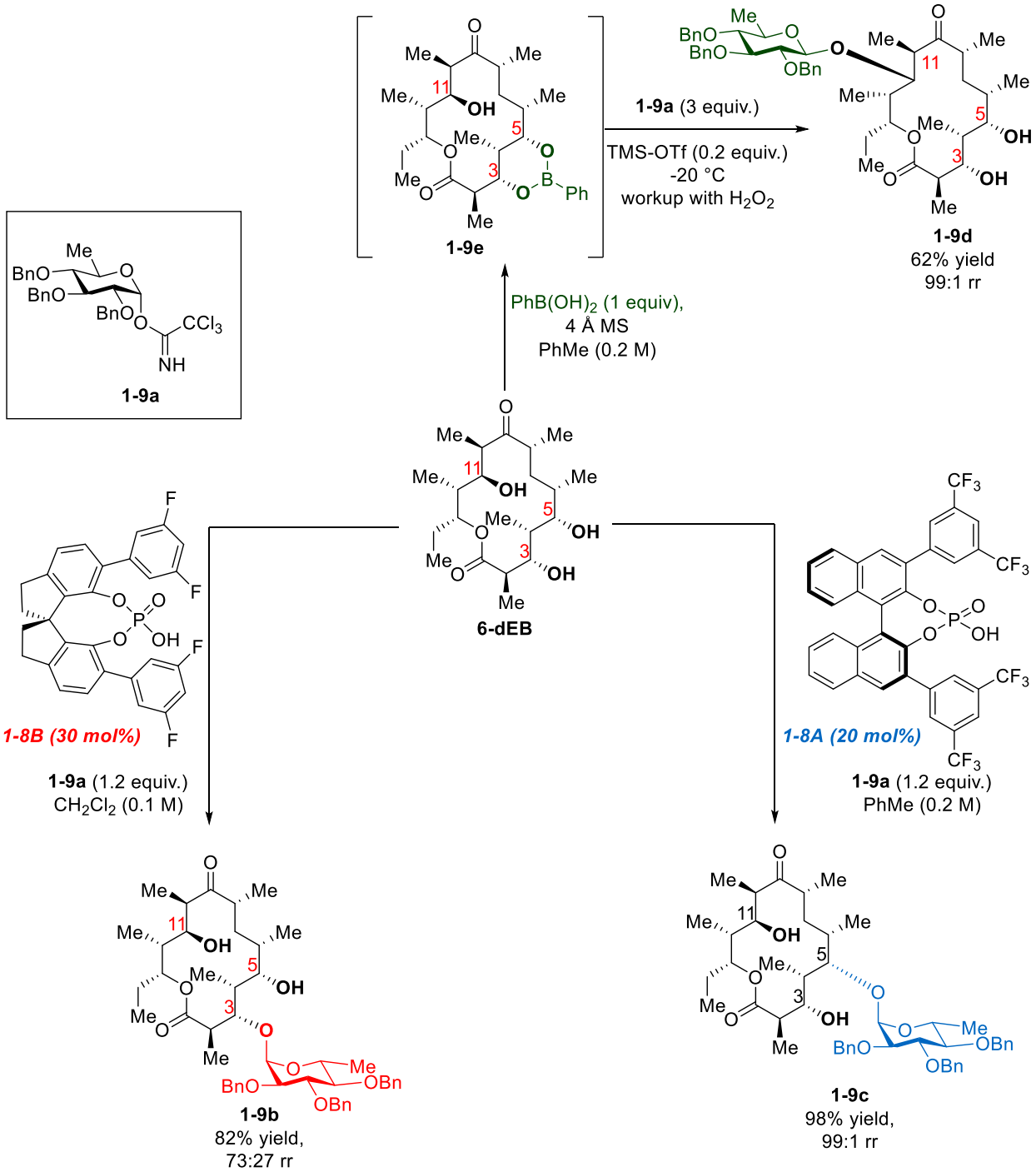

Scheme 1.8 Glycosylation of 6-dEB via chiral phosphoric acids.

In addition to the aforementioned examples that involved using the CPAs to control site-selectivity, CPA-controlled diastereoselective transformations have been of great utility for the synthesis of natural products. Thus, in 2013 the Toshima group demonstrated that CPAs could be used to accomplish glycosylation of racemic alcohols that proceed with the recognition of chirality (i.e. resolution).[36] This concept was employed in the total synthesis of flavan glycoside **1-10c** (cf. Scheme 1.9). Using the catalyst **(*S*)-1-10A** and racemic flavone derivative **1-10a**, the authors have accomplished a highly diastereoselective glycosylation with 2,3,4,6-tetra-*O*-benzyl-*D*-glucose trichloroacetimidate **1-10b** as the donor. The desired glycoside **1-10c** was obtained in 65% yield from trichloroacetimidate donor, and in excellent α/β stereo- and diastereoselectivity. In addition, they also observed no glycosylation occurred with the other enantiomer **(+)-1-10a** and it was fully recovered. At the same time, no diastereoselectivity was observed when either an achiral phosphoric acid or (*R*)-enantiomer of **1-10A** were used as the catalysts. Even though the authors were not clear about the high diastereoselectivity, they suggest (-)-**1-10a** could potentially form a more stable intermediate **1-10d** compared to (+)-**1-10a** due to steric clash. These studies suggested that CPAs may serve as important element of the chiral recognition leading to the highly stereoselective product formation.

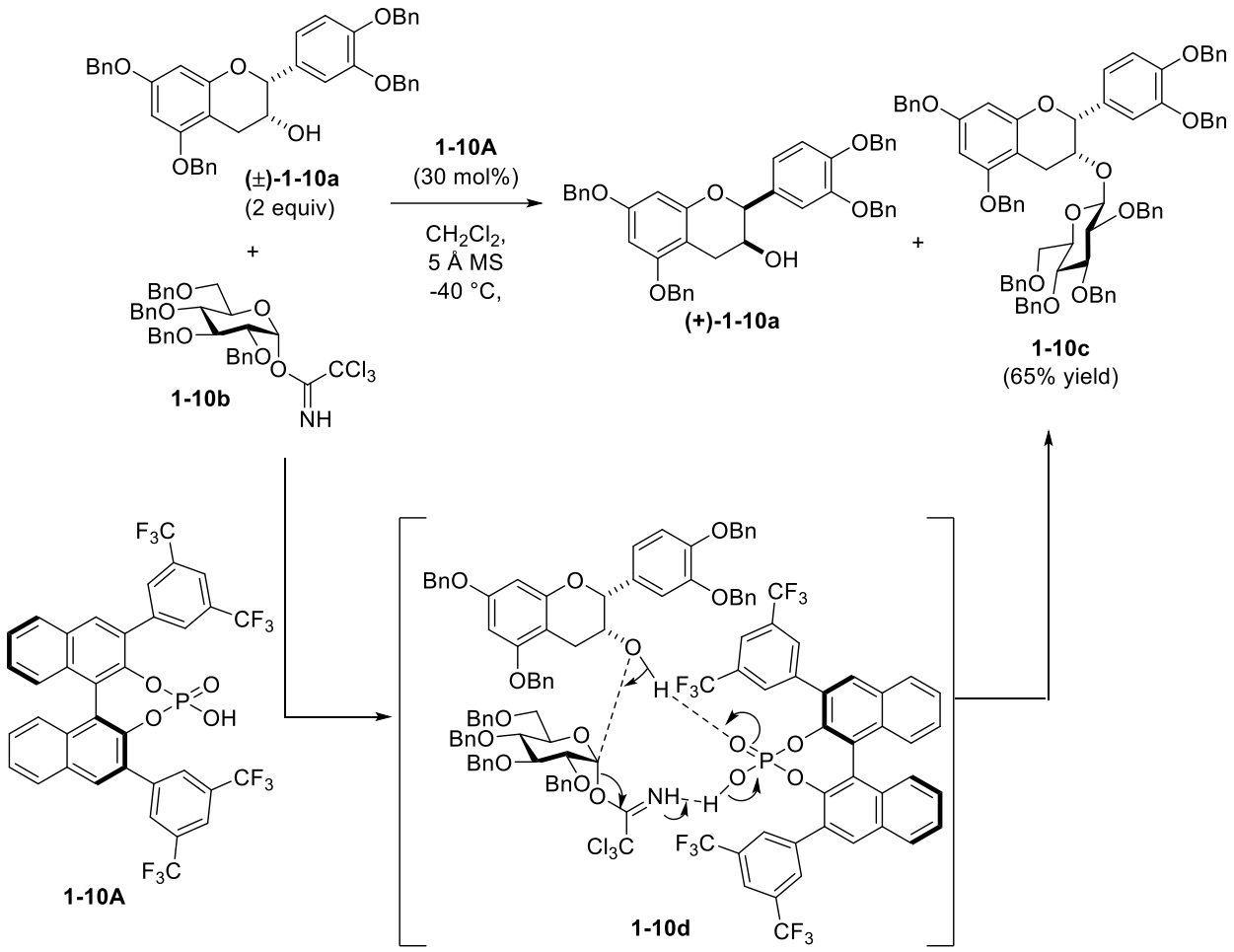

Scheme 1.9 Diastereoselective glycosylation of 1-9a.

Another example highlighting the stereodifferentiating reactions with CPAs was published by Ghosh and co-workers in the context of the total synthesis of (-)-zampanolide (*cf.* Scheme 1.8).[37] This polyketide natural product contains a macrolactone moiety **1-11c** with a high degree of unsaturation and a side-chain that contains an unusual hemiaminal motif. The hemiaminal motif present in (-)-zampanolide exists in (*R*)-stereochemical configuration and is likely to arise from the hydration of the acyliminium intermediate arising from the reaction of aldehyde **1-11a** and primary amide **1-11b**. Following this proposal, the authors were able to access both the aldehyde precursor **1-11a** and amide **1-11b** and investigated their coupling (cf. Scheme 1.8). Using the

previously reported method for the 10-camphorsulfonic acid-catalyzed formation of hemiaminal from **1-11a** and **1-11b**, only 12 % of the desired (-)-zampanolide **1-11c** was obtained along with 12 % of its diastereomer epi-(-)-zampanolide **1-11d**, and 16% of bis-amide product **1-11e**.[38] Based on the previous work of List and Antila who demonstrated that CPAs could be used for enantioselective formation of hemiaminals[39], the authors decided to explore chiral phosphoric acids to control the diastereoselective formation of **1-11c**. Using **(*S*)-1-11A** as the catalyst, they could drastically increase the isolated yield of **1-11c** in 51% while only18% of **1-11d** and no **1-11e** were formed. At the same time, the enantiomeric **(*R*)-1-11A** catalyst provided ~1:1 mixture of **1-11c** and **1-11d**, indicating that depending on the chirality of the catalyst could be either matched or mismatched with the chirality of the aldehyde **1-11b**.

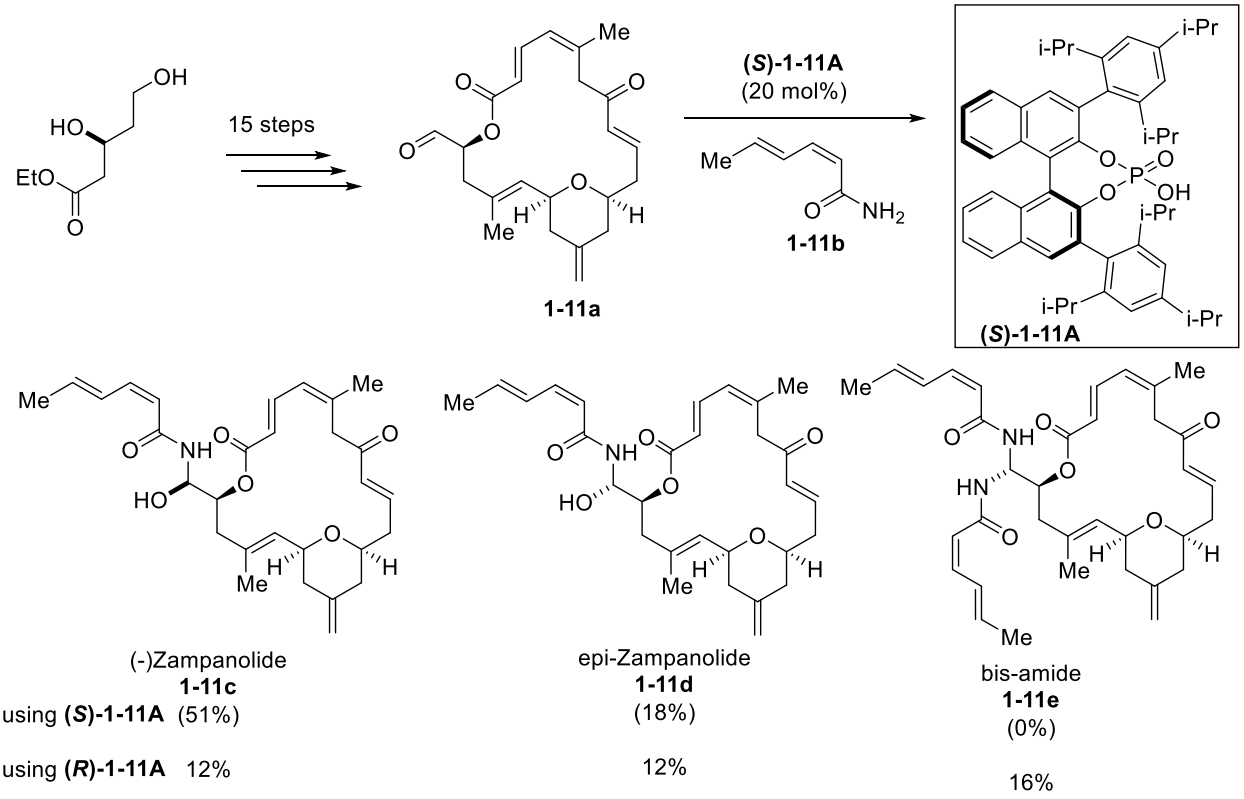

Scheme 1.10 CPA catalyzed amination towards total synthesis of (-)-Zampanolide.

In addition to the Nagorny group's use of CPAs in controlling the site-selective glycosylation, the Toste, Miller and Sigman groups have demonstrated the use of CPAs for the regioselective acylation of natural products for building regioisomeric acetates for potential medicinal chemistry exploration.[18] One of the targets in these studies was 19-hydroxy-DHEA (**1-12a**) (**Scheme 1.11A**). The authors discovered that for **1-12a** the primary alcohol at the C_{19}-position is more kinetically reactive than the secondary alcohol at the C_3-position. This selectivity could be overturned to form the C_3-acylated product **1-12b** with the C_{19}-hydroxyl in 98% yield and more than 50:1 r.r., favoring the less reactive secondary alcohol, if CPA **1-12A** was used as the catalyst. Moreover, a similar method was used for the acylation of the natural polyphenol naringenin (**1-12c**) (**Scheme 1.11B**). In this case, the use of classic acylating conditions (AcCl, K_2CO_3) resulted in the acylation at the $C_{4'}$-position of naringenin to form product **1-12d** in 65% yield and 33:1 r.r.. However, when acetic anhydride was used in combination with CPAs **1-12B**, the reversal of the regioselectivity was observed and the acylated at the C_7-position product **1-12e** was formed in 35% yield and 7:1 r.r.

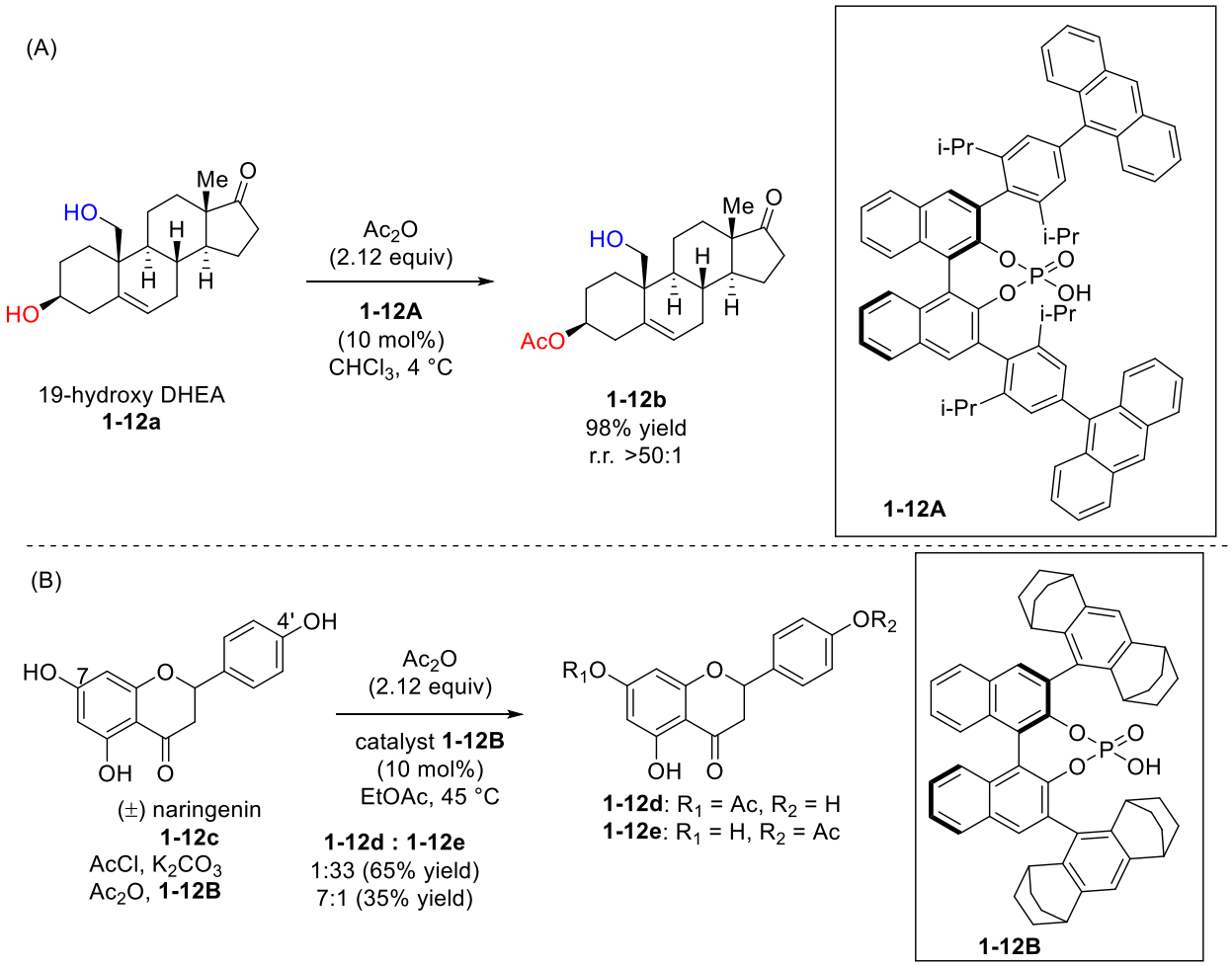

Scheme 1.11 Examples of regioselective CPA-controlled acylation of natural polyols (A) 19-hydroxy-DHEA (B) naringenin.

Another example of the CPA-controlled stereoselective transformation in the natural product synthesis was recently published by Shenvi and co-workers.[40] Working on the synthesis of natural product (-)-bilobalide, the authors faced the problem of controlling the stereoselectivity of acetalization leading to the formation of the oxetane intermediate **1-13b** (Scheme 1.12). After examining standard acidic catalysts, they found that the formation of the desired diastereomer of oxetane **1-13b** is not favored. For example, with *para*-toluenesulfonic acid, they could only obtain 1:3 mixture of the desired oxetane acetal diastereomer **1-13b** and the undesired product **1-13c**. Due to the instability of the oxetane acetal because of the ring strain, all of the initial attempts to

epimerize **1-13c** to **1-13b** under acidic conditions turned out to be futile. Instead of the epimerization, the authors were only able to recover the starting material **1-13a**. They hypothesized that this transformation failed due to the instability of the 4-membered oxocarbenium ion intermediate and steric effects due to the presence of multiple quaternary carbons and *tert*-butyl substituent in case of the *exo*-cleavage pathway. These effects make it impossible to epimerize and lead to kinetic stability of the starting material. However, when they used CPA **1-13A** to control the direct cyclization of **1-13a** into either **1-13b** or **1-13c**, they started observing a moderate selectivity (~5.3:1 dr) favoring the desired diastereomer of **1-13b** with >99% d.r. after the recrystallization. Therefore, the Shenvi group has shown the potential of CPAs to achieve efficient, highly diastereoselective, and functional group tolerance in complex natural products.

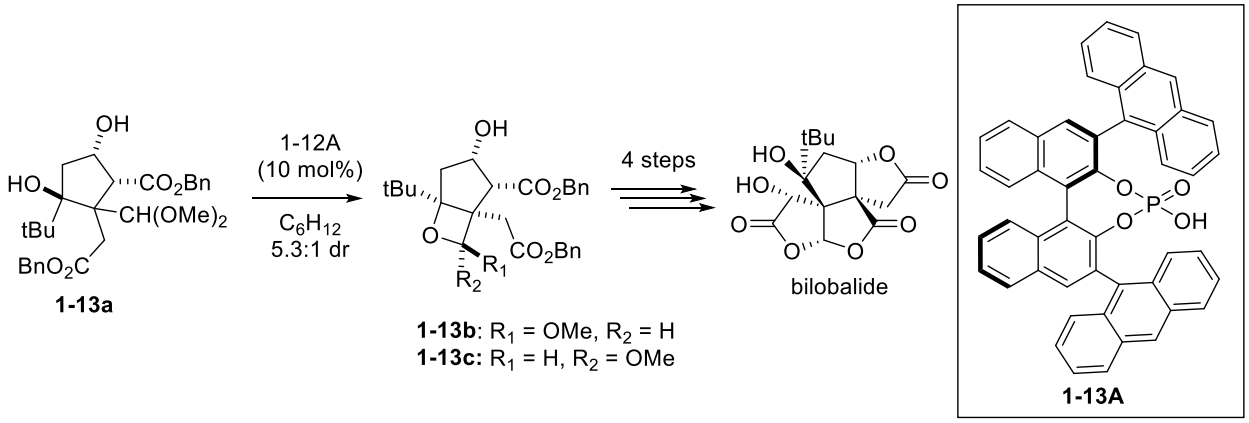

Scheme 1.12 CPA catalyzed oxetane for the synthesis of (-)-bilobalide.

The examples in this chapter highlight the power of chiral phosphoric acids for controlling the course of regio- and stereoselective transformations. In some instances, CPAs could be used to overcome the inherent selectivity bias of the substrate and result in the selectivity that otherwise would not be attained with achiral reagents or standard conditions. Considering the reach chemistry of CPA-catalyzed enantioselective transformations and multiple modes of substrate activation through which CPAs could operate, it is expected that many other types of

transformations relevant to the synthesis and derivatization of natural products and chiral substrates could be greatly improved through the use of CPA catalysis. The following chapters will demonstrate the first example of CPA-controlled regiodivergent epoxide ring opening leading to the formation of complex natural product derivatives with different heterocycle sizes. In addition, this dissertation will investigate the immobilized and recyclable CPA to address problems associated with the regioselective synthesis of the sugar derivatives. These applications further highlight the utility of CPAs in the natural product synthesis and demonstrate that practical and scalable CPA-catalyzed reactions could be achieved.

1.4. References

(1) Akiyama, T.; Itoh, J.; Yokota, K.; Fuchibe, K. Enantioselective Mannich-Type Reaction Catalyzed by a Chiral Brønsted Acid. *Angew. Chem.* **2004**, *116* (12), 1592–1594. https://doi.org/10.1002/ange.200353240.

(2) Uraguchi, D.; Terada, M. Chiral Brønsted Acid-Catalyzed Direct Mannich Reactions via Electrophilic Activation. *J. Am. Chem. Soc.* **2004**, *126* (17), 5356–5357. https://doi.org/10.1021/ja0491533.

(3) Maji, R.; Mallojjala, S. C.; Wheeler, S. E. Chiral Phosphoric Acid Catalysis: From Numbers to Insights. *Chem. Soc. Rev.* **2018**, *47* (4), 1142–1158. https://doi.org/10.1039/C6CS00475J.

(4) Rueping, M.; Kuenkel, A.; Atodiresei, I. Chiral Brønsted Acids in Enantioselective Carbonyl Activations – Activation Modes and Applications. *Chem. Soc. Rev.* **2011**, *40* (9), 4539. https://doi.org/10.1039/c1cs15087a.

(5) Yang, C.; Xue, X.-S.; Jin, J.-L.; Li, X.; Cheng, J.-P. Theoretical Study on the Acidities of Chiral Phosphoric Acids in Dimethyl Sulfoxide: Hints for Organocatalysis. *J. Org. Chem.* **2013**, *78* (14), 7076–7085. https://doi.org/10.1021/jo400915f.

(6) Cheon, C. H.; Yamamoto, H. A Brønsted Acid Catalyst for the Enantioselective Protonation Reaction. *J. Am. Chem. Soc.* **2008**, *130* (29), 9246–9247. https://doi.org/10.1021/ja8041542.

(7) Xie, Y.; Zhao, Y.; Qian, B.; Yang, L.; Xia, C.; Huang, H. Enantioselective N–H Functionalization of Indoles with a,b-Unsaturated g-Lactams Catalyzed by Chiral Brønsted Acids*. *Angew. Chem. Int. Ed.* **2011**, 5.

(8) Thomas, C. M.; Hothersall, J.; Willis, C. L.; Simpson, T. J. Resistance to and Synthesis of the Antibiotic Mupirocin. *Nat. Rev. Microbiol* **2010**, *8* (4), 281–289. https://doi.org/10.1038/nrmicro2278.

(9) Pathak, T. P.; Miller, S. J. Site-Selective Bromination of Vancomycin. *J. Am. Chem. Soc.* **2012**, *134* (14), 6120–6123. https://doi.org/10.1021/ja301566t.

(10) Dailler, D.; Dorst, A.; Schäfle, D.; Sander, P.; Gademann, K. Novel Fidaxomicin Antibiotics through Site-Selective Catalysis. *Commun. Chem.* **2021**, *4* (1). https://doi.org/10.1038/s42004-021-00501-6.
(11) Zhang, G.; Fang, L.; Zhu, L.; Zhong, Y.; Wang, P. G.; Sun, D. Syntheses and Biological Activities of 3‘-Azido Disaccharide Analogues of Daunorubicin against Drug-Resistant Leukemia. *J. Med. Chem.* **2006**, *49* (5), 1792–1799. https://doi.org/10.1021/jm050916m.
(12) Langenhan, J. M.; Peters, N. R.; Guzei, I. A.; Hoffmann, F. M.; Thorson, J. S. Enhancing the Anticancer Properties of Cardiac Glycosides by Neoglycorandomization. *PNAS* **2005**, *102* (35), 12305–12310. https://doi.org/10.1073/pnas.0503270102.
(13) Beale, T. M.; Taylor, M. S. Synthesis of Cardiac Glycoside Analogs by Catalyst-Controlled, Regioselective Glycosylation of Digitoxin. *Org. Lett.* **2013**, *15* (6), 1358–1361. https://doi.org/10.1021/ol4003042.
(14) Shugrue, C. R.; Miller, S. J. Applications of Nonenzymatic Catalysts to the Alteration of Natural Products. *Chem. Rev.* **2017**, 58.
(15) Mahatthananchai, J.; Dumas, A. M.; Bode, J. W. Catalytic Selective Synthesis. *Angew. Chem. Int. Ed.* **2012**, *51* (44), 10954–10990. https://doi.org/10.1002/anie.201201787.
(16) Lobsanov, Y. D.; Romero, P. A.; Sleno, B.; Yu, B.; Yip, P.; Herscovics, A.; Howell, P. L. Structure of Kre2p/Mnt1p. *J. Biol. Chem.* **2004**, *279* (17), 17921–17931. https://doi.org/10.1074/jbc.M312720200.
(17) Borisova, S. A.; Kim, H. J.; Pu, X.; Liu, H. Glycosylation of Acyclic and Cyclic Aglycone Substrates by Macrolide Glycosyltransferase DesVII/DesVIII: Analysis and Implications. *ChemBioChem* **2008**, *9* (10), 1554–1558. https://doi.org/10.1002/cbic.200800155.
(18) Li, J.; Grosslight, S.; Miller, S. J.; Sigman, M. S.; Toste, F. D. Site-Selective Acylation of Natural Products with BINOL-Derived Phosphoric Acids. *ACS Catal.* **2019**, *9* (11), 9794–9799. https://doi.org/10.1021/acscatal.9b03535.
(19) Lewis, C. A.; Miller, S. J. Site-Selective Derivatization and Remodeling of Erythromycin A by Using Simple Peptide-Based Chiral Catalysts. *Angew. Chem. Int. Ed.* **2006**, *45* (34), 5616–5619. https://doi.org/10.1002/anie.200601490.
(20) Reetz, M. T. What Are the Limitations of Enzymes in Synthetic Organic Chemistry? *Chem. Rec.* **2016**, *16* (6), 2449–2459. https://doi.org/10.1002/tcr.201600040.
(21) Stork, G.; La Clair, J. J. Stereoselective Synthesis of β-Mannopyranosides via the Temporary Silicon Connection Method. *J. Am. Chem. Soc.* **1996**, *118* (1), 247–248. https://doi.org/10.1021/ja9532291.
(22) Moitessier, N.; Englebienne, P.; Chapleur, Y. Directing-Protecting Groups for Carbohydrates. Design, Conformational Study, Synthesis and Application to Regioselective Functionalization. *Tetrahedron* **2005**, *61* (28), 6839–6853. https://doi.org/10.1016/j.tet.2005.04.060.
(23) Toshima, K.; Nozaki, Y.; Mukaiyama, S.; Tamai, T.; Nakata, M.; Tatsuta, K.; Kinoshita, M. Application of Highly Stereocontrolled Glycosidations Employing 2,6-Anhydro-2-Thio Sugars to the Syntheses of Erythromycin A and Olivomycin A Trisaccharide. *J. Am. Chem. Soc.* **1995**, *117* (13), 3717–3727. https://doi.org/10.1021/ja00118a008.
(24) Lewis, C. A.; Longcore, K. E.; Miller, S. J.; Wender, P. A. An Approach to the Site-Selective Diversification of Apoptolidin A with Peptide-Based Catalysts. *J. Nat. Prod.* **2009**, *72* (10), 1864–1869. https://doi.org/10.1021/np9004932.
(25) Fowler, B. S.; Laemmerhold, K. M.; Miller, S. J. Catalytic Site-Selective Thiocarbonylations and Deoxygenations of Vancomycin Reveal Hydroxyl-Dependent

Conformational Effects. *J. Am. Chem. Soc.* **2012**, *134* (23), 9755–9761. https://doi.org/10.1021/ja302692j.
(26) Yoganathan, S.; Miller, S. J. Structure Diversification of Vancomycin through Peptide-Catalyzed, Site-Selective Lipidation: A Catalysis-Based Approach To Combat Glycopeptide-Resistant Pathogens. *J. Med. Chem.* **2015**, *58* (5), 2367–2377. https://doi.org/10.1021/jm501872s.
(27) Ueda, Y.; Mishiro, K.; Yoshida, K.; Furuta, T.; Kawabata, T. Regioselective Diversification of a Cardiac Glycoside, Lanatoside C, by Organocatalysis. *J. Org. Chem.* **2012**, *77* (18), 7850–7857. https://doi.org/10.1021/jo301007x.
(28) Muramatsu, W.; Kawabata, T. Regioselective Acylation of 6-O-Protected Octyl β-d-Glucopyranosides by DMAP Catalysis. *Tetrahedron Lett.* **2007**, *48* (29), 5031–5033. https://doi.org/10.1016/j.tetlet.2007.05.098.
(29) Yanagi, M.; Ninomiya, R.; Ueda, Y.; Furuta, T.; Yamada, T.; Sunazuka, T.; Kawabata, T. Organocatalytic Site-Selective Acylation of 10-Deacetylbaccatin III. *Chem. Pharm. Bull.* **2016**, *64* (7), 907–912. https://doi.org/10.1248/cpb.c16-00037.
(30) Sun, Z.; Winschel, G. A.; Borovika, A.; Nagorny, P. Chiral Phosphoric Acid-Catalyzed Enantioselective and Diastereoselective Spiroketalizations. *J. Am. Chem. Soc.* **2012**, *134* (19), 8074–8077. https://doi.org/10.1021/ja302704m.
(31) Khomutnyk, Y. Ya.; Argüelles, A. J.; Winschel, G. A.; Sun, Z.; Zimmerman, P. M.; Nagorny, P. Studies of the Mechanism and Origins of Enantioselectivity for the Chiral Phosphoric Acid-Catalyzed Stereoselective Spiroketalization Reactions. *J. Am. Chem. Soc.* **2016**, *138* (1), 444–456. https://doi.org/10.1021/jacs.5b12528.
(32) Nagorny, P.; Sun, Z.; Winschel, G. A. Chiral Phosphoric Acid Catalyzed Stereoselective Spiroketalizations. *Synlett* **2013**, *24*, 661–665.
(33) Mensah, E.; Camasso, N.; Kaplan, W.; Nagorny, P. Chiral Phosphoric Acid Directed Regioselective Acetalization of Carbohydrate-Derived 1,2-Diols. *Angew. Chem. Int. Ed.* **2013**, *52* (49), 12932–12936. https://doi.org/10.1002/anie.201304298.
(34) Lee, J.; Borovika, A.; Khomutnyk, Y.; Nagorny, P. Chiral Phosphoric Acid-Catalyzed Desymmetrizative Glycosylation of 2-Deoxystreptamine and Its Application to Aminoglycoside Synthesis. *Chem. Comm.* **2017**, *53* (64), 8976–8979. https://doi.org/10.1039/C7CC05052F.
(35) Tay, J.-H.; Argüelles, A. J.; DeMars, M. D.; Zimmerman, P. M.; Sherman, D. H.; Nagorny, P. Regiodivergent Glycosylations of 6-Deoxy-Erythronolide B and Oleandomycin-Derived Macrolactones Enabled by Chiral Acid Catalysis. *J. Am. Chem. Soc.* **2017**, *139* (25), 8570–8578. https://doi.org/10.1021/jacs.7b03198.
(36) Kimura, T.; Sekine, M.; Takahashi, D.; Toshima, K. Chiral Brønsted Acid Mediated Glycosylation with Recognition of Alcohol Chirality. *Angew. Chem. Int. Ed.* **2013**, *52* (46), 12131–12134. https://doi.org/10.1002/anie.201304830.
(37) Ghosh, A. K.; Cheng, X. Enantioselective Total Synthesis of (−)-Zampanolide, a Potent Microtubule-Stabilizing Agent. *Org. Lett.* **2011**, *13* (15), 4108–4111. https://doi.org/10.1021/ol201626h.
(38) Uenishi, J.; Iwamoto, T.; Tanaka, J. Total Synthesis of (−)-Zampanolide and Questionable Existence of (−)-Dactylolide as the Elusive Biosynthetic Precursor of (−)-Zampanolide in an Okinawan Sponge. *Org. Lett.* **2009**, *11* (15), 3262–3265. https://doi.org/10.1021/ol901167g.

(39) Hoffmann, S.; Seayad, A. M.; List, B. A Powerful Brønsted Acid Catalyst for the Organocatalytic Asymmetric Transfer Hydrogenation of Imines. *Angew. Chem.* **2005**, *117* (45), 7590–7593. https://doi.org/10.1002/ange.200503062.
(40) Demoret, R. M.; Baker, M. A.; Ohtawa, M.; Chen, S.; Lam, C. C.; Khom, S.; Roberto, M.; Forli, S.; Houk, K. N.; Shenvi, R. A. Synthetic, Mechanistic, and Biological Interrogation of *Ginkgo Biloba* Chemical Space En Route to (−)-Bilobalide. *J. Am. Chem. Soc.* **2020**, *142* (43), 18599–18618. https://doi.org/10.1021/jacs.0c08231.

Chapter 2

Experimental and Computational studies on Regiodivergent Chiral Phosphoric Acids Catalyzed Cycloisomerization of Mupirocin Methl Ester

(This chapter was partially published in: Wang, S.; Arguelles, A. J.; Tay, J.-H.; Hotta, M.; Zimmerman, P. M.; Nagorny, P. *Chem. Eur. J.* **2020**, 26, 4583)

2.1. Introduction

The three membered cyclic ethers, called epoxides or oxiranes, are of great importance in both man-made applications and biosynthesis of natural products (Figure 2.1A).[1] An almost endless number of naturally occurring epoxides with a wide range of interesting biological activities are found in nature, which has further increased the interest of epoxides to biologists, pharmacologists, and synthetic chemists.[2] Epoxides are highly strained heterocycles (Figure 2.1B). According to the Dastoori group work, the unsubstituted epoxide has the highest ring strain energy of 27.5 kcal/mol, followed by ethyl substituted and dimethyl substituted with 24.4 and 23.0 kcal/mol, respectively.[3] There is not much difference in a*nti* or *syn* substituted epoxide with about 22 kcal/mol. In comparison, the ring strain for cyclohexane is only 2.2 kcal/mol. Therefore, the high ring strain energy allows epoxide to be synthetic useful as a building block.

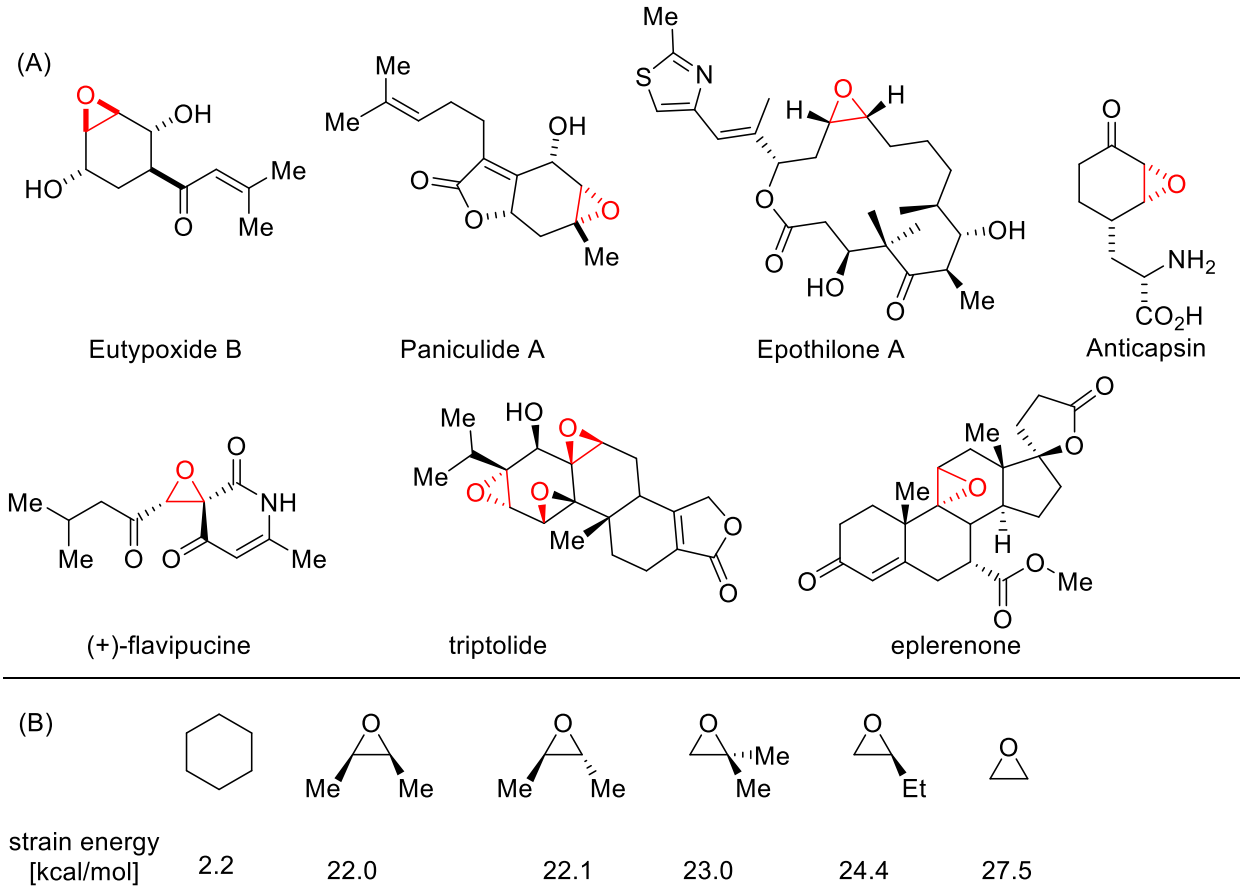

Figure 2.1 (A) Epoxides in natural products and drugs. (B) Ring strain energy for epoxides.

Because of the high strain energy, one of the most classic methods to open the epoxide ring is via S_N2 mechanism by a nucleophile (Figure 2.2). Some of the selected examples of nucleophile include dimethyl sulfoxide, lithium aluminum hydride, hydrogen halides, Grignard reagents, thiols, azides, amines, and even water.[2] Because of these easy, yet powerful, transformations, there have been multiple methods developed to obtained the enantiopure form by using asymmetric catalytic techniques such as the Sharpless asymmetric epoxidation of allylic alcohols,[4] the Jacobson epoxidation,[5] the Shi epoxidation[6] as well as a plethora of other methods.[2] These methods provide an efficient and straightforward route to synthesize various natural products, pharmaceutical compounds, and vaccines.

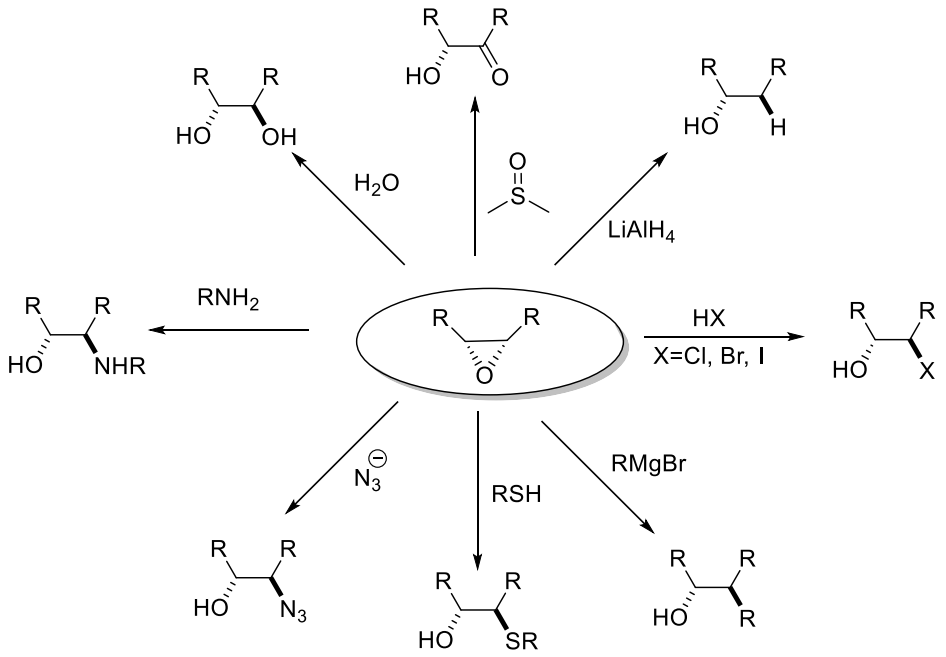

Figure 2.2 Applications of epoxides via ring openings by some selected nucleophiles.

Epoxide-based intermediates play an important role in the biosynthesis of various classes of natural products, and cyclic ether-containing natural products such as polyether ionophores, the annonaceous acetogenins and marine polyethers.[7] In 1983, Cane, Celmer and Westley proposed a unified stereochemical model of polyether antibiotic biogenesis that implied that such natural products are formed through the cascade cyclization of the epoxide-containing biosynthetic precursors.[8] Later, Nakanishi invoked the cascade cyclization of polyepoxide precursor in the biosynthesis of ladder polyether natural product brevetoxin B (Figure 2.3A).[9] Since then, epoxide intermediates became routinely proposed and observed in the biosynthesis of other cyclic ethers. It was known that enzymes are likely to play an important role in controlling the regioselectivity of these reactions. The factors affecting the regioselectivity of the epoxide opening are not well understood as such biosynthetic cascade reactions may often produce seemingly unfavored regioisomers. For instance, Oikawa group report that for the synthesis of lasalocid A, under the standard acidic conditions, 5-exo-cyclic product isolasalocid A is formed. However, when the

epoxide hydrolase Lsd19 is used, it promotes 6-endo-cyclization in the biosynthesis of natural lasalocid A (Figure 2.3B).[10]

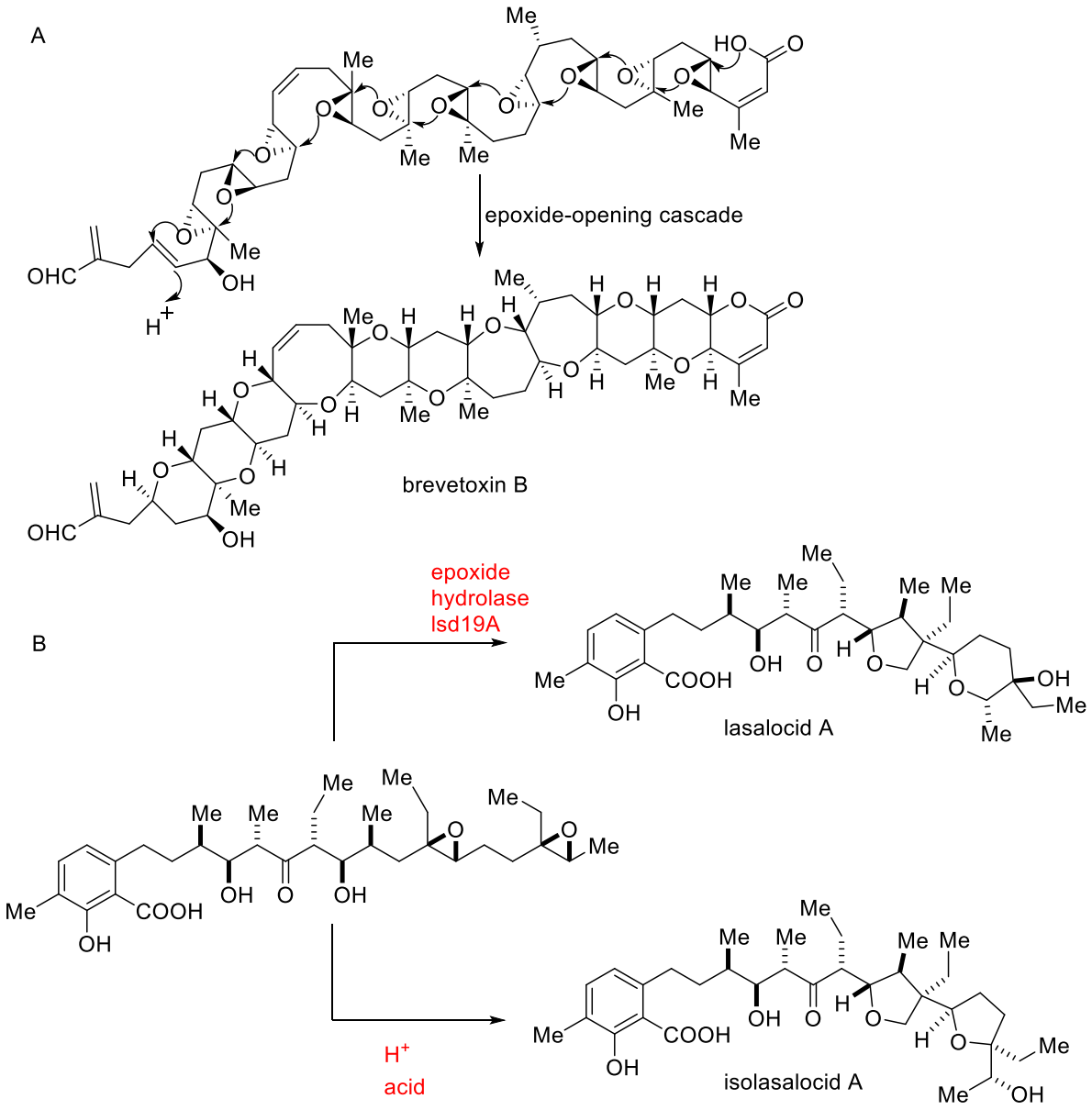

Figure 2.3 Biosynthetic epoxide cyclizations leading to the formation of cyclic ether containing natural products. A) Nakanishi's cascade hypothesis for the formation of brevetoxin A. B) Epoxide hydrolase Lsd 19-contrlled cyclization.

Inspired by the processes observed in nature, chemists extensively used epoxy alcohol cycloisomerizations to generate various cyclic ethers. However, one of the most common problems

associated with the intramolecular epoxide ring opening is achieving high levels of regiocontrol to control the regioselectivity in the formation of the *exo*- or *endo*- products, in particular tetrahydrofurans (THFs) and tetrahydropyrans (THPs). (**Scheme 2.1**). However, for such an approach to be a reliable strategy in the synthetic toolbox, effective ways to control the regioselectivity of the epoxide ring-opening (ERO) is mandatory. According to Baldwin's rules,[11] a set of empirical generalizations that help discern kinetically favored intramolecular cyclizations, the intramolecular *exo*-selective ERO reactions are preferred due to the easier-to-adopt spirocyclic transition state leading to the *exo*-product. Indeed, with only few exceptions, the majority of intramolecular ERO lead to the formation of 5-membered ring-containing products (*exo*-products) instead of the 6-membered rings (*endo*-products) (**Scheme 2.1**).[12] For this reason, methods that facilitate *endo*- control for intramolecular ERO are of high interest to synthetic chemists.

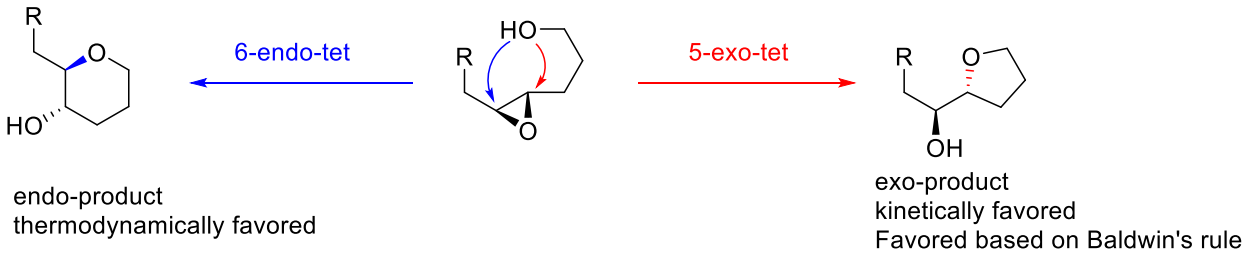

Scheme 2.1 Intramolecular ERO leading to endo- or exo-product.

Most of the strategies developed to control the regiochemistry of intramolecular EROs have relied on the use of directing groups covalently present in the substrates. A variety of modifications have been developed, including alkenyl,[13,14] alkynyl,[15] and silyl.[16] The majority of these methods justify their regioselectivity in electronic perturbations of the epoxide that stabilize the 6-*endo*-tet TS or disfavour the 5-*exo*-tet TS. For instance, the Nicolaou group,[14] pioneers of the regioselective ERO, used epoxy alcohols containing a simple ethyl substituent on the epoxide such as **2.1a**. They found that consistently with Baldwin's rules such epoxides undergo

regioselective 5-*exo*-tet cyclization leading to the tetrahydrofuran as the only observable product **2-1b**. However, when the substrate containing vinyl rather than ethyl substitution, such as **2-2a**, were subjected to acids, the selectivity of the cyclization was switched, and the *endo*-cyclization product **2-2b** was observed in such cases. The authors rationalized it by suggesting the formation of an allylic carbocation intermediate **2-2c**, which has a more electrophilic C5-position that preferably reacts leading to more thermodynamically stable 6-*endo*-tet product **2-2b** (**Scheme 2.2**). This seminal study by Nicolaou and co-workers suggests that a directing group might be used to override the inherent preference for the *exo*-cyclization mode and provide a less kinetically favored *endo*-product.

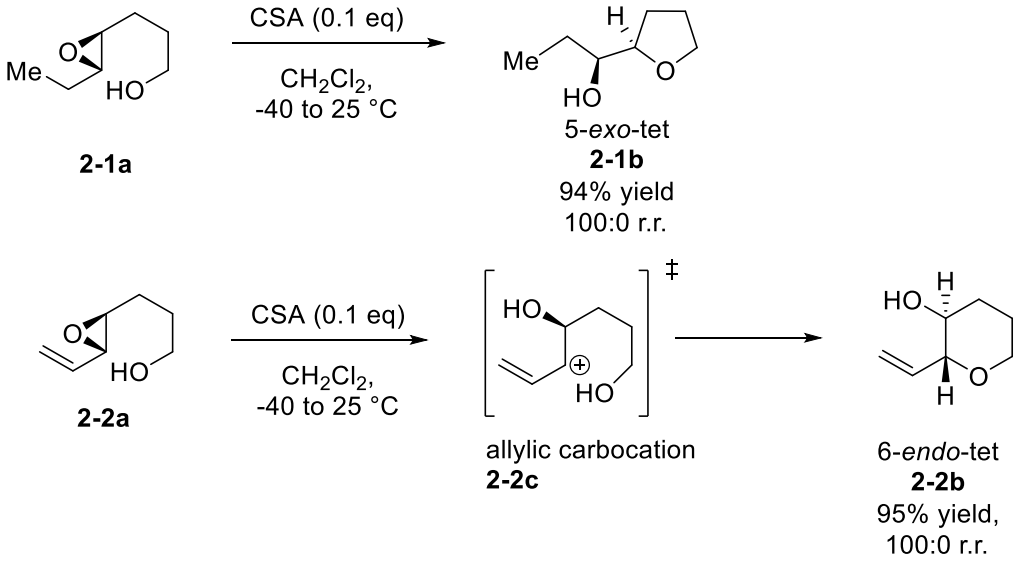

Scheme 2.2 Intramolecular ERO via alkenyl protecting group.

In line with this work, Schaumann and co-workers achieved a related stereoelectronic effect by using silyl-substituted epoxides **2.3a** that preferentially produce *endo*-product **2.3c** (Scheme **2.3**). They subsequently investigated the cyclization of silyl group-substituted epoxides and discovered that the relative configuration of the silyl-substituted epoxy alcohol is the determining for the outcome of the epoxide ring opening parameter.[16] When racemic epoxy

alcohol **2.3a** was tested, less kinetically favored 6-*endo*-product **2.3c** was obtained as the major product (56% yield), while more kinetically favored 5-*exo*-product **2.3b** was obtained as a minor product only (22% yield). These observations could be explained by proposing that the reaction with *syn*-**2.3a** proceeded through a favorable chair-like transition state. However, when anti-**2.3a** was used, a chair-like transition state could not be achieved, and instead the reaction proceeded through a less favored boat-like transition state that led to the 6-*endo*-cyclized product. Consequently, when *anti*-**2.3a** was tested, the mixture of epimeric 5-*exo*-tet were obtained. Based on these considerations, Schaumann and co-workers concluded that the configuration of the silyl-substituted epoxy alcohol could determine the regioselectivity of ERO.

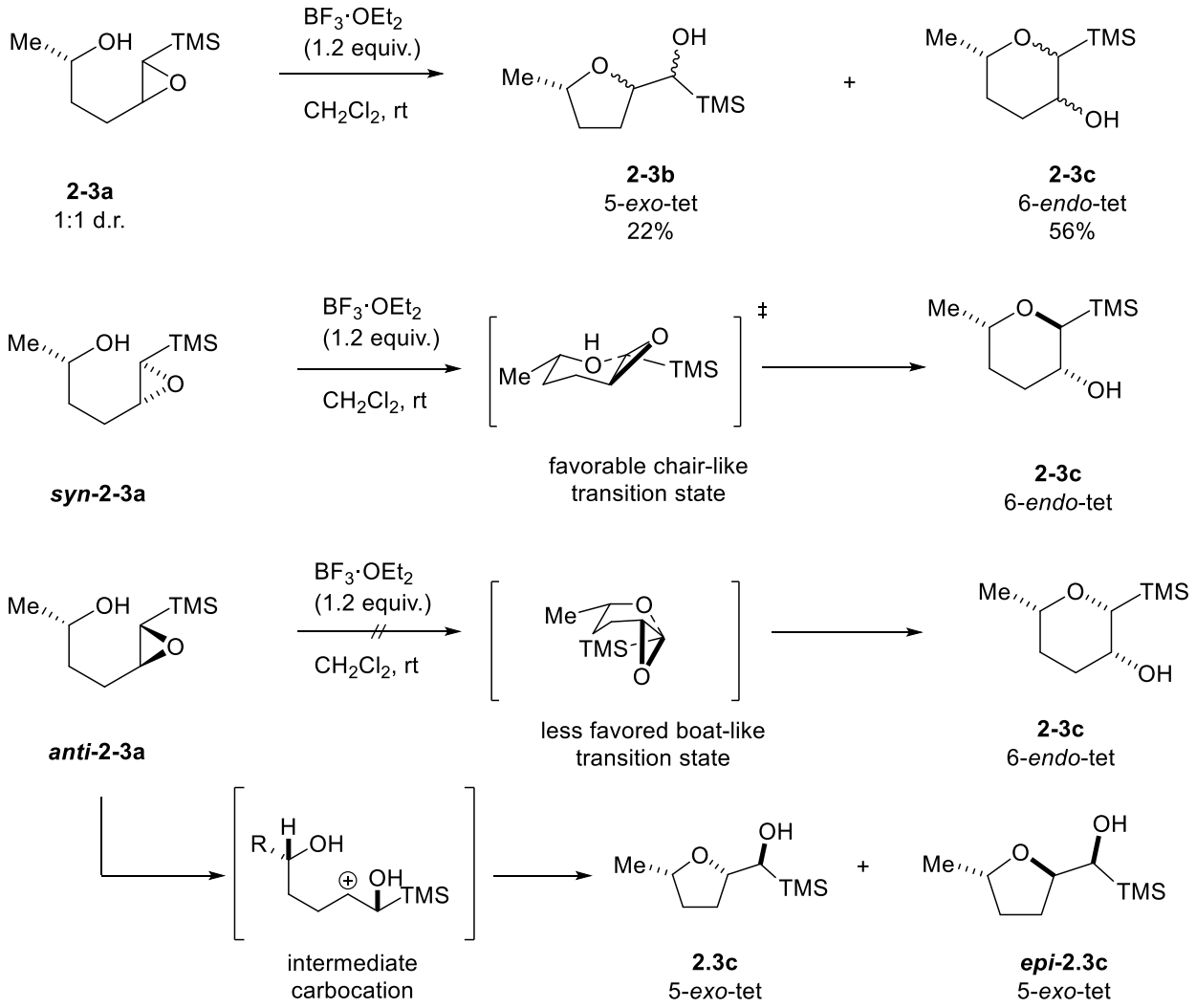

Scheme 2.3 Intramolecular ERO via configuration of silyl-substituted epoxy alcohols.

While the aforementioned strategies focused on modifying/adjusting the substrate, the ability to control the regioselectivity through the judicious selection of the reagents/reaction conditions for an unaltered substrate is by far more attractive. In search for such conditions, the Jamison group recently discovered an effective strategy that is based on the use of neutral water in combination with a preinstalled THP templates such as **2-4e** (Scheme 2.4) that results in the formation of poly-THP subunits.[17–21] In their initial optimization of reaction conditions, they observed that when epoxy alcohol **2-4a** was exposed to the strong basic conditions (Cs_2CO_3 in

methanol), the undesired *exo*-product **2-4c** was formed in 2.7:1 r.r. (entry 1). However, under either Lewis acidic or Brønsted acidic conditions, they were able to switch the regioselectivity and preferentially form *endo*-product **2-4b** (entries 2 and 3). Moreover, the authors discovered that these acidic aditives were not necessary as the cyclization also took place with neutral protic solvents, such as water, ethylene glycol and methanol, and **2-4b** was selectively formed with up to 10:1 r.r. (entry 4-6). These changes in regioselectivity due to the switch from basic to acidic conditions, and observation of the highest regioselectivities in neutral protic solvents, allowed Jamison and co-workers to hypothesize that the reaction medium acidity is critical for the ERO reaction selectivity. Therefore, a series of experiments focused on investigating the selectivity of ERO dependence on pH was carried out using various potassium phosphate buffers. These studies demonstrated that either high or low pH values led to poor regioselectivities (*cf.* Figure 2.4); and that the highest levels of selectivity for the endo-product **2-4b** (up to 10:1 r.r.) were observed in the pH range of 6-8.

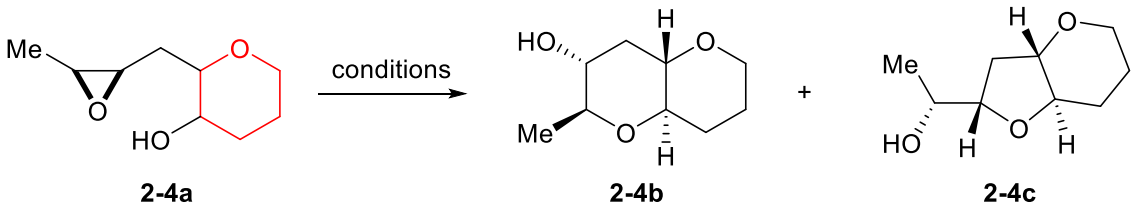

2-4a **2-4b** **2-4c**

entry	conditions	**2-4b**	:	**2-4c**
1	Cs_2CO_3, MeOH	1	:	2.7
2	BF_3•OEt_2, CH_2Cl_2	1.4	:	1
3	AcOH, PhMe	1.6	:	1
4	H_2O	>10	:	1
5	Ethylene glycol	9	:	1
6	MeOH	8	:	1

Scheme 2.4 Intramolecular ERO via various reaction conditions.

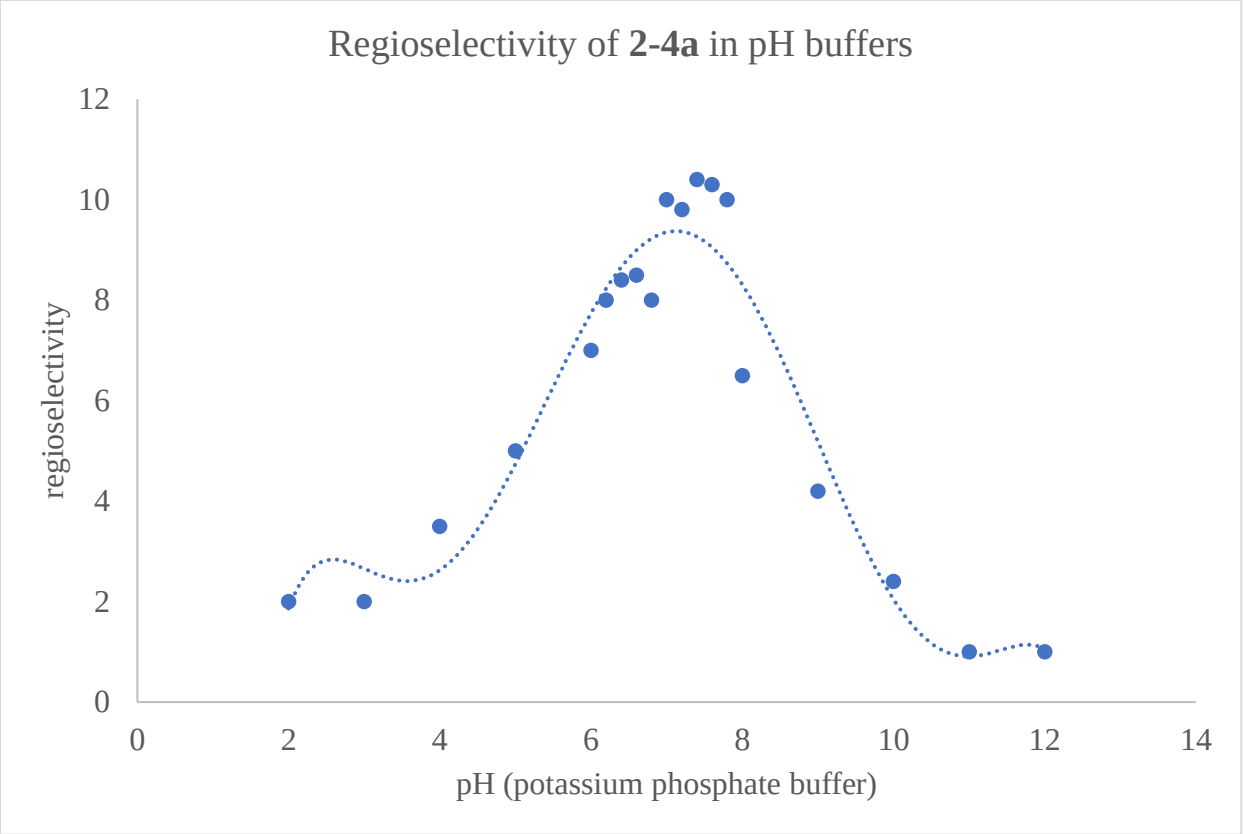

Figure 2.4 Regioselectivity of the ERO at various pH.

Following these inspiring results, they conducted several studies to reveal the potential of *endo*-selective ERO in water (Figure 2.5). The initial studies by the Jamison group suggested that using simple epoxide substrates such as compound **2-5a** would lead to preferential cyclization to the *exo*-product **2-5c** (86% yield), and the endo-product **2-5e** was formed in only 14% yield. In this situation, the authors proposed that the spiro transition state **2-5b** is more entropically favored than the fused transition state **2-5d**, leading to *exo*-product **2-5c**. However, if the structure of the starting epoxide is altered and the THP-containing material **2-5f** is used instead, a different regioisomer distribution is observed. In this situation, the impacts of the entropic factor on the transition state energy were minimized, while the enthalpic factor dominated in the transition state due to lesser ring strain. Therefore, the trans-6,5-spiro transition state **2-5g** was unfavored, while

the trans-6,6-fused transition state **2-5i** was preferred, leading to the *endo*-cyclization product **2-5j** in greater than 90% yield. Moreover, the Jamison group also found that in the less polar solvents (i.e. polar aprotic solvents) the selectivity of **2-5j** to **2-5h** is less than 3:1; however, in the protic solvents, such as water buffered to pH=7, they could observe *endo*-selectivities up to 11:1. These observations suggest that the formation of hydrogen bonds with epoxide is crucial to stabilizing the transition state **2-5i** leading to the endo-product **2-5j**.

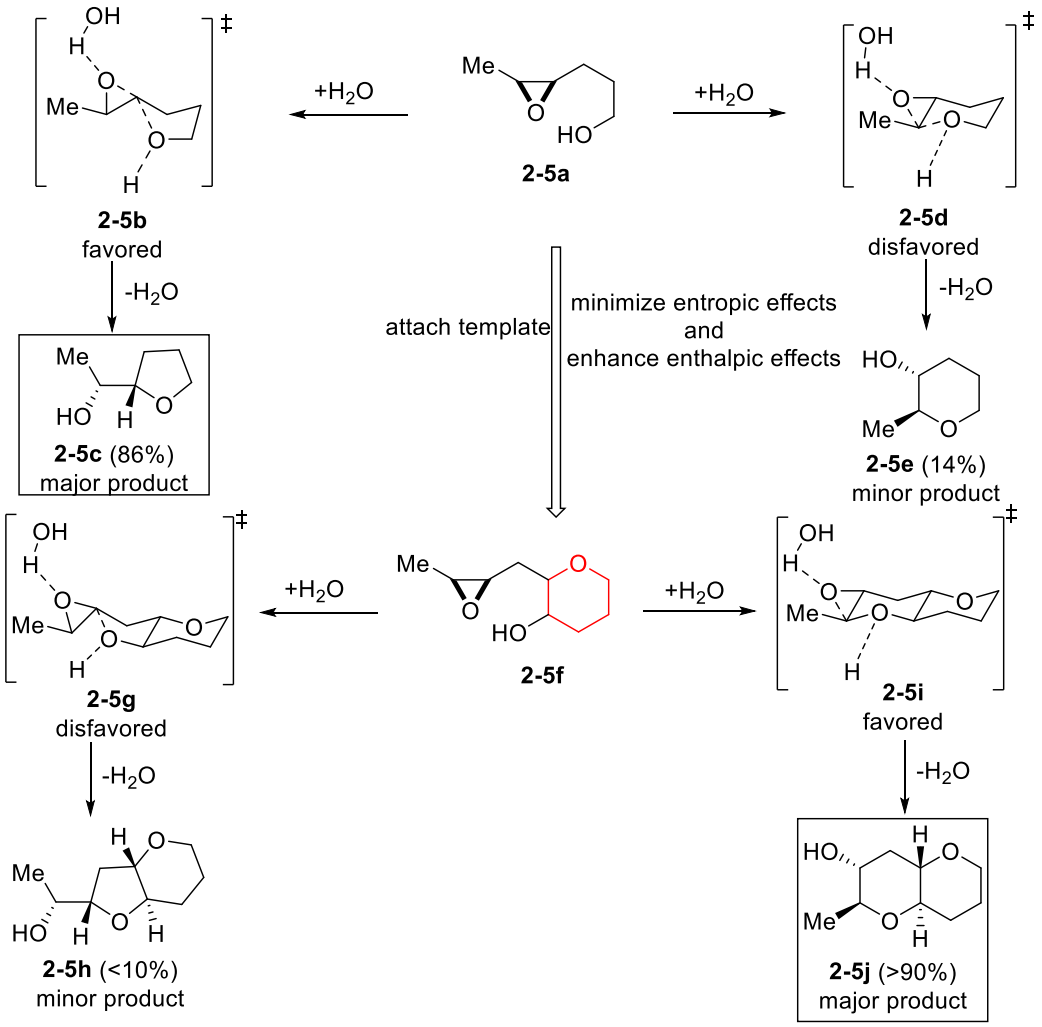

Figure 2.5 Regioselectivity of ERO via hydrogen bond and THP template.

With these developed methods and understanding of mechanisms, the Jamison group conducted cascade ERO via water to form polycyclic ethers **2-6b** and **2-6d** (Scheme 2.5).[21] The

chiral poly-epoxide precursors **2-6a** and **2-6c** were synthesized via Shi epoxidation.[6] Subsequently, these epoxides were subjected to aqueous medium to promote ERO resulting in the selective formation of **2-6b** and **2-6d**. Their method is highly attractive because it was the very first example mimicking enzymatic route for the cascade ERO formation of brevotoxin shown in Scheme 2.1A.

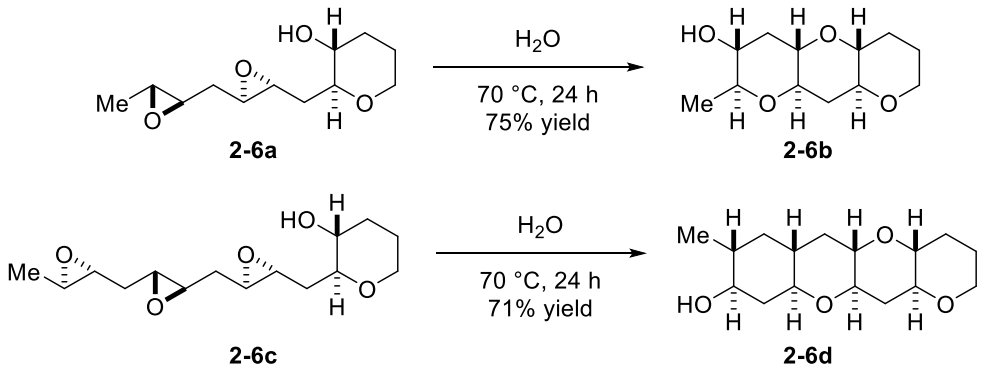

Scheme 2.5 Regioselectivity of ERO via hydrogen bond and THP template

These substrate- or medium-controlled strategies offered a breakthrough in the ability to divert the course of the intramolecular ERO. However, the use of the covalently linked directing groups as the sole source of regiocontrol has some evident drawbacks. For instance, the most obvious one is that these methods are restricted in scope and tend to lack generality. In order to achieve tetrahydropyran-selective cascades, every epoxide moiety presented in substrate would require a directing group, which could be synthetically challenging.[21] Yet, ERO reaction is of great importance towards synthesis of natural products.

Towards their synthesis of α-tocopherol, commonly known as vitamin E, the Woggon group was able to achieve the *anti*-Baldwin's rule of ERO via using acid (Scheme 2.6).[22] They observed that when no acid was added, the ERO of **2-6a** primarily produced Baldwin's rule favored *exo*-product **2-6b** (entry 1); however, after the acidic additive was introduced, the amounts of produced *endo*-product **2-6c** significantly increased, and 1:1 mixture of products was obtained

(entry 2). Further optimization of the solvent provided no significant improvement in regioselectivity (entries 3-5). However, increasing the concentration of HCl in acetonitrile resulted in slight improvement in the selectivity (~2:1 r.r., entries 6-7), and theother acids were infereior to HCl in terms of promoting the formation of **2-6c** (entries 8-10). Further optimization of the HCl-promoted cyclization resulted in **2-6c** formed in 3.3:1 r.r. (entry 12). With this key intermediate core-structure obtained, the authors were able to complete the synthesis of α-tocopherol in 4 more steps. However, one of the significant drawbacks in their synthesis was the ERO step, as the low selectivity resulted in the 23% of the undesired product **2-6b**.

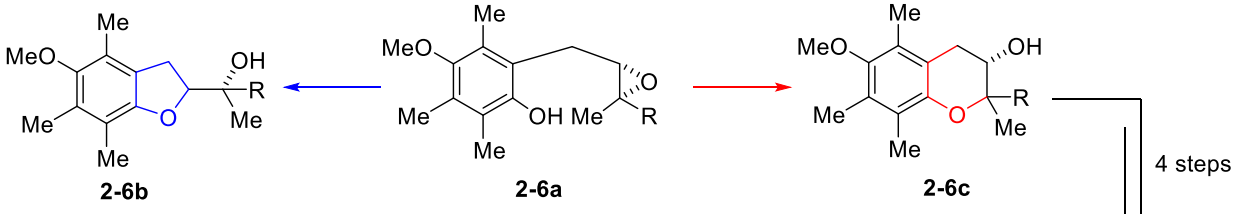

entry	acid	solvent	conv (%)	**2-6b** : **2-6c**
1	none	MeOH	99	98 : 2
2	1 N HCl_{aq}	MeCN	94	51 : 49
3	1 N HCl_{aq}	THF	90	67 : 33
4	1 N HCl_{aq}	MeOH	92	56 : 44
5	1 N HCl_{aq}	acetone	92	58 : 42
6	6 N HCl_{aq}	MeCN	92	35 : 65
7	12 N HCl_{aq}	MeCN	94	37 : 67
8	TFA (20 mol%)	MeCN:H_2O (3:1)	99	49 : 51
9	(+)-CSA (1 equiv)	MeCN:H_2O (3:1)	99	47 : 53
10	(+)-CSA (1 equiv)	MeCN	99	40 : 60
11	2 M HCl_{MeOH}	MeOH	98	62 : 38
12	2 M HCl_{ether}	MeCN	98	23 : 77

Scheme 2.6 Application of ERO towards total synthesis of α-tocopherol.

Following the studies above, the Li group was able to achieve regiodivergent synthesis of natural products (+)-corinandrone A and B by controlling the acidity of the medium for the ERO reactions (Scheme 2.7).[23] One of the key intermediates in this synthesis was epoxide **2-7a** that was synthesized asymmetrically using the Shi epoxidation. Using epoxide **2-7a** was obtained, the

authors could regiodivergently form *exo*-product **2-7b** using basic buffer condition or *endo*-product **2-7c** under acidic condition. These ERO-products would allow them access final (+)-corinandrone A and B in six steps to finish the total synthesis. Similarly, many others studies, including the ones by Coster[24] and the Kimachi[25] have utilized ERO for the synthesis of natural products.

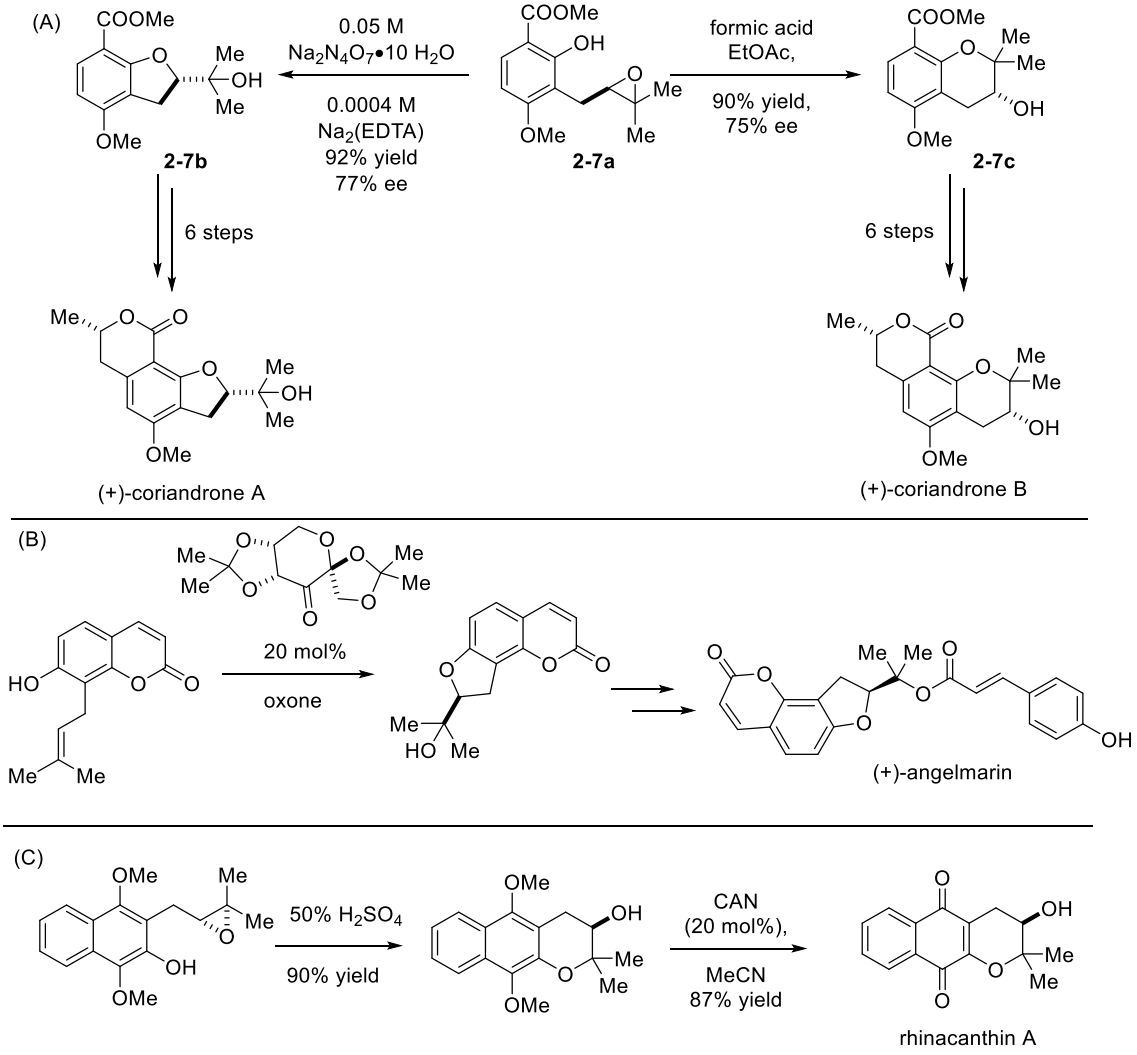

Scheme 2.7 Application of ERO towards total synthesis of (A) Li, (B) Coster, (C) Kimachi.

In view of the recent successes in chiral catalyst-controlled selective functionalization of natural products (*cf.* Chapter 1), chiral catalyst-controlled regioselective intramolecular ERO could

provide a more robust method that is applicable to a variety of substrates. Our group has a long-standing interest in the application of chiral phosphoric acids (CPAs) to control regio- and stereoselective functionalization of natural products.[26–30] In our recent efforts, we demonstrated that CPAs could mimic enzymatic processes and control the regioselectivity and/or stereoselectivity of acetalization,[31] spiroketalization,[32] and glycosylation[33] reactions. Inspired by the *endo*- regiocontrol exhibited by the epoxide hydrolase Lsd19 that catalyzes the selective formation of lasalocid A rather than its kinetically-favored regioisomer isolacid A (cf. Figure 1B),

We sought to investigate the possibility of controlling the formation of *exo*- and *endo*-products through the CPA catalysis. Our group is particularly interested in utilizing CPAs as the catalysts that mimic enzymatic function and control the selective transformations of complex substrates or natural products. As an encouraging precedent, both the Sun[34] and the List[35] groups independently demonstrated the usefulness of CPAs **2-8A** and **2-8B** in the desymmetrizative intermolecular ERO of meso-epoxide **2-8a** with thiols and carboxylic acids as the nucleophiles, respectively (**Scheme 2.8**). They hypothesized that the epoxide was activated by Brönsted acid moiety imbedded in CPAs, while the nucleophile, likely to be in its tautomer form, was activated by the phosphoryl oxygen. Both of these activations were accomplished via hydrogen bonds (Scheme 2.8A). Moreover, the desymmetrization of epoxide was achieved through a pathway that has minimized steric repulsions between the epoxide and CPAs via transition state **2-8c**. Conversely, an alternatively oriented transition state **2-8d** is less favored because of the strong steric repulsions between the epoxide and CPA. Similarly, List and co-workers also reported a similar study of desymmetrizative benzoylation of epoxide **2-8a** using catalyst **2-8B**, in as high as 86% yield and 93% ee (Scheme 2.8B). While these prior results provide the strong foundation for

our subsequent studies on using CPAs to control the regioselectivity of ERO, no applications of the CPAs for controlling the regioselectivity of the epoxide opening have been reported to date.

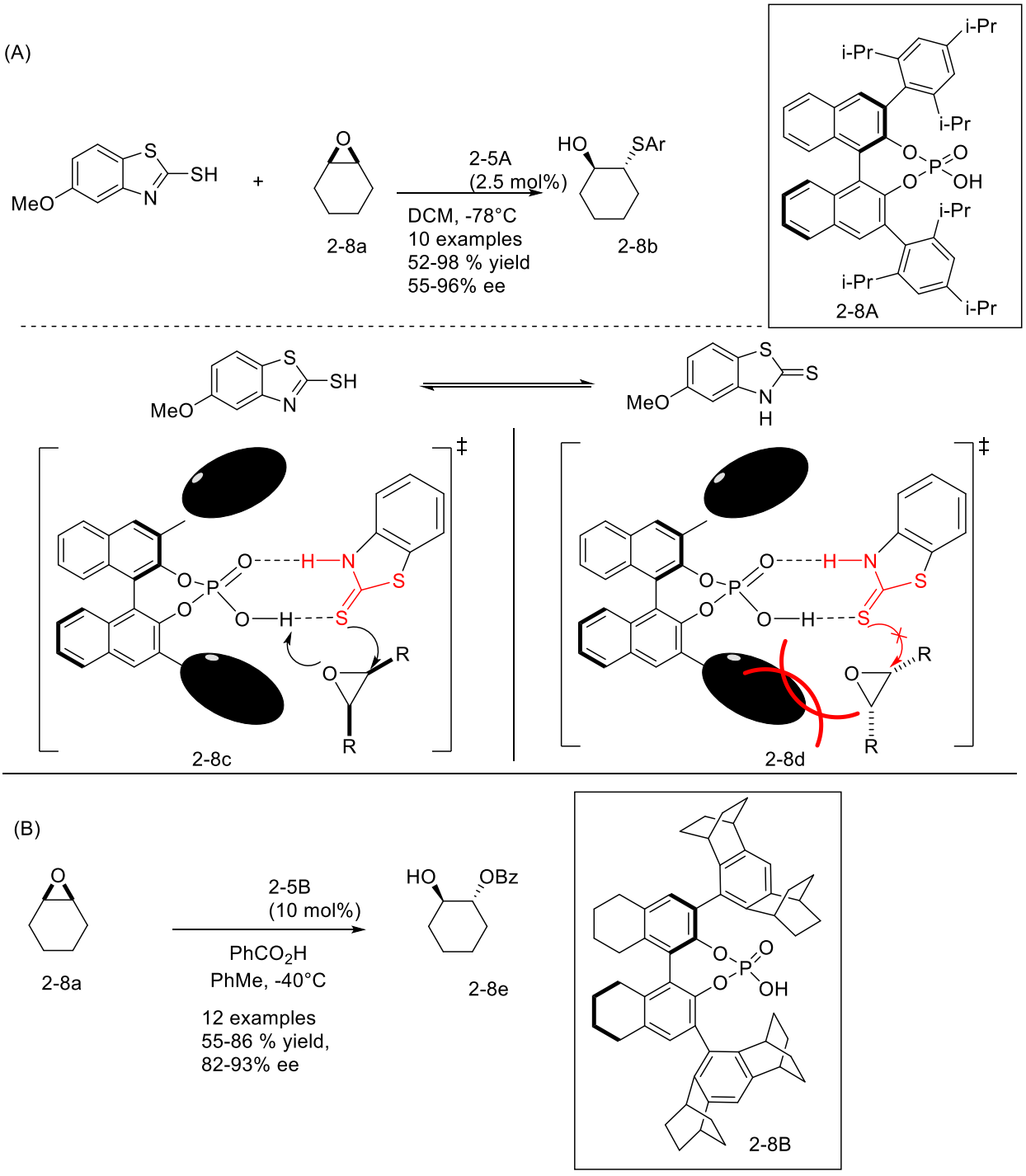

Scheme 2.8 Examples of CPA-catalyzed epoxide desymmetrization by (A) J. Sun and (B) B. List.

This chapter describes the development and studies of CPA-controlled *endo*- and *exo*-selective cyclization of antibiotic mupirocin methyl ester, leading to the selective formation of either THP or THF-containing derivatives. To the best of our knowledge, this is the first example of a strategy that achieves regiocontrol by using the chiral catalysts rather than achiral reagents or enzymes. The mechanisms of these transformations were investigated using a combination of experimental techniques as well as computational methods based on the single-ended growing string (SE-GSM), a quantum chemical tool developed by the Zimmerman group and explored by Dr. Alonso Arguelles.[36] These mechanistic studies provide a description of the potential energy surface and suggest a concerted and highly synchronous mechanism for the formation of both the *exo*- and *endo*-products.

2.2. Results and Discussion

Inspired by the Nagorny group's work on CPA catalyzed glycosylation of different hydroxyl groups on 6-dEB, Dr. Tay Rosenthal investigated the possibility of accomplishing a CPA-controlled site-selective glycosylation of the antibiotic mupirocin methyl ester (*cf.* Scheme 2.9). During these studies, he observed that instead of achieving direct glycosylation, the reaction proceeded through an intramolecular epoxide cyclization followed by glycosylation to produce compounds **2-9b** and **2-9c** (Scheme 2.9). This result was counterintuitive as the *endo*-product **2-9b** was formed as the major regioisomer in 83% yield. Moreover, the control study using diphenyl hydrogenphosphate demonstrated that with this achiral catalyst, the reaction was not selective and a complex mixture of both the *endo*- and *exo*-cyclization product glycosides was formed. Therefore, we proposed that (*R*)-TRIP has altered the course of ERO, and that the *endo*-product **2-9d** underwent glycosylation to get observed product **2-9b**. To test the hypothesis that CPAs could

be used to control the regioselectivity of the intramolecular cyclization of muprocin methyl ester, we have undertaken the studies described in this chapter.[37]

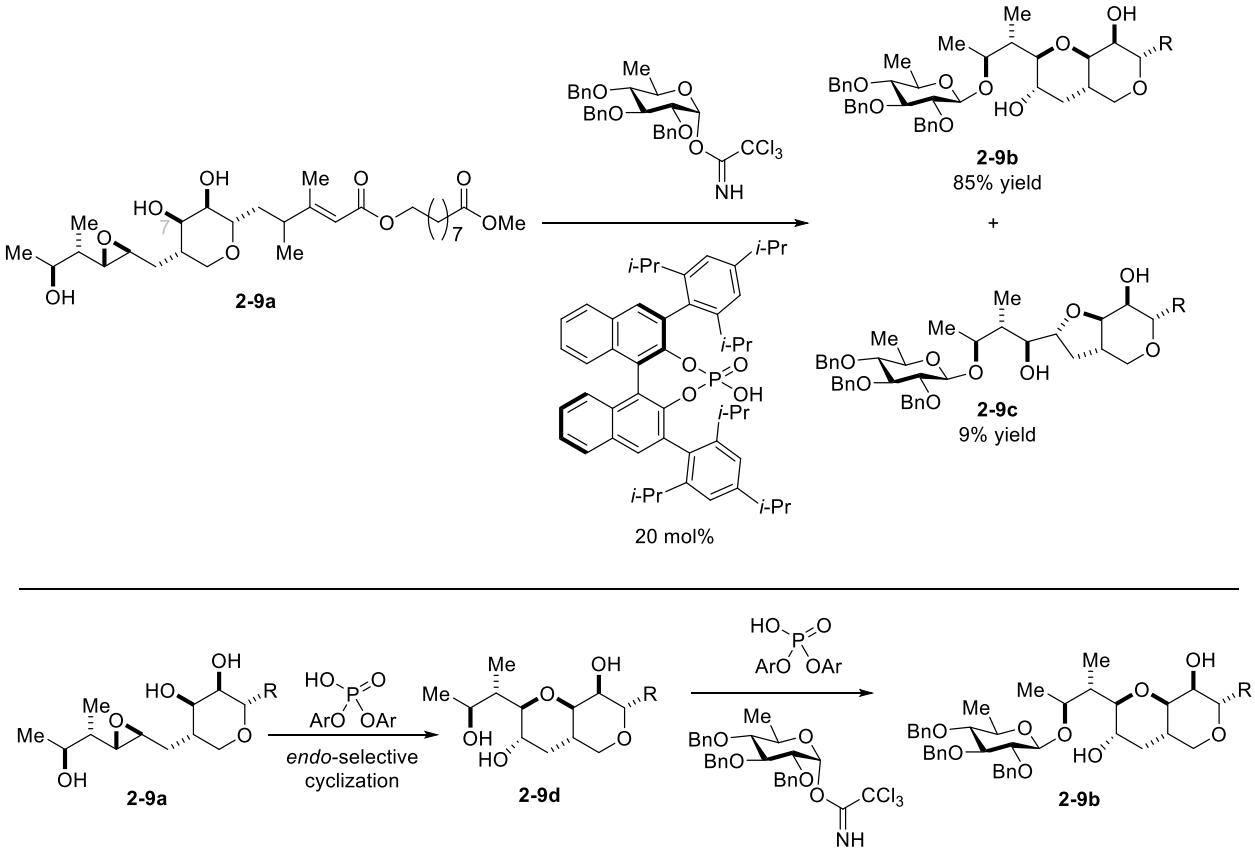

Scheme 2.9 Previous studies of CPA catalyzed glycosylation of 2-9a by Dr. Tay Rosental (Nagorny group).

While Dr. Rosenthal has obtained encouraging preliminary results for the *endo*-selective cyclization with (*R*)-TRIP as the catalyst, it was not clear if such selectivity is not achievable with other achiral reagents or conditions. Therefore, a series of control experiments to investigate the inherent reactivity of mupirocin methyl ester were carried (*cf.* Table 2.1). These control experiments indicated that the use of acidic, neutral, and basic conditions that have been previously reported in literature,[12,38–41] resulted in either poor conversion or the unselective formation of both the *endo*- and *exo*-products (**2-10b** and **2-10c**, Table 2.1). While the use of LiCl as the Lewis acid,

did not result in successful cyclization (entry 1), $ZnCl_2$ and $Sc(OTf)_3$ catalyzed the unselective formation of **2-10b** and **2-10c** (entries 2 and 3). Interestingly, using Jamison's method of suspending **2-10a** in deionized water underwent slow cyclization in the course of 4 days and provided 71:29 mixture of **2-10b** and **2-10c** in 24% conversion (entry 4). The reaction rate could be significantly improved if pH=7 phosphate buffer is used instead (entry 5); however, this reaction proceeded with no selectivity and produced an equimolar mixture of **2-10b** and **2-10c**. The use of more basic conditions did not produce the desired cyclization products (entries 6 and 7). However, using catalytic amounts of the acidic phosphoric acid (p-NO_2-$C_6H_4O)_2PO_2H$, resulted in complete conversion of mupirocin methyl ester **2-10a**, and low levels of *endo*-selectivity were observed (entry 8). This suggests that, contrary to what might be expected by Baldwin's rules, phosphoric acid catalysis has small inherent endo-selectivity for the intramolecular ERO of mupirocin methyl ester, but high selectivity for either **2-10b** and **2-10c** is unlikely to achieve using achiral catalysts or conditions.

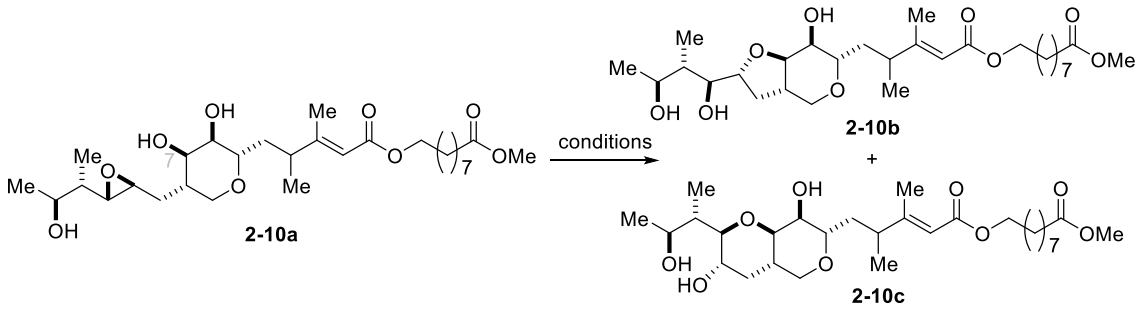

entry	catalyst	Solvent	Time	Conv. [%]	**2-10b:2-10c**[b]
1[c]	LiCl	DCM	o/n	<5	-
2[c]	ZnCl2	DCM	o/n	82	52:48
3[c]	$Sc(OTf)_3$	DCM	o/n	77	43:57
4[d]	-	H_2O	4d	24	29:71
5	KH_2O_4 buffer (7 pH)	H_2O	4d	>98	52:48
6[e]	Cs_2CO_3	MeOH	4d	nr	-
7[f]	LiHMDS	THF	4d	nr	-
8[g]	$(p\text{-}NO_2\text{-}C_6H_4O)PO_2H$	DCM	5d	>98	30:70

[a] Conditions: 14 (0.02 mmol), catalyst (20 mol%), CH_2Cl_2 (0.01 M); [b]Determined by RP-HPLC; [c]Conditions: catalyst (20 mol%), CH_2Cl_2 (0.2 M); [d] 70 ºC; [e] Cs_2CO_3 (10 equiv), CH_2Cl_2 (0.02 M); [f] LiHMDS (3 equiv), CH_2Cl_2 (0.01 M); [g] catalyst (20 mol%), CH_2Cl_2 (0.2 M).

Table 2.1 Initial control experiments on the intramolecular ERO of 1.[a]

To further demonstrate the potential of CPAs in controlling the regioselectivity of the mupirocin methyl ester cyclization, we focused on developing both regiodivergent pathways leading to the formation of the *endo*-and *exo*-products **2-10b** and **2-10c**. Following these control studies, we then investigated if the use of CPAs could further enhance the formation of **2-10c** or even revert the observed trend and favour the *exo*-product **2-10b**. To this end, we screened several BINOL-derived CPAs (Table 2.2). We selected methylene chloride dried with 4 Å MS as the starting solvent due to its excellent solvating properties and good compatibility with phosphoric acid catalysis. Subsequently, we evaluated an array of BINOL- based CPAs. Encouragingly, we found that the axial chirality of the BINOL backbone had a significant impact on the regioselectivity of this transformation, with (*R*)-CPAs consistently favoring *endo*-product **2-10c** formation more than the (*S*)-enantiomers (entries 1-12). While CPAs bearing 3,5-substituted aryl groups at the 3,3'-positions of the BINOL scaffold were not effective (catalysts **2-1A** to **2-1D**,

entries 1-8), the 2,4,6-substituted CPAs such as (*R*)-TRIP (**2-1D**) and (*R*)-TCYP (**2-1D**) were found to be superior catalysts for the formation of *endo*-product **2-10c** (entries 6-10). As before, the (*S*)-enantiomers of **2-1D** and **2-1D** did not provide good selectivities and were not further investigated (entries 7 and 9). Those results supported our initial hypothesis that the chiral of CPA has critical influence on regioselectivity of ERO and the outcome of the regioselectivity could be further controlled via the steric impacts on the 3,3'-positions in CPAs. Even with the more steric hindered substituents at the 3,3'-position, regioselectivity could not improve further using catalyst **2-1F** and **2-1G** (entries 11-13). Similarly, the use of more acidic *N*-triflyl phosphoramide **2-2B** and sulfonamides **2-3B** and **2-3D** did not result in a selective reaction, and no further attempts to investigate this class of Brönsted acids was pursued (entries 14-18).

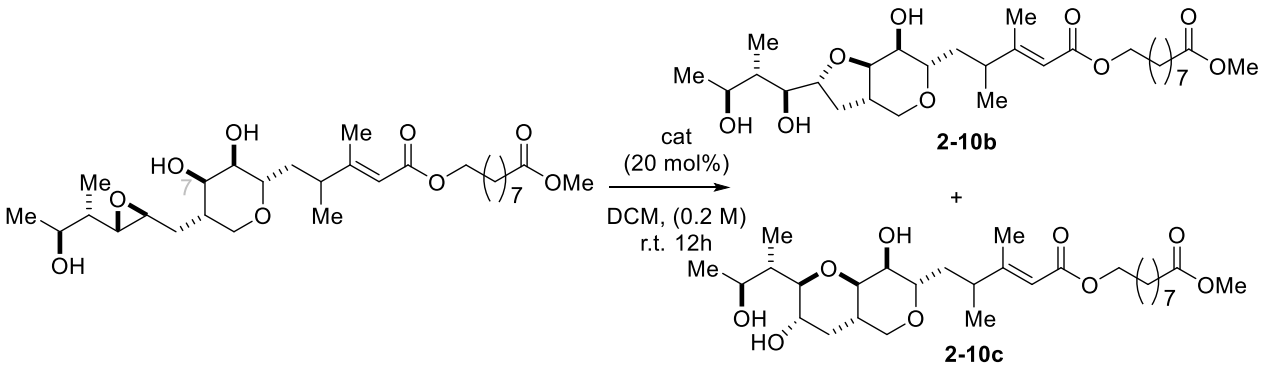

entry	catalyst	conversion (%)	**2-10b:2-10c**[b]
1	**(S)-2-1A**	>98	34:66
2	**(R)-2-1A**	>98	26:74
3	**(S)-2-1B**	95	38:62
4	**(R)-2-1B**	>98	20:80
5	**(S)-2-1C**	>98	34:66
6	**(R)-2-1C**	>98	27:73
7	**(S)-2-1D**	>98	43:57
8	**(R)-2-1D**	>98	7:93
9	**(S)-2-1E**	>98	55:45
10	**(R)-2-1E**	>98	6:94
11	**(S)-2-1F**	>98	45:55
12	**(R)-2-1F**	>98	23:77
13	**(S)-2-1G**	>98	43:57
14	**(S)-2-2C**	>98	28:72
15	**(S)-2-2D**	97	52:48
16	**(R)-2-3C**	>98	45:55
17	**(S)-2-4B**	90	40:60
18	**(R)-2-4B**	>98	43:57

a conditions: 1 (0.02 mmol), 4Å MS
b Determined by RP-HPLC.

Table 2.2 Catalyst screening for the optimization of endo-product 2-10c.

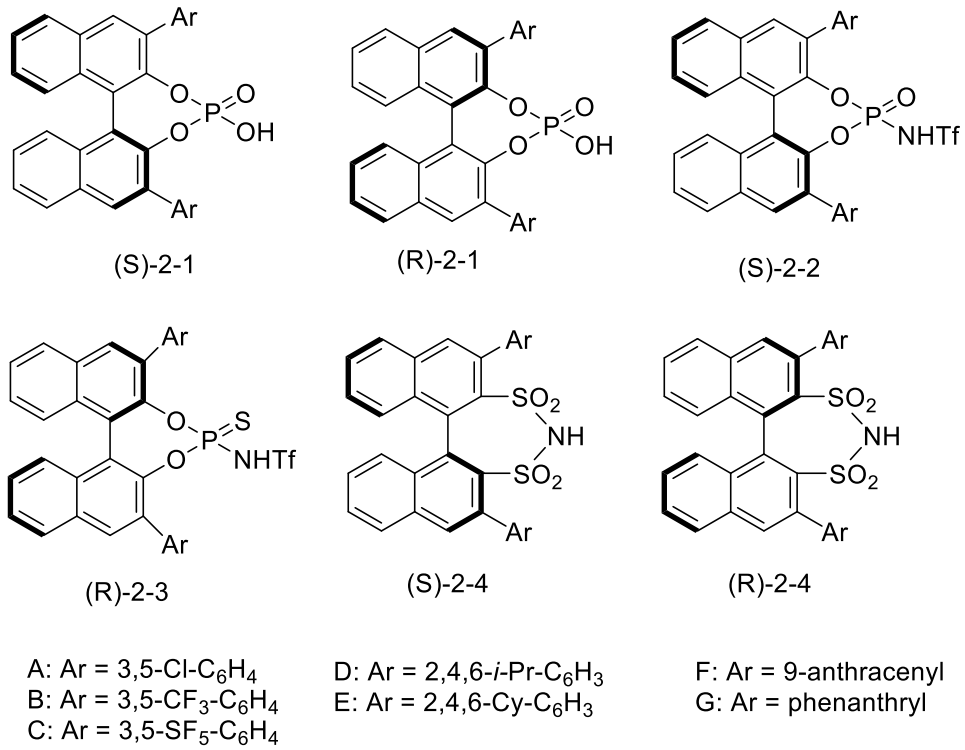

Figure 2.6 Catalyst screening for the optimization of *endo*-product 2-10c.

Based on these results, catalyst **(*R*)-2-1E** was selected and the reaction conditions were further optimized (**Table 2.3**). Initially, 4 Å molecular seives was added to the reaction media, and it was found to have no impact on regioselectivity, as the same selectivity was observed (entries 1 and 2). When the non-polar non-coordinating solvents such as hexanes and cyclohexane were used (entries 3 and 4), the conversion could be reduced dramatically due to the solubility of catalysts. Therefore, when increasing the polarity of solvent, such as ether and tetrahydrofuran, the reaction rate increased, even though lower regioselectivity was still observed (entries 5 and 6). Other solvents, such as ethyl acetate, chloroform, and acetonitrile were tested out and no improvement of regioselectivity was observed (entries 7-9) Eventually, toluene was identified as the solvent of choice in the absence of 4 Å MS (entries 10) as the use of this solvent resulted in high *endo*-product selectivity (95:5 rr). Our attempts to further optimize the solvent by using trifluorotoluene did not

lead to increase of regioselectivity (entry 11). Therefore, the optimum solvent for the subsequent experiments focused on optimizing the formation of the *endo*-product was toluene.

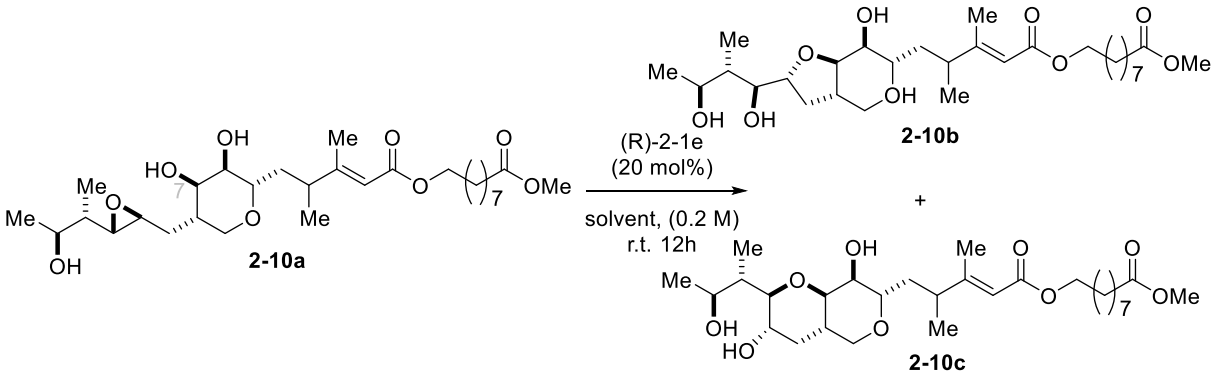

entry	solvent	conversion (%)	**2-10b:2-10c**[b]
1[c]	Dichloromethane	>98	6:94
2	Dichloromethane	>98	6:94
3	Cyclohexane	33	12:88
4	Hexane	47	15:85
5	Ether	81	12:88
6	Tetrahydrofuran	86	11:89
7	Ethyl acetate	>98	8:92
8	Chloroform	>98	8:92
9	Acetonitrile	94	15:85
10	**Toluene**	**>98**	**5:92**
11	Trifluorotoluene	>98	8:95

a conditions: 1 (0.02 mmol),
b Determined by NMR
c 4Å MS were used

Table 2.3 Solvent screening for the optimization of *endo*-product 2-10c.

After identifying the most optimal catalyst and solvent, we subsequently investigated the possibility of reducing the catalyst loading while still maintaining high regioselectivity (**Table 2.4**). We observed no depletion of regioselectivity and reactivity after decreasing the catalyst loading from 20 mol% to 10 mol%, and then to 5 mol% (entries 1-3). However, with the further decrease of the catalyst loading, we started observing the loss of reactivity and the conversion dropped to 44% when 2.5 mol% of catalyst was used, even though the regioselectivity was not dramatically

decreased (entry 4, 94:6 rr). The further decrease of the catalyst loading to 1 mol% resulted in even lower conversion and selectivity (33%, 93:7 rr, entry 5), and running the cyclization for 120 h instead of 1 h was required to achieve synthetically useful conversion and selectivity (92%, 95:5 rr, entry 6). In line with these observations, using 0.5 mol% of the catalyst resulted in significantly lower conversion even after running the cyclization for 120 h (51%, 94:6 rr, entry 7). Finally, in order to evaluate the possibility of non-linear effects, the reaction with 100 mol% of the catalyst was performed (entry 8). This transformation proceeded with full conversion and selectivity and resulted in 97:3 ratio of **2-10c:2-10b**. These observations suggested that our optimum catalyst loading was 5 mol%. We were capable of running this reaction on a larger reaction scale (0.20 mmol) with minimal impact on the regioselectivity (entry 3).

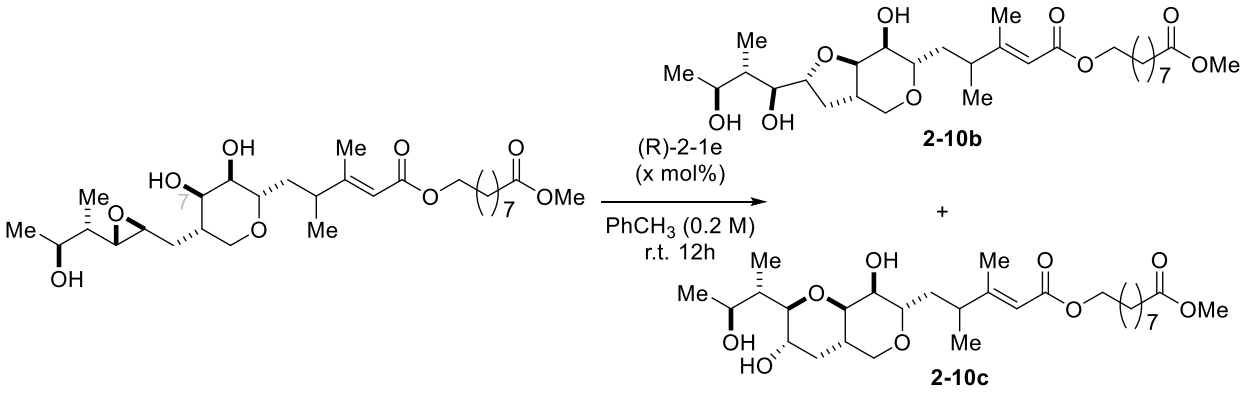

entry	cat. loading (mol%)	t (h)	conversion (%)	**2-10b:2-10c**[b]
1	20	12	>98	5:95
2	10	12	>98	5:95
3[c]	5	12	97	5:95
4	2.5	12	44	6:94
5	1	12	32	7:93
6	1	120	92	5:95
7	0.5	120	51	6:94
8	100	12	>98	3:97

a conditions: 1 (0.02 mmol),
b determined by NMR
c reaction was run in 0.2 mmol scale.

Table 2.4 Catalyst loading screening for the optimization of *endo*-product 2-10c.

Having been successful in identifying the catalyst and conditions for the highly selective and efficient formation of the *endo*-product **2-10c**, we surmised that this selectivity could be overturned to favor the *exo*-product **2-10b** through the judicious choice of a CPA. We hypothesized that (*S*)-chirality based CPAs would give better *exo*-selectivity (Table 2.5). Initially, (*S*)-CPAs with different substituents at the 3,3'-positions were studied. When increasing the bulkiness of the substituents at the meta-positions of the 3,3'-aryl group from Cl to CF_3 to SF_5 groups, there were no significant improvements of regioselectivity (entries 1, 2, 3, compared to Table 2.1 entry 8). Therefore, we decided not to continue with the evaluation of the meta-substituted aryl groups at the 3,3'-position, and instead focused on exploring other types of substitution patterns. Thus, when catalyst (*S*)-**2-1D** with isopropyl group at *ortho*- and *para*-position of the phenyl ring was tested, we observed improvement in the *exo*-selectivity (entry 4, 43:57 rr). However, its more acidic *N*-triflyl phosphoramide analog, (*S*)-**2-2D,** provided worse regioselectivity (entry 9, 52:48 rr). Further examining of larger cyclohexyl substituents at the *para*- and *ortho*-positions did not lead to a higher selectivity (entry 5, 55:45 rr). Therefore, changing different substituents at the *para*- and *ortho*-positions was ineffective for improving the *endo*-selective formation of **2-10b**. Moreover, (*S*)-CPAs with either 9-anthrancenyl or phenanthryl substituents at the 3,3'-positions also failed to yield a higher selectivity for the formation of **2-10b** (entries 6 and 7). At the same time, it was evident that 3,3'-diarylsubstituted BINOL-based CPAs (*cf.* Table 2.2) did not significantly increase the *exo*-product selectivity, and other subtypes of CPAs or organic acids were evaluated in our subsequent screens.

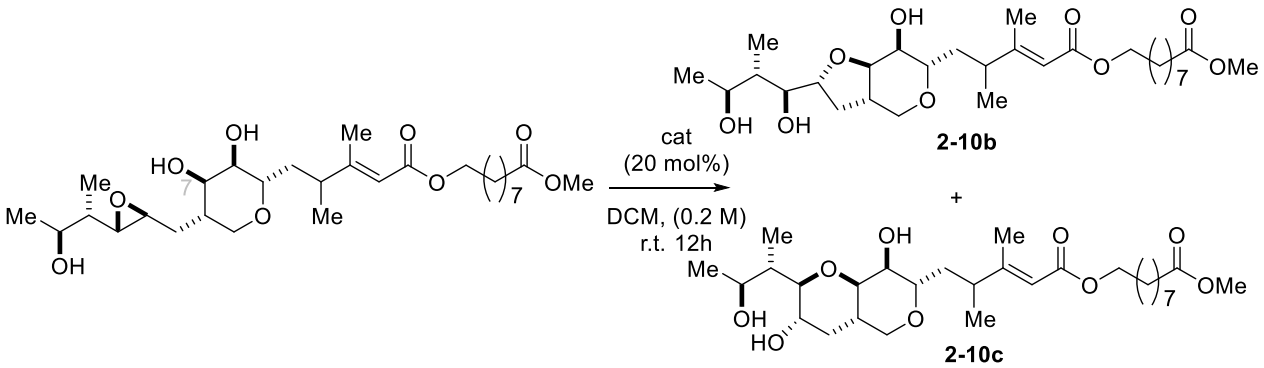

entry	catalyst	conversion (%)	**2-10b:2-10c**[b]
1	**(S)-2-1A**	>98	34:66
2	**(S)-2-1B**	95	38:62
3	**(S)-2-1C**	>98	34:66
4	**(S)-2-1D**	>98	43:57
5	**(S)-2-1E**	>98	55:45
6	**(S)-2-1F**	>98	45:55
7	**(S)-2-1G**	>98	43:57
8	**(S)-2-2C**	>98	28:72
9	**(S)-2-2D**	97	52:48
10	**(S)-2-4B**	90	40:60

a conditions: 1 (0.02 mmol), 4Å MS
b Determined by RP-HPLC.

Table 2.5 (*S*)-chirality CPAs for the optimization of *exo*-product 2-10b.

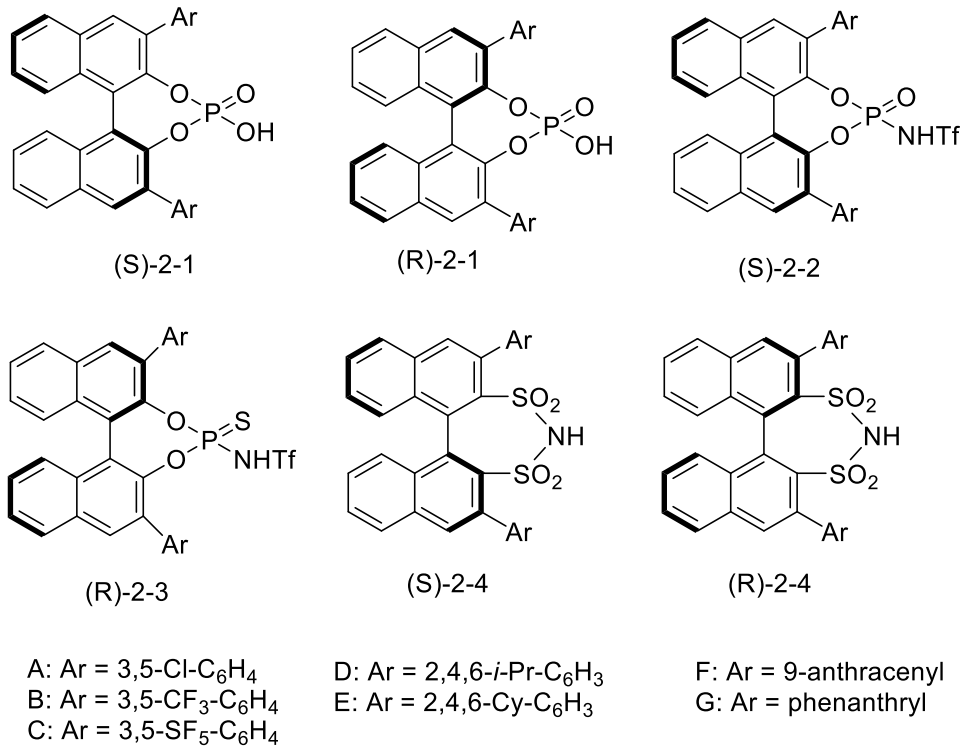

Figure 2.7 Catalyst screening for the optimization of *exo*-product 2-10b.

Inspired by our previous work, in which we everturned the site-selectivity of macrolactone-based triol 6-dEB glycosylation by changing the backbone of CPA (cf. Scheme 1.8 Chapter 1),[33] we decided to evaluate SPINOL-based CPAs. To this end, we evaluated several (*R*)-SPINOL CPAs, which possess axial chirality similar to (*S*)-BINOL CPAs, with *meta*-aryl substituents ranging from F to CF_3 and SF_5 (Table 2.6 entries 1-4), using toluene as the solvent. With smaller *meta*-aryl substituents, such as F or CF_3 groups, we observed decrease in regioselectivity of **2-10b** in comparison to what we observed with BINOL-based acid (*S*)-**2-1D** (entries 1 and 2, compared to Table 2.4, entry 9). However, the increase in the steric size of the substituents resulted in more regioselective formation of **2-10b** to 60:40 rr (entry 3, compared to Table 2.4, entry 9). Further evaluation of the SPINOL-based CPAs carrying 9-anthrancenyl substituents led to similar regioselectivity (entry 4, compared to entry 3). These results obtained for the SPINOL-based CPAs

confirmed our hypothesis and supported the observations previously made by the Nagorny[27] and Houk groups[42] that SPINOL-based CPAs have a rigid spironbiindane backbone with a different bite-angle, which makes them complementary to the BINOL-based acids for the stereodifferentiating reactions.

Despite the observed improvements (*vide supra*), further selectivity optimization was necessary, and non-CPA hydrogen bond donors were evaluated next (entries 5-11). The Jørgensen group recently reported using thiourea-derived cinchona alkaloids **2-11A** to achieve a desymmetrizative β-elimination of epoxide **2-11a** (Scheme 2.10).[43] They proposed that the ketone moiety of the susbstrate forms hydrogen bonds with **2-11A** resulting in a rigid six-membered ring with the thiourea catalyst, and the resultant enhancement in the acidity of the α-proton enables the deprotonation by the quinuclidine nitrogen resulting in an E_1cb-like elimination leading to product **2-11c**.

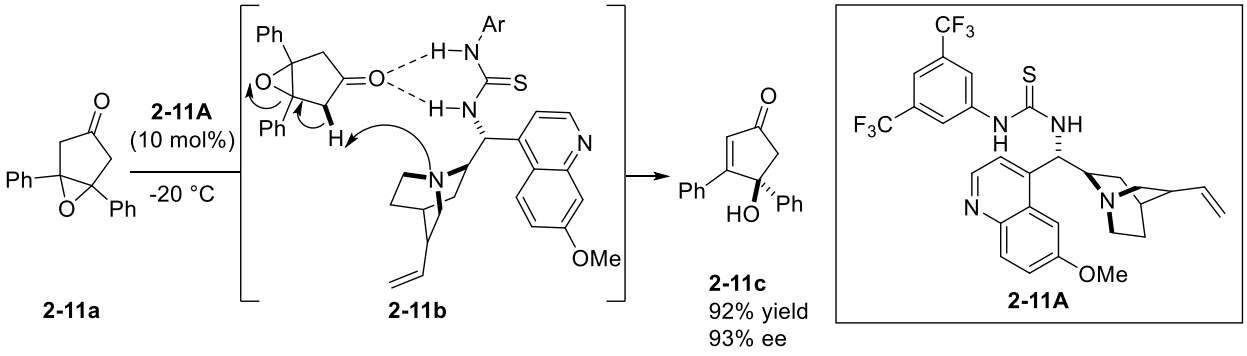

Scheme 2.10 Desymmetrization of epoxides via thiourea-containing cinchona alkaloids catalyst.

Inspired by this work, we investigated the thiourea-containing cinchona alkaloids and other hydrogen bond donor catalysts. These studies commenced with evaluating squaramide-based catalyst **2-6** (entry 5). While this reaction led to similar regioselectivity as what was observed with the SPINOL-base CPAs (entry 5, compared to entry 4), the reaction was much slower, and only

10% of conversion was observed. Further evaluation of thiophosphoramide **2-7** and thiourea **2-8** provided similar results with less than 10% conversion. Moreover, the thiourea-based cinchona alkaloids catalysts **2-9** and **2-10** did not lead to the productive formation of product and less than 5% conversion was observed (entries 8-11). These results suggested that standard HBD catalysts are not suitable for promoting ERO of mupirocin methyl ester, and we continued evaluating CPA-based catalysts containing silyl groups as the 3,3'-substituents (entries 12 and 13). Indeed, CPA catalyst **(*S*)-2-11** developed by the MacMillan group was found to promote ERO with highest levels of regioselectivity (entry 13, >98% conversion, 66:34 rr). Therefore, we selected it as the catalyst of choice for our subsequent optimization of the *exo*-selective ERO leading to **2-10b**.

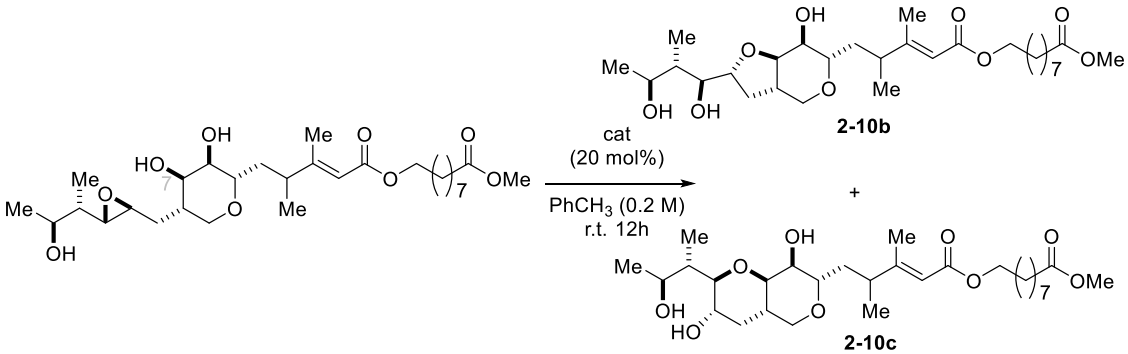

entry	catalyst	conversion (%)	2-10b:2-10c[b]
1	**(R)-2-5A**	>98	42:58
2	**(R)-2-5B**	>98	52:48
3	**(R)-2-5C**	91	60:40
4	**(R)-2-5D**	>98	60:40
5	**2-6**	10	61:39
6	**2-7**	10	60:40
7	**2-8**	6	63:37
8	**2-9A**	<5	N/A
9	**2-9B**	<5	N/A
10	**2-9C**	<5	N/A
11	**2-10**	<5	N/A
12	**(S)-2-11**	>98	66:34
13	**(R)-2-11**	>98	28:72

a conditions: 1 (0.02 mmol), 4Å MS
b Determined by RP-HPLC.

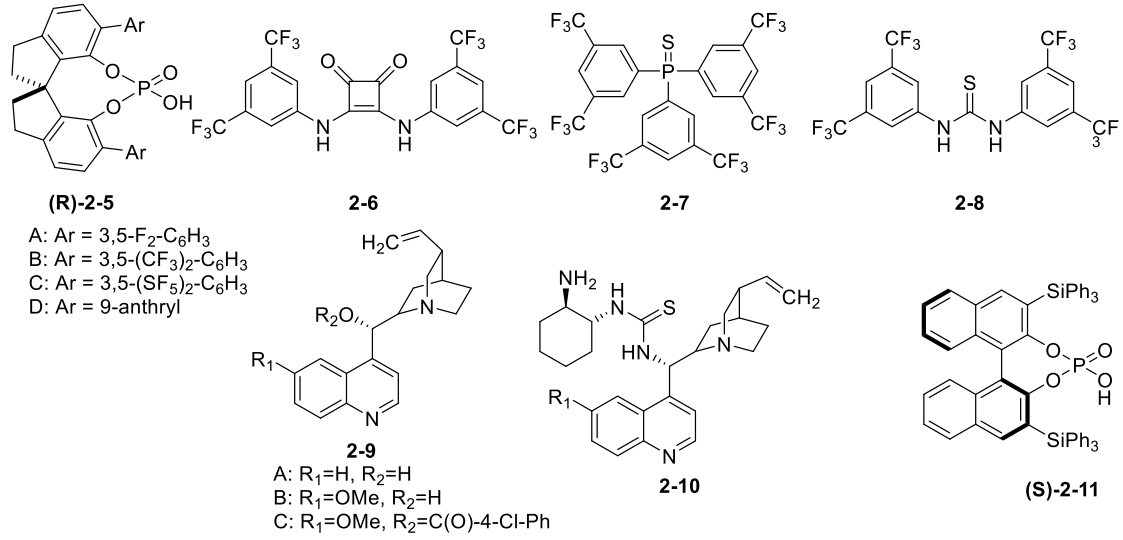

Table 2.6 Catalyst screening for the optimization of *exo*-product 2-10b.

Having identified the most optimal for the *exo*-product catalyst **(*S*)-2-11**, we pursued additional optimization studies in order to further increase the selectivity of this reaction. During the catalyst optimization studies, we have discovered that the saddle changes in the reaction conditions for the *exo*-selective formation of **2-10b** with **(*S*)-2-11** may lead to significant changes in the reaction selectivity. Surmising that these observations might result from different modes of CPA to substrate complexation, we subsequently decided to evaluate the dependence of the substrate and catalyst concentrations on the reaction selectivity (Table 2.7). When increasing the concentration, the regioselectivity decreased and it could potentially override the regioselectivity and favor *endo*-product **2-10c** (entry 1). However, when lowering the concentration from 0.2 M to 0.1 M, we started observing the increase of regioselectivity, even though there was slightly decreased in the reaction rate (entry 3, 85% conversion, and 62:38 rr). Further and gradual decrease in the concentration (from 0.1 M to 0.05 M, to 0.025 M, and to 0.01 M) demonstrated an enhancement of the **2-10b**:**2-10c** selectivity (entries 2–6). When the reaction concentration was set at 0.01 M, we were able to obtain the highest regioselectivity ratio of **2-10b** in 74:26 (entry 6) Therefore, we hypothesized the regioselectivity of the **2-10b** was likely due to the concentration dependent.

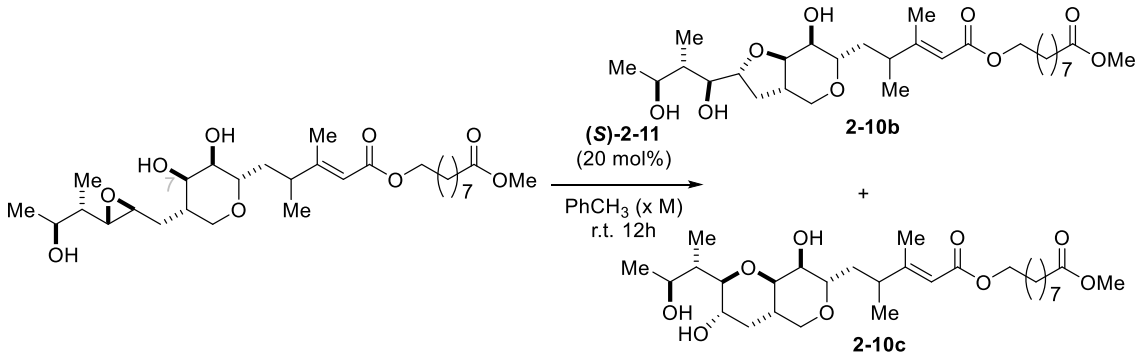

entry	solvent (conc.)	conversion (%)	**2-10b:2-10c**[b]
1	Toluene (0.5 M)	94	45:55
2	Toluene (0.2 M)	90	52:48
3	Toluene (0.1 M)	85	62:38
4	Toluene (0.05 M)	90	62:38
5	Toluene (0.025 M)	83	65:35
6	Toluene (0.01 M)	95	74:26

a conditions: 1 (0.02 mmol),
b Determined by rp-HPLC

Table 2.7 Concentration screening for the optimization of *exo*-product 2-10b

The observed selectivity dependence on the reaction concentration (*cf.* Table 2.7) suggests that the complexation and proper hydrogen bond network formation between the **(*S*)-2-11** and mupirocin methyl ester play an important role for the formation of the *exo*-product **2-10b**. Considering that the choice of solvent may significantly impact the hydrogen bonding between the catalyst and substrates, the dependence of the solvent on the reaction regioselectivity was evaluated next (*cf.* Table 2.8). The use of coordinating solvents such as ether, THF, and ethyl acetate dramatically decreased both the reaction rate and selectivity (entry 4-6). In addition, the polar solvents led to lower reactivity (entry 4-8), with less than 75% conversion were observed, while the non-polar solvents typically resulted in almost full conversion, under the same reaction conditions (entry 1, 2, 3, and 9). While the reactions in chloroform have shown promising selectivity (entry 7, 67:44 rr), the toluene was found to be the best solvent that provided 77:23 *exo*:*endo* selectivity.

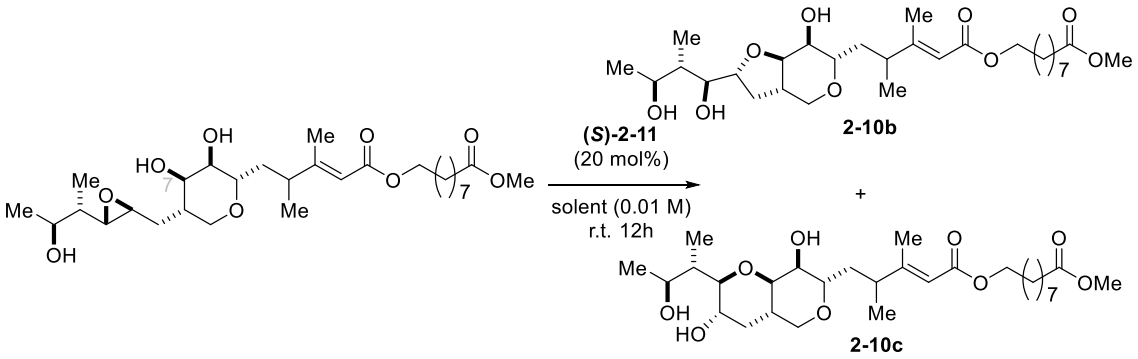

entry	solvent (conc.)	conversion (%)	**2-10b:2-10c**[b]
1	Toluene (0.01 M)	>98	77:23
2	Cyclohexane (0.01 M)	91	44:56
3	Hexane (0.01 M)	93	38:62
4	Ether (0.01 M)	22	50:50
5	Tetrahydrofuran (0.01 M)	46	52:48
6	Ethyl acetate (0.01 M)	40	55:45
7	Chloroform (0.01 M)	75	67:33
8	Acetonitrile (0.01 M)	67	52:48
9	Trifluorotoluene (0.01 M)	98	55:45

a conditions: 1 (0.02 mmol),
b Determined by rp-HPLC

Table 2.8 Solent screening for the optimization of *exo*-product 2-10b

Similar to the optimization studies for the endo-selective cyclization outlined above, we next pursued the optimization of the catalyst loading (*cf.* Table 2.9). While the originally used 20 mol% catalyst loading resulted in complete conversion in 12 h (entry 1), the reduction of the catalyst loading to 15 mol% (entry 2) or to 10 mol% (entry 3) resulted in lower conversions (88% and 75%, correspondingly). To address the conversion problem, the subsequent experiments with lower catalysts loadings were carried for 72 h instead (entries 4–7). To our delight, the use of 5 mol% of **(*S*)-2-11** did not significantly erode the selectivity, and 75% of the *exo*-product **2-10b** was obtained after stirring the reaction mixture for 72 h (77:23, entry 4). Moreover, similar levels of regioselectivity were maintained even at much lower catalyst loadings such as 0.5 mol% (70:30 rr, entry 6). However, this significant reduction in the catalyst loading resulted in great increase

in the reaction times as after 72 hours less than 30 % of conversion was observed. Unlike the *endo*-selective reaction with **(*R*)-2-1E** (Table 2.2, entry 19), this *exo*-selective transformation catalyzed by **(*S*)-2-6** was highly sensitive to the presence of water, as the addition of 5 mol% to the reaction catalyzed by 5 mol% of **(*S*)-2-6** resulted in complete loss of the regioselectivity and significantly slower reaction rate (Table 2.9, entry 7). This observation suggests that water may disrupt the pre-complexation of **(*S*)-2-11** and mupirocin methyl ester and that the formation of the *exo*-product **2-10b** requires specific network of hydrogen bonds between the substrate and catalyst that is different from the hydrogen bonding pattern that leads to the *endo*-product.

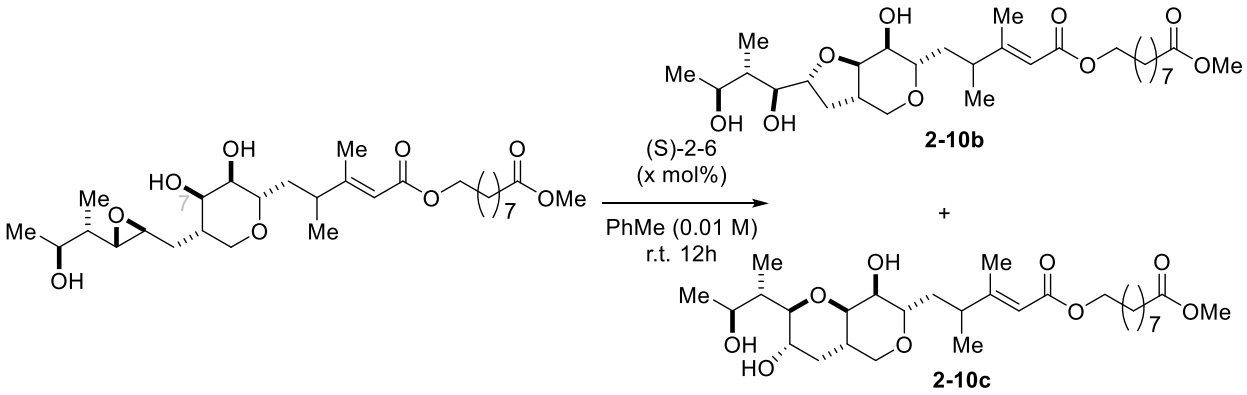

entry	cat. loading (mol%)	conversion (%)	**2-10b:2-10c**[b]
1	20	>98	77:23
2	15	88	73:27
3	10	74	70:30
4[c]	5	75	73:27
5[c]	1	38	68:32
6[c]	0.5	30	70:30
7[c,d]	5	44	55:45

a conditions: 1 (0.02 mmol),
b Determined by rp-HPLC
c reaction time was 72h
d 5 mol% of H_2O was added

Table 2.9 Catalyst loading screening for the optimization of *exo*-product 2-10b

With the catalyst-controlled pathways leading to both **2-10b** and **2-10c** being established, some experimental studies to probe the potential reaction mechanism were performed (Figure 2.8). To rule out the CPA-catalyzed equilibration between the *exo*- and *endo*-products, both **2-10b** and **2-10c** were subjected to **(*R*)-2-1E** and **(*S*)-2-11**, and no isomerization, reversed mupirocin methyl ester formation or material degradation was noted at room temperature (Figure 2.8A and 2.8B). In addition, when a 1:1 mixture of **2-10b** and **2-10c** were subjected to **(*R*)-2-1E** and **(*S*)-2-11** either at room temperature or elevated temperature at 80 ˚C, no isomerization was observed (Figure 2.8C and 2.8D). Similarly, neither **2-10b** nor **2-10c** acted as the catalysts when stirred with mupirocin methyl ester (**2-10a**), as no reaction occurred (Figure 2.8E). However, the addition of 0.5 equiv of either the *endo*- or *exo*-products **2-10b** and **2-10c** to the initial reaction mixture did not affect the selectivity vs. conversion profiles (Figure 2.8F). These control studies demonstrate that both *exo*- and *endo*-products are kinetically stable even at the elevated temperature, and that the formation of the product does not affect the selectivity of the reaction. Therefore, interconversion between the *exo*- and *endo*- products is unlikely to happen under the reaction conditions.

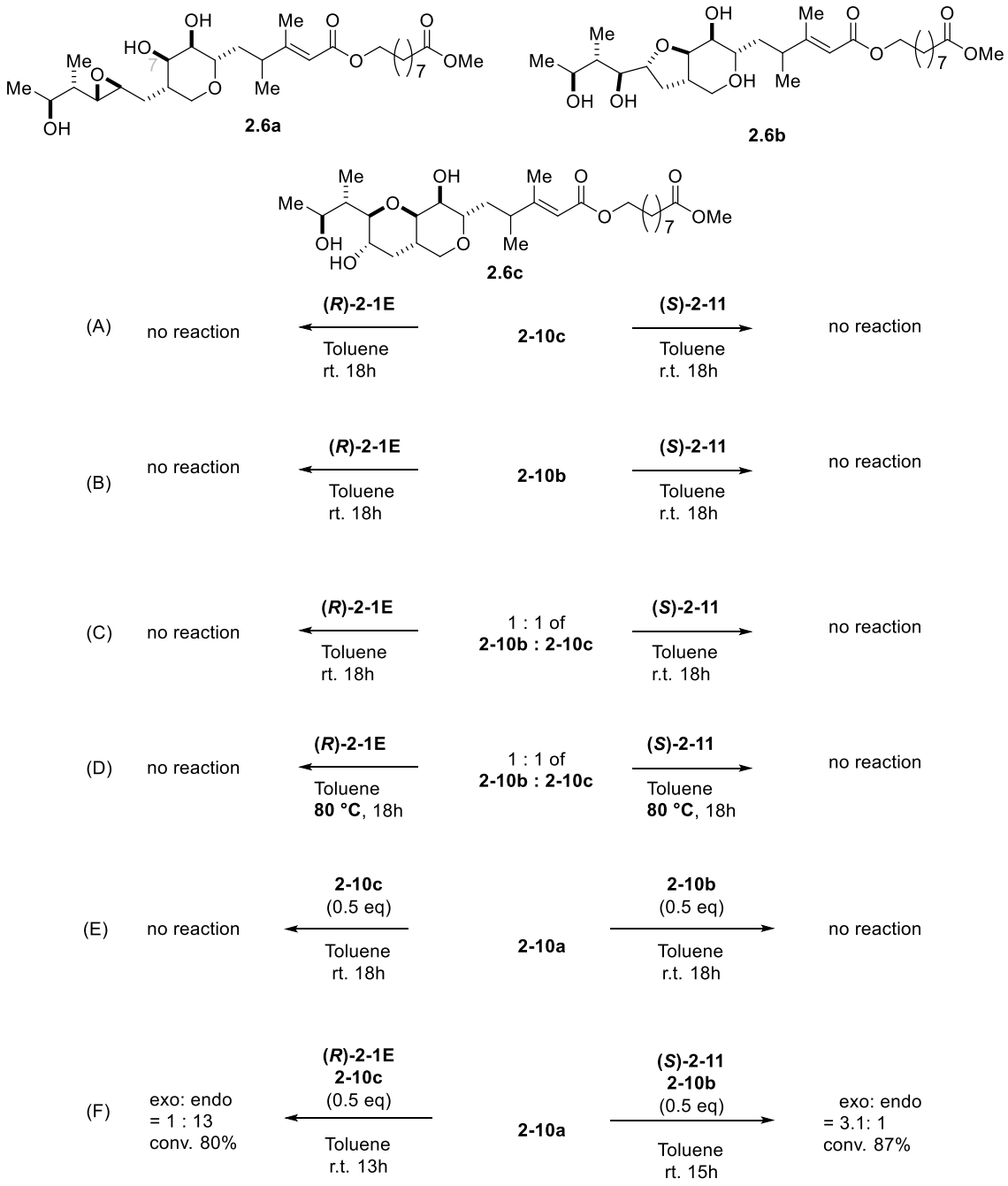

Figure 2.8 Control experiments to probe the isomerization of 2-10b and 2-10c under the reaction conditions.

Our studies focused on probing the mechanisms of the regiodivergent cyclizations continued with investigating the conversion vs. selectivity profiles for both the *exo*- and *endo*-selective transformations (Figure 2.8A and Figure 2.8B). The reaction progression was monitored

by HPLC, and the selectivity was plotted as the function of the reaction conversion for both the *exo*- and *endo*- products. Our initial studies commenced with probing the selectivity versus conversion dependence for the *exo*-selective cyclization catalyzed by **(*S*)-2-11** (*cf.* Figure 2.9). At low conversions (20-40%), moderate selectivity of ~60:40 r.r. was observed. However, as the reaction progressed, the r.r. value slowly, but steadily increased until when it reached to ~80% conversion after 6 hours. At this point, no significant changes in the reaction selectivity were observed, until reaching the reaction completion, and the final r.r. value was similar to what we observed and described in our earlier studies (*vide supra*). The observations were consistent with noted earlier selectivity on concentration-dependence for the **(*S*)-2-11**-catalyzed *exo*-cyclization (Figure 2.9). These results suggest that higher concentrations of substrate negatively impact the substrate/catalyst pre-complexation that leads to the productive formation of the *exo*-product.

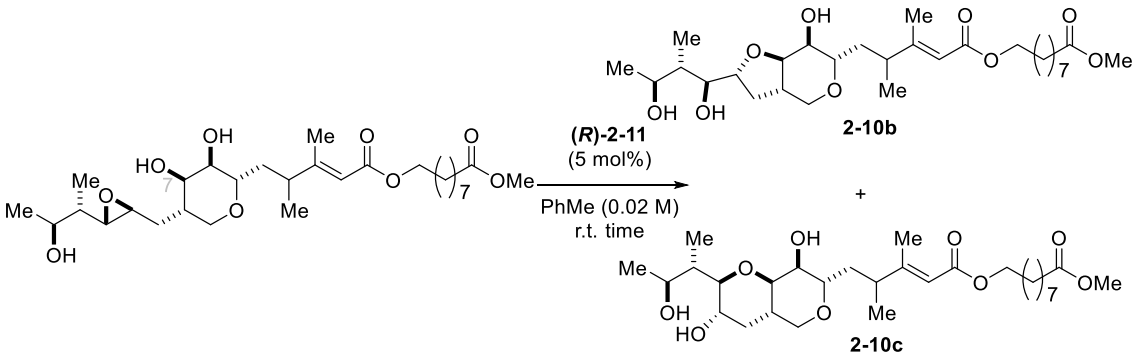

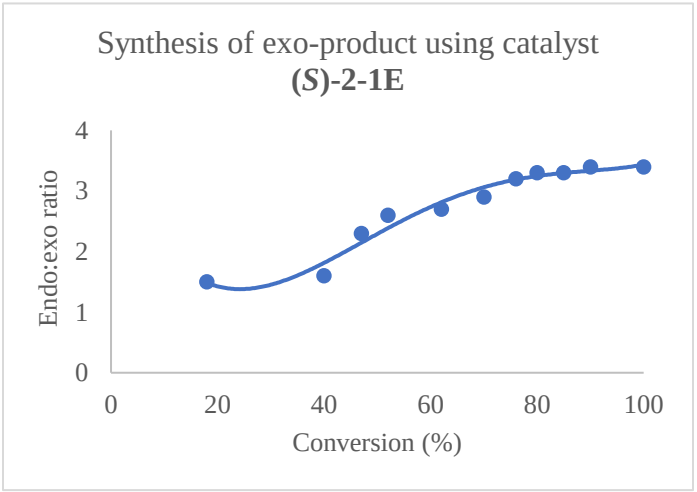

[1]Reaction was executed on 0.02 mmol scale, using 5 mol% of catalyst, toluene (0.02 M) for the indicated period of time. The selectivity and conversion were determined by NMR.

Figure 2.9 Time studies for the *exo*-product[1]

Similar reaction profile was subsequently obtained for the *endo*-product (*cf.* Figure 2.10). As before, we observed increase of the regioselectivity as the reaction progressed; however, in the case of the *endo*-product formation this dependence was more significant. Thus, at low conversions (~10-20%) the initial ratio of **2-10b:2-10c** was as low as 6.6:1; however, this value lineary increased with the reaction progression and after 86% conversion, the r.r. had increased up to 19:1 r.r. As before, these observations suggest that *endo*-product formation is also affected by the starting material concentration, and the selectivities are high at lower concentrations of mupirocin methyl ester. These results coupled with the observation that catalytic quantities of water diminish the reaction selectivity strongly suggest the formation of hydrogen bond complexes between **2-10a** and catalysts **(*R*)-2-1e** or **(*S*)-2-11**.

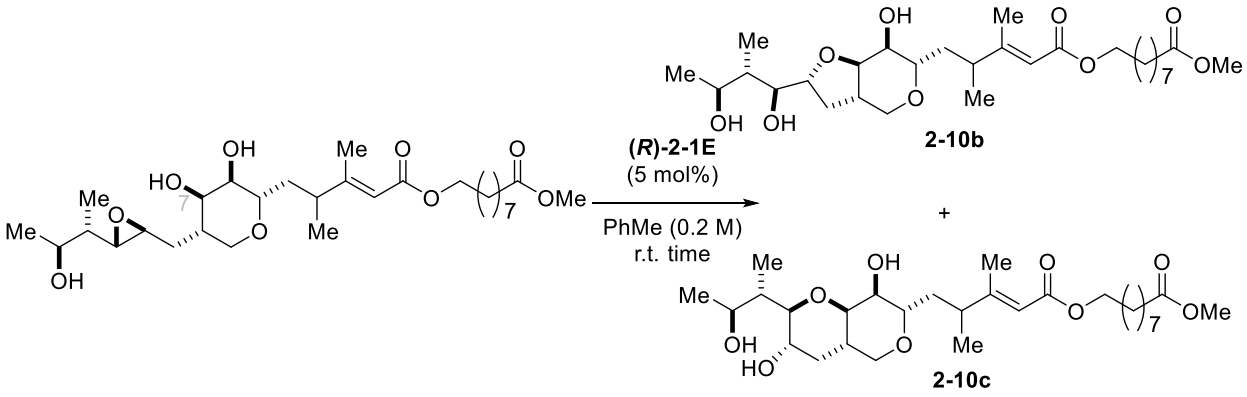

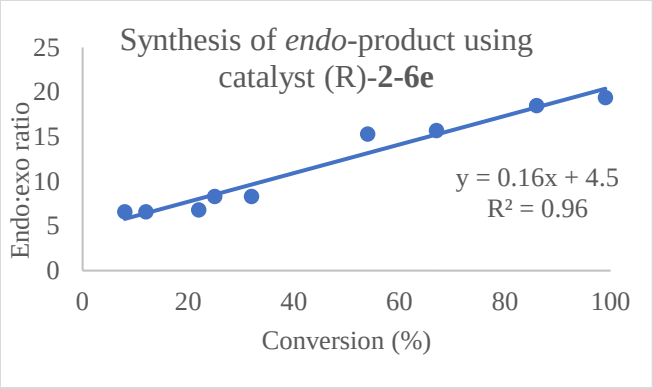

Reaction was executed on 0.02 mmol scale, using 5 mol% of catalyst, toluene (0.2 M) for the indicated period of time. The selectivity and conversion were determined by NMR.

Figure 2.10 Time studies for the *endo*-product

Based on these experimental observations, we searched for computational studies to help understand the reaction mechanism and obtained selectivity. The computational studies were performed by Dr. Alonso Arguelles and Professor Paul Zimmerman via using the single-ended growing string method (GSM). These simulations (Figure 2.11A) revealed that the formation of a substrate-BPA complex [**2-10a** – BPA] was thermodynamically favored by 3.5 kcal/mol over the separated reactant and catalyst, giving 3 hydrogen bonds between C6, C7, and C13 hydroxy groups and the phosphoric acid. Upon transforming this complex, **2-10c** was found to be 12.6 kcal/mol downhill from the substrate-BPA complex [**2-10a** – BPA], while **2-10b** was only 7.5 kcal/mol. These calculations indicated that **2-10c** was 5.1 kcal/mol more stable than **2-10b**. Concerted reaction pathways for the formation of *endo*- and *exo*-products were readily found using GSM (Figure 2.11A). These revealed that the preferred regiotopic pathways, while topologically distinct, shared almost identical activation barriers of around 19.06 vs 19.22 kcal/mol. The *endo*-pathway was preferred minutely by 0.16 kcal/mol, a number that, while within the error of the computational methods, agrees with the small intrinsic *endo*-selectivity that is observed with achiral phosphoric acids experimentally (Figure 2.11A *endo* TS vs. *exo* TS and Table 2.1, entry

8). An alternative mechanism through epoxide opening and involving a phosphate intermediate was ruled out because the barrier was substantially higher (~8.3 kcal/mol, Phosphate formation) than the concerted pathways.

The reverse reactions for the concerted mechanism have activation barriers of 36.0 and 32.1 kcal/mol for *endo*- and *exo*-product formation, respectively, indicating the transformation is irreversible at room temperature. This is consistent with the observation that no interconversion was observed between **2-10b** or **2-10c** in our control experiments (Figure 2.11A). As mentioned earlier, the preferred *endo*- and *exo*-pathways are close in energy and share some common features. For instance, in both cases the hydroxyl group at C13 is required to serve as a proton donor/acceptor relay for the concerted pathway to be operative (Figure 2.11B). Indeed, models lacking this functional group require a stepwise sequence of events (protonation, rotation, and cyclization) to yield the product and thus, have a higher activation barrier. Another shared feature for this pathway is that protonation of the epoxide (red arrows) and cyclization (blue arrows) occur simultaneously in the TS. There are, however, important differences between the *endo*- and *exo*-pathways. The geometrical demands of 5-*exo*-tet cyclizations require a more closed and tight transition state, and the C13 hydroxyl group serves as a relay to protonate the epoxide, while the phosphoric acid activates the C7 hydroxyl group. However, the 6-*endo*-tet mechanism involves a more open transition state, and the C13 hydroxyl group serves as a relay to activate the C7 hydroxyl group, while the phosphoric acid protonates the epoxide directly.

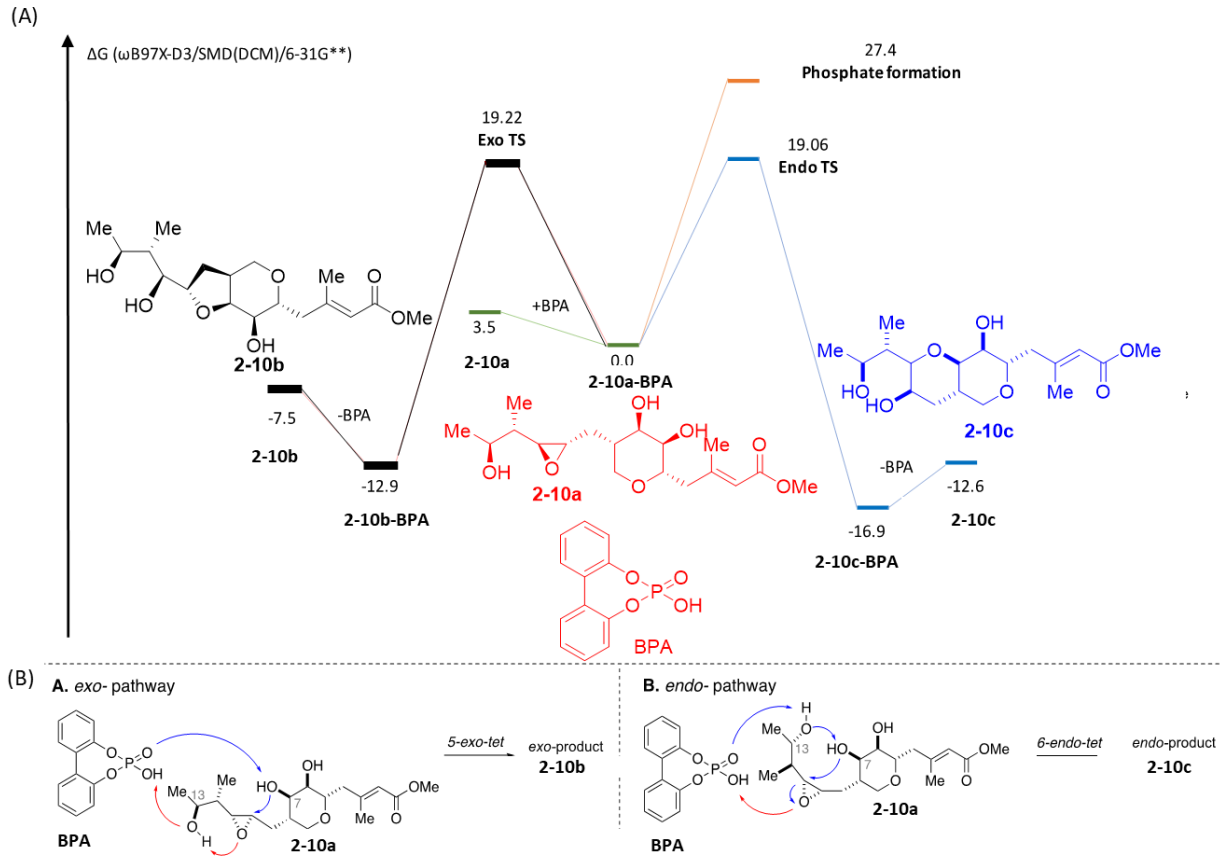

Figure 2.11 Energy diagram for the intramolecular ERO of 2-10a (developed by Dr. Alonso J. Arguelles and Dr. Paul M. Zimmerman).

The quadrant-based analysis, developed by Himo and Terada to explain the selectivity of BINOL-based CPAs,[44,45] has been previously used to describe the steric profile imposed by these acids (Figure 2.12A). Herein we use a similar analysis to explain the observed selectivity pattern. This qualitative model uses the TS for *endo*- and *exo*-cyclization obtained with BPA (Figure 2.12B) as a template to juxtapose the steric profile of (*R*)- or (*S*)-BINOL-derived CPAs. Figures 2.12C and 2.12D show that the 6-*endo*-tet pathway leading to **2-10c** would not have significant contacts with either (*R*)-CPAs, and most of the interactions are with torsionally flexible parts of the substrate, colored blue in Figure 2.12C. But it has strong steric interaction with (*S*)-BINOL-derived CPAs. This is consistent with the more open and flexible TS compared to the 5-*exo*-tet

pathway and suggests that the choice of chirality of the CPA has a drastic impact on the 6-*endo*-tet cyclization activation barrier (Table 2.2 entries 9 and 10). On the other hand, the tighter TS of the 5-*exo*-tet mechanism places an inflexible and bulky group (colored in red in Figure 2.12) in the bottom right quadrant pointing towards the phosphoric acid (Figures 2.12E and 2.12F). This implies that (*R*)-BINOL-derived CPAs would disfavor the *exo*-pathway due to steric clashes in this quadrant. On the other hand, CPAs with (*S*)-chirality, that have an inverse steric profile, would not suffer from these interactions and would therefore have lower barriers for the formation of *exo*-product **2-10b** (Figure 2.12E). Taking both considerations together, this model explains why catalysts with (*R*)-chirality favor endo-product formation more than those with (*S*)-chirality and is in agreement with the experimental results (Tables 2.5, entries 12 and 13).

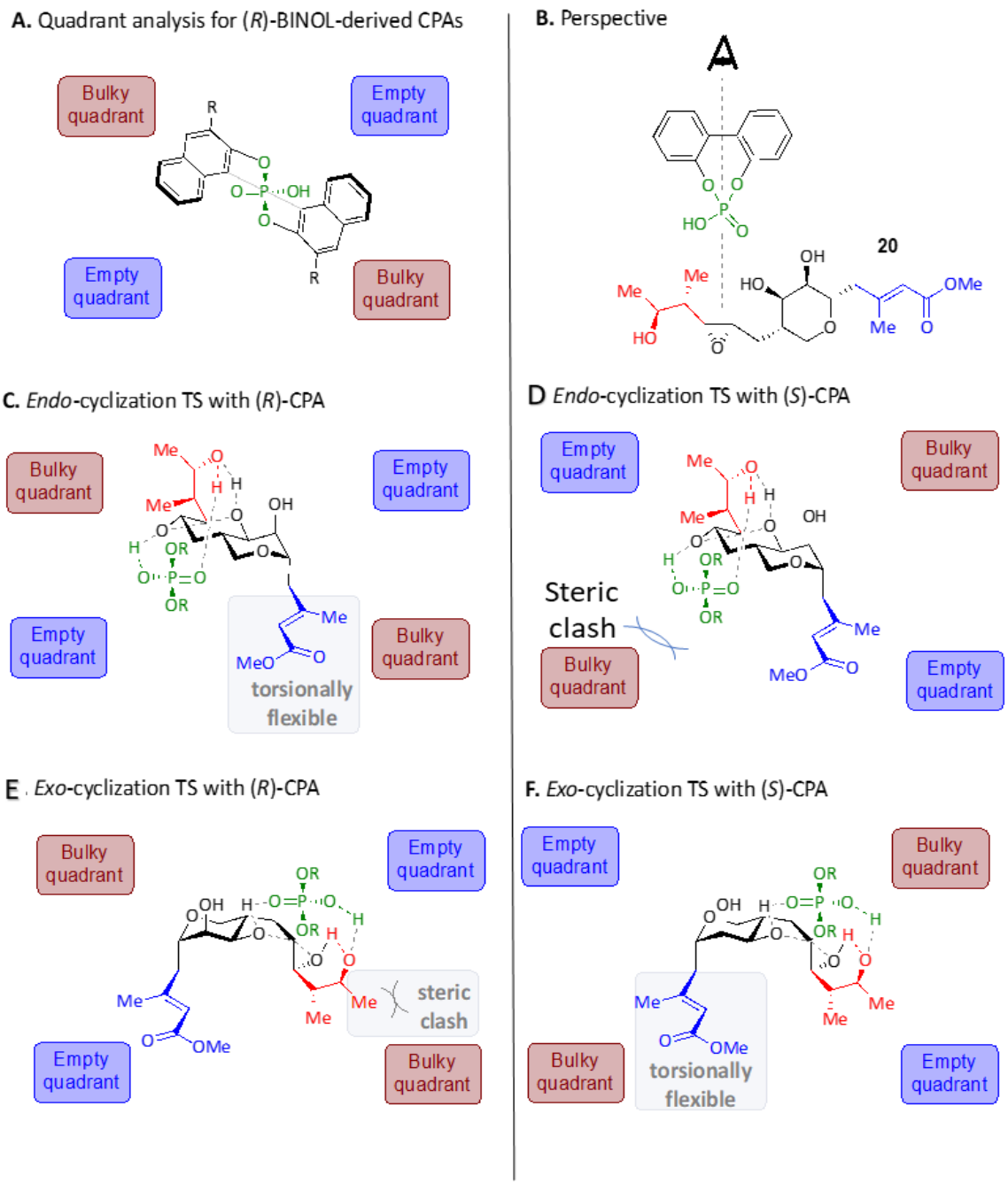

Figure 2.12 Quadrant-based perspective for key TSs. (A) Quadrant analysis for (R)-BINOL-derived CPAs generated by Dr. Alonso J. Arguelles and Dr. Paul M. Zimmerman. (B). Perspective taken. (C). 6-*endo*-tet pathway in a (R)-CPA quadrant framework. (D). 6-*endo*-tet pathway in a (S)-CPA quadrant framework. (E). 5-*exo*-tet pathway in a (R)-CPA

quadrant framework. F. 5-*exo*-tet pathway in a (S)-CPA quadrant framework. Biphenyl backbone of the catalyst is omitted from the perspective for clarity.

2.3. Conclusion

In summary, controlling the regioselectivity of the intramolecular epoxide opening represents a significant challenge, in particular in the context of the formation of the 5- and 6-membered oxygen-containing heterocycles. While nature often uses enzymes to divert such pathways and produce kinetically unfavored products, the existing synthetic solutions have been primarily focused on altering the substrate structure to enhance the formation of the otherwise slower-to-form *endo*-regioisomer. Although emulating the enzymatic pathways through the use of chiral catalysts seems to be a more direct way of controlling the regioselectivity of ERO reactions, the successful examples of such transformations have not been reported prior to this work.

In this chapter we describe the study focused on controlling the regioselectivity of ERO for the natural product derivative mupirocin methyl ester. Unlike many other systems, this natural epoxide does not preferentially cyclize to form the *exo*-product, and the survey of known reaction conditions and achiral catalysts/promoters indicated that both *endo*- and *exo*-products are formed with almost equal rates (*cf.* Table 1). Based on the observations that phosphoric acids may serve as effective catalysts of ERO reactions, we have explored axially-chiral CPAs as the catalysts and developed a CPA-controlled method for the regioselective intramolecular epoxide ring openings. While the achiral catalysts and conditions did not lead to the selective formation the axial chirality of CPAs and the 3,3'-substituents were found to play a determining role on the reaction outcome. The majority of evaluated CPAs were found to provide *endo*-selective cyclization product albeit with low selectivities. After an extensive screening, we discovered that (*R*)-TCYP (**(*R*)-2-1E**) could catalyze a highly selective formation of *endo*-product **2-10b** in 95:4 r.r. when toluene was selected as the solvent.

In contrast, the search for the catalyst that would promote an *exo*-selective cyclization was by far more challenging. While the majority of the screened (*S*)-BINOL- and (*R*)-SPINOL-based CPAs were found to promote this reaction unselectively, (*S*)-TIPSY (catalyst (*S*)-**2.6**) was unique in promoting the formation of *exo*-product **2-10c** in 77:23 r.r. This transformations have shown strong dependence on the solvent polarity, concentration and water content, which suggests that the productive pre-complexation of the catalyst and substrate is key for the formation of the *exo*-product. Importantly, significant insights regarding the difference between the *endo*- and *exo*-pathways were gained through the collaborative computational studies of the reaction mechanism carried in collaboration with Dr. Alonso J. Arguelles and Prof. P. Zimmerman. On the basis of our results, we postulate that both reactions proceed through the concerted and highly synchronous mechanisms. We obtained highly detailed reaction paths for the formation of *exo*- and *endo*-products. These computations indicated that both pathways have similar activation barriers, an observation that is well-aligned with the observed experimental results. These compuations helped to establish the key structural dissimilarities explaining the origin of regiocontrol of these reactions, and confirm the observed experimentally importance of hydrogen bond networks between the acid and substrate. The *endo*-selectivity could be explained by the steric clashes of the epoxide alkyl substituents with the 3- and 3′- substituents of BINOL-derived CPAs with (*R*)-chirality that arise in the transition state leading to the product. The exo-selectivity, in turn arises from the destabilizing interactions with the 3- and 3'-substituents of (*S*)-TiPSY catalyst that distabilize an easier to form pre-complex leading to the *endo*-product. Catalyst-controlled regiodivergent methods for epoxide opening are scarce but synthetically useful and versatile. We hope that our mechanistic insights can assist in developing this methodology further to make it more broadly applicable to the cases such and useful to the organic chemists. We also envision

that CPAs could be broadly applied to affect other intramolecular ERO reactions such as the ones depicted in Figure 1 and Scheme 1, and these studies are currently ongoing in our laboratories.

2.4. Experimental Information

All reactions were carried out under an atmosphere of nitrogen in flame- or oven-dried glassware with magnetic stirring. Mupirocin was purchased from Sigma Aldrich and used as such. Chiral phosphoric acids (*R*)-**2-1e** and (*S*)-**2-11** are commercially available or could be synthesized using the known procedures. Deionized water was used in the preparation of all aqueous solutions and for all aqueous extractions. Solvents used for extraction and chromatography were ACS or HPLC grade. Purification of reactions mixtures was performed by flash chromatography using SiliCycle SiliaFlash P60 (230-400 mesh). Diastereomeric ratios were determined by Diastereomeric ratios were determined by RP HPLC analysis using a Shimadzu SBM-20A Separations Module with a photodiode array detector equipped with C18 Nova-Pack® column (60 Å, 4 mM, 3.9 x150 mm). All spectra were recorded on Varian vnmrs 700 (700 MHz), Varian vnmrs 500 (500 MHz), Varian MR400 (400 MHz), Varian Inova 500 (500 MHz) spectrometers and chemical shifts (δ) are reported in parts per million (ppm) and referenced to the ^{1}H signal of the internal tetramethylsilane according to IUPAC recommendations. Data are reported as (br = broad, s = singlet, d = doublet, t = triplet, q = quartet, qn = quintet, sext = sextet, m = multiplet; coupling constant(s) in Hz; integration). High resolution mass spectra (HRMS) were recorded on MicromassAutoSpecUltima or VG (Micromass) 70-250-S Magnetic sector mass spectrometers in the University of Michigan mass spectrometry laboratory. Infrared (IR) spectra were recorded as thin films on NaCl plates on a Perkin Elmer Spectrum BX FT-IR spectrometer and are reported in wavenumbers (cm^{-1}).

I. **Synthesis of mupirocin methyl ester**.

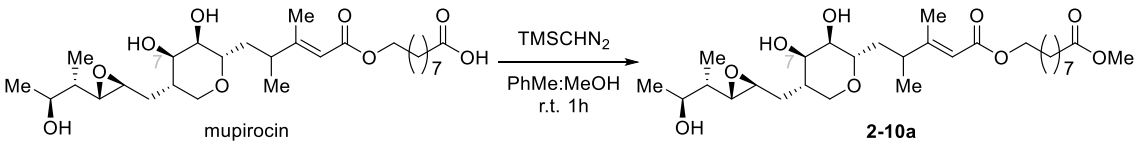

Mupirocin (2.0 g, 4mmol) was initially dissolved in toluene (16 mL) and methanol (4 mL). Then trimethylsilyldiazomethane (2.4 mL, 4.8 mmol, 1.2 eq) was added in dropwise. The reaction mixture was stirred for 1h at room temperature under N_2. After reaction is completed, the reaction was diluted with EtOAc (15 mL) and quenched with 10 v/v % AcOH (15 mL). Then the organic layer was separated from aqueous layer, which was extracted with EtOAc (15 mL x 3). The combined organic layer was washed with brine, dried over with Na_2SO_4, and concentrated *in vacuo* to obtain white solid. The crude product was purified by recrystallization via hexane (10 mL) and diethyl ether (20 mL) and filtered through a Büchner funnel to afford mupirocin methyl ester **2-10a** (1.93g, 85%) as a white solid.

IR (thin film, cm^{-1}): 3564, 3399 (br), 1737, 1712, 1647, 1218, 1142, 1110, 1075, 941, 922, 890, 814, 754, 669.

^{1}H NMR (700 MHz, Chloroform-*d*) δ 5.74 (s, 1H), 4.05 (t, *J* = 6.7, 2.1 Hz, 2H), 3.91 (t, *J* = 3.3 Hz, 1H), 3.86 (d, *J* = 11.7, 3.0 Hz, 1H), 3.80 (t, *J* = 6.7 Hz, 1H), 3.74 (t, *J* = 8.7 Hz, 1H), 3.65 (d, *J* = 2.4 Hz, 3H), 3.54 (d, *J* = 11.8 Hz, 1H), 3.45 (q, *J* = 3.5 Hz, 1H), 2.80 (dd, *J* = 7.4, 4.2 Hz, 1H), 2.69 (d, *J* = 8.0 Hz, 1H), 2.58 (d, *J* = 14.6 Hz, 1H), 2.28 (dtd, *J* = 17.6, 9.0, 8.3, 4.7 Hz, 3H), 2.19 (d, *J* = 2.4 Hz, 3H), 1.99 (tt, *J* = 6.9, 3.3 Hz, 1H), 1.77 – 1.66 (m, 2H), 1.61 (q, *J* = 7.7 Hz, 4H), 1.38 – 1.26 (m, 10H), 1.21 (dd, *J* = 6.5, 2.2 Hz, 3H), 0.93 (dd, *J* = 7.2, 2.2 Hz, 3H).

^{13}C NMR (176 MHz, Chloroform-*d*) δ 174.4, 166.7, 156.6, 117.6, 74.8, 71.40, 70.38, 69.0, 65.3, 63.8, 61.3, 55.6, 51.5, 42.8, 42.8, 39.5, 34.1, 31.5, 29.1, 29.03, 29.01, 28.6, 25.9, 24.9, 20.8, 19.0, 12.7.

HRMS (ESI+) (m/z): $[M+Na]^+$ calcd for C27H46O9, 537.3040, found 537.3014;

$[\alpha]_D^{25}$ = -9.4˚ (c=2.06, $CHCl_3$).

Synthesis of *exo*- and *endo*-products.

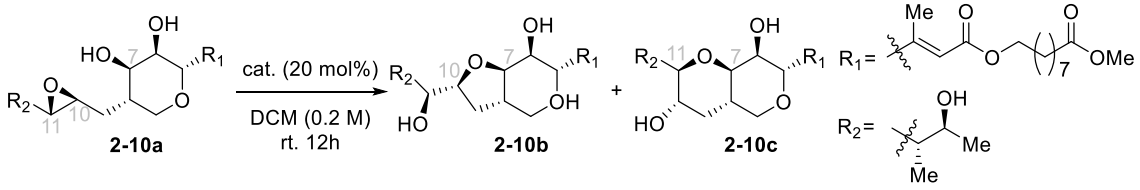

Experimental Procedure for *exo*-product (2-10b):

To a flame dried, N_2 flushed 1 dram vial, a stir bar and mupirocin methyl ester (10 mg, 0.02 mmol) was placed. Then chiral phosphoric acids **(*S*)-2-13** (0.001 mmol, 0.05 eq) was added in and dissolved in toluene (2 mL). The reaction was stirred for 18 hours at room temperature.

Experimental Procedure for *endo*-product (2-10c):

To a flame dried, N_2 flushed 1 dram vial, a stir bar and mupirocin methyl ester (10 mg, 0.02 mmol) was placed. Then chiral phosphoric acids **(*R*)-2-1E** (0.001 mmol, 0.05 eq) was added in and dissolved in toluene (0.2 mL). The reaction was stirred for 18 hours at room temperature.

Exo-product (**2-10b**).

IR (thin film, cm^{-1}): 3407(br), 2929, 2856, 1714, 1646, 1436, 1223, 1149, 1059, 993, 913, 842, 800, 755, 667, 610.

^{1}H NMR (700 MHz, Chloroform-*d*) δ 5.70 (s, 1H), 4.28 (ddd, *J* = 9.4, 5.9, 3.3 Hz, 1H), 4.14 (ddd, *J* = 9.5, 5.4, 1.8 Hz, 1H), 4.07 (t, *J* = 6.7 Hz, 2H), 4.03 – 3.98 (m, 2H), 3.91 (dd, *J* = 9.5, 3.3 Hz, 1H), 3.89 – 3.83 (m, 1H), 3.66 (s, 3H), 3.64 (dd, *J* = 11.3, 3.1 Hz, 1H), 2.50 (dd, *J* = 14.2, 9.4 Hz, 1H), 2.41 (qq, *J* = 13.5, 8.0, 6.6 Hz, 1H), 2.30 (t, *J* = 7.5 Hz, 2H), 2.25 (dd, *J* = 14.1, 5.4 Hz, 1H), 2.20 (d, *J* = 1.3 Hz, 3H), 1.91 (dt, *J* = 11.6, 5.9 Hz, 1H), 1.80 (td, *J* = 12.1, 9.8 Hz, 1H), 1.61 (hept,

J = 6.8 Hz, 5H), 1.49 (dp, *J* = 9.1, 7.1 Hz, 1H), 1.38 – 1.27 (m, 10H), 1.19 (d, *J* = 6.2 Hz, 3H), 0.81 (d, *J* = 6.9 Hz, 3H).

^{13}C NMR (176 MHz, Chloroform-*d*) δ 174.3, 166.4, 155.2, 118.3, 81.1, 80.6, 77.3, 76.2, 72.2, 69.0, 65.6, 63.9, 51.5, 42.0, 41.4, 36.3, 34.1, 29.1, 29.03, 29.01, 28.6, 26.4, 25.9, 24.9, 20.9, 18.4, 12.5;

HRMS (ESI+) (m/z): $[M+Na]^+$ calcd for C27H46O9, 537.3040, found 537.3041;

[α]D^{25} = -2.1˚ (c=2.23, $CHCl_3$).

Endo-product (**2-10c**).

IR (thin film, cm^{-1}): 3407(br), 2930, 2856, 1713, 1646, 1436, 1223, 1149, 1095, 1056, 997, 914, 862, 808, 753, 610.

^{1}H NMR (700 MHz, Chloroform-*d*) δ 5.69 (d, *J* = 1.9 Hz, 1H), 4.22 (ddd, *J* = 10.0, 5.3, 1.4 Hz, 1H), 4.06 (t, *J* = 6.7 Hz, 2H), 3.79 (p, *J* = 6.5 Hz, 1H), 3.74 (t, *J* = 2.0 Hz, 1H), 3.65 (s, 3H), 3.63 (d, *J* = 2.0 Hz, 1H), 3.60 (ddd, *J* = 16.2, 10.8, 5.1 Hz, 2H), 3.33 – 3.24 (m, 2H), 2.57 (dd, *J* = 14.2, 9.9 Hz, 1H), 2.28 (t, *J* = 7.5 Hz, 2H), 2.24 – 2.17 (m, 5H), 2.17 – 2.08 (m, 1H), 2.01 (dt, *J* = 11.7, 3.9 Hz, 1H), 1.93 (pd, *J* = 7.1, 1.8 Hz, 1H), 1.66 – 1.55 (m, 5H), 1.37 – 1.27 (m, 10H), 1.25 (d, *J* = 6.3 Hz, 3H), 0.96 (d, *J* = 7.1 Hz, 3H).

^{13}C NMR (176 MHz, Chloroform-*d*) δ 174.3, 166.4, 155.1, 118.3, 82.0, 77.1, 75.9, 70.2, 69.1, 66.3, 64.2, 63.9, 53.4, 51. 5, 40.0, 39.9, 34.6, 34.1, 32.9, 29.1, 29.03, 29.00, 28.6, 25.9, 24.9, 22.2, 18.3, 10.8;

HRMS (ESI+) (m/z): $[M+Na]^+$ calcd for C27H46O9, 537.3040, found 537.3054;

[α]D^{25} = -8.5˚ (c=1.91, $CHCl_3$).

The Spectrum of ^{1}H NMR for mupirocin **2-10a**, *exo*-product **2-10b**, and *endo*-product **2-10c** was shown below. The assigned peaks range from 0.9-1.2 ppm was used to determine the ratio of **2-10a : 2-10b : 2-10c**. The full assignment of every proton peak was initially studied by Rogers and co-workers and was used as reference.[41]

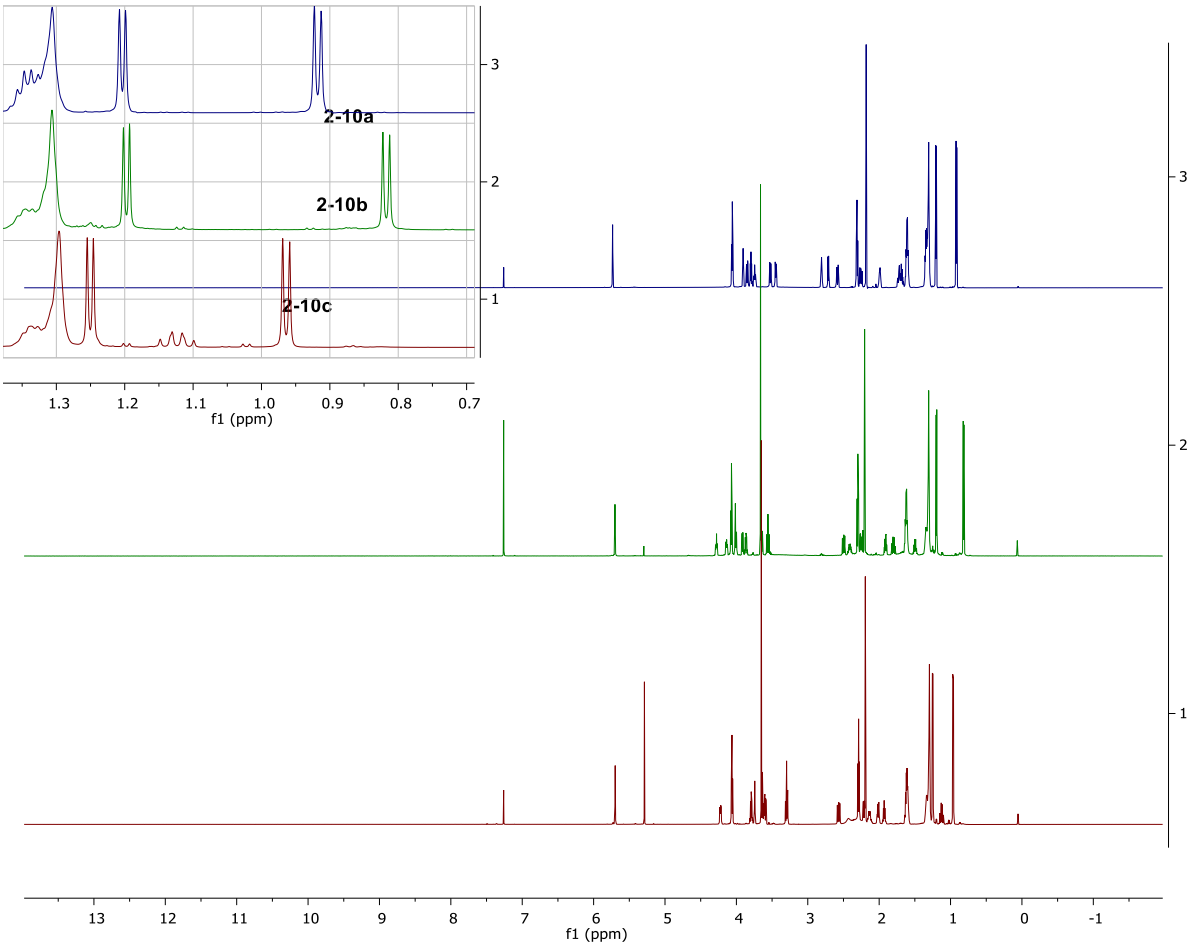

Figure 2.13 Superimpose of 2-10a and 2-10b and 2-10c in ^{1}H NMR.

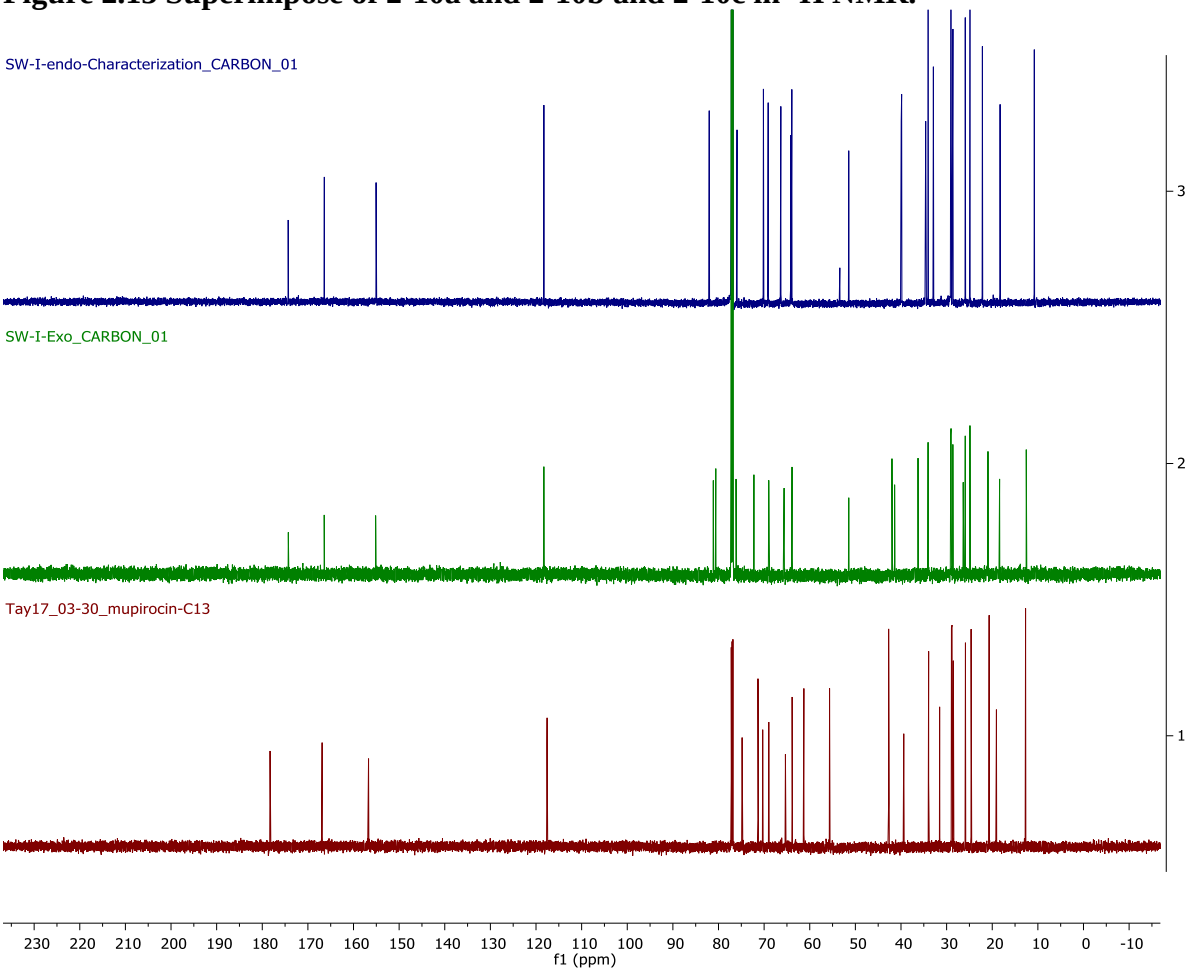

Figure 2.14 Superimpose of 2-10a and 2-10b and 2-10c in ^{13}C NMR.

Control Studies

i. **Control studies for LiCl, $ZnCl_2$, and $Sc(OTf)_3$ (entry 1-3)**[46]

To a flame dried, N_2 flushed 1 dram vial, a stir bar and mupirocin methyl ester (10 mg, 0.02 mmol) was placed. Then the entitled catalysts (0.001 mmol, 0.2 eq) were added in, followed by dissolved in dichloromethane. The concentration of LiCl and $ZnCl_2$ were 0.01 M, while it is 0.2 M for $Sc(OTf)_3$. The reaction was stirred for 18 hours at room temperature. And the results were analyzed by rp-HPLC.

ii. Control studies for H_2O and H_2O in pH 7 buffer (entry 4-5) [21,40]

To a flame dried, N_2 flushed 1 dram vial, a stir bar and mupirocin methyl ester (10 mg, 0.02 mmol) was placed. Water or KH_2PO_4 buffer with a pH of 7 aqueous solution were directly used as solvent and catalyst. The reaction concentration was 0.2 M. Then the reaction was stirred at 70 ^oC for 96 h. The results were analyzed by rp-HPLC.

iii. Control studies for Cs_2CO_3 (entry 6) [47]

To a flame dried, N_2 flushed 1 dram vial, a stir bar and mupirocin methyl ester (10 mg, 0.02 mmol) was placed. Then Cs_2CO_3(10 eq) was added in, followed by dissolving in methanol (0.002 M). The reaction was stirred for 90 hours at room temperature. And the results were analyzed by rp-HPLC.

iv. Control studies for LiHMDS (entry 7) [48]

To a flame dried, N_2 flushed 1 dram vial, a stir bar and mupirocin methyl ester (10 mg, 0.02 mmol) was placed. Then lithium bis(trimethylsilyl)amide (LiHMDS) (3 eq) was added in, followed by dissolving in tetrahydrofuran (0.01 M). The reaction was stirred for 90 hours at room temperature. And the results were analyzed by rp-HPLC.

v. Control studies for $(p\text{-}NO_2\text{-}C_6H_4O)_2PO_2H$ (entry 8)

To a flame dried, N_2 flushed 1 dram vial, a stir bar and mupirocin methyl ester (10 mg, 0.02 mmol) was placed. Then achiral phosphoric acid $(p\text{-}NO_2\text{-}C_6H_4O)_2PO_2H$ (0.2 eq) was added in, followed by dissolving in dichloromethane (0.2 M). The reaction was stirred for 120 hours at room temperature. And the results were analyzed by rp-HPLC.

II. Calibration Curve of *exo*-product and *endo*-product on rp-HPLC

The isolated *exo*- and *endo*-products were initially dissolved in toluene to make stock solutions (0.1 mg/mL in toluene). Afterwards, different volumes of *exo*-product to *endo*-product were mixed to prepare the theoretical ratio of *exo*-product to *endo*-product. The mixture was then

injected into rp-HPLC to analyze the experimental *exo*-product to *endo*-product ratio (Scheme 2.11).

theoretical *exo:endo* ratio	experimental *exo:endo* ratio
10	9.8
3	3.9
2	1.8
1	1.1
0.5	0.5
0.2	0.2
0.1	0.1

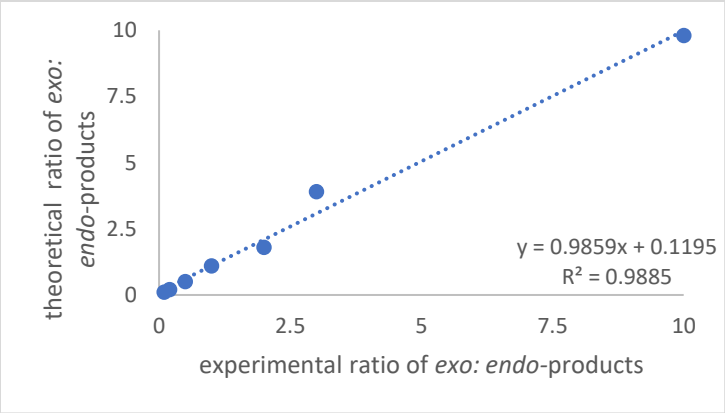

Figure 2.15 Calibration curve of *exo:endo*-product in reverse-phase HPLC.

2.5. Reference

(1) Lu, Q.; Harmalkar, D. S.; Choi, Y.; Lee, K. An Overview of Saturated Cyclic Ethers: Biological Profiles and Synthetic Strategies. *Molecules* **2019**, *24* (20), 3778. https://doi.org/10.3390/molecules24203778.

(2) Marco-Contelles, J.; Molina, M. T.; Anjum, S. Naturally Occurring Cyclohexane Epoxides: Sources, Biological Activities, and Synthesis. *Chem. Rev.* **2004**, *104* (6), 2857–2900. https://doi.org/10.1021/cr980013j.

(3) Morgan, K. M.; Ellis, J. A.; Lee, J.; Fulton, A.; Wilson, S. L.; Dupart, P. S.; Dastoori, R. Thermochemical Studies of Epoxides and Related Compounds. *J. Org. Chem.* **2013**, *78* (9), 4303–4311. https://doi.org/10.1021/jo4002867.

(4) Katsuki, T.; Sharpless, K. B. The First Practical Method for Asymmetric Epoxidation. *J. Am. Chem. Soc.* **1980**, *102* (18), 5974–5976. https://doi.org/10.1021/ja00538a077.

(5) Chang, S.; Galvin, J. M.; Jacobsen, E. N. Effect of Chiral Quaternary Ammonium Salts on (Salen)Mn-Catalyzed Epoxidation of Cis-Olefins. A Highly Enantioselective, Catalytic Route to Trans-Epoxides. *Journal of the American Chemical Society* **1994**, *116* (15), 6937–6938. https://doi.org/10.1021/ja00094a059.

(6) Wang, Z.-X.; Tu, Y.; Frohn, M.; Zhang, J.-R.; Shi, Y. An Efficient Catalytic Asymmetric Epoxidation Method. *J. Am. Chem. Soc.* **1997**, *119* (46), 11224–11235. https://doi.org/10.1021/ja972272g.

(7) Gallimore, A. R. The Biosynthesis of Polyketide-Derived Polycyclic Ethers. *Nat. Prod. Rep.* **2009**, *26* (2), 266–280. https://doi.org/10.1039/B807902C.

(8) Cane, D. E.; Celmer, W. D.; Westley, J. W. Unified Stereochemical Model of Polyether Antibiotic Structure and Biogenesis. *J. Am. Chem. Soc.* **1983**, *105* (11), 3594–3600. https://doi.org/10.1021/ja00349a040.

(9) Nakanishi, K. The Chemistry of Brevetoxins: A Review. *Toxicon* **1985**, *23* (3), 473–479. https://doi.org/10.1016/0041-0101(85)90031-5.

(10) Shichijo, Y.; Migita, A.; Oguri, H.; Watanabe, M.; Tokiwano, T.; Watanabe, K.; Oikawa, H. Epoxide Hydrolase Lsd19 for Polyether Formation in the Biosynthesis of Lasalocid A: Direct Experimental Evidence on Polyene-Polyepoxide Hypothesis in Polyether Biosynthesis. *J. Am. Chem. Soc.* **2008**, *130* (37), 12230–12231. https://doi.org/10.1021/ja8040543.

(11) Baldwin, J. E.; Thomas, R. C.; Kruse, L. I.; Silberman, L. Rules for Ring Closure: Ring Formation by Conjugate Addition of Oxygen Nucleophiles. *J. Org. Chem.* **1977**, *42* (24), 3846–3852. https://doi.org/10.1021/jo00444a011.

(12) Vilotijevic, I.; Jamison, T. F. Epoxide-Opening Cascades in the Synthesis of Polycyclic Polyether Natural Products. *Angew. Chem. Int. Ed.* **2009**, *48* (29), 5250–5281. https://doi.org/10.1002/anie.200900600.

(13) Matsukura, H.; Morimoto, M.; Koshino, H.; Nakata, T. Stereoselective Synthesis of Tetrahydropyran and Oxepane Systems by the Endo-Cyclization of Hydroxy Styrylepoxides. *Tetrahedron Lett.* **1997**, *38* (31), 5545–5548. https://doi.org/10.1016/S0040-4039(97)01197-0.

(14) Nicolaou, K. C.; Prasad, C. V. C.; Somers, P. K.; Hwang, C. K. Activation of 6-Endo over 5-Exo Hydroxy Epoxide Openings. Stereoselective and Ring Selective Synthesis of Tetrahydrofuran and Tetrahydropyran Systems. *J. Am. Chem. Soc.* **1989**, *111* (14), 5330–5334. https://doi.org/10.1021/ja00196a043.

(15) Mukai, C.; Sugimoto, Y.; Ikeda, Y.; Hanaoka, M. A New Procedure for Highly Stereoselective and Regioselective Synthesis of 2-Ethynyl-3-Hydroxytetrahydropyran Derivatives Based on Alkyne-Co2(CO)6 Complex. *Tetrahedron* **1998**, *54* (5–6), 823–850. https://doi.org/10.1016/S0040-4020(97)10357-X.
(16) Adiwidjaja, G.; Flörke, H.; Kirschning, A.; Schaumann, E. Cyclizations of 5-Silyl-Substituted 4,5-Epoxy-1-Alkanols: A Configuration Dependent Mode of Ring Closure. *Tetrahedron Lett.* **1995**, *36* (48), 8771–8774. https://doi.org/10.1016/0040-4039(95)01915-5.
(17) Van Dyke, A. R.; Jamison, T. F. Functionalized Templates for the Convergent Assembly of Polyethers: Synthesis of the HIJK Rings of Gymnocin A. *Angew. Chem. Int. Ed.* **2009**, *48* (24), 4430–4432. https://doi.org/10.1002/anie.200900924.
(18) Byers, J. A.; Jamison, T. F. On the Synergism Between H $_2$ O and a Tetrahydropyran Template in the Regioselective Cyclization of an Epoxy Alcohol. *J. Am. Chem. Soc.* **2009**, *131* (18), 6383–6385. https://doi.org/10.1021/ja9004909.
(19) Morten, C. J.; Byers, J. A.; Van Dyke, A. R.; Vilotijevic, I.; Jamison, T. F. The Development of Endo-Selective Epoxide-Opening Cascades in Water. *Chem. Soc. Rev.* **2009**, *38* (11), 3175. https://doi.org/10.1039/b816697h.
(20) Sittihan, S.; Jamison, T. F. Total Synthesis of the Marine Ladder Polyether Gymnocin B. *J. Am. Chem. Soc.* **2019**, *141* (28), 11239–11244. https://doi.org/10.1021/jacs.9b04696.
(21) Vilotijevic, I.; Jamison, T. F. Epoxide-Opening Cascades Promoted by Water. *Science* **2007**, *317* (5842), 1189–1192. https://doi.org/10.1126/science.1146421.
(22) Chapelat, J.; Buss, A.; Chougnet, A.; Woggon, W.-D. Diastereoselective Synthesis of α-Tocopherol: A New Concept for the Formation of Chromanols. *Org. Lett.* **2008**, *10* (22), 5123–5126. https://doi.org/10.1021/ol8019583.
(23) Wang, W.; Xue, J.; Tian, T.; Jiao, Y.; Li, Y. The First Asymmetric Total Synthesis of (+)-Coriandrone A and B. *Org. Biomol. Chem.* **2013**, *11* (39), 6686. https://doi.org/10.1039/c3ob41497c.
(24) Magolan, J.; Coster, M. J. Total Synthesis of (+)-Angelmarin. *J. Org. Chem.* **2009**, *74* (14), 5083–5086. https://doi.org/10.1021/jo900613u.
(25) Kimachi, T.; Torii, E.; Ishimoto, R.; Sakue, A.; Ju-ichi, M. Asymmetric Total Synthesis of Rhinacanthin A. *Tetrahedron: Asymmetry* **2009**, *20* (14), 1683–1689. https://doi.org/10.1016/j.tetasy.2009.06.025.
(26) Lee, J.; Borovika, A.; Khomutnyk, Y.; Nagorny, P. Chiral Phosphoric Acid-Catalyzed Desymmetrizative Glycosylation of 2-Deoxystreptamine and Its Application to Aminoglycoside Synthesis. *Chem. Comm.* **2017**, *53* (64), 8976–8979. https://doi.org/10.1039/C7CC05052F.
(27) Tay, J.-H.; Argüelles, A. J.; DeMars, M. D.; Zimmerman, P. M.; Sherman, D. H.; Nagorny, P. Regiodivergent Glycosylations of 6-Deoxy-Erythronolide B and Oleandomycin-Derived Macrolactones Enabled by Chiral Acid Catalysis. *J. Am. Chem. Soc.* **2017**, *139* (25), 8570–8578. https://doi.org/10.1021/jacs.7b03198.
(28) Khomutnyk, Y. Ya.; Argüelles, A. J.; Winschel, G. A.; Sun, Z.; Zimmerman, P. M.; Nagorny, P. Studies of the Mechanism and Origins of Enantioselectivity for the Chiral Phosphoric Acid-Catalyzed Stereoselective Spiroketalization Reactions. *J. Am. Chem. Soc.* **2016**, *138* (1), 444–456. https://doi.org/10.1021/jacs.5b12528.

(29) Sun, Z.; Winschel, G. A.; Borovika, A.; Nagorny, P. Chiral Phosphoric Acid-Catalyzed Enantioselective and Diastereoselective Spiroketalizations. *J. Am. Chem. Soc.* **2012**, *134* (19), 8074–8077. https://doi.org/10.1021/ja302704m.
(30) Mensah, E.; Camasso, N.; Kaplan, W.; Nagorny, P. Chiral Phosphoric Acid Directed Regioselective Acetalization of Carbohydrate-Derived 1,2-Diols. *Angew. Chem. Int. Ed.* **2013**, *52* (49), 12932–12936. https://doi.org/10.1002/anie.201304298.
(31) Mensah, E.; Camasso, N.; Kaplan, W.; Nagorny, P. Chiral Phosphoric Acid Directed Regioselective Acetalization of Carbohydrate-Derived 1,2-Diols. *Angew. Chemie.* **2013**, *125* (49), 13170–13174. https://doi.org/10.1002/ange.201304298.
(32) Khomutnyk, Y. Ya.; Argüelles, A. J.; Winschel, G. A.; Sun, Z.; Zimmerman, P. M.; Nagorny, P. Studies of the Mechanism and Origins of Enantioselectivity for the Chiral Phosphoric Acid-Catalyzed Stereoselective Spiroketalization Reactions. *J. Am. Chem. Soc.* **2016**, *138* (1), 444–456. https://doi.org/10.1021/jacs.5b12528.
(33) Tay et al. - 2017 - Regiodivergent Glycosylations of 6-Deoxy-Erythrono.Pdf.
(34) Wang, Z.; Law, W. K.; Sun, J. Chiral Phosphoric Acid Catalyzed Enantioselective Desymmetrization of *Meso* -Epoxides by Thiols. *Org. Lett.* **2013**, *15* (23), 5964–5966. https://doi.org/10.1021/ol402797v.
(35) Monaco, M. R.; Prévost, S.; List, B. Organocatalytic Asymmetric Hydrolysis of Epoxides. *Angew. Chem. Int. Ed.* **2014**, *53* (31), 8142–8145. https://doi.org/10.1002/anie.201400170.
(36) Zimmerman, P. M. Growing String Method with Interpolation and Optimization in Internal Coordinates: Method and Examples. *The Journal of Chemical Physics* **2013**, *138* (18), 184102. https://doi.org/10.1063/1.4804162.
(37) Thomas, C. M.; Hothersall, J.; Willis, C. L.; Simpson, T. J. Resistance to and Synthesis of the Antibiotic Mupirocin. *Nat. Rev. Microbiol* **2010**, *8* (4), 281–289. https://doi.org/10.1038/nrmicro2278.
(38) Meyer, O.; Ponaire, S.; Rohmer, M.; Grosdemange-Billiard, C. Lewis Acid Mediated Regioselective Ring Opening of Benzylglycidol with Dibenzyl Phosphate: Short and Attractive Synthesis of Dihydroxyacetone Phosphate. *Organic Letters* **2006**, *8* (19), 4347–4350. https://doi.org/10.1021/ol061748a.
(39) Chong, J. M.; Sharpless, K. B. Nucleophilic Opening of 2,3-Epoxy Acids and Amides Mediated by Titanium Isopropoxide. Highly Enhanced C-3 Selectivity. *The Journal of Organic Chemistry* **1985**, *50* (9), 1560–1563. https://doi.org/10.1021/jo00209a048.
(40) Czabaniuk, L. C.; Jamison, T. F. Hydroxyl-Substituted Ladder Polyethers via Selective Tandem Epoxidation/Cyclization Sequence. *Organic Letters* **2015**, *17* (4), 774–777. https://doi.org/10.1021/ol503400j.
(41) Clayton, J. P.; Oliver, R. S.; Rogers, N. H.; Pharmaceuticals, B.; Park, B.; Rh, S.; King, T. J. The Chemistry of Pseudomonic Acid. Part 3.l The Rearrangement of Pseudomonic Acid A in Acid and Basic Solution. *J.C.S. Perkin I* **1979**, 838.
(42) Champagne, P. A.; Houk, K. N. Origins of Selectivity and General Model for Chiral Phosphoric Acid-Catalyzed Oxetane Desymmetrizations. *J. Am. Chem. Soc.* **2016**, *138* (38), 12356–12359. https://doi.org/10.1021/jacs.6b08276.
(43) Dickmeiss, G.; De Sio, V.; Udmark, J.; Poulsen, T. B.; Marcos, V.; Jørgensen, K. A. Organocatalytic Asymmetric Desymmetrization-Fragmentation of Cyclic Ketones. *Angew. Chem. Int. Ed.* **2009**, *48* (36), 6650–6653. https://doi.org/10.1002/anie.200903253.

(44) Gridnev, I. D.; Kouchi, M.; Sorimachi, K.; Terada, M. On the Mechanism of Stereoselection in Direct Mannich Reaction Catalyzed by BINOL-Derived Phosphoric Acids. *Tetrahedron Lett.* **2007**, *48* (3), 497–500. https://doi.org/10.1016/j.tetlet.2006.11.017.
(45) Oikawa, M.; Hashimoto, R.; Sasaki, M. Asymmetric Synthesis and in Vivo Biological Inactivity of the Right-Hand Terpenoid Fragment of Terpendole E. *Eur. J. Org. Chem.* **2011**, *2011* (3), 538–546. https://doi.org/10.1002/ejoc.201001104.
(46) Marques, M. V.; Sá, M. M. Lithium Chloride-Mediated Stereoselective Synthesis of Cyclopropanecarboxamides from γ,δ-Epoxy Malonates through a Domino Cyclopropanation/Lactonization/Aminolysis Process. *J. Org. Chem.* **2014**, *79* (10), 4650–4658. https://doi.org/10.1021/jo500712t.
(47) Duprez, V.; Heumann, A. An Efficient Synthesis of β-Hydroxyethylpyrazoles from Propylene and Styrene Oxide Using Cs 2 CO 3. *Tetrahedron Lett.* **2004**, *45* (29), 5697–5701. https://doi.org/10.1016/j.tetlet.2004.05.124.
(48) Rastelli, E. J.; Bolinger, A. A.; Coltart, D. M. Stereodivergent Synthesis of β,γ-Fused Bicyclic γ-Lactones via a Multicomponent Ring-Expansion Cascade. *Chem* **2018**, *4* (9), 2228–2238. https://doi.org/10.1016/j.chempr.2018.08.007.

Chapter 3

Studies of Catalyst-Controlled Regioselective Acetalization and Its Application to Single-Pot Synthesis of Differentially Protected Saccharides

3.1. Introduction to carbohydrates

Carbohydrates are essential molecules that not only serve as immediate energy sources but are also associated with numerous biological activities. Accordingly, the studies of carbohydrates have been the focus of many ongoing investigation in various stages in the fields of organic chemistry, biochemistry, drug discovery, and vaccines.[1,2] However, in many instances, gaining access to these complex oligosaccharides and glycoconjugates has been the bottleneck for the exploration of their biological and medicinal properties.[3–6] Complex oligosaccharides are comprised of the simpler monosaccharides, such as D-glucose, D-galactose, and D-mannose, which are abundant in nature. However, in order for these monosaccharides to be synthetically useful as building blocks for the synthesis of oligosaccharides or polysaccharides, they are commonly required to be functionalized or protected. Not surprisingly, modern synthetic approaches to oligosaccharides strongly rely on the ability to access differentially protected building blocks (Scheme 3.1).[7] For instance, Schmidt and co-workers illustrated the synthesis of various oligosaccharides via different mono-*O*-unprotected sugar acceptors. Moreover, in order to synthesize glycosylphosphatidylinositol glycan-based vaccine, Seeberger and co-workers have demonstrated the significance of accessing to the individual building units efficiently and rapidly.[1] However, synthesis of such differentially protected monosaccharides often requires multiple step

sequences to differentiate numerous hydroxyl groups, stereogenic carbon centers, and may suffer from low yields and tedious purifications due to the formation of undesirable regioisomers throughout these sequences.[8,9] To address these challenges associated with selective functionalization of monosaccharides, there have been many ongoing studies focused on developing new and efficient methods and catalysts.

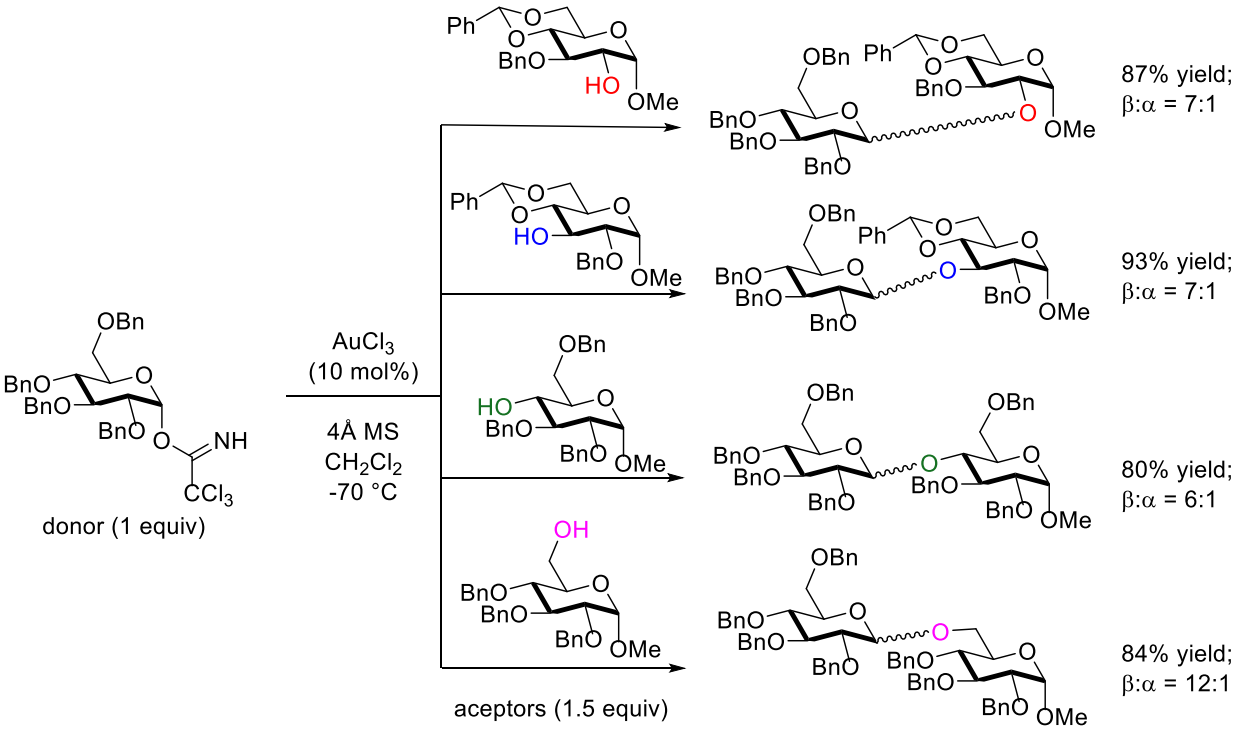

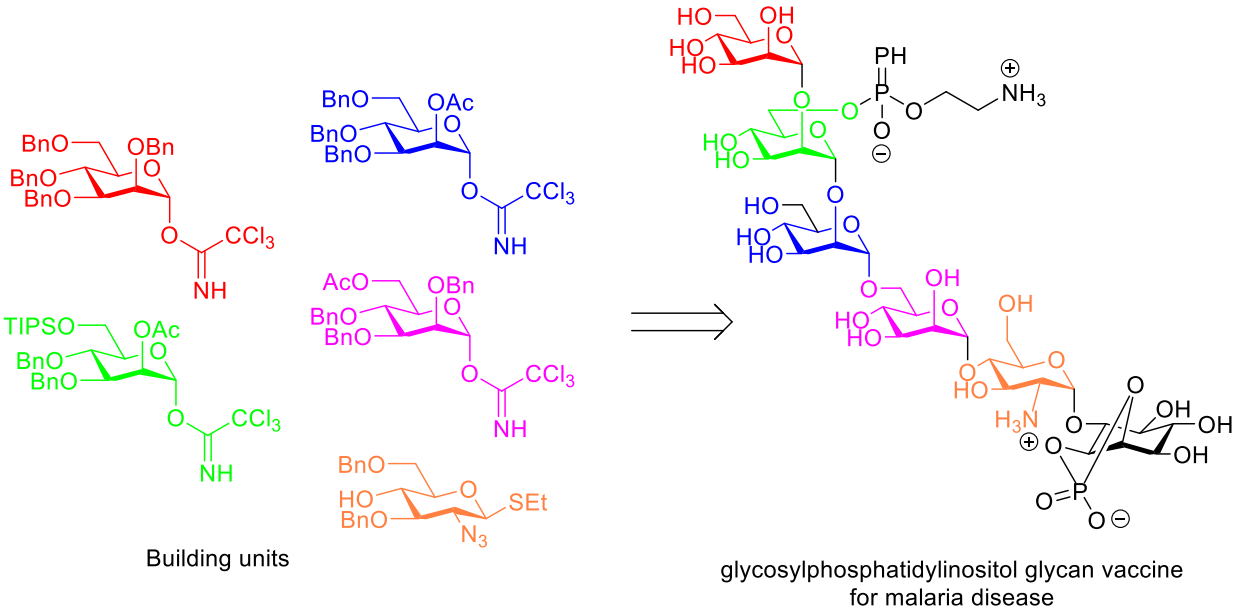

Scheme 3.1 Examples of (A) synthesis of oligosaccharides via different mono-O-unprotected sugar acceptors. (B) synthesis of vaccines via different building units of monosaccharides.

3.2. Overview of the known methods for the regioselective functionalization of carbohydrates based on achiral reagents and catalysts.

While a number of methods have been developed to accomplish site-selective functionalization of hydroxyl groups in saccharides, differentiating equatorial hydroxyls represents a significant challenge. This subsection provies a brief overview of the state-of-the-art in using achiral reagents and conditions to achieve selectivities. A particular emphasis is placed on overviewing the problem of selective functionalization of the C2/C3-positions of the monosaccharides as the selectivities of such reactions are highly dependent on many different factors. The problem of the selective C2/C3 functionalization is common to various types of pyranoses due to the fact that the C6 and C4 hydroxyls could be easily differentiated from the C2 and C3 ones through the installation of the cyclic acetals such as benzylidene acetals.

Achiral nucleophilic organic catalysts and reagents such as pyridine, *N,N*-diisopropylethylamine (DIPEA), and 4-dimethylaminopyridine (DMAP) have been extensively used for the regioselective functionalization of monosaccharides. For instance, the Jeanloz group reported the usage of pyridine for the site-selective C2-tosylation of methyl 4,6-benzylidine-α-D-glucopyranoside **3-1a** (Table 3.1).[10] The initial studies focused on the acylation and benzoylation of **3-1a** and did not provide the desired C2-regioselectivity (entries 1-4). Thus, using the acetic anhydride resulted in the selective acetylation of the C3-OH group leading to **3-1c** in 42% yield (entry 1) along with substantial quantities of the *bis*-protected product **3-1d** (26% yield) and small quantities of the C3-regioisomer **3-1b** (3% yield). The use of acyl chloride as the acylating agent resulted in higher amounts of the acylation at the C2-OH group, and product **3-1b** was now obtained in 16% yield (entry 2). However, regardless of whether the acylation is carried with either acetic anhydride or acyl chloride, significant amount of diacyl product **3-1d** was obtained in 26% and 23% yield, respectively. Similar results were observed when using either benzoic anhydride or benzoyl chloride in 9% and 35% yield, respectively (entries 3 and 4). However, when attempting

to tosylate **3-1a,** significantly better C2-selectivity was achieved. Either tosyl anhydride or tosyl chloride in pyridine provided **3-1b** as the major product in 83% and 68% yield, even though about 15% of **3-1d** was also obtained in each case (entries 5 and 6). It was hypothesized that the low regioselectivity observed for the acylation reactions could be due to the migration of esters under the basic conditions, leading to low selectivity at the C2-OH and C3-OH, as well as the formation of the di-ester product. These results as well as other studies suggest that the usage of pyridine, as well as other Lewis bases such as imidazole[11] or *N*-methyl imidazole[12] as the catalysts to achieve regioselective acylation of monosaccharides with equatorial alcohols will not lead to highly selective monofunctionalizations.

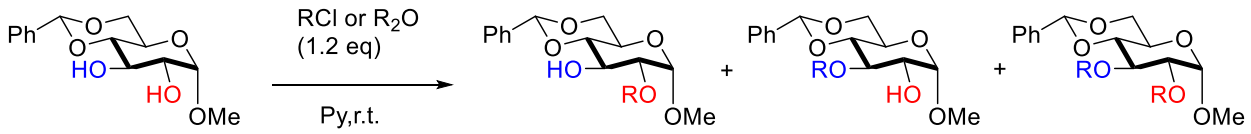

3-1a **3-1b** **3-1c** **3-1d**

entry	RCl or R_2O	R_2	**3-1b**	:	**3-1c**	:	**3-1d**
1	Ac_2O	Ac	3	:	**42**	:	26
2	AcCl	Ac	16	:	NA	:	**23**
3	Bz_2O	Bz	13	:	**25**	:	9
4	BzCl	Bz	24	:	6	:	**35**
5	Ts_2O	Ts	**83**	:	NA	:	15
6	TsCl	Ts	**68**	:	NA	:	16

Table 3.1 Pyridine based esterification of 4,6-benzylidine-α-D-glucopyranoside.

Around the same time as the studies above, the Haines' group developed a new method based on benzoyl cyanide and triethylamine as the reagents for the regioselective benzoylation of various monosaccharides (Table 3.2).[11] Their results indicated that when BzCN was used with the catalytic triethylamine, they could selectively functionalize the axial C2-OH group of 4,6-O-

benzylidene-β-D-mannopyranoside, forming product **3-2b** with a r.r. of 2.3:1 (entry 1). Similar results were obtained with either glucopyranoside or allopyranoside (entries 2 and 4). However, when galactopyranoside was used, the C3-OH group was regioselected with 2.8:1 r.r. (entry 3).

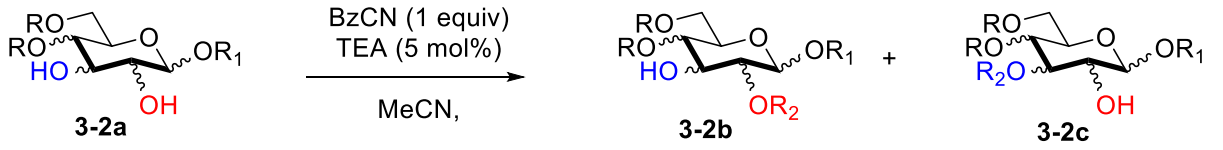

entry	starting material	3-2b	:	3-2c
1	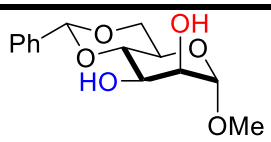	**70**	:	**30**
2	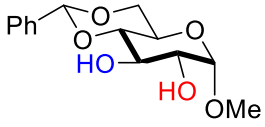	**62**	:	**38**
3	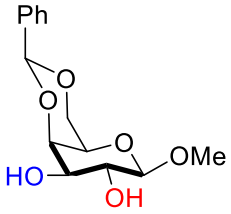	26	:	74
4	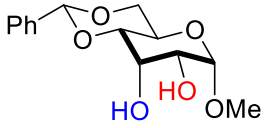	**62**	:	**38**

Table 3.2 Benzoyl cyanite catalyzed site-selective benzoylation.

Even though Haines group did not perform a mechanistic study, later reports by Schmidt and Peng suggested that the hydrogen bond between the cyanite anion and axial hydroxyl group is kinetically more stable than a similar bond the equatorial hydroxyl group (Table 3.3).[13] In addition, once this hydrogen bond forms (intermediates **3-3d** and **3-3f**), it creates a partial negative charge for the axial oxygen, which is stabilized by the intramolecular hydrogen bond formation from the

equatorial hydroxyl group and increases the nucleophilicity of the axial oxygen to allow regioselective benzoylation, forming product **3-3e** or **3-3g**.

Based on this process, Schmidt and co-workers carried the optimization of the catalytic base and found that 4-dimethylaminopyridine (DMAP) could yield more reactive cyanide anions, which allowed them to do site-selective benzoylation of both *cis*-diols (with the r.r. values increased from 70:30 with TEA to 85:15 with DMAP) as well as *trans*-diol (with the r.r. values increased from 62:38 with TEA to 89:11 with DMAP). However, when other *trans*-diols, such as allyl 4,6-O-benzylidene-α-D-galactopyranoside were used, the regioselectivity decreased from 26:74 to 25:64 r.r. favoring the C3-OH group acylation now. Therefore, usage of acyl cyanides for the selective acylation is primarily limited to substrates with the axial hydroxyl groups or substrates with equatorial groups next to the axial substituents.

entry	Starting material	3-5b : 3-5c
1	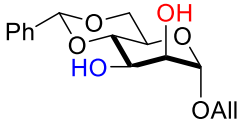	**85:15**
2	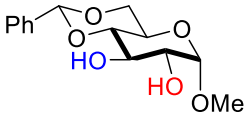	**89:11**
3	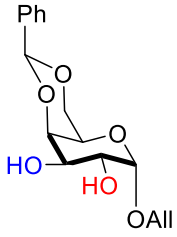	25:64

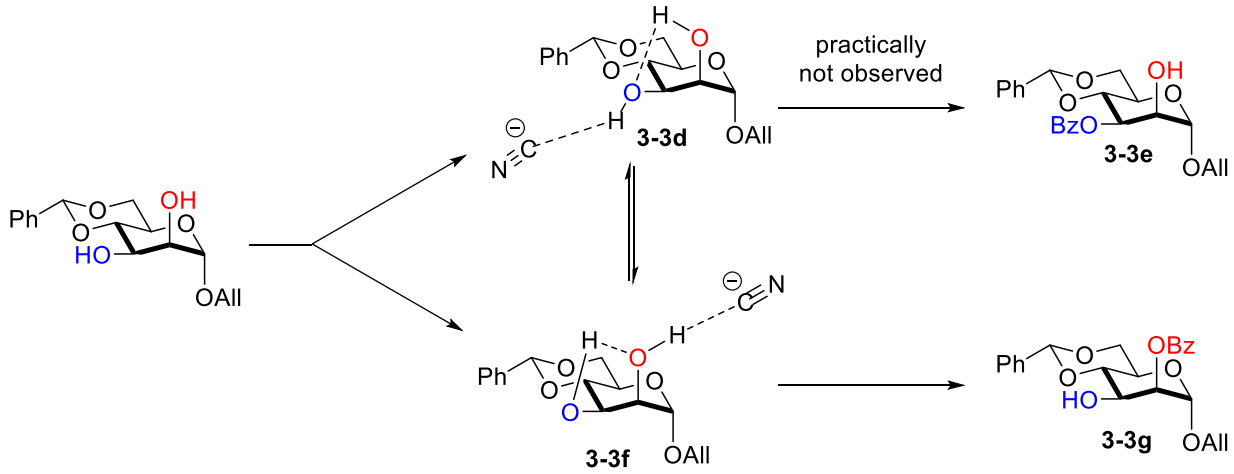

Table 3.3 Site-selective functionalization of diols using DMAP and BzCN.

In addition to the Lewis base activation of the acylating agents, neutral reagents have been developed to control the site-selective functionalization of monosaccharides. The Ye group reported potassium iodide (KI) catalyzed regioselective esterification of pyranosides in the presence of silver(I) oxide.[14] Their initial results showed promising selectivities for the C3-

selective acylation, benzoylation, and tosylation of glycopyranosides regardless of either the α- or β-configuration at the anomeric position was used (Table 3.4A entries 1-5). However, not all substrates provided high selectivities as the tosylation of methyl 4,6-O-benzylidene-α-D-galactopyranoside resulted in **3-4c** in only 72:26 r.r. (entry 6). Further studies indicated that this is not an exception, and that the C3-regioselectivity is not always observed when β-thiophenyl group is attached to the anomeric position. Thus, in the case β-thiogalactoside, acylation allowed them to obtain 87% of **3-4c**, but benzoylation favored **3-4b** in 70% yield (entries 7 and 8). However, under the same condition for the β-thioglucoside, both acylation and benzoylation favored **3-4b** in 74 % and 86% yield correspondingly (entries 10 and 11). However, highly C3-selective tosylation leading to product **3-4c** could be obtained in in each case (entries 9 and 12).

Ye and co-workers hypothesized that the preferences for the C3- or C2- product are dictated by the way the internal hydrogen bonds between the C2 and C3 hydroxyls are set up (Table 3.4B). If such a hydrogen bond is formed between the H_b and O_a **(3-4d)**, the acidity of H_b is decreased, allowing Ag_2O to deprotonate/coordinate H_a and increase the nucleophilicity of O_a thus leading to the regioselective functionalization at the C3-OH position. If the directionality of this hydrogen bond is reversed **3-4e** (i.e. the H_a and O_b case), the selectivity is also reversed. However, the mechanistic studies explaining the switch of regioselectivity from the acyl group to benzoyl group in β-thiogalactoside (entries 7 and 8) and the switch of acylation from thiogalactoside to thioglucoside (entries 7 and 10) are insufficient and the precise origins of these effects are yet to be established. Therefore, there are significant limitations due to the lack of generalization and good predictive model that would allow to predict the regioselectivity of the protection using KI and Ag_2O as electrophile/hydroxyl activators.

(A)

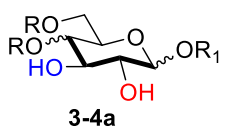

3-4a

Ag_2O (1.5 equiv)
KI (0.2 equiv)

RCl (1.1 equiv)
CH_2Cl_2, r.t.

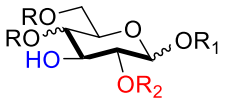

3-4b

+

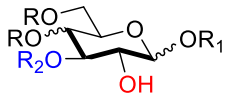

3-4c

entry	starting material	R_2	**3-4b**	:	**3-4c**
1	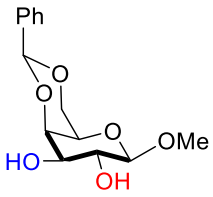	Ac	<5	:	95
2		Bz	<2	:	98
3		Ts	<2	:	98
4	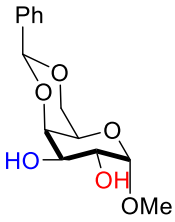	Ac	<5	:	95
5		Bz	<2	:	98
6		Ts	26	:	72
7	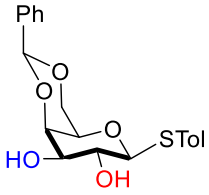	Ac	12	:	87
8		Bz	70	:	12
9		Ts	<5	:	87
10	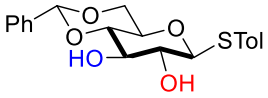	Ac	74	:	20
11		Bz	86	:	13
12		Ts	<3	:	97

(B) Plausible mechanism

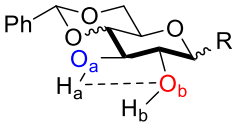

3-4d

VS

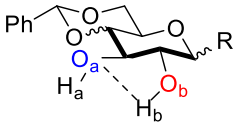

3-4e

Table 3.4 (A) Examples of site-selective functionalization of diols using KI catalyst (B) Plausible mechanism for selective functionalization of diols.

In addition to the aforementioned methods, tin(IV)-alkoxides have been extensively used to achieve regioselective functionalization of hydroxide moieties in sugar polyols.[15] Ever since their discovery, there have been a lot of studies focused on using tin(IV) reagents to accomplish

regioselective alkylations, acylations or even glycosylations.[16] One of the very first studies of tin(IV) alkoxides was conducted by the Szmant group.[17] Szmant and co-workers found that tin(IV) alkoxides derived from 4,6-O-benzylidene-α-D-glucopyranoside, 4,6-O-benzylidene-α-D-galactopyranoside, or 4,6-O-benzylidene-α-D-allopyranoside could be selectively benzoylated at the C2-positions with up to 91:5 r.r. of **3-5b** and **3-5c** (Table 3.5 entries 1-3). However, substrates without the axial methoxy group, such as methyl 4,6-O-benzylidene-β-D-glucopyranoside, are benzoylated in poor selectivity (30:20 r.r., entry 4). Similarly poor selectivities were observed with methyl 4,6-O-benzylidene-α-D-mannopyranoside, for which 25:35 r.r. was observed (entry 5). Thus, the use of Sn(IV)-based methods may lead to the promising regioselectivities for the cases when the hydroxyl groups are in *cis*-arrangements or have cis-substituents that can complex with Sn(IV) next to them. However, for the sugars containing only equatorial substituents, selective functionalization of Sn(IV) alkoxide is challenging. Another significant drawback of this method is that it requires the use of a stoichiometric amount of tin(IV) reagent, which creates problems with waste handling as Sn(IV) derivatives are toxic to a variety of organisms.[18] Further studies showed there is obligatory use of stoichiometric amounts of tin(IV) reagent as the reaction pathway proceeds through the formation of methyl 4,6-O-benzylidene-2,3-O-dibutylstannylene-α-D-glucopyranoside. This five-membered stannylene ring is considered to be more stable in pyranoside containg a α-methoxyl group due to the coordination between Sn(IV) and anomeric methoxy group (**3-5d**). Therefore, methyl 4,6-O-benzylidene-b-D-mannopyranoside could not result in high regioselectivity because of the lack of this coordination due to the strained nature of the bis-coordinated Sn(IV) alkoxide intermediate (**3-5e**). Even though tin(IV)-alkoxide-based methods have shown promise at controlling the regioselective functionalizations, these methods

suffer from significant limitations as far as the substrate scope is concerned and their large scale use is limited by the toxicity of Sn(IV) reagents and side-products.

(A) Site-selective benzoylation with different monosaccharides

3-5a **3-5b** **3-5c**

entry	starting material	**3-5b**	:	**3-5c**
1	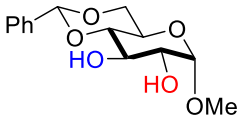	85	:	<5
2	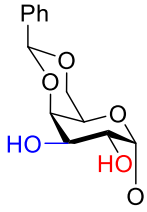	62	:	<5
3	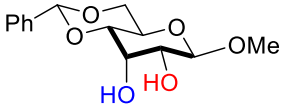	91	:	<5
4	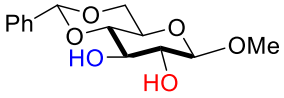	30	:	20
5	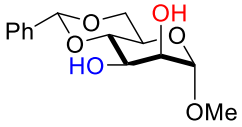	25	:	35

(B) Reaction pathway of forming stannylene complex

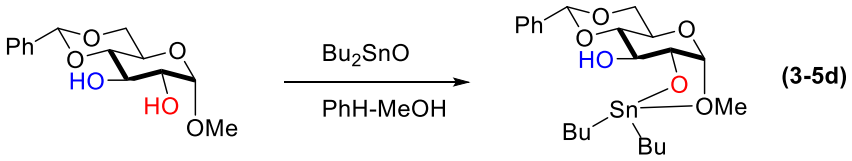

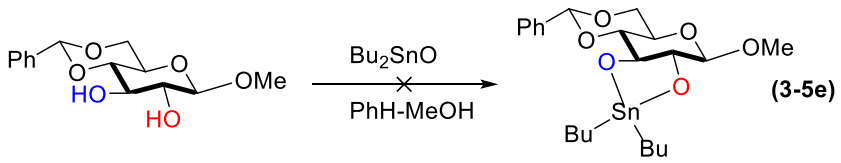

Table 3.5 (A) Examples of site-selective functionalization of diols using tin catalyst (B) Reaction pathway for selective functionalization of diols.

3.3. Overview of chiral catalysts-controlled methods for the regioselective functionalization of carbohydrates.

Since most of the previously reported methods are highly dependent on the substrate structural features, a lot of the recent studies have been focused on using chiral-based catalysts to discriminate between the axial and equatorial hydroxyl groups and to differentiate the hydroxyl groups that are in similar steric and electronic environment.

Among the various significant contributions in using chiral catalysts to control the course of regioselective functionalization of saccharides are the ones by the Tang group. The Tang group explored the commercially available benzotetramisoles (BTMs) as the catalysts for the regioselective esterification of *trans*-1,2-diols **3-6a** (Scheme 3.2).[19] When (*R*)-BTM **3-6A** was used, the C3-ester **3-6b** was obtained in 92% yield and more than 20:1 r.r.; while using the enantiomeric catalyst (*S*)-BTM, the C2-ester **3-6c** was produced in 91% yield, also with greater than 20:1 r.r. In contrast, the use of achiral catalyst, such as DMAP, resulted in no regioselectivity. Based on the computational studies in collaboration with Peng and coworkers, they hypothesized that the catalytic cycle begins with the nucleophilic addition of **3-6A** to anhydride forming the positively charged acylated BTM intermediate **3-6d**. Then, **3-6d** undergoes association with **3-6A** due to the lone pair electrons on the C4 oxygen interaction with the electron deficient acylated catalyst, which allows the C3-hydroxyl group to abstract the acyl group from the **3-6d** to do the esterification. The acylation of the C2-hydroxyl group was less favored with **3-6A** due to the steric interactions with the C1-axial OMe group of the substrate. However, when using enantiomeric catalyst **3-6B**, the steric interactions with the catalyst prevented the C4-OH group coordination

with the catalyst. Instead, **3-6B** forms a much stronger cation-lone pair electron interaction with the C3-OH group, but not with C2-OH due to steric clush with the anomeric axial OMe group. Therefore, the use of enantiomeric catalyst **3-6B** favors the C2-esterification pathway. Even though Tang and co-workers have demonstrated that the use of enantiomeric chiral catalysts may lead to the regiodivergent functionalization of saccharides, their method is limited as far as the substrate scope is concerned. For instance, when b-anomer of **3-6a** was subjected to the same acylation conditions, the catalyst **3-6A** indeed provided the regioselective C3-OH acylation in 90% yield and 20:1 r.r.; however, the reaction with catalyst **3-6B** was not selective.

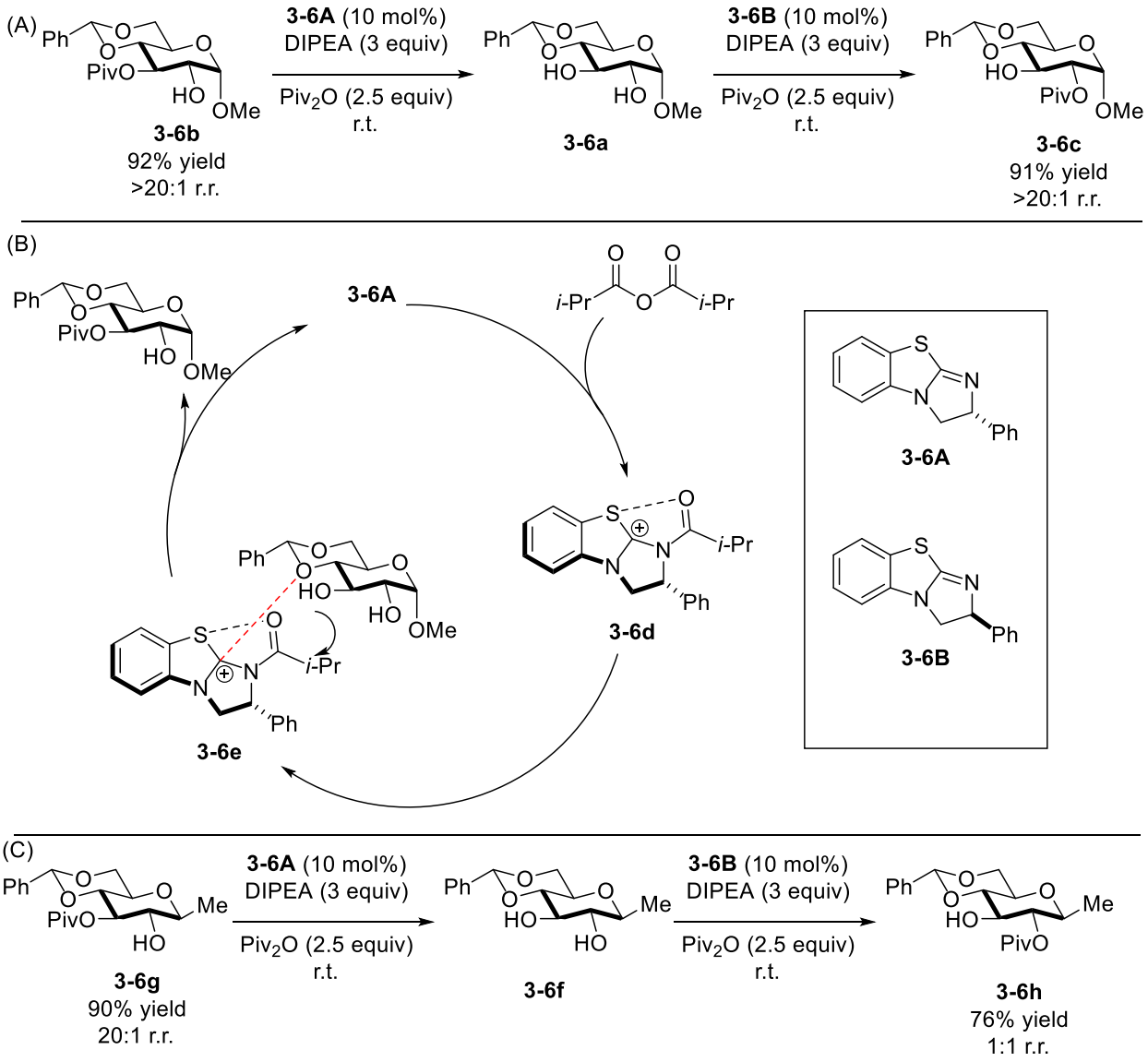

Scheme 3.2 Tang's methods (A) using chiral BTM catalysts regioselective acylate methyl 4,6-O-benzylidene-α-D-glucopyranoside. (B) proposed mechanism. (C) using chiral BTM catalysts regioselective acylate methyl 4,6-O-benzylidene-β-D-deoxyglucopyranoside.

In 2013, Tan and coworkers have demonstrated the utility of covalent chiral catalysis for achieving regiocontrolled protection of monosaccharides as well as complex natural products (Scheme 3.3).[20] The authors developed acetal-based catalysts **3-7A** and **3-7B** that contain orthoamide functionalities. In the presence of acid, these catalysts may undergo S_N1-type of reaction with the substrate and substitute the MeO group with a hydroxyl group of the substrate.

This mode of binding to substrate through a reversible covalent bond has many advantages that include minimizing the number of interactions necessary for high selectivities, lowering the energy barriers, maximizing the effective substrate localization, and enabling the desired proximity conformational effects. For instance, when D-mannose-based substrates were tested, Tan and co-workers found that in the presence of catalyst **3-7A**, a regioselective functionalization of the C2-OH resulting in products **3-7a** was observed. The authors discovered that this reaction is compatible with various electrophiles, and triethyl silyl (TES), acyl, and mesyl protecting groups were installed in 84%, 74% and 80% yield and 90:10, 84:9, and 91:8 d.r., respectively (Scheme 3.3A). However, when **3-7b** was used, they could reverse the selectivity, yielding product **3-7c** with TES, acyl and mesyl protecting group in 98%, 99% and 97% yield and 0:100, 15:84, and 0:100 d.r., respectively. In addition to the aforementioned D-mannose example, the Tan group demonstrated that their methods are applicable to achieve protection of 8 monosaccharides with great regioselectivity and reactivity. However, even though Tan's approach provides simple and yet effective way to achieve regiodivergent functionalization of monosaccharides, their major limitation is the requirement of containing a α-methoxyl group at the anomeric position. The observed selectivity trends are different with the substrates that have b-configuration of the anomeric position. An example of such substrate is **3-7d** containing C1-b-alkoxy substituent (*cf.* Scheme 3.3B). Its functionalization at the C2-position was accomplished with catalyst **3-7A**, in 90% yield and 95:5 r.r. However, the functionalization at the C3-OH group with **3-2B** turned out to be more challenging due to the presence of the b-anomeric substituent, and the C4-protected product **3-7f** was isolated as major product in only 63% yield and 77:10 r.r. while the expected C3-product was isolated in less than 13% yield.

Another additional factors that hinder the use of this method is the lack of the mechanistic and computational studies that would provide a reliable predictive stereochemical model. Tan and co-workers hypothesized that the covalently linked catalyst interacts with the diol moiety via hydrogen bond network, which results in differentiation of the hydroxyl groups and activation of a specific hydroxyl for the protection. At the same time, the precise factors resulting in the selectivity and the detailed understanding of the mechanism for these remarkable transformations are yet to be established.

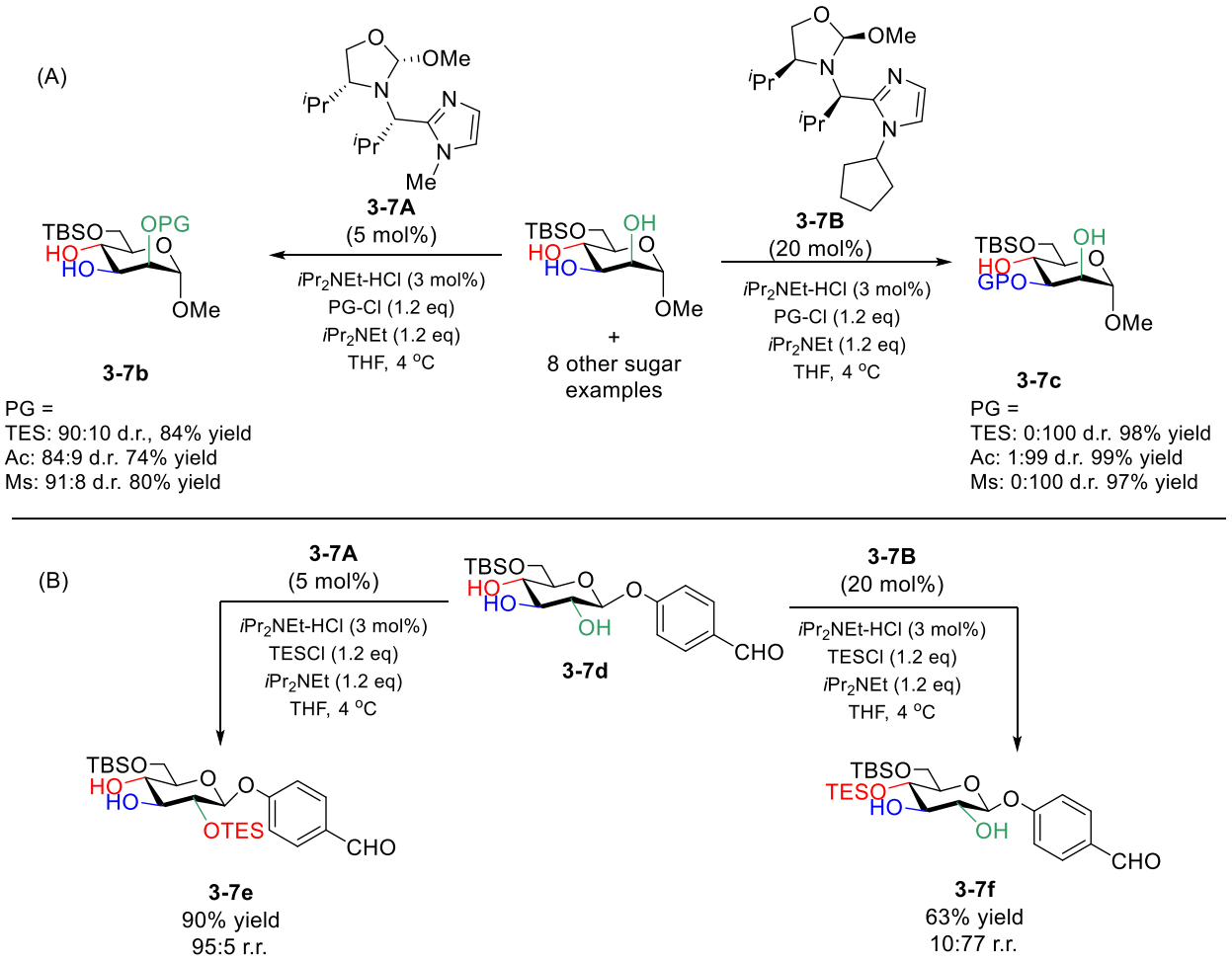

Scheme 3.3 Tan's methods of using chiral oxazolidine catalyst to regioselective functionalization of (A) α-D-glucopyranoside (B) β-D-glucopyranoside.

In addition to the Tan and Tang groups of using chiral catalysts in site-selective functionalization of monosaccharides, multiple groups has reported using peptide-based chiral catalysts to regioselective protect erythromycin A[21], vancomycin[22,23], and lanatoside C[24] (for details, see chapter 1, Scheme **1.4-1.6**). Collectively, these results suggest that chiral catalysts might be of great utility for the site-selective functionalization of monosaccharides.

Based on the promising results obtained for the CPA-controlled enantio- and diastereoselective spiroketalization reactions disclosed in 2012, the Nagorny group explored the use of CPAs for the site-selective functionalization of monosaccharides and in 2013 they described CPA-catalyzed regioselective protection of monosaccharide-based diols with acetal-based protecting groups (Scheme 3.4).[25] Acetal formation is a classical organic chemistry transformation that is believed to proceed through S_N1-like mechanism involving highly reactive oxocarbenium ion intermediates. The formation of the high energy oxocarbenium ions is typically a rate-limiting step while their reaction with strong nucleophiles, like hydroxyl groups, is very fast and proceeds unselectively. The resultant acetals are also acid labile, and equilibration/isomerization leading to the most thermodynamically stable product under the reaction conditions is common. Being very useful in organic synthesis and carbohydrate chemistry, mixed acetal protecting groups such as 1-methoxycyclohexyl (MOC) and 2-methoxy-2-propyl (MOP) are very sensitive to acids and may easily hydrolyze back to hydroxyl groups, allowing acetals to be ideal protecting groups to install and easily to remove.[17]

In order to demonstrate the application of CPAs in controlling regioselective functionalization of diols, Nagorny and coworkers initially selected a D-glucose-based diol **3-8a**. Their control studies with **3-8a** demonstrated that when achiral catalysts $(PhO)_2PO_2H$ or PPTS were used, there was almost no regioselectivity (**Table 3.6.** entries 1 and 2). Subsequent evaluation

of chiral phosphoric acids as the catalysts (entries 3-12) demonstrated that CPAs containing 2,4,6-functionalized aryl substituents at the 3,3'-positions of the BINOL scaffold were uniquely selective for promoting the regioselective formation of **3-8b** (entries 6, 10, 12) or **3-8c** (entries 5 and 9). Among these results it was noted that (*R*)-enantiomers of CPA favored the formation of the C2 product **3-8b** while the (*S*)-enantiomers exhibited low levels of selectivity for **3-8c**. Thus, when catalyst **(*R*)-3-8D** was tested, significant selectivity favoring C2-OH was observed (19:1 r.r., entry 10), even though its enantiomer **(*S*)-3-8D** led to only ~1:4 r.r. (entry 9). Among the evaluated CPAs, catalyst **(*R*)-3-8E** provided the greatest selectivities for the formation of **3-8b** (25:1 r.r., entry 12).

However, selective acetalization of a single alcohol moiety within a sugar-derived diol possessing alcohols in similar steric and electronic environment represents a challenge. Consistent with these general principles, Nagorny and co-workers investigated acetalization of sugar-based diols with various achiral sulfonic acids (*p*-TsOH, CSA, etc.) and achiral phosphoric acids (DPPA and BPPA). As expected for the classical reactions involving diffusion-controlled reactions of oxocarbenium ions and strong nucleophiles, little regioselectivity was observed for the protection of the C2- and C3-positions, and approximately equimolar mixtures of the C2 and C3 protected acetals were obtained in each instance in low yields.

In order to demonstrate the application of CPAs in controlling regioselective functionalization of diols, we initially selected glucose-based diols to optimize CPA catalysts. Our studies showed that when achiral catalysts were used, there was almost no regioselectivity (**Table 3.6.** entries 1 and 2). However, when switching to chiral phosphoric acids, we observed much better regioselectivity, and different regioselectivities could be obtained using different enantiomer of CPAs with up to 3:1 r.r. (entries 5 and 6). When catalyst **(*R*)-3-8D** was tested, we observed significant selectivity favoring C2-OH, up to 19:1 r.r. (entry 10), even though its enantiomer **(*S*)-**

3-8D led to only ~1:4 r.r. (entry 9). Further optimization of catalysts showed that **(*R*)-3-8E** outperformed the rest of CPAs with greater than 25:1 r.r. (entry 12).

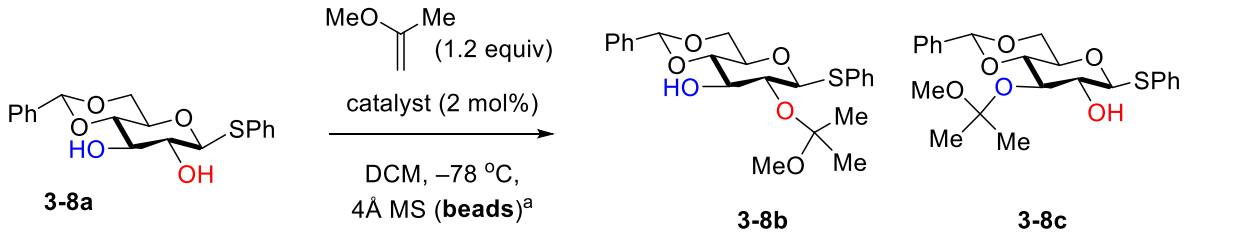

Entry	catalyst	Conv. (%)[b]	3-8a[c]	:	3-8C[c]
1	$(PhO)_2PO_2H$	>95	1	:	1.2
2	PPTS	>95	1	:	1
3	(*S*)-**3-8A**	>95	1	:	1.6
4	(*R*)-**3-8A**	25	1	:	1.7
5	(*S*)-**3-8B**	92	1	:	3.0
6	(*R*)-**3-8B**	>95	3.8	:	1
7	(*S*)-**3-8C**	>95	1	:	1.1
8	(*R*)-**3-8C**	93	1	:	1.7
9	(*S*)-**3-8D**	90	1	:	3.7
10	(*R*)-**3-8D**	>95	19	:	1
11	(*S*)-**3-8E**	69	1	:	1.7
12	(*R*)-**3-8E**	>95	>25	:	1

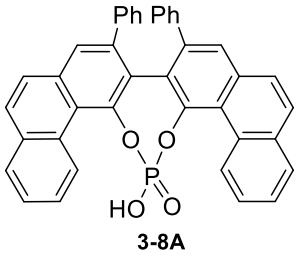

3-8A

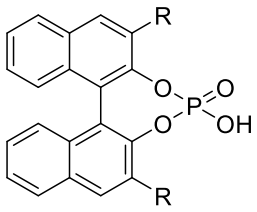

3-8B, R = 2,4,6-*i*Pr$_3$C$_6$H$_2$
3-8C, R = 3,5-(CF$_3$)$_2$C$_6$H$_3$
3-8D, R = 2,4,6-Cy$_3$C$_6$H$_2$
3-8E, R = 4-(1-adamantyl)-2,6-*i*Pr$_2$C$_6$H$_2$

The reactions were performed with 2 mol% of catalysts at either –78 ºC (2-MOP-protection) on 0.056 mmol scale (0.042 M solution) for 18-24 h in the presence of 4Å MS. The rr values were determined by ^{1}H NMR analysis of the crude reaction mixtures of the products as well as their acetylated derivatives.

Table 3.6 Evaluation of the catalysts for regioselective acetalization of diols.

With the (*R*)-**3-8E** in hand, Mensah *et al.* investigated other electrophiles and discovered that this transformation was also compatible with the use of 1-methoxycyclohexene and dihydropyrane. The subsequent evaluation of substrates other than **3-8a** indicated that various *D*-glucose, *D*-galactose, and *D*-mannose-derived diols may undergo selective protection with both

THP, MOC and MOP groups. The selected examples of such reactions relevant to the studies described in this chapter are provided in Scheme 3.4. In all of these cases, control experiments that used DPPA resulted in an unselective formation of the regioisomeric products. Similarly, the reactions with enantiomeric (*S*)-**3-8E** were also unselective for the *D*-sugars (substrates **3-10a-3-10e**), but selective with the *L*-fucose-derived triol **3-10f** resulting in the C3-protection in 52% yield and >25:1 rr. However, with the (*R*)-enantiomer of **3-8E**, the opposite outcome was observed, and selective acetalization at the C2-position of the *D*-sugars, and unselective reaction of the *L*-fucose took place. While the MOC-protections were found to be more selective than the MOP-protections, often both types of acetals were installed with similar levels of selectivity (*cf.* substrates **3-10a** and **3-10b**, Scheme 3.4). These transformations tolerated modifications of the anomeric substituent (*cf.* substrate **3-10c**) and modifications of the C6/C4 protection. The reactions with *D*-galactose derivatives were equally selective as exemplified by substrate **3-10d** (51% yield, >25:1 rr). While *D*-mannose was successfully subjected to the MOP-protection at the equatorial C3-position (60% yield, 13:1 rr), the corresponding MOC-protection was sluggish and provided the corresponding MOC acetal in low conversions. Altogether, the observed selectivities with **(*R*)-3-8E** differed from the selectivities observed for the functionalization with achiral reagents (*vide supra*). This coupled with the fact that these transformations featured mild reaction conditions and required the use of easily available and non-toxic electrophiles such as dihydropyrane (DHP), 2-methoxypropene (2-MP), and 1-methoxycyclohexene (1-MCH) prompted us to investigate the use of this transformation for the synthesis of differentially protected monosaccharides described in this chapter.

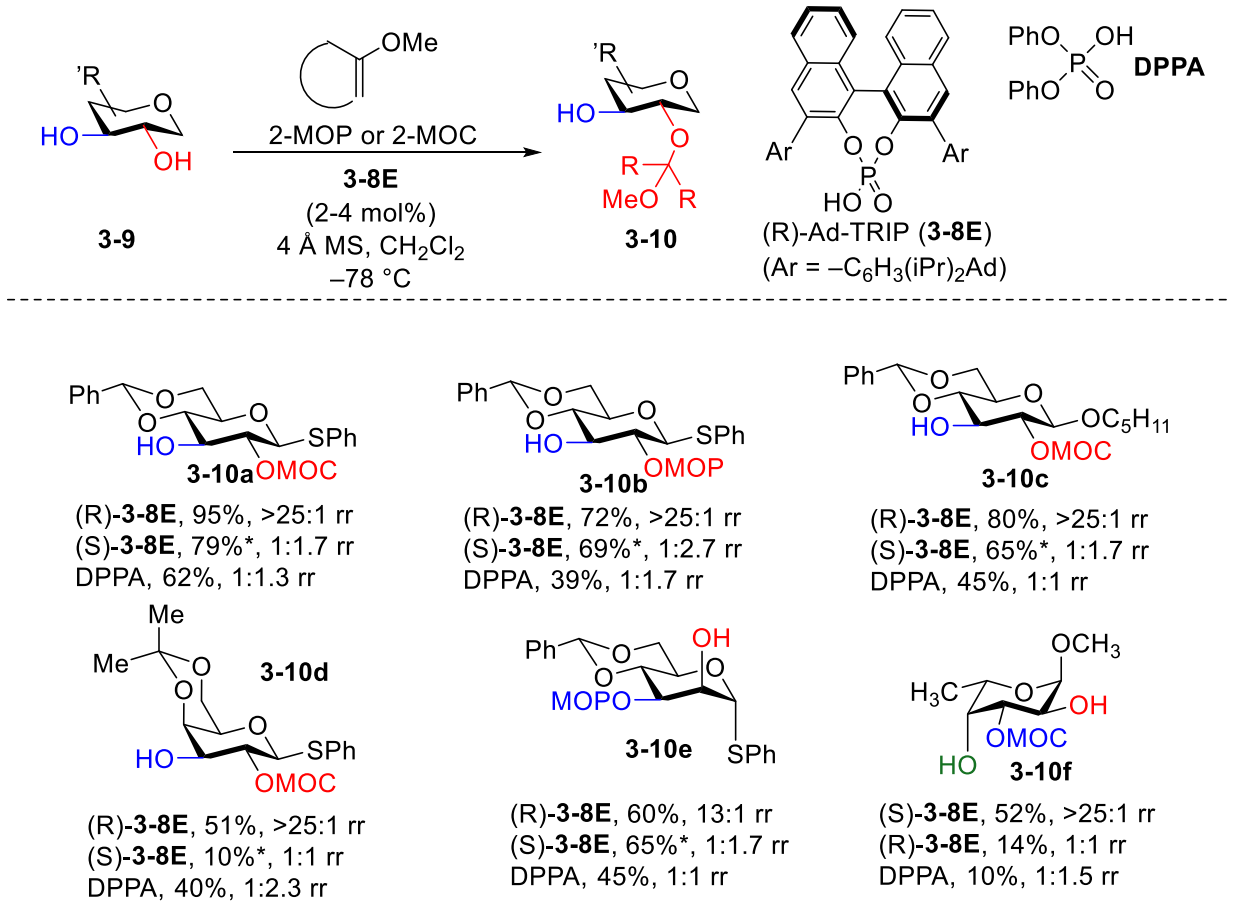

Scheme 3.4 Selected examples of regioselective acetalization using CPAs.

Mixed acetal protecting groups such as MOC and MOP are unstable to even trace amounts of acids, but stable to a variety of the basic and neutral conditions. Therefore, the installation of the MOP and MOC groups may be viewed as the traceless protection of the carbohydrate moiety that could be combined with a variety of other transformations. One particular application of this chemistry that we decided to pursue was inspired by the recent work of Hung and coworkers, in which they were able to access a variety of differentially protected D-glucose derivatives using single-pot functionalizations of persilylated *D*-glucose thioglycosides.[26] Not only these methods provided access to the fully functionalized monosaccharide building blocks, but also helped to

reduce production costs and times as only one work up and single purification is needed to access the products.

Building on the aforementioned approaches, the current chapter demonstrates the use of CPA-catalyzed regioselective acetalizations for the scalable single-pot synthesis[27] of various differentially protected *D*-glucose, *D*-galactose and *D*-mannose-based mono- and disaccharides (Scheme 3.4). These telescoped single-pot multiple step protocols proceed with high selectivities and efficiencies and require minimum purifications to access valuable protected building blocks from commercially available diol precursors. To address the challenges associated with the accessibility of the catalyst (*R*)-**3-8E**, immobilized catalysts **PS-(*R*)-3-10E** was found to promote highly selective acetalization reactions and could be recycled and re-used multiple times. The use of catalyst **PS-(*R*)-3-10E** that is structurally equivalent to (*R*)-**3-8E** allowed to achieve substantial reduction of the catalyst loading (0.5 to 0.1 mol% for gram-scale reactions) and significantly improve the selectivity of acetalization for several different substrates.

3.4. Result and Discussion

While mixed acetal protecting groups are less common in carbohydrate synthesis then acyl or benzyl protection, their stability to bases and significant lability under the mildly acidic conditions offer excellent opportunities for carrying the subsequent functionalizations in a single operation (*vide supra*). Therefore, our following studies were focused on demonstrating that regioselective products **3-10a**-**3-10s** are of great utility for the telescoped preparation of differentially protected monosaccharide derivatives from commercially available building blocks such as **3-9a**. Inspired by the streamline method for the single-pot synthesis of various *D*-glucose derivatives by the Hung and coworkers,[28] Dr. Jeonghyo Lee investigated one-pot derivatizations of **3-10a** (Scheme 3.5). Considering that both the MOC and 2-MOP protecting groups are highly

labile in the presence of an acid (*vide supra*), our single pot protocol included *in situ* removal of the MOC protection with 0.05 M HCl without deprotecting the 4,6-benzylidine acetal. The high volatility of 0.05 M HCl solution in DCM was also suitable for the overall single-pot functionalization process as it could be removed by passing a nitrogen stream over the reaction mixture without the necessity of carrying the reaction work up.

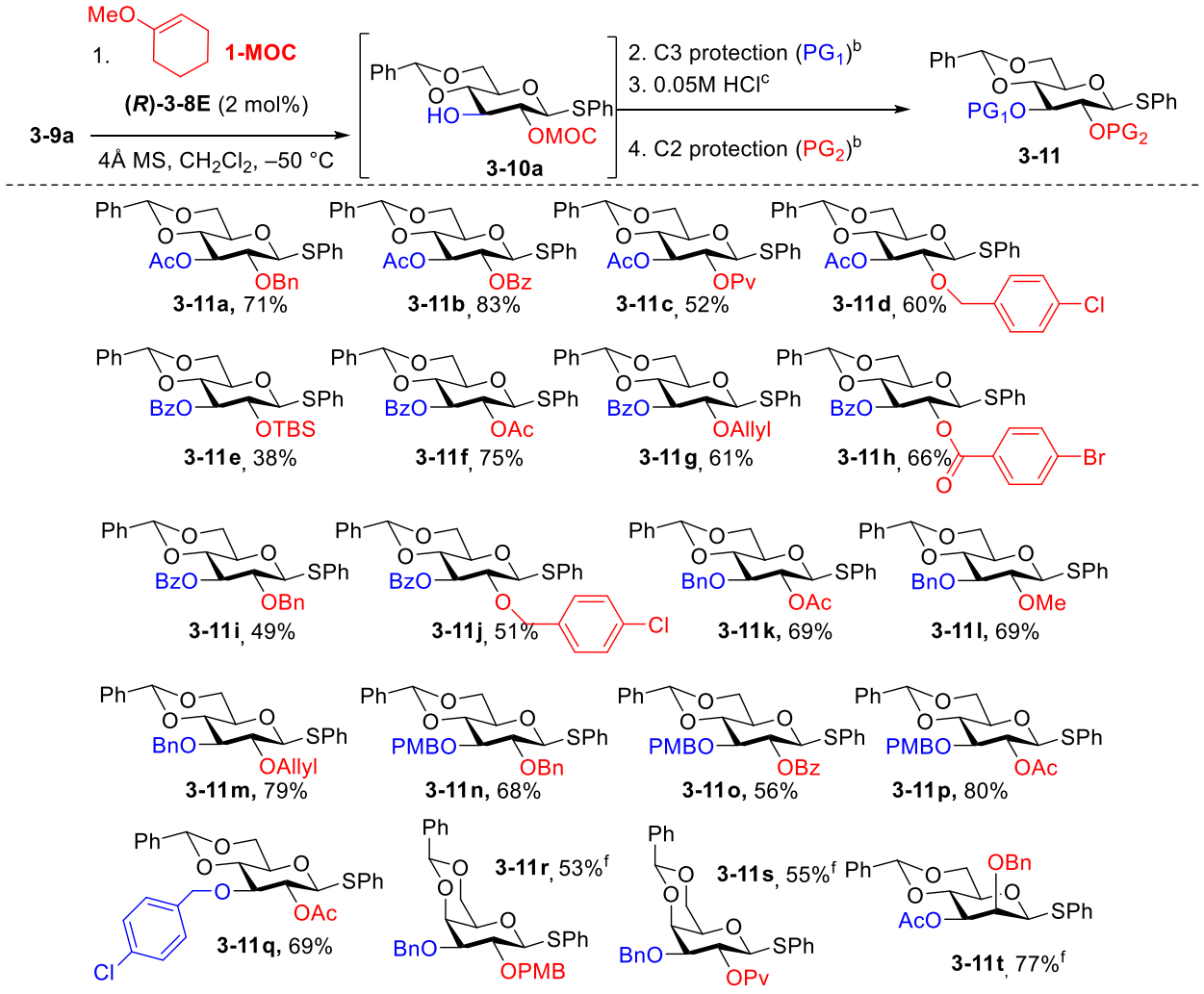

[a]Isolated yield after one-pot sequence leading to **3-11**. The reaction mixtures were concentrated by the stream of N_2 prior to each protection step. Unless noted otherwise, these experiments were carried on 0.056 mmol scale. MOC protection was accomplished as described in Scheme 3.4. [b]Acylations were carried using Ac_2O (1.1 equiv), DMAP (10 mol%), Et_3N (5.0 equiv) or BzCl (1.2 equiv), DMAP (20 mol%), Py (10 equiv). Alkylation was accomplished by addition of NaH (1.2 equiv), alkyl halide (1.1 equiv), TBAI (0.1 equiv) and DMF (cat). [c]The MOC cleavage was achieved by addition of 0.05M HCl in CH_2Cl_2 (pH=5).

Scheme 3.5 Regioselective single-pot synthesis of the differentially protected mono- and disaccharide derivatives enabled by (*R*)-3-8E-catalyzed regioselective MOC- and MOP-protections.[a] Experiment were performed by Dr. Jeonghyo Lee.

The one-pot transformations leading to differentially protected C2/C3 products **3-11a-3-11t** (Scheme 3.5) commenced with CPA ((*R*)-**3-8E**)-directed regioselective acetalization, and the resultant C2-acetal **3-10a** (or **3-10q** and **3-10s**) was successfully obtained in full conversion. At this point, the mixture was dried by sequentially applying a gentle N_2 flow and flask evacuation before the next step. Initially the crude mixture containing compound **3-10a** was subjected to free C3-hydroxyl group protection without affecting the C2-acetal. Since mixed acetals are acid- and heat- labile, acidic conditions and high reaction temperatures were avoided. The regioselective acylations of the C3-OH were accomplished using $(RCO)_2O$/Py or RCOCl/Et_3N in the presence of catalytic DMAP (substrates **3-11a–3-11j**). Alternatively, the C3-alkylation was accomplished using alkyl halides and sodium hydride as the base in the presence of catalytic TBAI (**3-11k–3-11t**). The C2 MOC (or MOP) acetal was removed by adding excess of HCl solution in DCM to the reaction mixture. The resultant acidic solutions were concentrated by passing N_2 stream to blow out the volatiles and subsequent evacuation of the reaction vessel, and the concentrated crude oils were subjected to the C2-protection to provide products **3-11a-3-11t** in good yields (49-83% overall yield). In addition to the *D*-glucose-based derivatives **3-11a-3-11q**, this method was also successfully applied to generate *D*-galactose-based substrates **3-11r** and **3-11s** as well as *D*-mannose-derived substrate **3-11t** using MOP (rather than MOC) protection strategy. Unlike other substrates, *D*-mannose derivative **3-10s** contained MOP acetal at the C3 position, which required functionalization in a reverse way (C2-benzylation, C3-acetal cleavage, and C3-acetylation) to afford compound **3-11t** in good overall yield (77%) and selectivity (>12:1 rr for the first step).

It is noteworthy that while some of the derivatives (i.e. **3-11k–3-11q**) might be potentially accessible through one-pot glucose functionalization strategy developed by the Hung group, one-pot synthesis of the derivatives **3-11a–3-11j** featuring the C3 acyl protection has not been previously described and would be challenging to accomplish via a single-pot protocol in good yields. Similarly, previously published one-pot protection protocols could not be readily adopted to the synthesis of *D*-galactose and *D*-mannose derivatives similar to **3-11r–3-11t**. Finally, the operational simplicity for the deprotection of the MOC and MOP groups allows to expand the scope of the protecting groups (to include substrates like **3-11e**) and achieve flexibility in controlling the C2/C3 protection to generate regioisomeric substrates like **3-11d** and **3-11q** in similar yields (60% and 69%, correspondingly).

These transformations could be further combined with benzylidene acetal opening/C4 protection steps to accomplish single-pot generation of differentially protected *D*-glucose derivatives **3-12a–3-12f** depicted in Scheme 3.6. Thus, the previously developed protocol included regioselective benzylidene acetal reduction with CF_3CO_2H/Et_3SiH leading to product containing free C4 alcohol that was subsequently protected. These single-pot transformations proceeded in 25-38% overall yield (~85% yield per operation) with high levels of overall regiocontrol. These procedures were scalable, and the derivative **3-12a** was made on 1.0 g scale (31% yield).

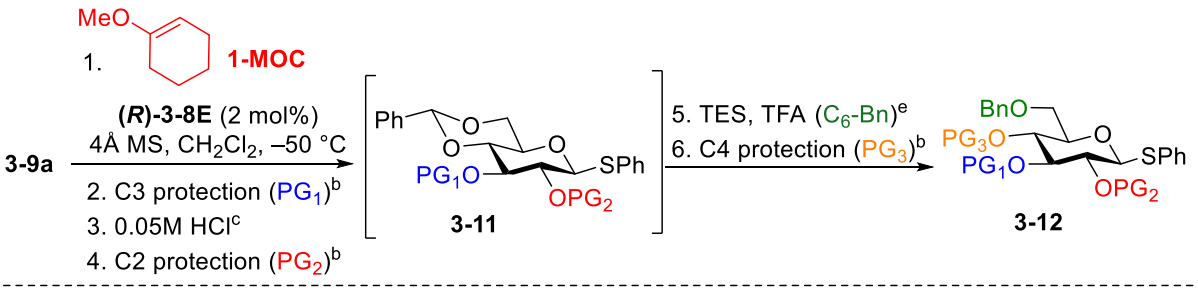

C. (Single Pot, 6 steps)

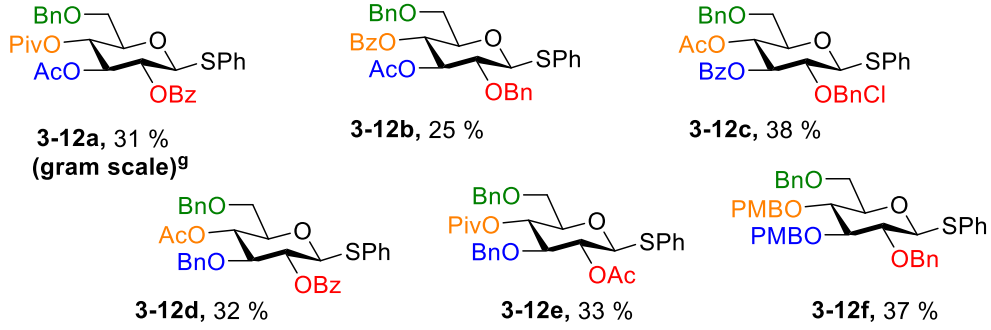

[a]Isolated yield after one-pot sequence leading to **3-12**. The reaction mixtures were concentrated by the stream of N_2 prior to each protection step. Unless noted otherwise, these experiments were carried on 0.056 mmol scale. MOC protection was accomplished as described in Scheme 3.4. [b]Acylations were carried using Ac_2O (1.1 equiv), DMAP (10 mol%), Et_3N (5.0 equiv) or BzCl (1.2 equiv), DMAP (20 mol%), Py (10 equiv). Alkylation was accomplished by addition of NaH (1.2 equiv), alkyl halide (1.1 equiv), TBAI (0.1 equiv) and DMF (cat). [c]The MOC cleavage was achieved by addition of 0.05M HCl in CH_2Cl_2 (pH=5). [d]Benzylidene acetal cleavage was accomplished using Et_3SiH (5 equiv), CF_3CO_2H (5 equiv), DCM, 0 °C, 2h. [e]The synthesis of **3-12a** was carried on 1.0 g scale.

Scheme 3.6 Regioselective single-pot synthesis of the fully and differentially protected mono- and disaccharide derivatives enabled by (*R*)-3-8E-catalyzed regioselective MOC- and MOP-protections.[a] Experiment were performed by Dr. Jeonghyo Lee.

The aforementioned results demonstrate that CPA-catalyzed regioselective acetalizations are of great use for the single pot protection and glycosylation of monosaccharides. While this method allows to expand the repertoire of sugar derivatives and transformations developed from Hung[26], it suffers from the obligatory use of expensive chiral acid **(*R*)-3-8E**. We surmised that the costs associated with the use of **(*R*)-3-8E** could be dramatically reduced if the catalyst is

immobilized on solid support as numerous recent studies suggest that such catalysts could be readily recovered and recycled or employed for the catalysis in continuous flow.[29]

Initially developed by the Rueping group, polymer-supported CPAs (PS-CPAs) have been used to catalyze heterogeneous transfer hydrogenation of quinolines (Scheme 3.7).[30] In the control studies, the use of monomeric **3-13A** for the homogenous transfer hydrogenation resulted in 65% ee (entry 1). The use of polymeric acid PS-CPAs **3-13B** lead to the similar levels of enantiocontrol (55-65% ee), but the polymeric catalyst could be easily separated from the reaction mixture, washed and directly resubjected to the next run. The authors tested recyclability of PS-CPAs **3-13B** for ten cycles, and in all of these cases the observed enantioselectivity for the reduction was 55-65% ee (entry 2). However, one of the major limitations of catalyst PS-CPAs **3-13B** is that no variation of the substituent in the 3,3'-position was possible. As demonstrated in chapter one of this thesis, the ability to modify the substituents at the 3,3'-position of CPAs is of great importance for adjusting the catalytic properties of CPAs. Therefore, having the polystyrene matrix directly attached at the 3,3'-positions significantly limits the scope of applications for such CPAs. To address this, Rueping and co-workers' carried subsequent studies, in which they were successfully produced PS-CPAs **3-13D** containing polystyrene matrix at the 6,6'- rather than 3,3' positions. This modification allowed them to widen the scope of potential immobilized CPAs as this catalyst design now allows to modify 3,3'-substituents. Remarkably, the introduction of additional functionalities at the 6,6'-position of the BINOL core led to an unexpected improvements in ee of **3-13b** from 64% to 96% (entries 2 and 4, Scheme 3.7). As before, catalyst **3-13D** was recycled and reused multiple times (10 cycles) without significant erosion in the product enantioselectivity (entry 4). This study by Rueping and co-workers highlights the potential of immobilized CPAs in reducing the costs associated with the preparation of these catalysts.

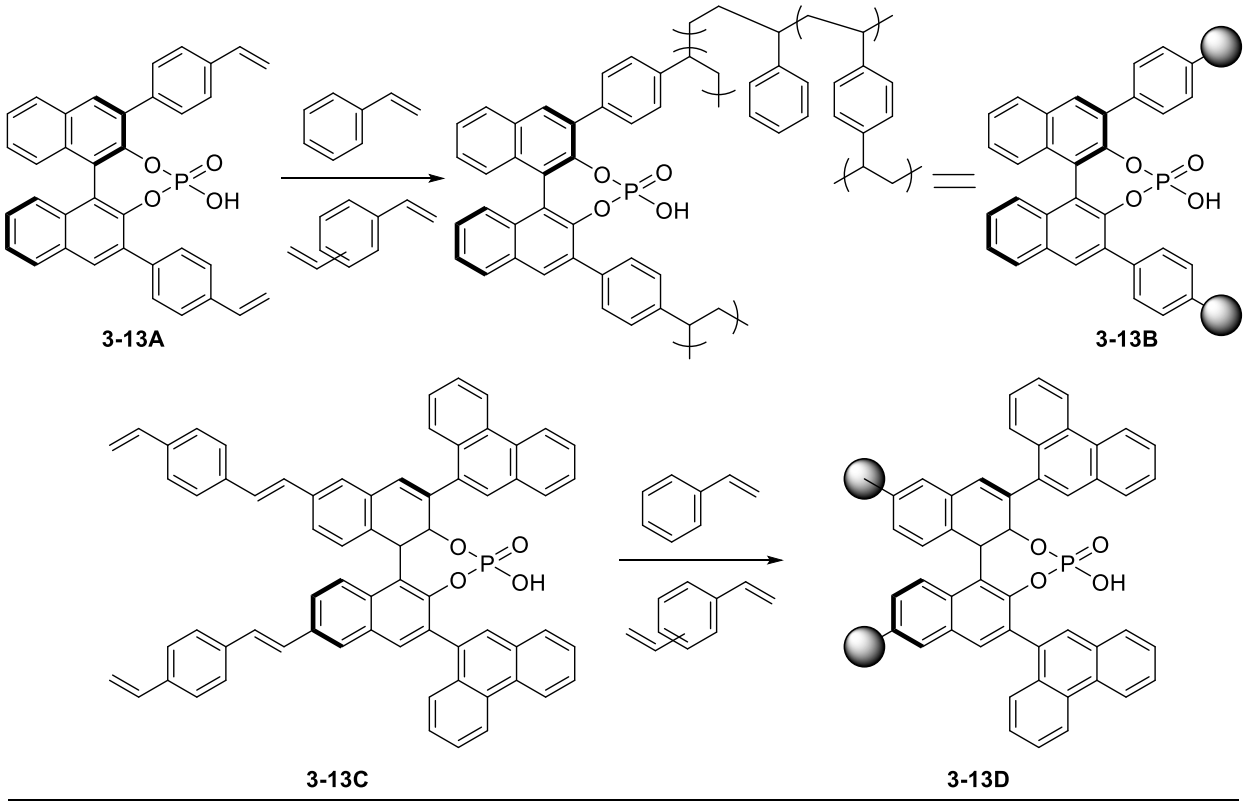

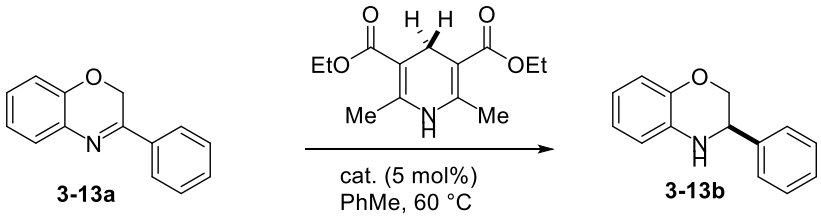

entry	catalyst	yield (%)	ee (%)	notes
1	3-13A	88	64	
2	3-13B	80-90	55-65	after 10 cycles still maintain 55-65% ee
3	3-13C	92	64	
4	3-13D	87-96	94-96	after 10 cycles still maintain 94-96% ee

Scheme 3.7 Polymerization of CPAs via styrene-based polymers.

Around the same as the aforementioned studies by the Rueping group, Thomas and co-workers have also reported a similar design of polymeric CPAs (Scheme 3.8).[31] However, unlike the Rueping and coworkers who utilized styrene-based polymerization, Thomas and co-workers used thiophene based monomer **3-14A** that underwent polymerization at the 3,3'-positions leading to the polymeric catalyst **3-14B**. Not surprisingly, even though the resultant polymeric acid **3-14B**

could promote hydrogenation of **3-14a**, the enantioselectivity for this transformation was not high (55% ee) although higher than with the monomeric catalyst **3-14A** (34% ee). The enhanced selectivity observed with the polymeric CPA was proposed to occur because the polymeric backbone is close to the reactive phosphoric acid center, which effectively enhances the steric size of the 3,3'-substituents.

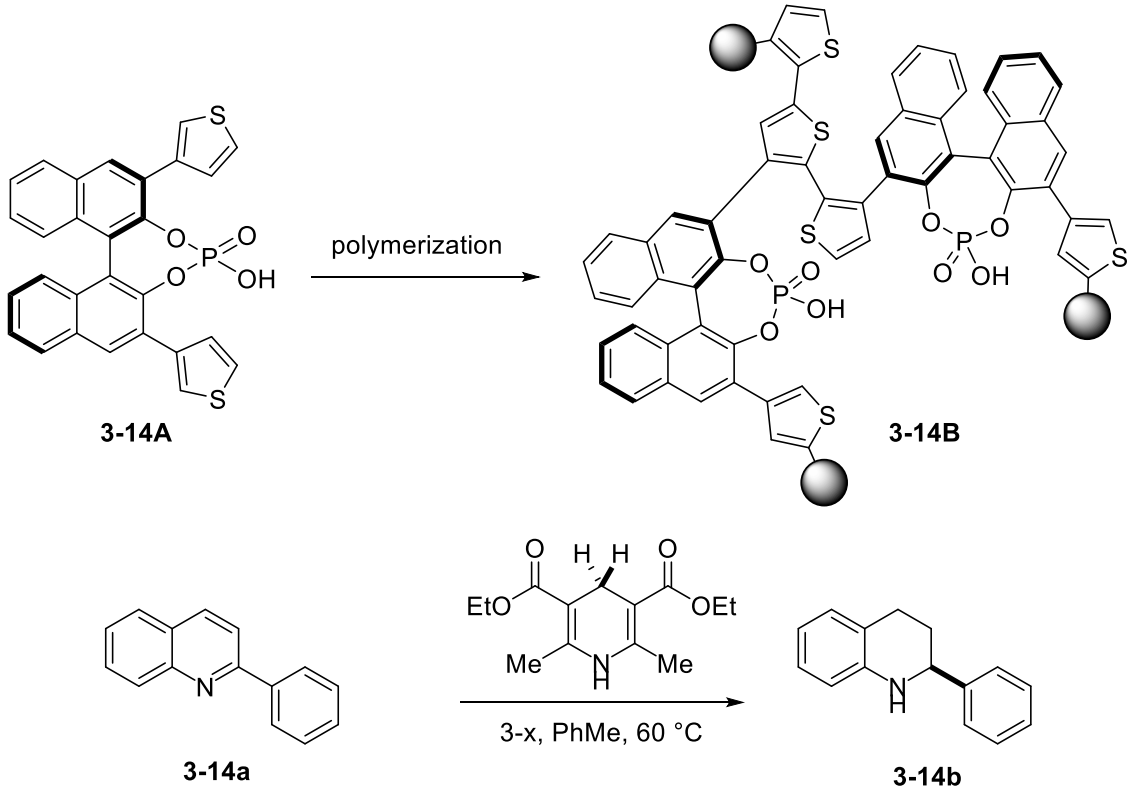

entry	catalyst	conv. (%)	ee (%)
1	**3-14A**	99	34
2	**3-14B**	99	47
3	**3-14B** 2nd run	99	54
4	**3-14B** 3rd run	99	55
5	**3-14B** 4th run	97	56

Scheme 3.8 Polymerization of CPAs via thiophene-based polymers.

Following these studies, the Pericas group have reported a polystyrene-supported 2,4,6-tris-isopropyl CPAs that has the polystyrene matrix attached at the 6,6' positions of the BINOL

core (Scheme 3.9).[32] Pericas and co-workers discovered that their immobilized catalyst **3-15A** could catalyze highly enantioselective (up to 96% ee) allylboration of aldehydes, and then be recycled and reuses for up to 18 cycles. In addition, a continuous flow variant of this reaction was also developed. These results highlight the stability and robustness of polymeric CPAs in catalysis and indicate that immobilization of the catalyst may significantly reduce the costs associated with its production and use.

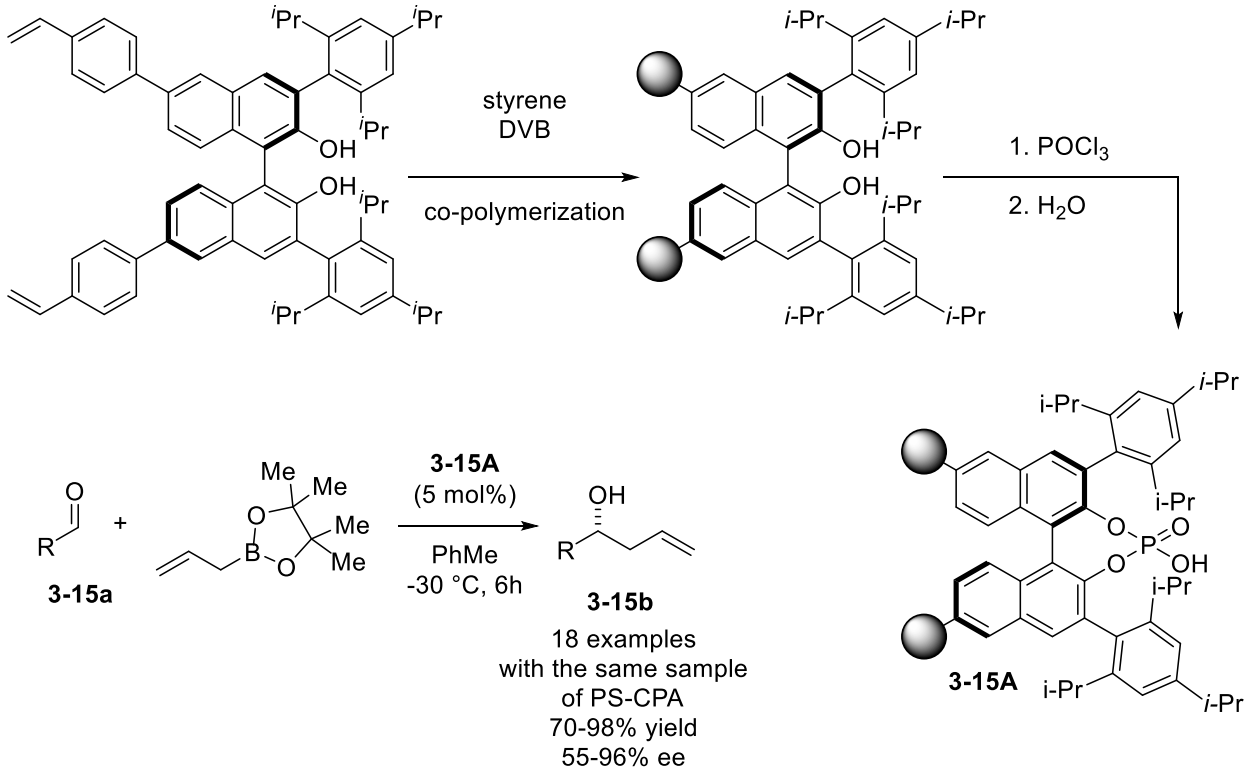

Scheme 3.9 Polymerization of CPAs via styrene and divinylbenzene-based polymers.

Therefore, the subsequent efforts were focused on developing a catalytically active immobilized version of **3-8E** (cf. Scheme 3.10).[30,33] Based on the previously developed strategies for the **3-15B** immobilization (*vide supra*),[34,35] similar method were applied for the synthesis of immobilized on polystyrene support catalyst **PS-(*R*)-3-8E**. While the previously published route

did not lead to catalytically active in acetalization reactions **PS-(*R*)-3-8E**, we were able to modify this approach (*cf.* Scheme 3.10 to produce a viable immobilized catalyst **PS-(*R*)-3-8E**. Our studies commenced with the bromination of the known derivative **3-16a** that proceeded in 92% yield on a multigram scale. However, the subsequent cross-coupling reaction turned out to be more challenging to develop. Initial exploration of the reaction conditions reported by the Pericas group did not result in the desired product **3-16c**, regardless of the quality of the boronic acid or Pd catalyst used (Table 3.7 entries 1 and 2). However, when these conditions were tried on the brominated TRIP derivative previously described by Pericas and co-workers, the desired cross-coupling product was obtained in 36% yield. This led us to believe that the adamantyl groups in **3-16b** alter its reactivity in the cross-coupling reactions, and that we would need to develop new reaction conditions that would be optimal for this specific substrate. Initially, stronger bases in various solvents were tested; however, no **3-16c** was obtained (entries 3-5). In addition, more reactive Pd catalysts were also tested with no desired product obtained (entries 6-7). With these disappointing results, we initially hypothesized that the isopropyl to admantyl group switch results in the increased hydrophobicity of **3-16b**. Therefore, polar co-solvents such as water dramatically decrease the solubility of **3-16b** in THF, which prevents the cross-coupling from happening. Therefore, the use of a less polar solvent may improve the solubility and lead to desire product. Consequently, when THF and ethanol were used as the co-solvents, for the first time, we were able to observe the desired product **3-16c** in 19% yield (entry 9). Further optimization of the reaction temperature led to 65% yield of the isolated cross-coupling product **3-16c** (entry 10).

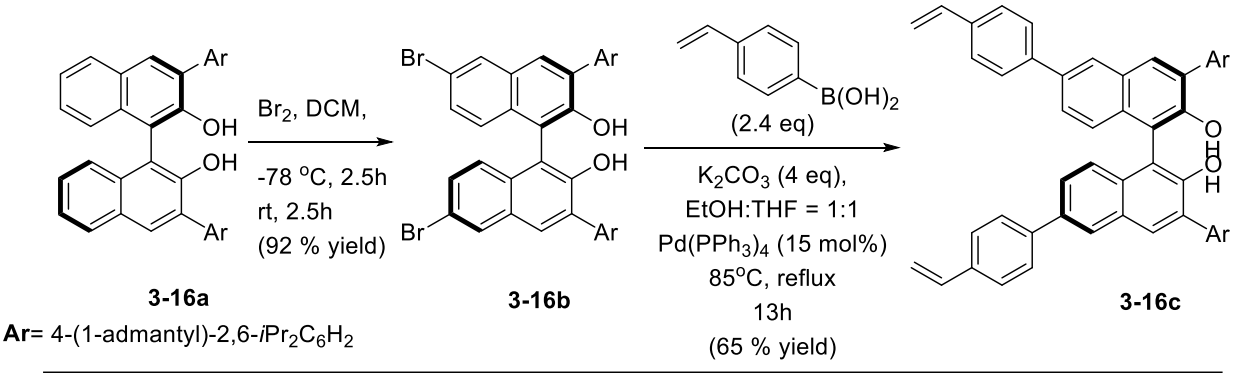

3-16a

Ar= 4-(1-admantyl)-2,6-*i*$Pr_2C_6H_2$

3-16b

3-16c

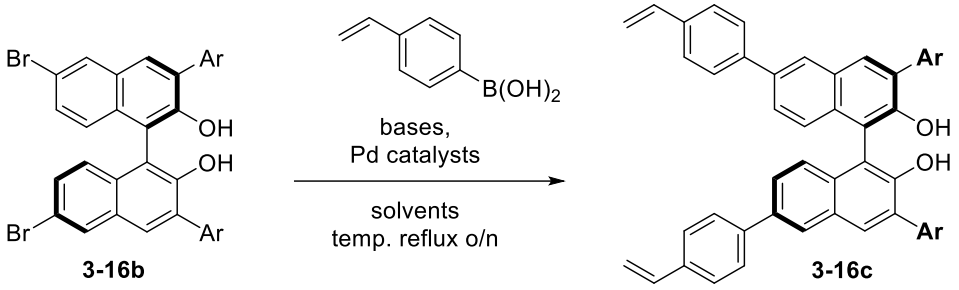

3-16b **3-16c**

entry	condition	results
1	new boronic acid	N.R.
2	new Pd catalyst	N.R.
3	TRIP model studies	36%
4	Cs_2CO_3	N.R.
5	Cs_2CO_3 in DMF at 100 °C	N.R.
6	Cs_2CO_3 in dioxane and water at 100 °C	N.R.
7	$PdCl_2$ in EtOH	N.R.
8	$Pd(dba)_2$ and KF in THF at r.t.	N.R.
9	EtOH:THF at 80 °C	19%
10	EtOH:THF reflux	60%

Table 3.7 Optimization of Suzuki cross coupling reactions.

With the Suzuki cross-coupling product **3-16c** in hand, different routes towards PS-CPAs **PS-3-8E (1-3)** were investigated next (Scheme 3-11). Based on the method previously reported by the Pericas group, both styrene and divinylbenzene were mixed as co-polymerizing reagents and the co-polymerization was catalyzed by azobisisobutyronitrile (AIBN) at 80 ℃ at 440 rpm. Thus obtained BINOL-based polymer **3-16d** underwent phosphorylation to yield **PS-3-8E-1**. However,

our subsequent evaluation of **PS-3-8E-1** in acetalization reaction resulted in only trace amount of the desired product **3-10a** being produced, and the majority of the unreacted starting material was recovered (Table 3.7, entry 3). It led us to search for an alternative route for the synthesis of **3-16e** using benzoyl peroxide as radical initiator at 1100 rpm. The subsequent phosphorylation provided acid **PS-3-8E-2**, which was also tested in acetalization reaction (Table 3.7, entry 4). This catalyst resulted in the significantly higher conversion and selectivity (83%, 22:1 r.r.), albeit these results were inferior to the ones observed with the monomeric CPA. In our attempts to further improve the polymeric catalyst, we noted that Pericas and coworkers avoided polymerizing the monomers containing the pre-installed hydrogen phosphate moiety due to their low solubility in pyridine. As the result, the strategy based on co-polymerization and then phosphorylation was adopted for the synthesis of immobilized TRIP CPA. However, our substrate contains admantyl groups, which decrease the polarity of the CPA and improve its solubility in pyridine. Based on these considerations, we generated monomeric CPAs could be obtained in 92% yield in gram scales. Followed by that, the co-polymerization CPA **3-16f**, which was then subjected to co-polymerization promoted by benzoyl peroxide to provide **PS-3-8E-1** in 92% yield on a gram scale.

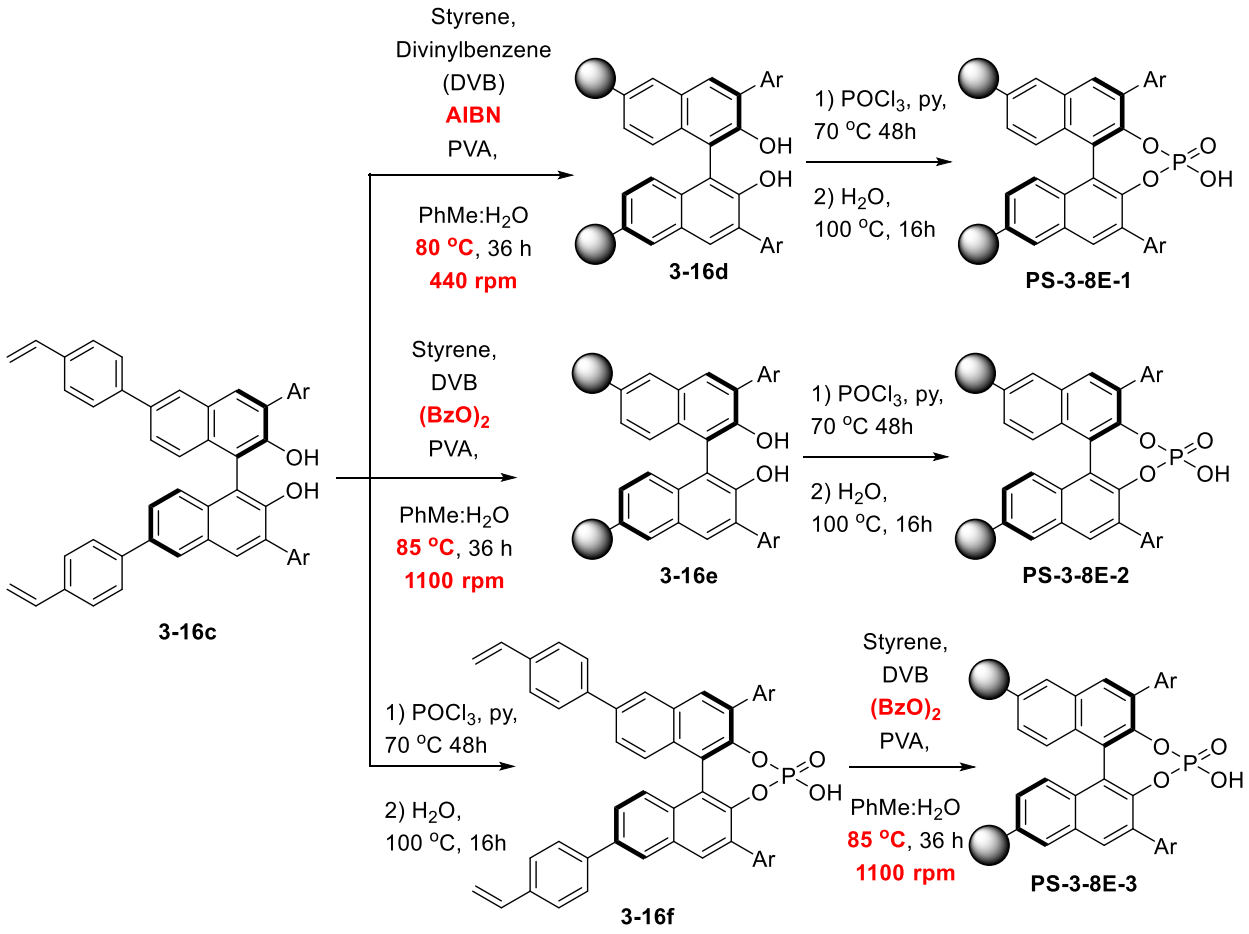

Scheme 3.10 Different methods to synthesize polystyrene-supported CPA catalyst PS-(*R*)-3-8E.

The subsequent evaluation of **PS-3-8E-3** suggested that it surpasses its monomeric equivalent **3-8E** in terms of the reactivity. Thus, with **PS-3-8E-3**, the complete reaction conversion could be achieved in 18 h with the catalyst loading as low as 0.5 mol%, while under the same conditions (Table 3.8 and 3.9), the use of 0.5 mol% of monomeric **3-8E** requires significantly longer reaction time (38 h). This encouraging observation prompted the subsequent evaluation of **PS-3-8E-3** at low catalyst loadings (*cf.* Table 3.8).

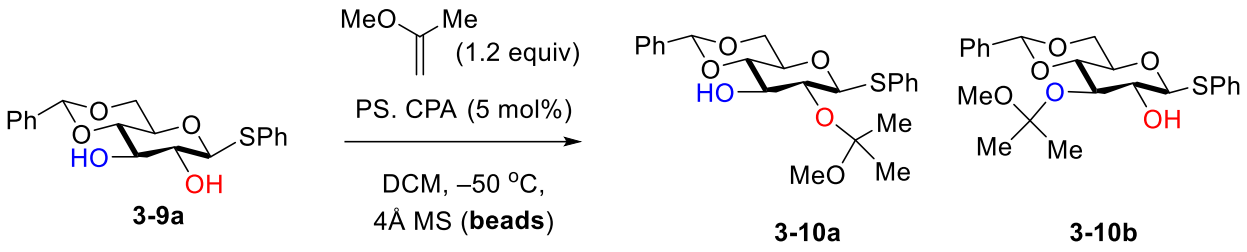

entry	CPA	Conv. by NMR (%)	3-10a:3-10b	time (h)	yield (%)
1	A	97	>25:1	24	95
2	B	96	>25:1	24	87
3	**PS-3-8E-1**	<5	-	-	-
4	**PS-3-8E-2**	83	22:1	24	80
5	**PS-3-8E-3**	95	>25:1	24	93
6	**PS-3-8E-3 (0.5 mol%)**	**97**	**>25:1**	**24**	**95**

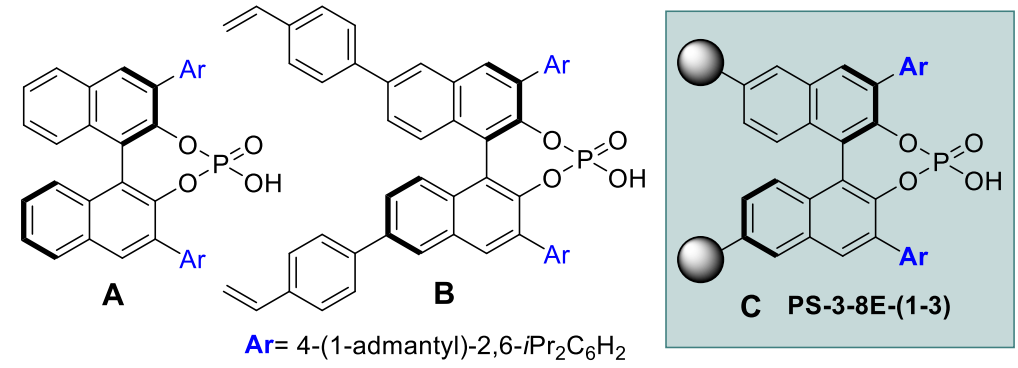

Table 3.8 Experimental test for the reactivity and selectivity of PS-CPAs towards regioselective acetalization of diols.

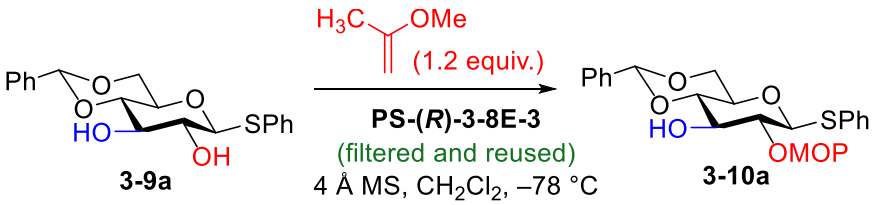

recovered by filtration and washh

cycle number	CPA loading (mol%)	scale	time	conversion (%)	**3-10a:3-10b** (r.r.)
1	0.5	1.0 g	18 h	99	>25:1
2	0.5	1.0 g	18 h	95	23:1
3	0.5	1.0 g	18 h	97	>25:1
4	0.5	1.0 g	18 h	99	>25:1
5	0.5	1.0 g	18 h	97	>25:1
6	0.5	1.0 g	18 h	99	>25:1
7	0.5	1.0 g	18 h	99	>25:1
8	0.5	1.0 g	18 h	99	>25:1
9	0.5	1.0 g	18 h	99	>25:1
10	0.5	1.0 g	18 h	99	>25:1
11	**0.1**	**5.0 g**	**36 h**	**99 (94%)**	**>25:1**

Table 3.9 Testing the recyclability of PS-(*R*)3-8E-3.

Not only the use of immobilized catalyst **PS-(*R*)-3-8E-3** resulted in improved catalytic activity and selectivity in acetalization of **3-9a**, but also this catalyst could be conveniently recovered and recycled by filtration and wash (Table 3.9). Most importantly, we were able to repeatedly run nine consecutive 1.0 g scale MOP-protections of **3-9a** with only 0.5 mol% (50 mg) of the same batch of catalyst **3-8E-3** without erosion in yield or selectivity.

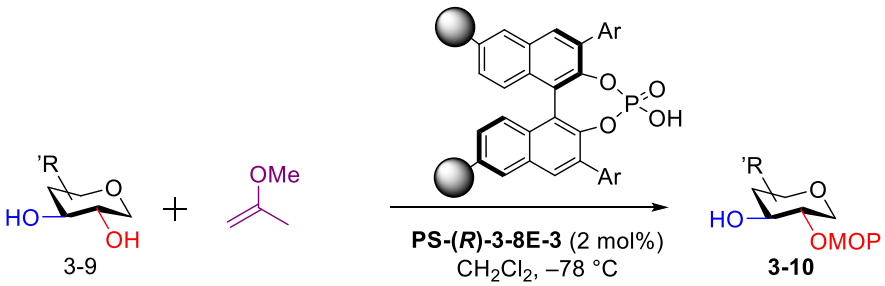

A.

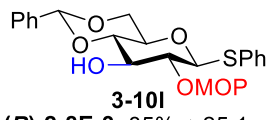

3-10l
(*R*)-2-8E-3, 85%, >25:1 rr
(*R*)-2-8E, 72%, >25:1 rr

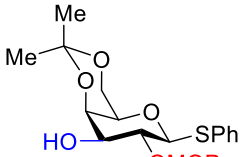

3-10r
(*R*)-2-8E-3, 81%, 21:1 rr
(*R*)-2-8E, 84%, 20:1 rr

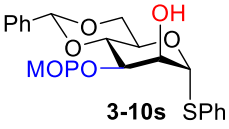

3-10s
(*R*)-2-8E-3, 50%, 12:1 rr
(*R*)-2-8E, 60%, 13:1 rr

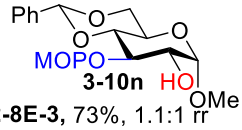

3-10n
(*R*)-2-8E-3, 73%, 1.1:1 rr
(*R*)-2-8E, 69%, 6.3:1 rr

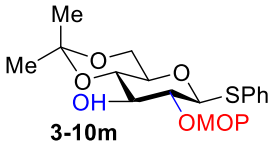

3-10m
(*R*)-2-8E-3, 89%, 19:1 rr
(*R*)-2-8E, 98%, 12:1 rr

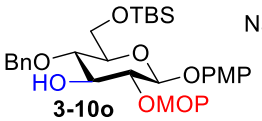

3-10o
(*R*)-2-8E-3, 95%, >25:1 rr
(*R*)-2-8E, 88%, 7:1 rr

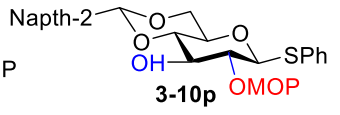

3-10p
(*R*)-2-8E-3, 89%, >25:1 rr
(*R*)-2-8E, 92%, 3:1 rr

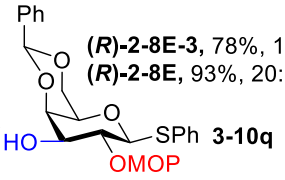

3-10q
(*R*)-2-8E-3, 78%, 15:1 rr
(*R*)-2-8E, 93%, 20:1 rr

B.

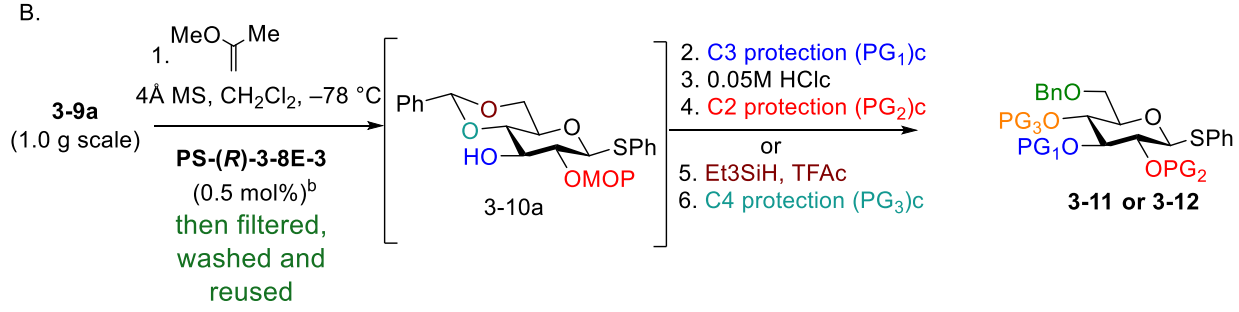

Substrates generated with the same batch of the recycled catalyst **PS-(*R*)-3-8E-3** (50 mg) using one-pot protection protocolsc

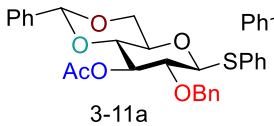

3-11a
70% (0.96 g)

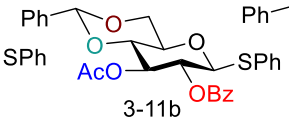

3-11b
85% (1.2 g scale)

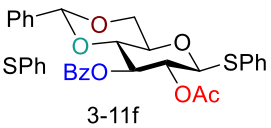

3-11f
80% (1.1 g)

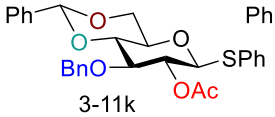

3-11k
74% (0.98 g)

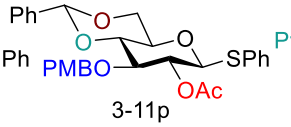

3-11p
85% (1.2 g scale)

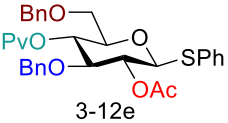

3-12e
47% (0.67 g scale)

[a]The reactions were performed with 2 mol% of catalysts **PS-(*R*)-8E-3** at either –78 ºC (2-MOP-protection) on 0.056 mmol scale (0.042 M solution) for 18-24 h in the presence of 4Å MS. The rr values were determined by ^{1}H NMR analysis of the crude reaction mixtures of the products **3-10** as well as their acetylated derivatives. Each entry represents an average of 2 experiments. [b]These experiments were performed with 50 mg (0.5 mol%) of catalyst **PS-(*R*)-8E-3** as described in Scheme 3.4. The reaction mixture was quenched with Et_3N and the catalyst **PS-(*R*)-8E-3** was filtered, washed, and reused. [c]The single pot-protection for steps 2-4 was executed following the protocols described in Scheme 3.5. The yields represent the yield for the overall single operation from **3-9a**.

Scheme 3.11 Regiodivergent protection of monosaccharides with immobilized catalysts PS-(*R*)3-8E-3, and the use of recycled PS-(*R*)-3-8E-3 for multiple gram-scale regioselective syntheses of differentially protected *D*-glucose derivatives 3-11a, 3-11b, 3-11f, 3-11k, 3-11p, and 3-12e.

Based on the aforementioned promising results obtained for the regioselective acetalization of **3-9a** using immobilized catalysts **PS-(*R*)-3-8E-3**, our subsequent studies focused on investigating these polymeric catalysts in the acetalizations of other substrates and comparing them to the monomeric catalysts **(*R*)-3-8E-3** (Scheme 3.12A). Gratifyingly, catalyst **PS-(*R*)-3-8E-3** demonstrated great selectivity profile for the generation of the corresponding 2-MOP protected derivatives, and with the exception of one case (**3-10n**), the resultant products were obtained in excellent C2-selectivity (*cf.* Scheme 3.12A). It is noteworthy that the selectivities and yields for substrates **3-10l**, **3-10r**, and **3-10s** obtained with the immobilized catalyst **PS-(*R*)-3-8E-3** matched the corresponding results previously obtained for **(*R*)-3-8E.** Remarkably, in three instances (**3-10m**, **3-10o**, and **3-10p**), **PS-(*R*)-3-8E-3** provided significantly higher regioselectivities than the monomeric acid **(*R*)-3-8E-3** (25:1 rr vs 3:1 rr for **3-10p**, 25:1 rr vs. 6:1 rr for **3-10o**, and 19:1 rr vs 12:1 rr for **3-10m**). Finally, in instances of **3-10n** and **3-10q**, the selectivities obtained with **PS-(*R*)-3-8E-3** were lower than the selectivities obtained with **(*R*)-3-8E** (1:1 rr vs 6:1 rr for **3-5n** and 20:1 rr vs 15:1 rr for **3-5q**). These observations suggest that the additional structural features present in **PS-(*R*)-3-8E-3** that are not present in **(*R*)-3-8E** such as the linker and polystyrene matrix may impact the steric interactions between the CPA and substrate. This could have both positive or negative consequences for the reaction outcome although in the majority of cases presented in Schemes 3-12A improvements in the selectivity were observed, which was confirmed by the Thomas group in their studies.[31]

To demonstrate the utility of the immobilized CPAs for the gram scale synthesis of differentially protected monosaccharide derivatives, we performed series of 1.0 g scale functionalizations of **3-9a** using the same batch (50 mg or 0.5 mol%) of **PS-(*R*)-3-8E-3** (*cf.* Scheme 3.8). The selective MOP-protections of **3-9a** was followed by the filtration, and the filtrate was subjected to the previously developed one-pot derivatizations (*cf.* Scheme 3.8). The recovered and recycled catalyst **PS-(*R*)-3-8E-3** was then reused to accomplish subsequent cycle of regioselective functionalization of **3-4a**. Following this protocol allowed to achieve consecutive one-pot syntheses of **3-11a** (0.96 g), **3-11b** (1.2 g), **3-11f** (1.1 g), **3-11k** (0.98 g), **3-11p** (1.2 g), and **3-12e** (0.67 g) using the same batch of catalyst **PS-(*R*)-3-8E-3**. It is also noteworthy that the single-pot procedures leading to **3-11a**, **3-11b**, **3-11f**, **3-11k**, **3-11p**, and **3-12e** were readily scalable and proceeded with improved overall yields. Altogether, these studies suggest that immobilized CPA-catalysts **PS-(*R*)-3-8E-3** hold great potential for the regioselective preparation of differentially protected monosaccharide derivatives, and that the use of the regioselective CPA-catalyzed acetalization allows to expand the single-pot methods previously developed by Hung and others.[26,28]

Finally in order to test these transformations in more complex settings, we investigated the possibility of carrying C2-selective functionalization of disaccharide-based triol **3-13a** provided by Professor Xuefei Huang. In the presence of **(*R*)-3-8E**, our catalyst could selectively acetalize the C2-hydroxyl in 61% yield with 20:1 r.r.; while with **PS-(*R*)-3-8E-3**, similar selectivity was observed with 73% yield and 16:1 r.r.. These results suggested both monomeric and polymeric catalysts might be used in the more complex settings in a predictable manner.

Moreover, we have also showed the possibility of our catalysts in regioselective acetalization of disaccharides. In the presence of **(*R*)-8E**, our catalyst could selectively acetalize

C2-OH in 61% yield with 20:1 r.r.; while when changing to **PS-(*R*)-8E-3**, similar results was observed with 73% yield and 16:1 r.r.. These results suggested our methods provided a mild reaction condition that could tolerate various functional groups such as azide, silyl ether, and acetal.

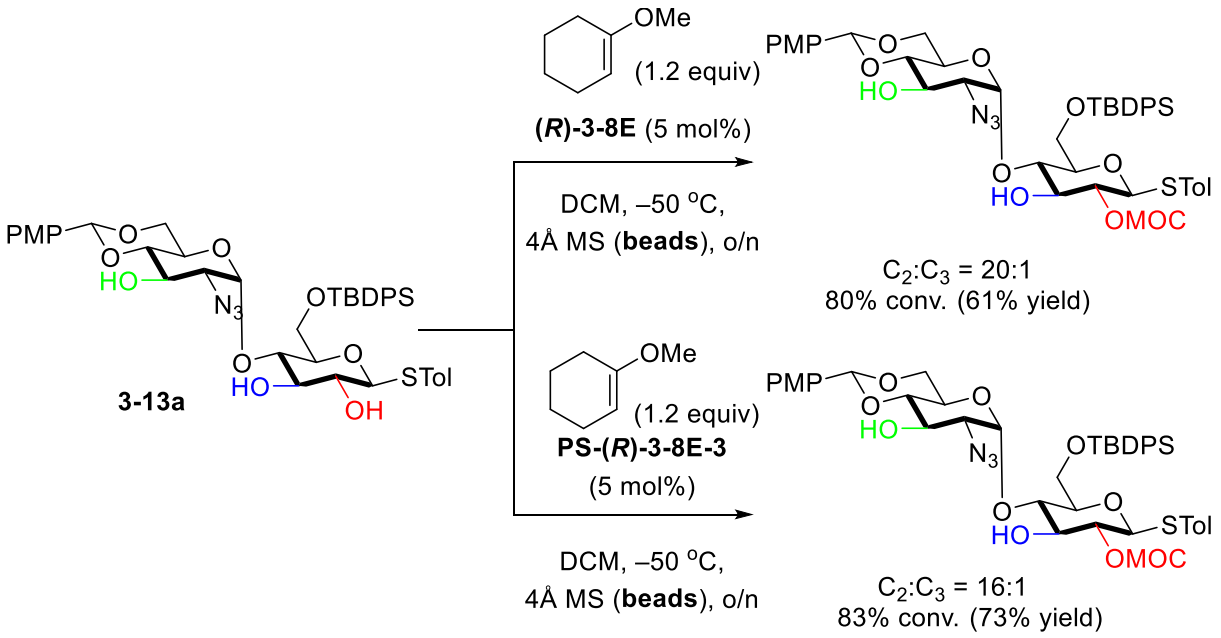

Scheme 3.12 Regioselective acetalization of disaccharides 3-13a provided by Prof. Xuefei Huang.

With these developments in hand, our subsequent studies were focused on experimental and computational exploration of the mechanism for the regioselective acetalizations and development of a stereochemical model explaining the observed selectivity trends. Both MOC and MOP acetalizations demonstrated unusual selectivity versus temperature profiles (*cf.* Scheme 3.9). Thus, both types of acetalization were unselective at the temperatures above –30 ºC, but demonstrated significant jump in selectivity once cooled below –50 ºC. These unusual temperature vs. selectivity profiles are not consistent with the theoretically predicted using Arrhenius

regioselectivity on temperature dependence computed for DDG°=1.2 kcal/mol (*cf.* Scheme 3.9). The regioselectivity should exponentially be dependent on temperature, and the profiles in Scheme 6A should not involve abrupt increase of selectivity at some threshold temperature. The observed temperature dependence suggests that the acetalization may happen through competing mechanisms, and that the mechanism prevailing at the temperatures below –50 ºC might be different from the reaction mechanism at higher temperatures.

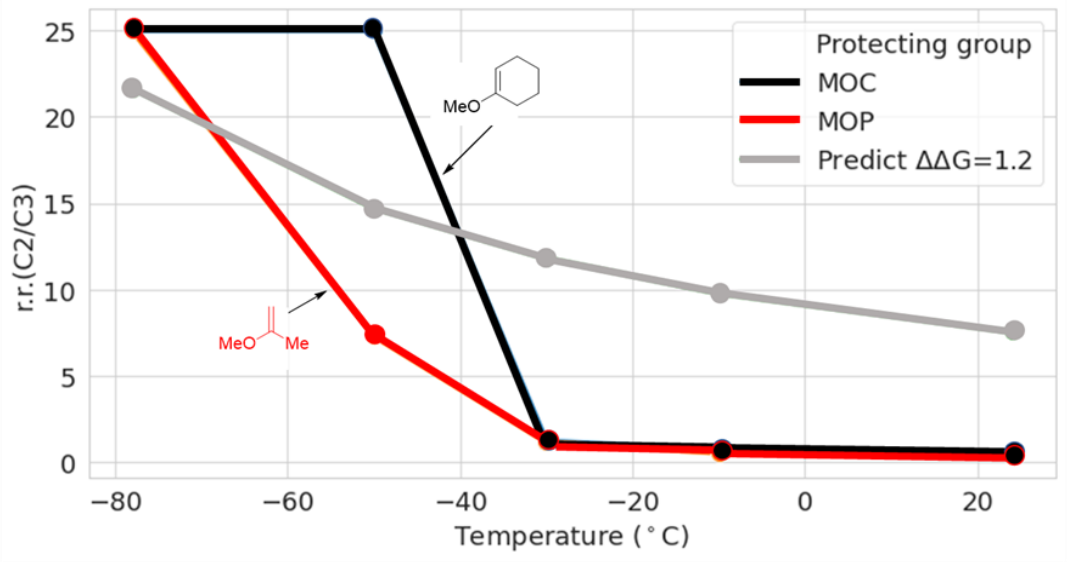

[a]The reactions with 2-methoxy-2-propene (2-MOP) and 1-methoxy-1-cyclohexene (1-MOC) were performed overnight at the specified temperature on 0.056 mmol scale (0.042 M solution) in the presence of 4Å MS. The C2/C3 ratio was determined by 1H NMR analysis of the crude mixture.

Scheme 3.13 A. Selectivity versus temperature profile for the MOC and 2-MOP protection of 3-9a, and theoretically predicted selectivity profile for a reaction with no mechanism switch using Arrhenius model with DDG° = 1.2 kcal/mol.[a] Experiment were performed by Dr. Jeonghyo Lee and Oleksii Zhelavskyi.

To test whether the product is stable at higher temperatures, regioisomerically enriched product **3-9a** was resubjected to acid **3-8E** at different temperatures (Scheme 3.14) for 12 h. At room temperature, this resulted in significant isomerization of **3-10a** into the regioisomeric product **3-10b**, and the crude reaction mixture contained ~1.7:1 ratio of **3-10a**: **3-10b**, in addition to 41%

of starting material of diols **3-9a**. However, with decreasing of temperature, the conversion of **3-10a** to **3-10b** and **3-9a** drastically decreased, which at -78 ˚ C, only less than 3% of **3-10b** and no **3-9a** were observed. Significant amounts of diol **3-9a** were also present in the mixture and suggested that the formation of **3-10b** proceeded through **3-9a** and that the overall acetal formation is reversible at room temperature.

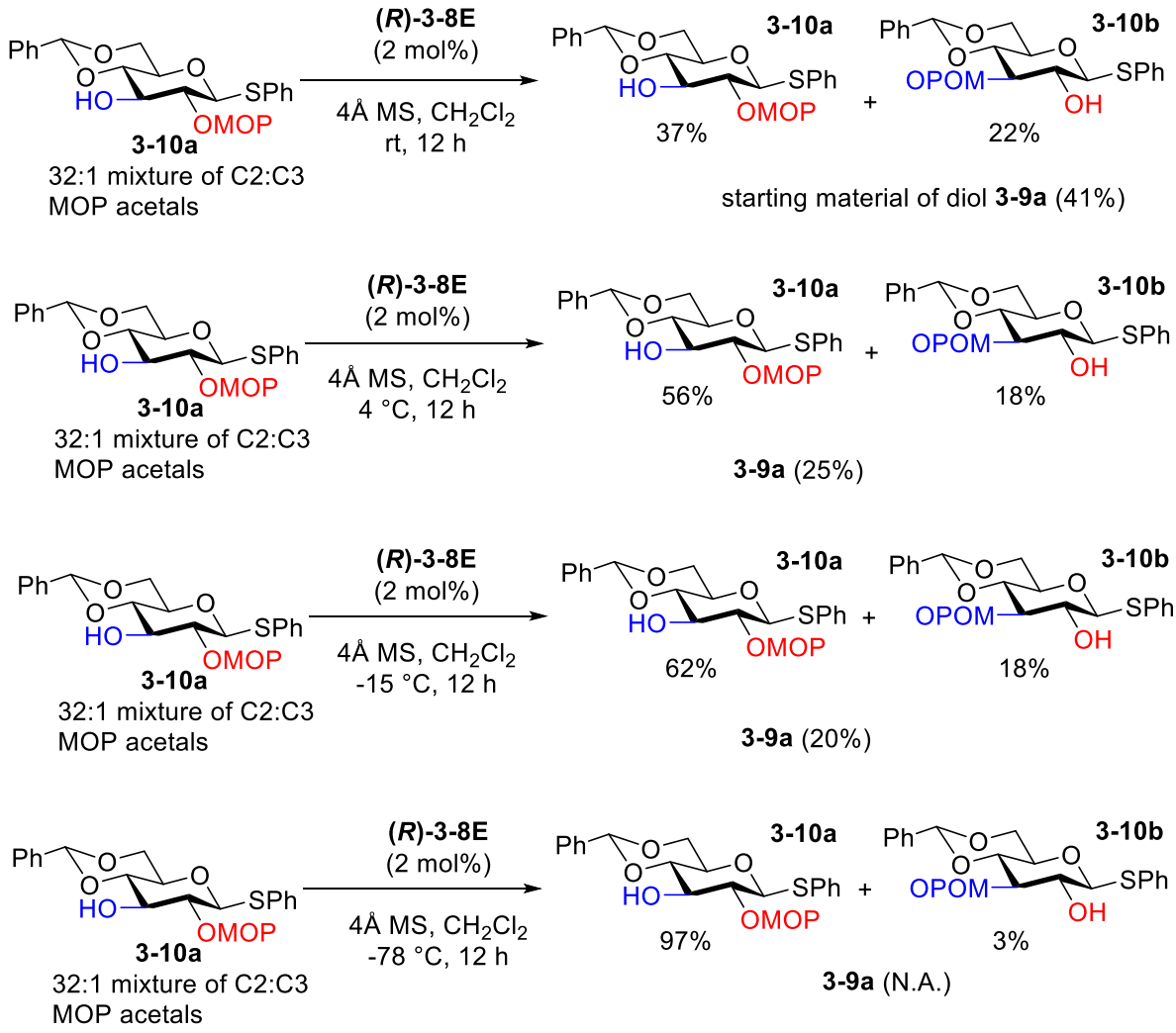

Compound **3-10a** containing 32:1 mixture of C2:C3 MOC acetal regioisomers was subjected to the standard acetalization conditions above without 1-MOC at r.t. for 12 h. The resultant mixture composition was analyzed by ^{1}H NMR.

Scheme 3.14 Control studies for the stability of obtained C2 acetal products under varies temperatures.

With these observations in mind, three different reaction mechanisms depicted in Scheme 3-15 were proposed. These involved the conventional mechanism proceeding through the oxocarbenium ion (Scheme 3.15A),[36,37] as well as direct synchronous or asynchronous concerted addition, as previously proposed by us for CPA-catalyzed spiroketalizations (Scheme 3.15B).[38] Alternatively, the catalyst may react with the MOC or 2-MOP enol ethers to form a phosphate intermediate, which then proceeds through S_N1 or S_Ni mechanisms that were observed by us for CPA-catalyzed glycosylation of 6-dEB (Scheme 3.15C).[39] Our collaborative mechanistic studies with the Professor Zimmerman, Oleksii Zhelavskyi and Alonse J. Arguelles suggest that this transformation is likely to proceed via a concerted asynchronous mechanism depicted in pathway B. These results are consistent with the extensive NMR experiments carried with *D*-labeled substrates and performed by Oleksii Zhelavskyi.

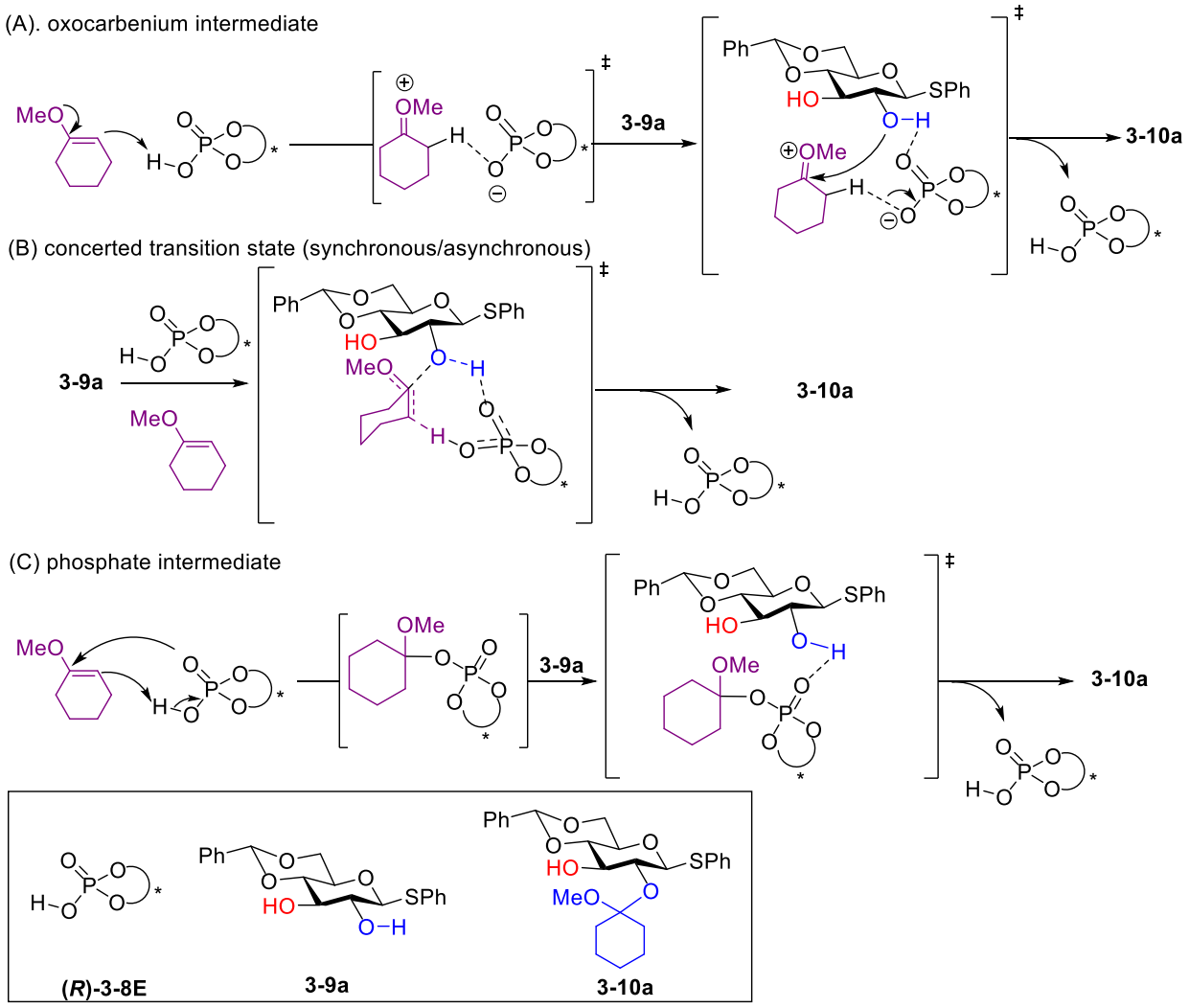

Scheme 3.15 Proposed mechanism for the regioselective acetalization.

3.5. Conclusion

In conclusion, this chapter overviews the challenges associated with using achiral reagents for achieving regioselective functionalization of the equatorial moieties in monosaccharides. While many useful methods for the regioselective protection have been developed to date, these methods demonstrate strong dependence on the substrate structure and electrophile and often lack generality. Many of these challenges might be addressed through the use of chiral catalyst for controlling the site of functionalization, and several methods demonstrating this concept have been

developed up-to-date. In particular, the Nagorny group has pioneered the use of CPA-catalyzed acetalization reactions that fueled the studies described in this chapter.

This chapter illustrated the use of CPAs catalyst **(*R*)-3-8E** for controlling highly regioselective acetalization reactions that are carried in one pot with other transformations to provide access to a diverse set of monosaccharides. Unlike their achiral counterparts, catalyst **(*R*)-3-8E** allows to differentiate equatorial hydroxy groups and selectively produce regioisomeric products. To further improve the practicality of this approach, the immobilized catalyst **PS-(*R*)-3-8E-3** have also been synthesized to accomplish regiodivergent acetal protection in good-to-excellent selectivities. In particular, **PS-(*R*)-3-8E-3** demonstrated superior to **(*R*)-3-8E** catalytic performance and selectivity, and it could be readily recycled by filtration and wash, and reused for more than ten cycles on 1.0 to 5.0 g scale of acetalizations with catalyst loadings as low as 0.5 to 0.1 mol%. This enabled achieving significant catalyst economy, and regioselective one-pot gram scale syntheses of 6 differentially protected *D*-glucose derivatives **3-11a**, **3-11b**, **3-11f**, **3-11k**, **3-11p**, and **3-12e** were accomplished with the same 50 mg batch of catalyst **PS-(*R*)-3-8E-3**.

The computational and mechanistic studies on the site-selective acetalization were performed in collaboration with Professor Paul M. Zimmerman, Oleksii Zhelavskyi, Dr. Jenghyuo Lee and Dr. Alonso J. Arguelles. The studies of site-selective acetalization under different temperatures, developed by Dr. Jeonghyo Lee, indicate a complex temperature-dependent interplay of two reaction mechanisms. Based on the temperature studies, three different mechanisms have been proposed: oxocarbenium intermediate, concerted transition states and phosphate intermediate. Out stability test of acetal **3-10a** (Scheme 3.14) and additional computational studies suggest that at low temperature, concerted asynchronous mechanism is dominant and the high selectivity for the formation of the C2 isomer is likely due to destabilizing

the TS leading to the C3 isomer interactions between the benzylidene acetal moiety of **3-9a** and catalyst **PS-(*R*)-3-8E-3**. The developed stereochemical models allow expanding the scope of this transformation, and further studies focused on exploring more complex substrates, such as oligosaccharides, and applying these transformations in continuous flow are the subjects of ongoing studies by our groups. Furthermore, it is still unclear about the effects of the polymeric backbones in controlling the site-selectivity. Further studies will focus on developing different polymer-supported CPAs and analyzing their catalytic performance.

3.6. Experimental Information

General Information:

The assessment of the regioselectivity was accomplished by adapting methods developed by Nagorny Group using COSY NMR studies.[1] The assessment of the regioselectivity of the acetal was accomplished by analysis of the 1H NMR spectra of the products obtained by the CPA-controlled tetrahydropyranylation. This analysis was based on comparison with the independently synthesized C2 and C3 regioisomers of the diol. A typical procedure for the synthesis of C2 and C3 regioisomeric standards of the diol began using galactose diol as starting material (see Scheme above). Mono acetylation afforded the C2/C3 mixture of mono acetates, which were separated by a preparative TLC. The identity of the regioisomers was accessed by COSY NMR techniques (the protons next to the acetoxy group are typically shifted downfield and have the d > 4.2 ppm).

In case with substrate **3-10a** benzylidene proton can be used for quantitative evaluation of the regioisomer ratio (r.r.) during the acetalization (see spectrum on Figure 3.1).

Figure 3.1 ^{1}H NMR regioselectivity evaluation of carbohydrate 3-10a acetalization (at –50 °C with MOC)

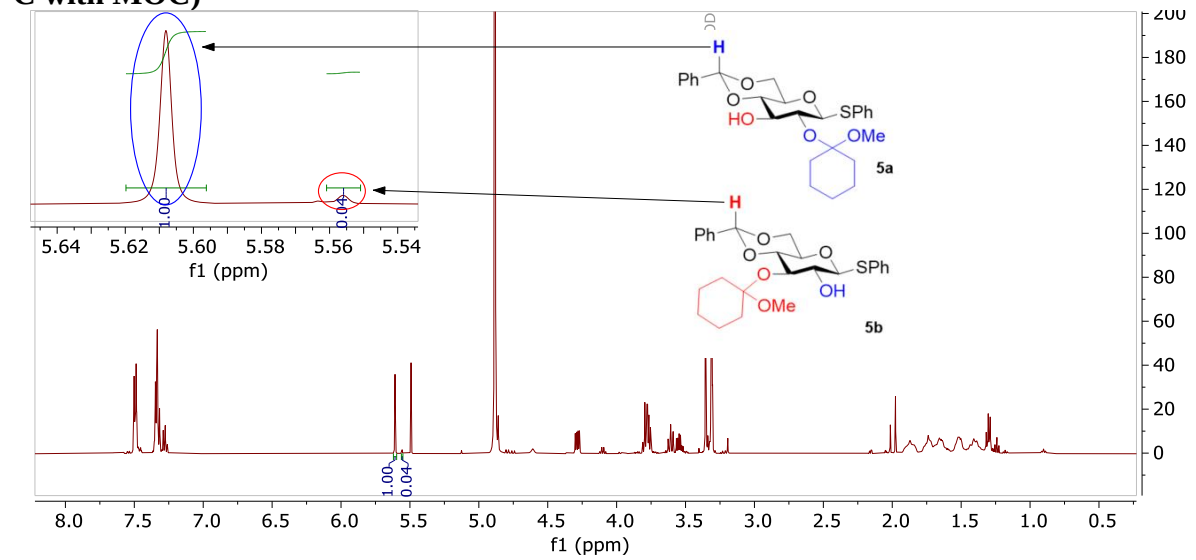

Synthesis and characterization of polystyrene-supported CPA catalysts (*R*)-Ad-TRIP-PS (3-8E)

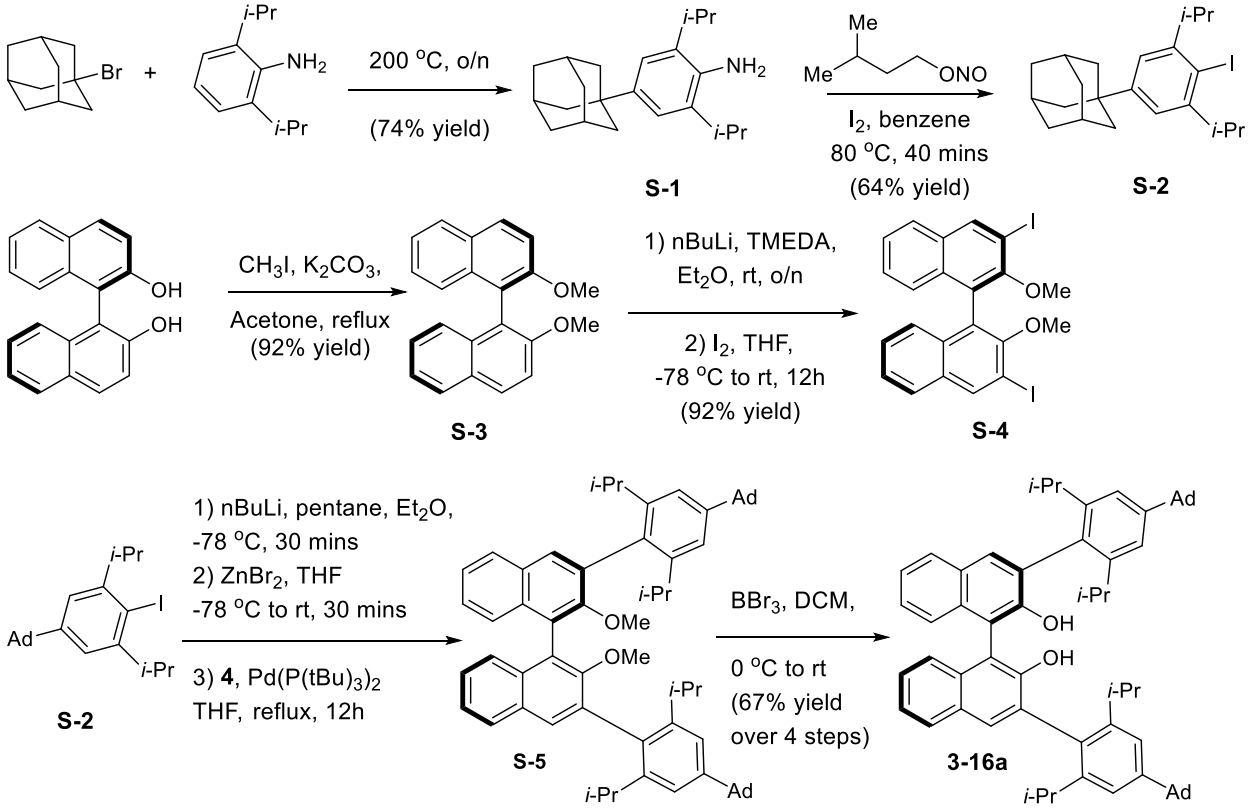

Scheme 3.16 Summary of the synthesis of known intermediate S-6 for the PS-(*R*)-3-8E-3 synthesis.

Reagent **S-2** and **S-4** were prepared using the previously reported methods. Reagent **S-2** (1.43 g, 3.4 mmol) was initially dissolved in pentane (30 mL, 0.1 M) and diethyl ether (15 mL, 0.2 M). The mixture was then cooled to –78 ^{o}C, and formation of the cloudy solution was noticed. Follow by that, 1.6 M solution of *n*-BuLi (2.1 mL, 3.4 mmol, 1.0 equiv.) was slowly added in and warmed up to 0 ^{o}C and stirred for 30 minutes. After that, the reaction mixture was cooled back to –78 ^{o}C and drop-wisely added in $ZnBr_2$ (0.92 g, 4.10 mmol, 1.2 equiv.) solution in THF. The reaction mixture was then warmed up to room temperature and stirred for 1.5 h. After that, the reaction was dried under reduced pressure to form off-white solid, which was used directly without purification. The obtained off-white solid was then mixed with reagent **S-4** (0.57 g, 1.00 mmol, 0.33 equiv.) and $Pd(P(t\text{-}Bu)_3)_2$ (3.3 mg, 68 mmol, 0.02 equiv.), followed by dissolving in THF (5 mL) and reflux at 80 ^{o}C for 12 h. After TLC indication of full conversion, the reaction was worked up by diluted with hexane and ether (1:1 ratio, 200 mL), then washed with 1N HCl (40 mL), followed by saturated $NaHCO_3$ (30 mL) and dried with brine and Na_2SO_4. Under the reduced pressure, a foaming brown solid was obtained without further purification. The crude product was then mixed with dichloromethane (0.16 M, 6 mL) and cooled to 0 ^{o}C. Then BBr_3 (6 equiv. 6 mL) was added dropwisely and warmed up to room temperature upon completing addition. The reaction was stirred for 12 h, until TLC indicated completion. The reaction was cooled to 0 ^{o}C, and extremely slowly added in water (20 mL). The organic layer was separated and the aquous layer was extracted with dichloromethane (40 mL x 3) and dried with brine and Na_2SO_4. The product was then purified with 5 % ethyl acetate in hexane to get a pale yellow product **3-16a** 0.59 g (67% yield over 3 step). ^{1}H NMR (700 MHz, Chloroform-*d*) δ 7.86 (d, *J* = 8.0 Hz, 2H), 7.77 (s, 2H), 7.37 (ddd, *J* = 8.1, 5.9, 2.1 Hz, 2H), 7.30 (dd, *J* = 6.1, 1.5 Hz, 4H), 4.91 (s, 2H), 2.86 (p, *J* = 6.7 Hz, 2H), 2.71 (p, *J* =

6.8 Hz, 2H), 2.12 (s, 6H), 1.99 (d, *J* = 2.9 Hz, 12H), 1.80 (s, 12H), 1.20 (d, *J* = 6.8 Hz, 6H), 1.10 (dd, *J* = 8.7, 6.9 Hz, 12H), 1.03 (d, *J* = 6.9 Hz, 6H).

^{13}C NMR (176 MHz, Chloroform-*d*) δ 151.5, 150.6, 147.3, 147.3, 133.4, 130.5, 130.0, 129.1, 129.0, 128.2, 126.5, 124.5, 123.7, 119.6, 113.2, 43.2, 36.9, 36.5, 31.0, 31.0, 29.0, 24.4, 24.4, 24.0, 23.8.

IR (thin film, cm^{-1}): 3520, 2958, 2901, 2847, 1601, 1497, 1422, 1382, 1361, 1344, 1315, 1255, 1234, 1147, 1121, 746.

HRMS (ESI+) (m/z): $[M+NH_4]^+$ calcd for $C_{64}H_{78}NO_2$: 892.6027, found:892.6011.

$[\alpha]_D^{25}$ = 35.1˚ (c=1.77, CH_2Cl_2).

Synthesis of (*R*)-3,3'-bis(2,6-bis(triisopropyl)-4-admantyl-phenyl)-6,6'-dibromo-1,1'-bi-2-naphthol (3-16b).

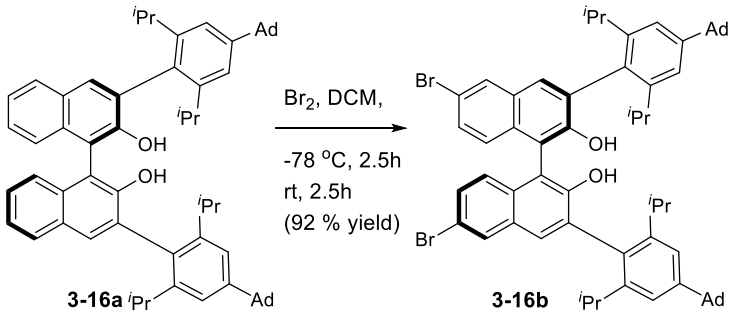

To pre-cooled (–78°C) solution of diol **3-16a** (2.1 g, 2.3 mmol) in dry DCM (12 mL) solution of Br_2 (0.25 mL, 5.3mmol, 2.2 equiv.) in 12 mL of dry DCM was added dropwise. Upon addition, almost instant discoloration of bromine solution happened. The reaction was stirred for 2.5h at –78°C, then heated up to room temperature and stirred for additional 12 h. After the reaction was indicated completion by TLC, the reaction was washed subsequently with 10% w/w aqueous solution of NaS_2O_3 (40 mL) and extracted with DCM (40 mL x 3). The organic layer was separated and washed with brine. DCM was removed by rotary evaporation. The crude product **3-16b** (2.2

g, 92% yield) was used directly without purification, as the purification typically leads to decomposition.

^{1}H NMR (401 MHz, Chloroform-*d*) δ 8.00 (d, *J* = 2.0 Hz, 2H), 7.66 (s, 2H), 7.38 (d, *J* = 2.0 Hz, 1H), 7.36 (d, *J* = 2.1 Hz, 1H), 7.29 (d, *J* = 1.9 Hz, 2H), 7.13 (s, 1H), 7.11 (s, 1H), 5.30 (s, 4H), 4.89 (s, 2H), 2.77 (q, *J* = 6.9 Hz, 2H), 2.71 – 2.58 (m, 2H), 2.13 (s, 6H), 1.98 (d, *J* = 3.0 Hz, 12H), 1.80 (s, 12H), 1.20 (d, *J* = 6.9 Hz, 6H), 1.09 (dd, *J* = 9.5, 6.8 Hz, 12H), 1.02 (d, *J* = 6.8 Hz, 6H).

^{13}C NMR (176 MHz, Chloroform-*d*) δ 152.1, 150.6, 150.2, 147.5, 147.4, 146.9, 132.0, 130.3, 130.1, 130.1, 130.0, 129.3, 128.9, 126.3, 123.6, 120.8, 119.9, 117.5, 113.6, 49.3, 43.2, 43.2, 36.9, 36.8, 36.6, 36.3, 35.5, 33.7, 32.6, 31.1, 31.0, 29.7, 29.0, 29.0, 29.0, 24.4, 24.3, 24.0, 23.8, 23.2.

IR (thin film, cm^{-1}): 3510, 2959, 2900, 2847, 1593, 1485, 1435, 1382, 1361, 1344, 1315, 1258, 1183, 1124, 1103, 1069, 935, 899, 873, 812.

HRMS (ESI+) (m/z): $[M+NH_4]^+$ calcd for $C_{64}H_{76}Br_2NO_2$: 1050.4222, found 1050.4224;

$[\alpha]_D^{25}$ = 37.2˚ (c=1.13, CH_2Cl_2).

Synthesis of (*R*)-3,3'-bis(2,6-bis(triisopropyl)-4-admantyl-phenyl)-6,6'-bis(4-vinylphenyl)-1,1'-bi-2-naphthol.

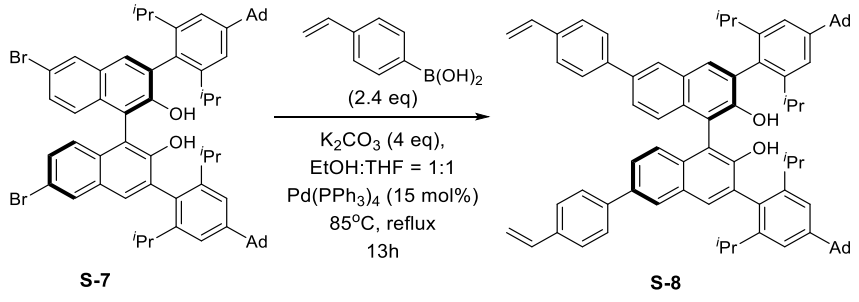

S-7 **S-8**

To a solution of **3-16b** (310 mg, 0.3 mmol) and 4-vinylphenylboronic acid (106 mg, 0.72 mmol, 2.4 equiv.) and K_2CO_3 (170 mg, 1.2 mmol, 4.0 equiv.) in a degassed mixture of ethanol: tetrahydrofuran 1:1 (3 mL). $Pd(PPh_3)_4$ (52 mg, 0.045 mmol, 15 mol%) was added in. The reaction

mixture was refluxed at 85˚C with stirring for 13 h. After cooling down to room temperature, volatiles were removed using rotatory evaporation. The resultant solid residue was then re-dissolved in dichloromethane (15 mL) and water (15 mL). The organic layer was separated, while the aqueous layer was extracted with dichloromethane (30 mL x 3). The combined organic layers were then dried with brine and sodium sulfate. Afterwards, the solution was concentrated by rotatory evaporation, and the residue was directly purified by flash column chromatography on silica using 5% EtOAc in hexanes to provide the desire product **3-16c** (211 mg, 0.195 mmol) as a brown-yellow solid in 65% yield.

^{1}H NMR (500 MHz, Chloroform-*d*) δ 8.06 (d, *J* = 1.9 Hz, 2H), 7.83 (s, 2H), 7.71 – 7.63 (m, 4H), 7.62 – 7.56 (m, 2H), 7.53 – 7.47 (m, 4H), 7.40 (d, *J* = 8.8 Hz, 2H), 7.26 (s, 4H), 6.76 (dd, *J* = 17.6, 10.9 Hz, 2H), 5.80 (dd, *J* = 17.6, 0.9 Hz, 2H), 5.27 (dt, *J* = 10.9, 1.6 Hz, 2H), 4.97 (s, 2H), 2.91 (p, *J* = 6.9 Hz, 2H), 2.75 (p, *J* = 6.8 Hz, 2H), 2.13 (s, 6H), 1.99 (d, *J* = 2.9 Hz, 12H), 1.88 – 1.72 (m, 12H), 1.25 – 1.20 (m, 6H), 1.16 – 1.09 (m, 12H), 1.05 (d, *J* = 6.9 Hz, 6H).

^{13}C NMR (176 MHz, Chloroform-*d*) δ 151.7, 150.7, 147.4, 147.4, 140.5, 136.4, 136.1, 132.7, 130.7, 129.7, 129.6, 129.2, 127.3, 126.7, 126.1, 126.0, 125.2, 120.0, 113.8, 113.3, 43.2, 36.9, 36.5, 31.1, 31.0, 29.0, 24.4, 24.4, 24.1, 23.8.

IR (thin film, cm^{-1}): 3518, 2958, 2901, 2847, 1602, 1495, 1464, 1382, 1361, 1315, 1255, 1233, 1103, 939, 904, 841.

HRMS (ESI+) (m/z): $[M+H]^+$ calcd for $C_{80}H_{85}O_2^+$, 1077.6555, found 1077.6580.

$[\alpha]_D^{25}$ = 49.1˚ (c=1.18, CH_2Cl_2).

Synthesis of (*R*)-3,3'-bis(2,6-bis(triisopropyl)-4-admantyl-phenyl)-6,6'-bis(4-vinylphenyl)-1,1'-bi-2-naphthol phosphoric acid.

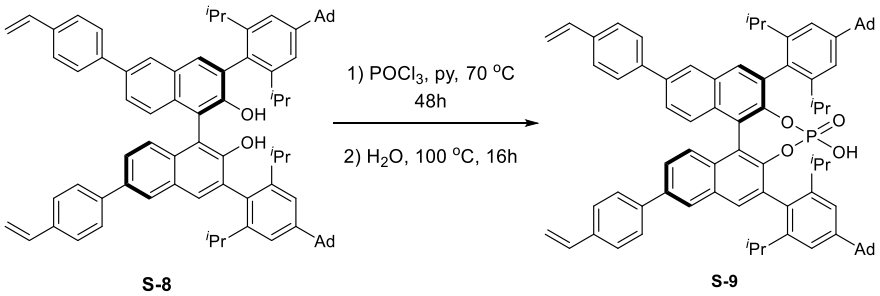

To a stirred solution of **3-16c** (216 mg, 0.20 mmol) and pyridine (0.1 M, 2.0 mL) was added $POCl_3$ (38 μL, 0.40 mmol, 2.0 eq). The mixture was stirred at 70 °C for 12 h. Then the reaction mixture was added in H_2O (2 mL) and continuous stirring at 100 °C for 12 h. After cooling to r.t., the reaction mixture was diluted with DCM (40 mL). The organic layer was separated and the aqueous layer was extracted with DCM (40 mL x 3). The organic layer was then washed with 6 N HCl (40 mL x 3). The combined organic layer was then dried with brine and anhydrous sodium sulfate and concentrated under reduce pressure to obtain a pale yellow solid. This crude product was then purified by column chromatography on silica gel using 2% MeOH in DCM. The obtained product was then dissolved in DCM, washed again with 6 N HCl, dried with anhydrous sodium sulfate, and concentrated under reduced pressure to obtain free acid form of **3-16d** in 128 mg in 57% yield.

^{1}H NMR (700 MHz, Chloroform-*d*) δ 8.11 (d, *J* = 1.9 Hz, 2H), 7.97 (s, 2H), 7.72 (d, *J* = 8.0 Hz, 4H), 7.65 (dd, *J* = 8.9, 1.9 Hz, 2H), 7.54 (dd, *J* = 16.6, 8.5 Hz, 6H), 7.23 – 7.10 (m, 4H), 6.80 (dd, *J* = 17.5, 10.9 Hz, 2H), 5.83 (d, *J* = 17.6 Hz, 2H), 5.31 (d, *J* = 10.8 Hz, 2H), 2.69 (dt, *J* = 14.7, 7.1 Hz, 4H), 2.12 (s, 6H), 2.01 – 1.92 (m, 12H), 1.84 – 1.72 (m, 12H), 1.34 – 1.23 (m, 6H), 1.19 – 1.06 (m, 12H), 0.99 (t, *J* = 12.0 Hz, 6H).

^{13}C NMR (176 MHz, Chloroform-*d*) δ150.8, 147.4, 146.8, 139.9, 138.1, 137.0, 136.3, 132.9, 132.8, 131.4, 130.8, 128.0, 127.5, 126.8, 125.9, 125.7, 121.8, 119.5, 118.6, 114.2, 43.2, 43.1, 36.9, 36.4, 31.2, 31.0, 29.7, 29.1, 26.8, 25.2, 23.5, 22.8, 20.8.

^{31}P NMR (283 MHz, Chloroform-*d*) δ 2.73.

IR (thin film, cm^{-1}): 2958, 2901, 2847, 1734, 1603, 1576, 1457, 1407, 1361, 1257, 1095, 1015, 974, 935, 873, 843, 732.

HRMS (ESI+) (m/z): $[M-H]^-$ calcd for $C_{80}H_{85}O_4P^-$, 1139.6113, found 1139.6100.

[α]D^{25} = –29.74˚ (c=1.06, CH_2Cl_2).

Synthesis of the catalyst PS-(*R*)-Ad-TRIP-PS (2)

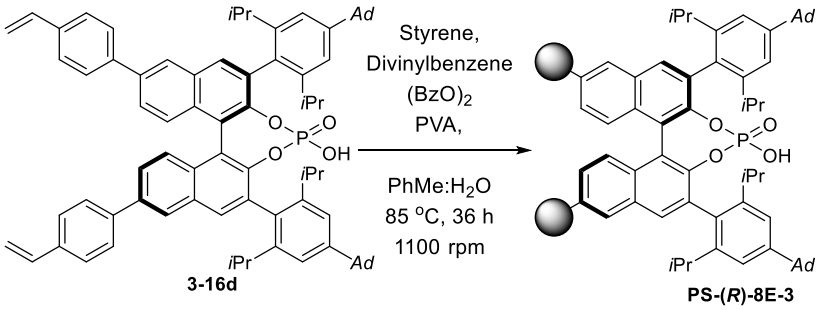

Solution **A** was prepared by dissolving polyvinyl alcohol (PVA, MW 31,000-35,000) (3.0 mg) in water (3.0 mL) to achieve full dissolution, heating up to 80 ºC while steering for 60 minutes was required. Clear solution then was cooled down to room temperature and degassed by sparging nitrogen for 15 minutes.

Solution **B** was prepared by mixing styrene (796 mg), divinyl benzene (28 mg, 80%) (both washed with 3N NaOH aqueous solution, and passed through alumina plug, and dried by sodium sulfate right before the experiment), monomer **S-9** (312 mg) and toluene (2.0 mL).

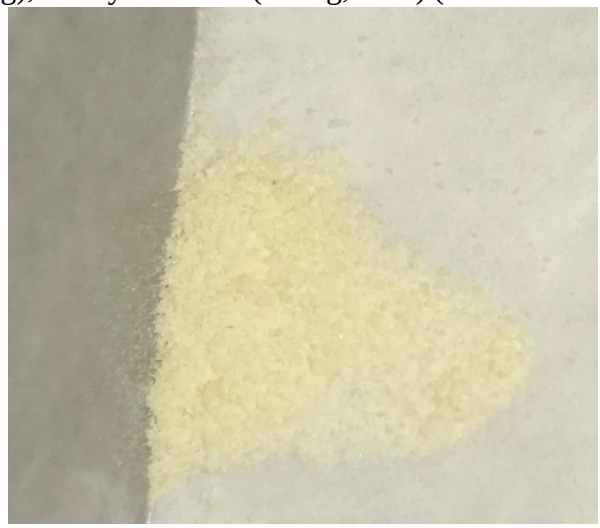

Solution A and Solution B were mixed in a screw thread tube and dibenzoyl peroxide (75%, water stabilized) (13.2 mg) was added. The mixture was degassed by sparging nitrogen for 5 minutes at RT and heated up to 95 ºC while steered at 1100 rpm. After 36 h, the reaction mixture was cooled down to room temperature, and solid material was collected by vacuum filtration. Copolymer **PS-(*R*)-3-8E-3** was washed successively with water, MeOH, THF, DCM, and finally with Hexane and dried in high vacuum overnight to get 1.07 g yellow powder particles.

Elemental Analysis: C: theoretical value: 89.9 %, observed (88.4 %); H: theoretical value: 7.7 %, observed (7.6 %).

General procedures A and B for MOP and MOC protection

General Procedure A for the Regioselective MOP protection with immobilized catalyst (*R*)-Ad-TRIP-PS (PS-3-2E) (Scheme 3.12A).

A one-dram vial was oven-dried and purged with nitrogen. Then the substrate diol (1.0 equiv.), which was previously pre-dried by azeotropic removal of moisture with toluene, was added. This followed by the addition of activated 4Å molecular sieves (beads) and anhydrous dichloromethane (0.04 M) and (*R*)-Ad-TRIP-PS-CPA (**PS-(*R*)-3-8E-3**) (2 mol% for Scheme 3.12A, and 0.5 mol% for Scheme 3.12B). Then the reaction mixture was submerged into a dry ice-acetone (–78 ^{o}C) bath, and 1-methoxycyclohexene or 2-methoxypropene (1.2 equiv.) was added. The reaction mixture was transferred to Neslab CB 80 immersion cooler and stirred at –78 ^{o}C for 12 to 18 h. After the reaction completion as judged by TLC, the reaction mixture was quenched with 5% of triethylamine in methanol. The residue was then filtered through a fritted funnel via the vacuum filtration. The filtrate was concentrated under reduced pressure to obtain the acetal-containing product, which was advanced to subsequent one-pot functionalization (i.e. Scheme 5C).

(IMPORTANT!) THE REACTION MIXTURE WAS COMPLETELY DRIED BY PASSING A GENTLE STREAM OF NITROGEN FOLLOWED BY APPLYING HIGH VACUUM AND SUBJECTED TO THE FURTHER SINGLE POT FUNCTIONALIZATIONS DESCRIBED IN THE SUBSEQUENT SECTIONS OF THIS SI WITHOUT WORK UP OR PURIFICATION.

The assessment of the regioselectivity was accomplished using previously published procedure outlined above.[1] The obtained crude product from CPA-catalyzed acetalization

was subjected directly into acetyl protection by treated with triethylamine (5.0 equiv) and anhydrous dichloromethane (0.3 M). Then anhydrous acetic anhydride (1.1 equiv), and 4-dimethyaminopyridine (DMAP) (0.1 equiv.) were added to the mixture. The reaction was stirred at room temperature until the reaction completion, which was judged by TLC. After the reaction was completed, the mixture was completely dried by gentle N_2 flow followed by high vacuum. The crude reaction mixture was analyzed by COSY NMR to determine the regioselective of C2 and C3. The acetylation result in significant shift of the proton next to the acetoxyl group to 4.2–4.6 ppm region.

Characterization of new acetalization products from Scheme 3.12.

Experimentals and characterization data for products of acetalization with PS-(*R*)-3-8E-3 (Scheme 3.12A).

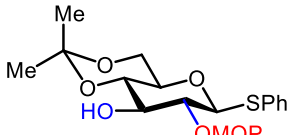

3-10m

Using diol **3-9m** (15.6 mg, 0.05 mmol, 1.0 equiv.) as the starting material, preparation of **3-10m** was accomplished following the **General Procedure A**. This product was purified by flash column chromatography on SiO_2 (1/1 Hexanes/Ethyl acetate + 1% triethylamine) to afford **3-10m** as a pale yellow oil (15.5 mg, 81%, C2:C3 = 21:1).

^{1}H NMR (500 MHz, Methanol-d_4) δ 7.55 – 7.44 (m, 2H), 7.38 – 7.30 (m, 2H), 7.30 – 7.24 (m, 1H), 4.76 (d, *J* = 9.3 Hz, 1H), 4.68 (d, *J* = 9.8 Hz, 0.04H), 3.95 (t, *J* = 10.1 Hz, 0.1H), 3.88 (dd, *J* = 10.7, 5.4 Hz, 2H), 3.78 (t, *J* = 10.5 Hz, 1H), 3.69 (dd, *J* = 9.4, 7.3 Hz, 1H), 3.66 – 3.53 (m, 2H), 3.37 (s, 3H), 1.53 (s, 3H), 1.46 (s, 3H), 1.41 (s, 3H), 1.38 (s, 3H).

^{13}C NMR (176 MHz, cd$_3$od) δ 133.9, 132.0, 128.6, 127.3, 101.8, 99.4, 88.4, 76.0, 72.7, 70.6, 61.8, 49.2, 28.0, 24.6, 24.0, 23.3, 17.9.

IR (thin film, cm^{-1}): 3395, 2991, 2939, 1583, 1479, 1462, 1373, 1262, 1199, 1143, 1073, 1022, 939, 860, 835, 742, 691.

HRMS (ESI+) Calcd. $C_{19}H_{28}NaO_6S$ $[M + Na]^+$: 407.1499, found : 407.1491;

$[\alpha]_D^{26}$ = –27.7° (c 2.0, DCM).

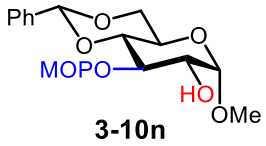

3-10n

Using diol **3-9n** (14 mg, 0.05 mmol, 1.0 equiv.) as the starting material, synthesis of **3-0n** was accomplished following the **General Procedure A**. This product was purified by flash column chromatography on SiO_2 (2/1 Hexanes/Ethyl Acetate + 1% triethylamine) to afford **3-10n** as a white foaming solid (12.9 mg, 85%, C2:C3 = 1.1:1). The spectral data of **this 1:1 mixture** is provided below:

^{1}H NMR (700 MHz, Methanol-d_4) δ 7.54-7.42 (m, 3H), 7.40-7.28 (m, 4H), 5.57 (s,0.5H), 5.52 (s, 0.5H), 4.77 (d, *J* = 3.6Hz, 0.5H), 4.73 (d, J 4.95 (d, *J* = 3.6 Hz, 0.5H), 4.25-4.16 (m, 1H), 4.01 (at, *J* = 9.2 Hz, 1H), 3.86 – 3.79 (m, 0.4H), 3.79 -3.65 (m, 3H), 3.51 (dd, *J* =9.2 Hz, 3.5 Hz, 1H), 3.49 – 3.45 (m, 1H), 3.43 (s, 1.5H), 3.41 (s, 1.5H), 3.27 (s, 1.5H), 3.15 (s, 1.5H), 1.41 (s, 1.5H), 1.40 (s, 1.5H), 1.38 (s, 1.5H), 1.36 (s, 1.5H)

^{13}C NMR (176 MHz, Methanol-d_4) δ 137.8, 137.7, 128.6, 128.5, 127.7, 127.6, 126.3, 126.1, 101.8, 101.6, 100.8, 100.2, 81.5, 81.4, 80.8, 73.0, 72.1, 71.7, 71.6, 70.6, 70.5, 69.0, 68.7, 68.6, 62.8, 62.1, 54.4, 54.3, 48.3, 48.1, 24.6, 24.0.

IR (thin film, cm^{-1}): 3429, 2993, 2932, 2913, 2855, 1506, 1456, 1387, 1374, 1206, 1147, 1075, 1072, 992.

HRMS (ESI+) (*m*/*z*): $[M+Na]^+$ calcd for $C_{18}H_{26}O_7SNa$ 377.1571, found 377.1583;

[α]$_D^{26}$ = +68.6° (c 0.37, DCM).

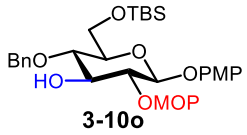

3-10o

Using diol **3-9o** (24.5 mg, 0.05 mmol, 1.0 equiv.) as the starting material, synthesis of **3-10o** was accomplished following the **General Procedure A**. This product was purified by flash column chromatography on SiO_2 (3/1 Hexanes/Ethyl Acetate + 1% triethylamine) to afford **3-10o** as a white foaming solid (23.9 mg, 95%, C2:C3 > 25:1).

^{1}H NMR (700 MHz, Methanol-d_4) δ 7.36 (d, J = 7.5 Hz, 2H), 7.32 (t, J = 7.6 Hz, 3H), 7.29 – 7.24 (m, 1H), 7.05 – 6.91 (m, 1H), 6.83 – 6.76 (m, 2H), 4.95 (d, J = 11.1 Hz, 1H), 4.82 – 4.77 (m 1H), 4.67 (d, J = 11.1 Hz, 1H), 3.85 (dd, J = 11.5, 1.9 Hz, 1H), 3.78 – 3.69 (m, 6H), 3.66 (t, J = 8.6 Hz, 1H), 3.53 – 3.46 (m, 1H), 3.46 – 3.38 (m, 1H), 1.51 (s, 3H), 1.46 (s, 3H), 0.90 (s, 3H), 0.88 (s, 9H), 0.03 (s, 3H), -0.01 (s, 3H).

^{13}C NMR (176 MHz, Methanol-d_4) δ 155.2, 151.6, 138.6, 128.0, 127.5, 127.3, 117.6, 114.1, 101.8, 100.7, 77.8, 76.3, 75.6, 74.60, 74.35, 62.3, 54.6, 49.1, 25.0, 23.8, 17.8, -6.4, -6.6.

IR (thin film, cm^{-1}): 3402, 2928, 2855,1506,1462,1372,1226,1056,1034,833,776, 698, 670.

HRMS (ESI+) (*m*/*z*): [M+Na]$^+$ calcd for $C_{30}H_{46}O_8SiNa$ 585.2854, found 585.2847.

[α]$_D^{26}$ = –9.9° (c=2.6, DCM).

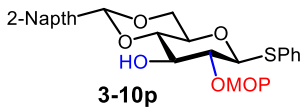

3-10p

Using diol **3-9p** (21 mg, 0.05 mmol, 1.0 eq.) as the starting material, preparation of **3-10p** was accomplished by following general procedure A. This product was purified by flash column chromatography on SiO_2 (7/1 Hexanes/Ethyl acetate + 2% triethylamine) to afford **3-10p** as a pale

yellow oil (21.9 mg, 91 % yield, C2:C3 > 25:1). C2 and C3 selectivity was determined based on the analysis of COSY for the acetylation of C3.

^{1}H NMR (500 MHz, Methanol-d_4) δ 8.29 (d, *J* = 8.3 Hz, 1H), 7.88 (d, *J* = 8.0 Hz, 2H), 7.76 (d, *J* = 7.2 Hz, 1H), 7.57 – 7.42 (m, 5H), 7.41 – 7.32 (m, 2H), 7.30 (t, *J* = 7.9 Hz, 1H), 6.20 (s, 1H), 4.38 (dd, *J* = 10.4, 5.0 Hz, 1H), 3.95 (t, *J* = 10.1 Hz, 1H), 3.83 – 3.73 (m, 3H), 3.69 (td, *J* = 9.5, 4.9 Hz, 1H), 3.36 (s, 3H), 3.32-3.24 (m, 1H), 1.48 (s, 3H), 1.44 (s, 3H).

^{13}C NMR (125 MHz, Methanol-d_4) δ 133.9, 133.8, 132.8, 131.1, 130.6, 129.2, 128.5, 128.0, 127.1, 125.7, 125.3, 124.5, 124.4, 124.2, 101.8, 100.8, 87.1, 80.4, 75.6, 74.3, 69.7, 68.4, 48.7, 24.1, 23.4.

IR (thin film, cm^{-1}): 2989, 2872, 1583, 1512, 1439, 1377, 1265, 1201, 1144, 1107, 1072, 1041, 1018, 858, 803, 743, 691.

HRMS (ESI+) Calcd. $C_{27}H_{30}NaO_6S$ $[M + Na]^+$: 505.1655, found : 505.1645.

$[\alpha]_D^{26}$ = –1.52° (c=0.17, DCM).

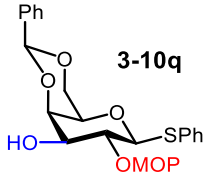

Using D-galactose diol **3-9q** (18 mg, 0.05 mmol, 1.0 eq.) as the starting material, preparation of **3-10q** was accomplished following the **General Procedure J**. This product was purified by flash column chromatography on SiO_2 (1/1 Hexanes/Ethyl acetate + 1% triethylamine) to afford **3-10q** as a pale yellow oil (16.8 mg, 78%, C2:C3 = 15:1).

^{1}H NMR (500 MHz, $CDCl_3$) δ 7.70 – 7.62 (m, 2H), 7.54 (dd, J = 7.5, 1.6 Hz, 2H), 7.42 – 7.33 (m, 3H), 7.25 – 7.18 (m, 3H), 5.58 (s, 1H), 5.16 (s, 1H), 4.60 (d, J = 9.3 Hz, 1H), 4.37 (dd, J = 12.3, 1.1 Hz, 1H), 4.31 (d, J = 3.2 Hz, 1H), 4.17 – 4.02 (m, 2H), 3.65 (dd, J = 8.6, 3.0 Hz, 1H), 3.50 (s, 1H), 3.31 (s, 3H), 1.43 (s, 3H), 1.14 (d, J = 18.0 Hz, 3H).

^{13}C NMR (125 MHz, $CDCl_3$) δ 138.0, 133.4, 131.7, 129.0, 128.8, 128.1, 127.1, 126.6, 101.9, 101.4, 86.0, 75.4, 73.8, 70.9, 70.1, 69.3, 49.7, 25.0, 23.6.

IR (thin film, cm^{-1}): 3382, 2989, 2923, 2857, 1471, 1456, 1439, 1375, 1156, 1099, 1044.

HRMS (ESI+) Calcd. for $C_{23}H_{28}O_6SNa$ $[M + Na]^+$ 455.1499, found 455.1509;

$[\alpha]_D^{26}$ = – 5.4° (c=0.02, DCM).

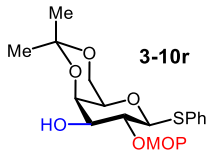

Using D-galactose diol **3-9r** (15.6 mg, 0.05 mmol, 1.0 eq.) as the starting material, preparation of **3-10r** was accomplished following the **General Procedure A**. This product was purified by flash column chromatography on SiO_2 (1/1 Hexanes/Ethyl acetate + 1% triethylamine) to afford **3-10r** as a pale yellow oil (15.6 mg, 81%, C2:C3 = 21:1).

^{1}H NMR (500 MHz, C_6D_6) δ 7.84 – 7.77 (m, 2H), 7.11 – 7.04 (m, 2H), 6.99 – 6.92 (m, 1H), 4.98 (d, J = 1.3 Hz, 1H), 4.50 (d, J = 9.3 Hz, 1H), 4.35 (at, J = 9.0 Hz, 1H), 3.91 (d, J = 2.8 Hz, 1H), 3.75 (dd, J = 12.6, 1.7 Hz, 1H), 3.48 – 3.40 (m, 2H), 2.90 (s, 3H), 2.49 (d, J = 0.9 Hz, 1H), 1.54 (s, 3H), 1.22 (s, 3H), 1.20 (s, 3H), 1.09 (s, 3H).

^{13}C NMR (125 MHz, C_6D_6) δ 134.7, 131.6, 128.6, 126.7, 101.7, 98.4, 86.2, 74.0, 71.4, 69.9, 68.2, 62.6, 49.1, 29.8, 29.4, 24.8, 23.3.

IR (film, cm-1) 3398, 2989, 2923, 1486, 1380, 1277, 1200, 1141, 1096, 1055, 1042.

HRMS (ESI+) Calcd. for $C_{19}H_{28}O_8SNa$ $[M + Na]^+$ 407.1499, found 407.1512;

$[\alpha]_D^{26}$ = –0.42° (c=0.24, DCM).

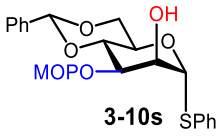

Using *D*-mannose derivative **3-9s** (18 mg, 0.04 mmol, 1.0 equiv.) as the starting material, synthesis of **10s** was accomplished following the **General Procedure A**. This product was purified by flash column chromatography on SiO_2 (3/1 Hexanes/Ethyl acetate + 1% triethylamine) to afford **3-10s** as a pale yellow oil (8.6 mg, 50%, C2:C3 = 1:12).

^{1}H NMR (500 MHz, CD_3OD) δ 7.54 – 7.43 (m, 4H), 7.39 – 7.25 (m, 6H), 5.58 (s, 1H), 5.48 (s, 1H), 4.29 (td, J = 9.8, 4.8 Hz, 1H), 4.22 (d, J = 3.0 Hz, 1H), 4.19 (dd, J = 10.0, 3.1 Hz, 1H), 4.11 (dd, J = 10.2, 4.8 Hz, 1H), 4.05 (at, J = 9.7 Hz, 1H), 3.82 (at, J = 10.3 Hz, 1H), 3.21 (s, 3H), 1.40 (d, J = 12.0 Hz, 3H), 1.37 (s, 3H).

^{13}C NMR (125 MHz, CD_3OD) δ 137.9, 133.7, 131.6, 128.8, 128.5, 127.6, 127.3, 126.0, 102.0, 101.5, 89.5, 77.3, 72.5, 68.1, 65.7, 48.6, 47.1, 24.5, 24.2.

IR (thin film, cm^{-1}): 3433, 2985, 2923, 2853, 1456, 1373, 1211, 1169, 1095, 1031, 970.

HRMS (ESI+) (*m*/*z*): $[M+Na]^+$ calcd for $C_{23}H_{28}O_6SNa$ 455.1499, found 455.1513.

$[\alpha]_D^{26}$ = +48.9° (c=0.51, DCM).

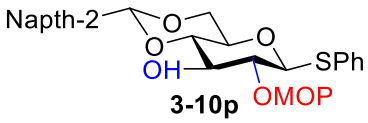

3-10p

Using diol **3-9p** (20.5 mg, 0.05 mmol, 1.0 equiv.) as the starting material, synthesis of **3-10p** was accomplished by following the **General Procedure A**. This product was purified by flash column chromatography on SiO_2 (3/1 Hexanes/Ethyl acetate + 1% triethylamine) to afford **3-10p** as a white foaming solid (21.5 mg, 89%, C2:C3 >= 25:1).

^{1}H NMR (500 MHz, Methanol-d_4) δ 8.29 (d, *J* = 8.3 Hz, 1H), 7.88 (d, *J* = 8.0 Hz, 2H), 7.76 (d, *J* = 7.2 Hz, 1H), 7.57 – 7.42 (m, 5H), 7.41 – 7.32 (m, 2H), 7.30 (t, *J* = 7.9 Hz, 1H), 6.20 (s, 1H), 4.38 (dd, *J* = 10.4, 5.0 Hz, 1H), 3.95 (t, *J* = 10.1 Hz, 1H), 3.83 – 3.73 (m, 3H), 3.69 (td, *J* = 9.5, 4.9 Hz, 1H), 3.36 (s, 3H), 3.32-3.24 (m, 1H), 1.48 (s, 3H), 1.44 (s, 3H).

^{13}C NMR (125 MHz, CD_3OD) δ 133.9, 133.8, 132.8, 131.1, 130.6, 129.2, 128.5, 128.0, 127.1, 125.7, 125.3, 124.5, 124.4, 124.2, 101.8, 100.79, 87.06, 80.37, 75.60, 74.26, 69.70, 68.41, 48.68, 24.05, 23.41.

IR (thin film, cm^{-1}): 2989, 2872, 1583, 1512, 1439, 1377, 1265, 1201, 1144, 1107, 1072, 1041, 1018, 858, 803, 743, 691

HRMS (ESI+) Calcd. $C_{27}H_{30}NaO_6S$ $[M + Na]^+$: 505.1655, found : 505.1645;

$[\alpha]_D^{26}$ = –1.52° (c=0.17, DCM).

Determination of the C2/C3 ratios was performed by acetylating the crude reaction mixture and analyzing the COSY NMR spectrum of the acetylated **5p** (acetylation result in significant shift of the proton next to the acetoxy group to 4.2-4.6 ppm region).

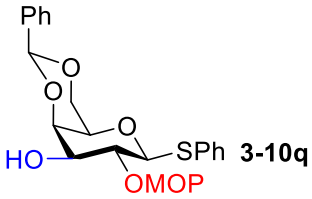

3-10q

Using D-galactose derivative **3-9q** (20 mg, 0.056 mmol, 1.0 equiv.) as the starting material, preparation of **3-10q** was accomplished following the **General Procedure A**. The product **3-10q** was purified by flash column chromatography on SiO_2 (1/1 Hexanes/Ethyl acetate + 1% triethylamine) to afford **3-10q** as a pale-yellow oil (22.2 mg, 93%, C2:C3 = 20:1).

^{1}H NMR (500 MHz, Chloroform-*d*) δ 7.70 – 7.62 (m, 2H), 7.54 (dd, J = 7.5, 1.6 Hz, 2H), 7.42 – 7.33 (m, 3H), 7.25 – 7.18 (m, 3H), 5.58 (s, 1H), 5.16 (s, 1H), 4.60 (d, J = 9.3 Hz, 1H), 4.37 (dd, J = 12.3, 1.1 Hz, 1H), 4.31 (d, J = 3.2 Hz, 1H), 4.17 – 4.02 (m, 2H), 3.65 (dd, J = 8.6, 3.0 Hz, 1H), 3.50 (s, 1H), 3.31 (s, 3H), 1.43 (s, 3H), 1.14 (d, J = 18.0 Hz, 3H).

^{13}C NMR (125 MHz, Chloroform-*d*) δ 138.0, 133.4, 131.7, 129.0, 128.8, 128.1, 127.1, 126.6, 101.9, 101.4, 86.0, 77.3, 77.0, 76.8, 75.4, 73.8, 49.7, 25.0, 23.6.

IR (thin film, cm^{-1}): 3382, 2989, 2923, 2857, 1471, 1456, 1439, 1375, 1156, 1099, 1044.

HRMS (ESI+) Calcd. for $C_{23}H_{28}O_6SNa$ $[M + Na]^+$ 455.1499, found 455.1509;

$[\alpha]^{26}_D$ = – 5.4° (c=0.02, DCM).

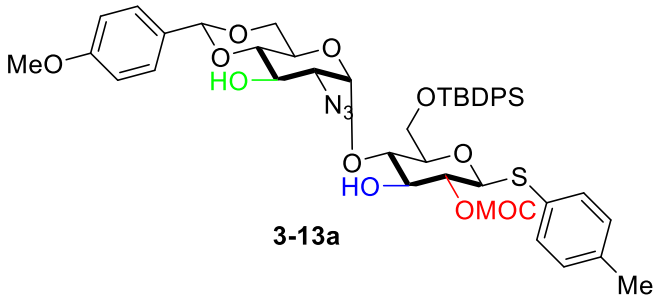

3-13a

^{1}H NMR (700 MHz, Methanol-*d*$_4$) δ 7.40 – 7.35 (m, 4H), 7.14 (d, *J* = 7.9 Hz, 2H), 6.90 – 6.86 (m, 2H), 5.65 (d, *J* = 3.8 Hz, 1H), 5.51 (s, 1H), 4.76 (d, *J* = 9.2 Hz, 1H), 4.20 – 4.13 (m, 1H), 4.09 (q, *J* = 7.1 Hz, 1H), 4.05 (d, *J* = 9.8 Hz, 1H), 3.96 (dd, *J* = 9.8, 8.5 Hz, 1H), 3.91 – 3.86 (m, 1H), 3.83 (s, 4H), 3.78 (s, 3H), 3.74 – 3.65 (m, 2H), 3.52 – 3.43 (m, 2H), 3.34 (d, *J* = 4.9 Hz, 4H), 3.26 – 3.21 (m, 1H).

^{13}C NMR (176 MHz, Methanol-*d*$_4$) δ 131.71, 129.30, 127.33, 112.96, 101.64, 98.70, 87.14, 81.28, 77.57, 76.95, 75.59, 73.31, 67.94, 63.55, 63.13, 47.94, 47.82, 47.69, 47.57, 47.45, 47.33, 47.21, 33.08, 32.79, 24.88, 22.29, 22.25.

HRMS (ESI+) Calcd. for $C_{50}H_{64}N_3O_{11}SSi$ $[M + H]^+$ 732.2802, found 732.2791;

Testing recyclability of PS-(*R*)-3-8E-3 .

Experimental Conditions for Entries 1–10 (Table 3.9**).** A 200 mL round-bottom flask was oven-dried and purged with nitrogen. Then substrate **3-9a** (1.00 g, 2.78 mmol, 1.0 equiv.) was mixed with activated 4Å molecular sieves (beads, 1.0 g) followed by anhydrous dichloromethane (70 mL, 0.04M) and **PS-(*R*)-3-8E-3** (50 mg, 0.014 mmol, 0.5 mol%). This reaction mixture was submerged in dry ice-acetone (–78 °C) bath, and 2-methoxypropene (0.32 mL, 3.34 mmol, 1.2 equiv.) was

added. The reaction mixture was transferred to Neslab CB 80 immersion cooler and stirred at –78 ^{o}C for 18 h. After the reaction completion as judged by TLC, the reaction mixture was quenched with 5% of triethylamine in methanol. The residue was then filtered through a fritted funnel via the vacuum filtration. The filtrate was under reduced pressure to obtain the acetyl product **3-5l** as a white solid (*ca.* ~1.2 g each run). The regioselectivity ratio of C2 and C3 was measured by ^{1}H NMR. The filtered **PS-(*R*)-3-8E-3** was partitioned in DCM to separate it from 4 Å MS beads (MS sediments in DCM while **3** floats on top), and then washed with 6N HCl, 1N HCl, H_2O, acetone, dichloromethane, and hexane. Thus obtained washed **PS-(*R*)-3-8E-3** was dried under reduced pressure and then re-used in the subsequent cycle.

Experimental Conditions for Entry 11 (Table 3.9**).** Run same as above using same 50 mg (0.1 mol%) batch of **PS-(*R*)-3-8E-3** and 5.00 g (13.9 mmol, 1.0 equiv.) of **3-9a**, 5.0 g of 4Å MS, 350 mL (0.04M) of DCM.

General Procedures C-E for the single-pot functionalization of diols (Scheme 3.3)

Scheme 3.17 General procedure for the single-pot protection of diols.

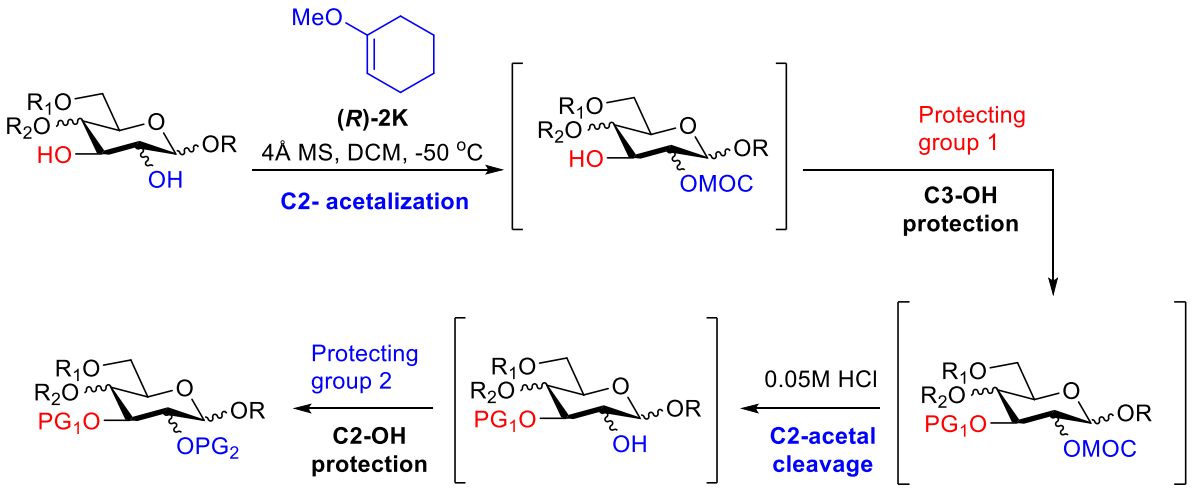

GENERAL PROCEDURE C:

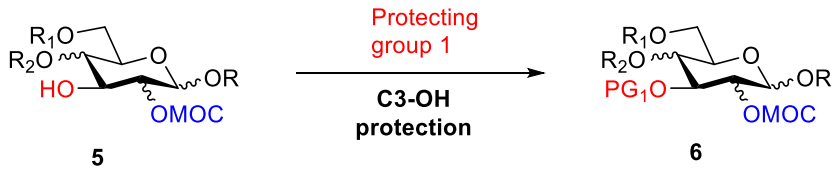

Instructions:

Most of reaction conditions for the protection of C3-OH are tolerated; however, the use of high temperature, acidic conditions, or a combination of acyl halide and pyridine may result in cleavage of MOP or MOC acetals. Acyl halides and pyridine form a pyridinium halide salts, which are acidic enough to remove the C2-acetal. The following procedure was written based on the functionalization of the D-glucose-derived substrate.

Procedure:

*The concentrated and dried MOP-protected substrate was subjected to one of the following conditions below.

1) **Acetylation**: Triethylamine (5.0 equiv.) and anhydrous dichloromethane (0.3M) were added to the concentrated MOC or MOP-protected substrate. This followed by the addition of acetic anhydride (1.1 equiv.), and 4-dimethyaminopyridine (DMAP) (0.1 equiv.). The resultant reaction was stirred at room temperature until the reaction completion, which was judged by TLC. After the reaction was completed, the mixture was completely dried using gentle N_2 gas flow followed by reaction vessel evacuation. The crude reaction mixture was subjected to the next reaction step without purification.

2) **Benzoylation**: Triethylamine (5.0 equiv) and anhydrous dichloromethane (0.3 M) were added to the concentrated MOC or MOP-protected substrate. Then, benzoyl chloride

(1.2 equiv.), and 4-dimethyaminopyridine (DMAP) (0.10 equiv.) were added to the resultant solution. This mixture was stirred at room temperature until the reaction completion by TLC and then dried by passing a gentle stream of N_2 followed by applying high vacuum. Thus obtained crude reaction mixture was subjected to the next reaction step without purification.

3) **Benzylation**: Anhydrous dichloromethane (0.2M) was added to the reaction mixture. Then sodium hydride (60% dispersion in mineral oil) (1.2 equiv.), and benzyl bromide (1.1 equiv.), tetrabutylammonium iodide (TBAI) (0.10 equiv.) were subsequently added to the mixture. Then 3-5 drops of anhydrous dimethylformamide (DMF) was added to the solution to dissolve the NaH efficiently. The reaction mixture was stirred at room temperature until the reaction completion, as judged by TLC. After completion, the reaction was carefully quenched with methanol. The solution was then, filtered through a HPLC filter to remove the slurry containing mineral oil from sodium hydride. The resulting filtered solution was completely dried by passing a stream of N_2 followed by applying high vacuum. The crude reaction mixture was subjected to the next reaction step without purification.

4) ***para*-methoxybenzylation (PMB-protection)**: same as benzyl protection, except using PMB chloride instead of benzyl bromide.

GENERAL PROCEDURE D:

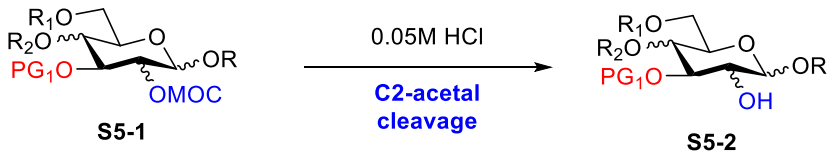

Instruction:

When clean MOP-acetal products were dissolved in $CDCl_3$ for NMR, the acetal cleavage was observed. We hypothesized that trace amounts of hydrochloric acid in the $CDCl_3$ could cleave the mixed acetal. To test this idea, 0.05M HCl solution was prepared in chloroform, and this solution was indeed acidic enough to cleave the C2-acetal (either MOC or MOP) within several minutes. Therefore, $CDCl_3$ should be avoided as the NMR solvent.

0.05M HCl solution did not cleave 4,6-benzylidine acetal moiety, which was excellent for our system. Furthermore, the HCl solution can be used to neutralize the previous basic conditions.

Procedure:

First, 0.05 M HCl solution in dichloromethane was added to the resulting reaction mixture to neutralize the basic reaction condition. While the HCl solution is added, the pH of the reaction mixture was monitored using pH paper. The solution of 0.05M HCl was added until the reaction medium became slightly acidic (around pH 5-6). This acidic solution was stirred until the reaction completion (C2-acetal cleavage), and the reaction can be monitored by TLC. Once the reaction was completed, the resulting reaction mixture was completely dried by passing a stream of N_2 followed by applying high vacuum.

GENERAL PROCEDURE E:

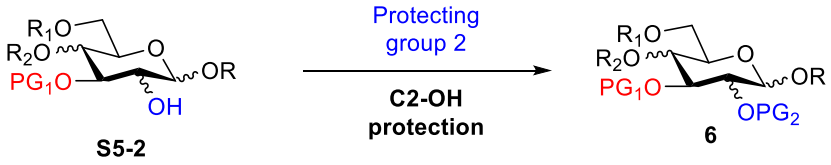

Instruction:

The scope of the C2-OH protecting groups for the subsequent re-protection was significantly wider due to the absence of the acid-labile mixed MOC and MOP acetals, and the combination of the acyl chlorides and pyridine was also available.

Procedure:

* The resulting from previous steps dried substrate **7** with free C2-OH was subjected to one of the following conditions below.

1) **Acetylation**: Triethylamine (5.0 equiv.) and anhydrous dichloromethane (0.3M) were added to the reaction mixture. Then anhydrous acetic anhydride (1.2 equiv.), and 4-dimethyaminopyridine (DMAP) (0.2 equiv.) were added to the resultant solution. The reaction was stirred at room temperature until TLC analysis indicated completion. The resultant mixture was slowly quenched with methanol, the solvent was then removed under vacuum, and the residue was dissolved in DCM and washed with NH_4Cl (x3). The resultant aqueous layers were extracted with DCM (x2), and the organic layers were combined and dried over $MgSO_4$ solution. The dried crude solution was concentrated *in vacuo* and purified by a flash column chromatography on SiO_2 (hexanes : ethyl acetate, 15:1 → 10:1 → 4:1).

2) **Benzoylation**: Pyridine (10.0 equiv.) and anhydrous dichloromethane (0.3M) were added to the reaction mixture. Then benzoyl chloride (1.2 equiv.), and 4-dimethyaminopyridine (DMAP) (0.2 equiv.) were subsequently added. The reaction mixture was stirred at room temperature until the TLC analysis indicated completion. Subsequently, the mixture was slowly quenched with methanol, the solvent was removed under vacuum, and the residue was re-dissolved in DCM and washed with NH_4Cl (x3). The resultant aqueous layers were extracted with DCM (x2), and the organic layers were combined and dried over $MgSO_4$ solution. The dried crude solution was concentrated *in vacuo* and purified by a flash column chromatography on SiO_2 (hexanes : ethyl acetate, 15:1 → 10:1 → 4:1). (Benzoyl chloride was found to be more reactive than benzoic anhydrides.)

3) **Benzylation**: Anhydrous dichloromethane (0.2M) was added to the reaction mixture. Then, sodium hydride (60% dispersion in mineral oil, 1.5 equiv.), benzyl bromide (1.2 equiv.), and tetrabutylammonium iodide (TBAI) (0.2 equiv.) were sequentially added to the mixture. This followed by the addition of 3-5 drops of anhydrous DMF to dissolve the NaH more efficiently. The reaction mixture was stirred at room temperature until the completion by the TLC analysis. The resultant mixture was slowly quenched with methanol, the solvent was removed under vacuum, and the residue was re-dissolved in DCM and washed with NH_4Cl (x3). The resultant aqueous layers were extracted with DCM (x2), and the organic layers were combined and dried over $MgSO_4$ solution. The dried crude solution was

concentrated *in vacuo* and purified by a flash column chromatography on SiO_2 (hexanes : ethyl acetate, 15:1 → 10:1 → 4:1).

Experimentals and Characterization Data for the Single-pot Protection with Immobilized (*R*)-Ad-TRIP (PS-3-2E) (Scheme 3.5C)

1) C2 acetalization

C2 acetalization with **3** → C3-OH protection → C2-acetal cleavage → C2-OH protection

Scheme 7S. General scheme for the single-pot functionalization of monosaccharide using the same 50 mg batch of **(R)-Ad TRIP-PS (2)**

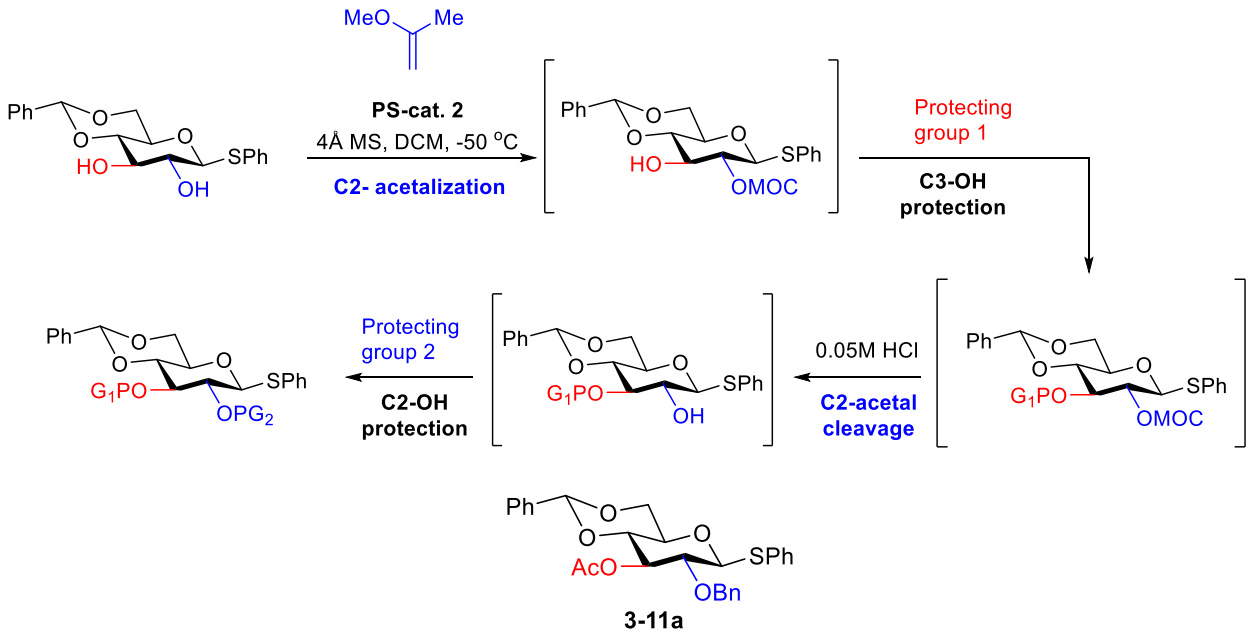

3-11a

Using **3-9a** (1.0 g, 2.78 mmol, 1.0 equiv.) as the starting material, the C2 MOP acetal installation was accomplished following the **General Procedure A**. After the reaction was completed, as judged by TLC, the reaction mixture was initially quenched with 5% triethylamine in methanol at –78 °C, then the residue was filtered through a fritted Buchner funnel. The catalyst **PS-(*R*)-3-8E-3** was recycled as described in Table 3.8. The filtrate was concentrated under reduced pressure to

obtain the acetal-containing product as a white solid that was used directly without further purification. This crude product was subjected to C3-**acetylation** as described in the **General Procedure C**. Upon completion, the reaction mixture was acidified following the **General Procedure D** to cleave the C2 MOP acetal moiety. After the cleavage of MOP acetal is completed, as judged by TLC, the solution was concentrated by applying nitrogen stream, and the resultant crude oil was **benzylated** as described in the **General Procedure E**. After purification by column chromatography, 957 mg (1.95 mmol) of the desired product **3-11a** was obtain in 70% yield.

^{1}H NMR (700 MHz, Chloroform-*d*) δ 7.57 – 7.51 (m, 2H), 7.44 – 7.39 (m, 2H), 7.37 – 7.28 (m, 11H), 5.48 (s, 1H), 5.39 (dd, *J* = 9.7, 8.8 Hz, 1H), 4.91 (d, *J* = 10.9 Hz, 1H), 4.83 (d, *J* = 9.7 Hz, 1H), 4.63 (d, *J* = 10.9 Hz, 1H), 4.37 (dd, *J* = 10.5, 4.9 Hz, 1H), 3.78 (t, *J* = 10.2 Hz, 1H), 3.60 (t, *J* = 9.5 Hz, 1H), 3.58 – 3.52 (m, 2H), 1.96 (s, 3H).

^{13}C NMR (176 MHz, Chloroform-*d*) δ 169.9, 137.7, 137.0, 133.0, 132.5, 129.3, 129.2, 128.6, 128.4, 128.3, 128.2, 128.1, 126.3, 101.5, 88.6, 79.3, 78.7, 75.4, 74.4, 70.5, 68.7, 21.1.

IR (thin film, cm^{-1}): 2960, 2923, 2854, 1748, 1450, 1369, 1230, 1029, 1001, 749, 698.

HRMS (ESI+) (*m*/*z*): $[M+Na]^+$ calcd for $C_{28}H_{28}O_6S$ 515.1504, found 515. 1496.

$[\alpha]_D^{26}$ = –13.2° (c=0.55, $CHCl_3$).

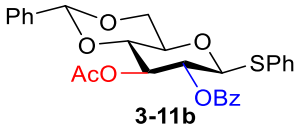

3-11b

With **3-9a** (1.0 g, 2.78 mmol, 1.0 equiv.) as the starting material, the C2 MOP acetal installation was accomplished following the **General Procedure J** using the catalyst **PS-(*R*)-3-8E-3** recovered above and re-used for the next substrate. After the reaction was completed, as judged by TLC, the reaction mixture was initially quenched with 5% triethylamine in methanol at –78 °C, then the residue was filtered through a fritted Buchner funnel. The catalyst **PS-(*R*)-3-8E-3** was recycled as

described in Table 3.8. The filtrate was concentrated under reduced pressure to obtain the acetal-containing product as a white solid that was used directly without further purification. This crude product underwent C3 **acetylation** as described in the **General Procedure C**. Upon completion, the reaction mixture was acidified using the **General Procedure D** to cleave the MOP acetal moiety. After the cleavage of acetal was completed, as judged by TLC, the resultant solution was concentrated by nitrogen stream, and the resultant crude oil was directly subjected to C2 **benzoylation** as described in the **General Procedure E**. After completion, the reaction was slowly quenched with methanol. The solvent was then removed under vacuum and the residue was dissolved in DCM and washed with NH_4Cl (x3). The resultant aqueous layers were extracted with DCM (x2), and the organic layers were combined and dried over $MgSO_4$ solution. The dried crude solution was concentrated *in vacuo* and purified by flash column chromatography on SiO_2 (hexanes : ethyl acetate, 15:1 → 10:1 → 4:1) to get 1.21 g (2.39 mmol) of white solid **3-11b** in 86% yield.

^{1}H NMR (700 MHz, Chloroform-*d*) δ 8.06 – 8.03 (m, 2H), 7.62 – 7.58 (m, 1H), 7.49 – 7.46 (m, 2H), 7.45 – 7.42 (m, 4H), 7.37 – 7.34 (m, 3H), 7.33 – 7.28 (m, 3H), 5.55 – 5.51 (m, 2H), 5.28 (dd, *J* = 10.0, 9.1 Hz, 1H), 4.95 (d, *J* = 10.0 Hz, 1H), 4.43 (dd, *J* = 10.6, 4.9 Hz, 1H), 3.85 (t, *J* = 10.3 Hz, 1H), 3.76 (t, *J* = 9.6 Hz, 1H), 3.67 (td, *J* = 9.7, 4.9 Hz, 1H), 1.94 (s, 3H).

^{13}C NMR (176 MHz, Chloroform-*d*) δ 170.1, 165.4, 136.9, 133.7, 133.2, 131.9, 130.1, 129.3, 129.3, 129.2, 128.7, 128.6, 128.4, 126.3, 101.7, 87.1, 78.4, 72.9, 71.3, 71.0, 68.7, 20.9.

IR (thin film, cm^{-1}): 2990, 2883, 2721, 1751, 1721, 1731, 1268, 1219, 1040, 1027, 963.

HRMS (ESI+) (*m*/*z*): $[M+Na]^+$ calcd for $C_{28}H_{26}O_7S$ 539.1900, found 539.1908.

$[\alpha]_D^{26}$ = –3.3° (c=0.13, $CHCl_3$).

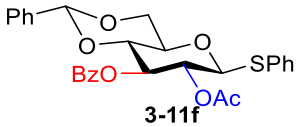

3-11f

With **3-9a** (1.0 g, 2.78 mmol, 1.0 equiv.) as the starting material, the C2 MOP acetal installation was accomplished following the **General Procedure J** using the catalyst **PS-(*R*)-3-8E-3** recovered above. After the reaction was completed, as judged by TLC, the reaction mixture was initially quenched with 5% triethylamine in methanol at –78 ^{o}C, then the residue was filtered through a fritted Buchner funnel. The catalyst **PS-(*R*)-3-8E-3** was recycled as described in Table 3.8 and re-used for the next substrate. The filtrate was concentrated under reduced pressure to obtain the acetal-containing product as a white solid that was used directly without further purification. This crude product was subjected to the C3-**benzoylation** as described in the **General Procedure C**. Upon completion, the reaction mixture was acidified using the **General Procedure D** to cleave the C2 MOP acetal moiety. After the cleavage of MOP acetal is completed, as judged by TLC analysis, the solution was concentrated by applying nitrogen stream, and the resultant crude oil was **acetylated** as described in the **General Procedure E**. Upon completion, the reaction mixture was slowly quenched with methanol. The solvent was then removed under vacuum and the residue was dissolved in DCM and washed with NH_4Cl (x3). The resultant aqueous layers were extracted with DCM (x2), and the organic layers were combined and dried over $MgSO_4$ solution. The dried crude solution was concentrated *in vacuo* and purified by a flash column chromatography on SiO_2 (hexanes : ethyl acetate, 15:1 → 10:1 → 4:1) to get 1.12 g (2.21 mmol) of white solid **3-11f** in 80 % yield.

^{1}H NMR (700 MHz, Chloroform-*d*) δ 8.03 – 7.98 (m, 2H), 7.57 – 7.52 (m, 1H), 7.51 (dd, *J* = 6.5, 3.0 Hz, 2H), 7.42 (t, *J* = 7.7 Hz, 2H), 7.38 (dt, *J* = 6.5, 4.0 Hz, 2H), 7.35 (dd, *J* = 5.0, 1.9 Hz, 3H), 7.30 (p, *J* = 3.6 Hz, 3H), 5.62 (t, *J* = 9.4 Hz, 1H), 5.51 (s, 1H), 5.22 (t, *J* = 9.6 Hz, 1H), 4.90 (d, *J*

= 10.0 Hz, 1H), 4.43 (dd, *J* = 10.6, 5.0 Hz, 1H), 3.83 (dt, *J* = 13.5, 9.9 Hz, 2H), 3.68 (td, *J* = 9.7, 5.0 Hz, 1H), 2.01 (s, 3H).

^{13}C NMR (176 MHz, Chloroform-*d*) δ 169.6, 165.8, 136.8, 133.4, 133.0, 132.0, 130.0, 129.5, 129.2, 129.2, 128.6, 128.5, 128.3, 126.2, 101.6, 86.9, 78.6, 73.5, 70.9, 70.7, 68.6, 20.9.

IR (thin film, cm^{-1}): 2903, 2866, 2721, 1752, 1728, 1374, 1280, 1099, 1068.

HRMS (ESI+) (*m*/*z*): $[M+Na]^+$ calcd for $C_{28}H_{26}O_7S$ 529.1297, found 529.1286.

$[\alpha]_D^{26}$ = –23.5° (c=0.19, $CHCl_3$).

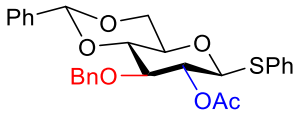

3-11k

With **3-9a** (1.0 g, 2.78 mmol, 1.0 equiv.) as the starting material, the C2 MOP acetal installation was accomplished by following the **General Procedure A** using the catalyst **PS-(*R*)-3-8E-3** recovered above. After the reaction was completed, as judged by TLC, the reaction mixture was initially quenched with 5% triethylamine in methanol at –78 °C, then the residue was filtered through a fritted Buchner funnel. The catalyst **PS-(*R*)-3-8E-3** was recycled as described in Table 3.8 and re-used for the next substrate. The filtrate was concentrated under reduced pressure to obtain the acetalated product as a white solid that was used directly without further purification. This crude product was subjected to C3-**benzylation** as described in the **General Procedure C**. Upon completion, the reaction mixture was acidified following the **General Procedure D** to remove the C2 MOP acetal moiety. After the cleavage of acetal was completed, as judged by TLC analysis, the solution was concentrated by applying nitrogen stream, and the resultant crude oil was **acetylated** as described in the **General Procedure E**. After concentration by rotatory evaporation, the resultant crude oil was purifide by column chromatography, to provide 984 mg (2.0 mmol) of the desired product **3-11k** in 72% yield.

^{1}H NMR (700 MHz, Chloroform-*d*) δ 7.51 – 7.44 (m, 4H), 7.42 – 7.27 (m, 11H), 5.58 (s, 1H), 5.06 – 5.00 (m, 1H), 4.86 (d, *J* = 12.0 Hz, 1H), 4.70 (d, *J* = 10.1 Hz, 1H), 4.66 (d, *J* = 12.0 Hz, 1H), 4.39 (dd, *J* = 10.6, 5.0 Hz, 1H), 3.81 (t, *J* = 10.3 Hz, 1H), 3.77 – 3.73 (m, 2H), 3.51 (td, *J* = 9.5, 4.8 Hz, 1H), 2.03 (d, *J* = 1.6 Hz, 3H).

^{13}C NMR (176 MHz, Chloroform-*d*) δ 169.5, 138.2, 137.2, 132.8, 132.4, 129.2, 129.1, 128.5, 128.4, 128.3, 128.1, 127.9, 126.1, 101.4, 87.0, 81.5, 79.8, 74.5, 71.5, 70.7, 68.7, 21.1.

IR (thin film, cm^{-1}): 3062, 2920, 2852, 2739, 1749, 1584, 1454, 1372, 1226, 1160, 1112, 1028, 1000.

HRMS (ESI+) Calcd. $C_{28}H_{28}NaO_6S$ $[M + Na]^+$: 515.1504, found : 515.1513;

$[\alpha]_D^{26}$ = +2.95° (c=0.24, $CHCl_3$).

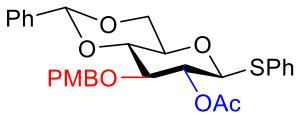

3-11p

With **3-9a** (1.0 g, 2.78 mmol, 1.0 equiv.) as the starting material, the C2 MOP acetal installation was accomplished by following the **General Procedure J** using the catalyst **PS-(*R*)-3-8E-3** recovered above. After the reaction was completed, as judged by TLC, the reaction mixture was initially quenched with 5% triethylamine in methanol at –78 °C, then the residue was filtered through a fritted Buchner funnel. The catalyst **PS-(*R*)-3-8E-3** was recycled as described in Table 3.8 and re-used for the next substrate. The filtrate was concentrated under reduced pressure to obtain the acetal-containing product as a white solid that was used directly without further purification. The obtained crude product underwent C3 protection using ***para*-methoxybenzylation (PMB protection)** as described in the **General Procedure C**. Upon completion, the reaction mixture was immediately acidified using the **General Procedure D** to cleave the C2 acetal moiety. After the cleavage of acetal was completed, as judged by TLC, the

reaction mixture was concentrated by nitrogen stream, and the resultant crude oil was directly subjected to the C2 **acetylation** as demonstrated in the **General Procedure E**. After the purification by column chromatography, 1.19 g (2.28 mmol) of the desired product **3-11p** was obtain in 82% yield.

^{1}H NMR (700 MHz, Chloroform-*d*) δ 7.52 – 7.43 (m, 4H), 7.41 – 7.36 (m, 3H), 7.31 (dd, *J* = 5.1, 2.0 Hz, 4H), 7.18 (d, *J* = 8.5 Hz, 2H), 6.85 – 6.82 (m, 2H), 5.57 (s, 1H), 5.00 (t, *J* = 9.4 Hz, 1H), 4.78 (d, *J* = 11.6 Hz, 1H), 4.69 (d, *J* = 10.1 Hz, 1H), 4.60 (d, *J* = 11.6 Hz, 1H), 4.39 (dd, *J* = 10.6, 5.0 Hz, 1H), 3.83 – 3.80 (m, 1H), 3.79 (s, 3H), 3.74 – 3.71 (m, 2H), 3.50 (dq, *J* = 9.6, 5.0 Hz, 1H), 2.05 (s, 3H).

^{13}C NMR (176 MHz, Chloroform-*d*) δ 169.4, 159.4, 137.3, 132.8, 132.4, 130.3, 129.8, 129.2, 129.1, 128.4, 128.3, 126.1, 113.9, 101.4, 87.0, 81.4, 79.3, 74.1, 71.5, 70.7, 68.7, 55.4, 21.2.

IR (thin film, cm^{-1}): 2918, 2849, 2720, 1749, 1612, 1513, 1465, 1372, 1228, 1098, 1067, 1029, 1002.

HRMS (ESI+) Calcd. $C_{29}H_{34}NO_7S$ $[M + NH_4]^+$: 540.2056, found : 540.2042.

$[\alpha]_D^{26}$ = +5.86° (c=0.13, $CHCl_3$).

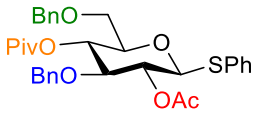

3-12e

With **3-9a** (1.0 g, 2.78 mmol, 1.0 equiv.) as the starting material, the C2 MOP acetal installation was accomplished by following the **General Procedure A** using the catalyst **PS-(*R*)-3-8E-3** recovered above. After the reaction was completed, as judged by TLC, the reaction mixture was initially quenched with 5% triethylamine in methanol at –78 °C, then the residue was filtered through a fritted Buchner funnel. The catalyst **PS-(*R*)-3-8E-3** was recycled as described in Table 3.8 and re-used for the next substrate. The filtrate was concentrated under reduced pressure to

obtain the acetal-containing product as a white solid that was used directly without further purification. The obtained crude product underwent C3-**benzylation** as described in the **General Procedure C**. Upon completion, the reaction mixture was immediately acidified following the **General Procedure D** to cleave the C2-acetal moiety. After the cleavage of acetal was completed, as judged by TLC, the solution was concentrated by nitrogen stream, and the resultant crude oil was directly subjected to C2-**acetylation** as described in the **General Procedure E**. Obtained via **General Procedure E** crude C2, C3-protected *D*-glucose derivative was dissolved in DCM (0.2 M) and the mixture was cooled to 0 ^{o}C. Then, triethylsilane (5.0 equiv.) was added to the mixture followed by the slow addition of trifluoroacetic acid (5 equiv.) at 0 ^{o}C. The reaction mixture was stirred for 2 h at 0 ^{o}C before being quenched with triethylamine (6 equiv.) and completely dried by passing a stream of N_2 followed by applying high vacuum. Then pyridine (20.0 equiv.) and anhydrous dichloromethane (0.5 M) were added to the reaction vessel. Afterwards pivaloyl chloride (2.0 equiv.), and 4-dimethyaminopyridine (DMAP) (0.3 equiv.) were added to the reaction mixture. The resultant mixture was stirred at room temperature until TLC analysis indicated reaction completion. At this point, the reaction mixture was slowly quenched with methanol. The solvent was then removed under vacuum and the residue was dissolved in DCM and washed with NH_4Cl (x3). The resultant aqueous layers were extracted with DCM (x2), and the organic layers were combined and dried over $MgSO_4$. The dried crude solution was concentrated *in vacuo* and purified by a flash column chromatography on SiO_2 (hexanes : ethyl acetate, 15:1 → 10:1 → 4:1). After purification by column chromatography, 674 mg (1.17 mmol) of the desired product **3-12e** was obtained in 42% yield.

^{1}H NMR (700 MHz, Chloroform-*d*) δ 7.51 (d, *J* = 7.7 Hz, 2H), 7.35 – 7.28 (m, 7H), 7.26 – 7.16 (m, 6H), 5.14 – 5.05 (m, 2H), 4.71 (d, *J* = 10.0 Hz, 1H), 4.62 (d, *J* = 11.1 Hz, 1H), 4.59 – 4.54 (m,

2H), 4.49 (d, *J* = 11.8 Hz, 1H), 3.78 (t, *J* = 9.2 Hz, 1H), 3.71 (t, *J* = 8.5 Hz, 1H), 3.60 – 3.55 (m, 1H), 3.50 (d, *J* = 11.0 Hz, 1H), 1.99 (s, 3H), 1.12 (s, 9H).

^{13}C NMR (176 MHz, Chloroform-*d*) δ 177.0, 169.5, 138.0, 137.8, 133.5, 132.5, 131.9, 129.1, 128.5(2C), 127.9, 127.8 (3C), 127.6, 86.5, 82.0, 78.5, 73.9, 73.8, 71.3, 69.9, 69.6, 38.9, 27.2 (2C), 21.1.

IR (thin film, cm^{-1}): 3031, 2958, 2923, 2869, 1714, 1584, 1479, 1454, 1370, 1279, 1251, 1226, 1191, 1091, 1039.

HRMS (ESI+) Calcd. $C_{33}H_{42}NO_7S$ $[M + NH_4]^+$: 596.2682, found : 596.2691;

$[\alpha]_D^{26}$ = +8.20° (c=0.14, $CHCl_3$).

Controlled equilibration experiment on stability of C2 MOP acetal isomerization

Using 32:1 ratio mixture of C2:C3 MOC acetal **3-10a** (43.2 mg, 0.1 mmol, 1.0 equiv.) as the starting material, following the **General Procedure B**, with the variable of different temperatures at room temperature, –78 ˚C, –15 ˚C and 4 ˚C. The reaction mixture was analyzed using ^{1}H NMR as described above.

3.7. References

(1) Lepenies, B.; Seeberger, P. H. The Promise of Glycomics, Glycan Arrays and Carbohydrate-Based Vaccines. *Immunopharmacol. Immunotoxicol.* **2010**, *32* (2), 196–207. https://doi.org/10.3109/08923970903292663.

(2) Ernst, B.; Magnani, J. L. From Carbohydrate Leads to Glycomimetic Drugs. *Nat. Rev. Drug Discov.* **2009**, *8* (8), 661–677. https://doi.org/10.1038/nrd2852.

(3) Bennett, C. S. Principles of Modern Solid-Phase Oligosaccharide Synthesis. *Org. Biomol. Chem.* **2014**, *12* (11), 1686. https://doi.org/10.1039/c3ob42343c.

(4) Krasnova, L.; Wong, C.-H. Oligosaccharide Synthesis and Translational Innovation. *J. Am. Chem. Soc.* **2019**, *141* (9), 3735–3754. https://doi.org/10.1021/jacs.8b11005.

(5) Seeberger, P. H.; Haase, W.-C. Solid-Phase Oligosaccharide Synthesis and Combinatorial Carbohydrate Libraries. *Chem. Rev.* **2000**, *100* (12), 4349–4394. https://doi.org/10.1021/cr9903104.

(6) Seeberger, P. H.; Werz, D. B. Synthesis and Medical Applications of Oligosaccharides. *Nature* **2007**, *446* (7139), 1046–1051. https://doi.org/10.1038/nature05819.

(7) Peng, P.; Schmidt, R. R. An Alternative Reaction Course in *O* -Glycosidation with *O* -Glycosyl Trichloroacetimidates as Glycosyl Donors and Lewis Acidic Metal Salts as Catalyst: Acid–Base Catalysis with Gold Chloride-Glycosyl Acceptor Adducts. *J. Am. Chem. Soc.* **2015**, *137* (39), 12653–12659. https://doi.org/10.1021/jacs.5b07895.
(8) Filice, M.; Palomo, J. M. Monosaccharide Derivatives as Central Scaffolds in the Synthesis of Glycosylated Drugs. *RSC Advances* **2012**, *2* (5), 1729. https://doi.org/10.1039/c2ra00515h.
(9) Wang, T.; Demchenko, A. V. Synthesis of Carbohydrate Building Blocks *via* Regioselective Uniform Protection/Deprotection Strategies. *Org. Biomol. Chem.* **2019**, *17* (20), 4934–4950. https://doi.org/10.1039/C9OB00573K.
(10) Lovett, W. Partial Esterification of Methyl 4,6-0-Benzylidene-a-D-Glucopyranoside in Pyridine Solution. *J. Am. Chem. Soc.* **1957**, *79*, 2579.
(11) Abbas, S.A., H., A. H. Benzoyl Cyanide as a Selective Acylating Agent. *Carbohydr. Res.* **1974**, *39*, 358–363.
(12) Seitz, A.; Wende, R. C.; Roesner, E.; Niedek, D.; Topp, C.; Colgan, A. C.; McGarrigle, E. M.; Schreiner, P. R. Site-Selective Acylation of Pyranosides with Oligopeptide Catalysts. *J. Org. Chem.* **2021**, *86* (5), 3907–3922. https://doi.org/10.1021/acs.joc.0c02772.
(13) Peng, P.; Linseis, M.; Winter, R. F.; Schmidt, R. R. Regioselective Acylation of Diols and Triols: The Cyanide Effect. *J. Am. Chem. Soc.* **2016**, 8.
(14) Wang, H.; She, J.; Zhang, L.-H.; Ye, X.-S. Silver(I) Oxide Mediated Selective Monoprotection of Diols in Pyranosides. *J. Org. Chem.* **2004**, *69*, 5774–5777.
(15) S. David; S. Hanessian. Regioselective Manipulation of Hydroxyl Groups via Organotin Derivatives. *Tetrahedron Lett 41*, 643.
(16) Kosugi, M.; Shimizu, Y.; Migita, T. Alkylation, Arylation, and Vinylation of Acyl Chlorides by Means of Organotin Compounds in the Presence of Catalytic Amounts of Tetrakis(Triphenylphosphine)Palladium (0). *Chem. Lett.* **1977**, 1423–1424.
(17) Munavu, R. M.; Szmant, H. H. Selective Formation of 2 Esters of Some Methyl .Alpha.-D-Hexopyranosides via Dibutylstannylene Derivatives. *J. Org. Chem.* **1976**, *41* (10), 1832–1836. https://doi.org/10.1021/jo00872a033.
(18) Gordon, R. G.; Prescia, J. W. Implications of the Toxicity of Tetramethyltin, Dimethyl Tin Dichloride, and Tin Tetrachloride in Selecting a Suitable Tin Precursor in the Chemical Vapor Deposition of Tin Oxide. In *AIP Conference Proceedings*; AIP, 1988; Vol. 166, pp 1–9. https://doi.org/10.1063/1.37122.
(19) Xiao, G.; Cintron-Rosado, G. A.; Glazier, D. A.; Xi, B.; Liu, C.; Liu, P.; Tang, W. Catalytic Site-Selective Acylation of Carbohydrates Directed by Cation– *n* Interaction. *J. Am. Chem. Soc.* **2017**, *139* (12), 4346–4349. https://doi.org/10.1021/jacs.7b01412.
(20) Sun, X.; Lee, H.; Lee, S.; Tan, K. L. Catalyst Recognition of Cis-1,2-Diols Enables Site-Selective Functionalization of Complex Molecules. *Nature Chemistry* **2013**, *5* (9), 790–795. https://doi.org/10.1038/nchem.1726.
(21) Lewis, C. A.; Miller, S. J. Site-Selective Derivatization and Remodeling of Erythromycin A by Using Simple Peptide-Based Chiral Catalysts. *Angew. Chem. Int. Ed.* **2006**, *45* (34), 5616–5619. https://doi.org/10.1002/anie.200601490.
(22) Yoganathan, S.; Miller, S. J. Structure Diversification of Vancomycin through Peptide-Catalyzed, Site-Selective Lipidation: A Catalysis-Based Approach To Combat Glycopeptide-Resistant Pathogens. *J. Med. Chem.* **2015**, *58* (5), 2367–2377. https://doi.org/10.1021/jm501872s.

(23) Fowler, B. S.; Laemmerhold, K. M.; Miller, S. J. Catalytic Site-Selective Thiocarbonylations and Deoxygenations of Vancomycin Reveal Hydroxyl-Dependent Conformational Effects. *J. Am. Chem. Soc.* **2012**, *134* (23), 9755–9761. https://doi.org/10.1021/ja302692j.

(24) Ueda, Y.; Mishiro, K.; Yoshida, K.; Furuta, T.; Kawabata, T. Regioselective Diversification of a Cardiac Glycoside, Lanatoside C, by Organocatalysis. *J. Org. Chem.* **2012**, *77* (18), 7850–7857. https://doi.org/10.1021/jo301007x.

(25) Mensah, E.; Camasso, N.; Kaplan, W.; Nagorny, P. Chiral Phosphoric Acid Directed Regioselective Acetalization of Carbohydrate-Derived 1,2-Diols. *Angew. Chem. Int. Ed.* **2013**, *52* (49), 12932–12936. https://doi.org/10.1002/anie.201304298.

(26) Wang, C.-C.; Lee, J.-C.; Luo, S.-Y.; Kulkarni, S. S.; Huang, Y.-W.; Lee, C.-C.; Chang, K.-L.; Hung, S.-C. Regioselective One-Pot Protection of Carbohydrates. *Nature* **2007**, *446* (7138), 896–899. https://doi.org/10.1038/nature05730.

(27) Hayashi, Y. Pot Economy and One-Pot Synthesis. *Chem. Sci.* **2016**, *7* (2), 866–880. https://doi.org/10.1039/C5SC02913A.

(28) Huang, T.-Y.; Zulueta, M. M. L.; Hung, S.-C. Regioselective One-Pot Protection, Protection–Glycosylation and Protection–Glycosylation–Glycosylation of Carbohydrates: A Case Study with D -Glucose. *Org. Biomol. Chem.* **2014**, *12* (2), 376–382. https://doi.org/10.1039/C3OB42097C.

(29) Benaglia, M.; Puglisi, A.; Cozzi, F. Polymer-Supported Organic Catalysts. *Chem. Rev.* **2003**, *103* (9), 3401–3430. https://doi.org/10.1021/cr010440o.

(30) Rueping, M.; Sugiono, E.; Steck, A.; Theissmann, T. Synthesis and Application of Polymer-Supported Chiral Brønsted Acid Organocatalysts. *Adv. Synth. Catal.* **2010**, *352* (2–3), 281–287. https://doi.org/10.1002/adsc.200900746.

(31) Bleschke, C.; Schmidt, J.; Kundu, D. S.; Blechert, S.; Thomas, A. A Chiral Microporous Polymer Network as Asymmetric Heterogeneous Organocatalyst. *Adv. Synth. Catal.* **2011**, *353* (17), 3101–3106. https://doi.org/10.1002/adsc.201100674.

(32) Clot-Almenara, L.; Rodríguez-Escrich, C.; Osorio-Planes, L.; Pericàs, M. A. Polystyrene-Supported TRIP: A Highly Recyclable Catalyst for Batch and Flow Enantioselective Allylation of Aldehydes. *ACS Catal.* **2016**, *6* (11), 7647–7651. https://doi.org/10.1021/acscatal.6b02621.

(33) Kundu, D. S.; Schmidt, J.; Bleschke, C.; Thomas, A.; Blechert, S. A Microporous Binol-Derived Phosphoric Acid. *Angew. Chem. Int. Ed.* **2012**, *51* (22), 5456–5459. https://doi.org/10.1002/anie.201109072.

(34) Lai, J.; Fianchini, M.; Pericàs, M. A. Development of Immobilized SPINOL-Derived Chiral Phosphoric Acids for Catalytic Continuous Flow Processes. Use in the Catalytic Desymmetrization of 3,3-Disubstituted Oxetanes. *ACS Catalysis* **2020**, *10* (24), 14971–14983. https://doi.org/10.1021/acscatal.0c04497.

(35) Clot-Almenara, L.; Rodríguez-Escrich, C.; Osorio-Planes, L.; Pericàs, M. A. Polystyrene-Supported TRIP: A Highly Recyclable Catalyst for Batch and Flow Enantioselective Allylation of Aldehydes. *ACS Catal.* **2016**, *6* (11), 7647–7651. https://doi.org/10.1021/acscatal.6b02621.

(36) Kanomata, K.; Toda, Y.; Shibata, Y.; Yamanaka, M.; Tsuzuki, S.; Gridnev, I. D.; Terada, M. Secondary Stereocontrolling Interactions in Chiral Brønsted Acid Catalysis: Study of a Petasis–Ferrier-Type Rearrangement Catalyzed by Chiral Phosphoric Acids. *Chem. Sci.* **2014**, *5* (9), 3515–3523. https://doi.org/10.1039/C4SC00611A.

(37) Lee, S.; Kaib, P. S. J.; List, B. Asymmetric Catalysis via Cyclic, Aliphatic Oxocarbenium Ions. *J. Am. Chem. Soc.* **2017**, *139* (6), 2156–2159. https://doi.org/10.1021/jacs.6b11993.
(38) Khomutnyk, Y. Ya.; Argüelles, A. J.; Winschel, G. A.; Sun, Z.; Zimmerman, P. M.; Nagorny, P. Studies of the Mechanism and Origins of Enantioselectivity for the Chiral Phosphoric Acid-Catalyzed Stereoselective Spiroketalization Reactions. *J. Am. Chem. Soc.* **2016**, *138* (1), 444–456. https://doi.org/10.1021/jacs.5b12528.
(39) Tay, J.-H.; Argüelles, A. J.; DeMars, M. D.; Zimmerman, P. M.; Sherman, D. H.; Nagorny, P. Regiodivergent Glycosylations of 6-Deoxy-Erythronolide B and Oleandomycin-Derived Macrolactones Enabled by Chiral Acid Catalysis. *J. Am. Chem. Soc.* **2017**, *139* (25), 8570–8578. https://doi.org/10.1021/jacs.7b03198.

Chapter 4

Closing remarks

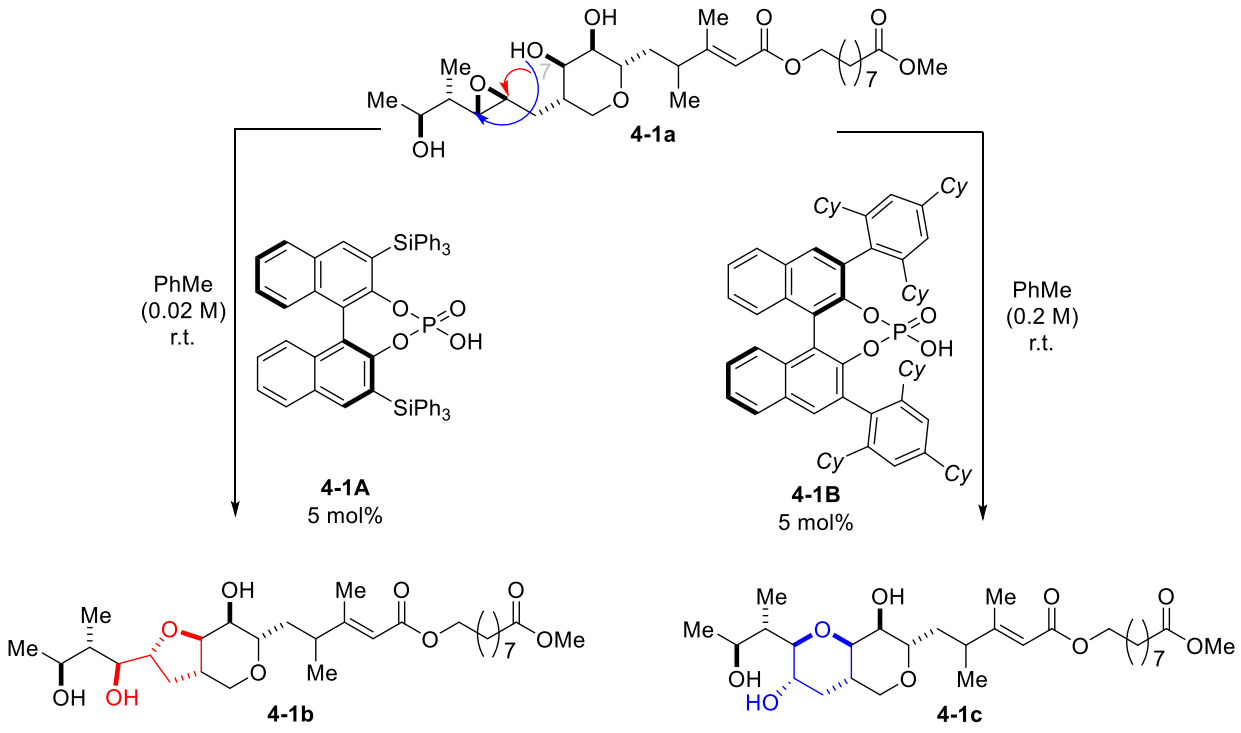

Figure 4.1 Catalyst-controlled epoxide ring openings via two different catalysts.

In summary, this dissertation demonstrates the applications of chiral phosphoric acids (CPAs) towards regiodivergent epoxide ring openings (ERO) of mupirocin methyl ester and regioselective acetalization, which leads to single-pot synthesis of differentially protected monosaccharides.

Catalyst-controlled regiodivergent methods for ERO are scarce but synthetically useful and versatile. In the second chapter, we demonstrated that mupirocin methyl ester **4-1a** may undergo

unselective intramolecular cyclization that leads to the formation of equimolar mixtures of both *exo*- and *endo*-regioisomers **4-1b** and **4-1c**. This situation is uncommon since the typical ERO reactions kinetically favor *exo*-product formation, and the observed lack of selectivity is due to the entropic restrictions imposed by the pyrane ring present in **4-1a**. Based on the strong precedents suggesting that CPAs may activate epoxide moiety towards the addition of nucleophiles, we evaluated various CPAs as the catalysts for the mupirocin methyl ester ERO, and discovered that catalysts **4-1A** could promote the *endo*-cyclization while catalyst **4-1B** favored the *exo*-cyclization product (Figure 4.1). Thus, using **4-1A**, we obtained *exo*-product **4-1b** in 77:23 rr, while catalysts **4-1B** yielded *endo*-product **4-1c** in 95:5 rr. Our studies indicated that the formations of both **4-1b** and **4-1c** are strongly dependent on the solvent polarity, concentrations, and water content, which suggests that the formation of pre-complexation of the catalyst and substrate is significant for the transformation. The proposed mechanism, computationally investigated by Dr. Alonso J. Arguelles and Prof. P. Zimmerman, suggested that both reactions proceed through concerted and highly synchronous mechanisms that were dependent on the specific hydrogen bond networks formed between **4-1a** and catalysts. In addition, these computational studies also explained the origin of regiocontrol. The *endo*-selectivity could be explained by the diminishing steric clashes of the epoxide alkyl substituents with the 3- and 3′- substituents of BINOL-derived CPAs with (*R*)-chirality that arise in the transition state leading to the product. However, stronger steric repulsion was observed with (*S*)-chirality, which led to poor regioselectivity. Similarly, in the *exo*-selectivity pathway, steric clashes were not present in between the 3- and 3’-substituents of (*R*)-chirality catalyst and epoxide alkyl, which stabilizes a more easily formed pre-complex, leading to the *exo*-product. We believe that these experimental and mechanistic insights can assist in further extending this methodology to make it more broadly applicable to other types of CPA-

catalyzed transformation. We also envision that CPAs could be broadly applied to affect other intramolecular ERO reactions such as the ones depicted in Figure 2.1 and Scheme 2.1, and these studies are currently ongoing in our laboratories.

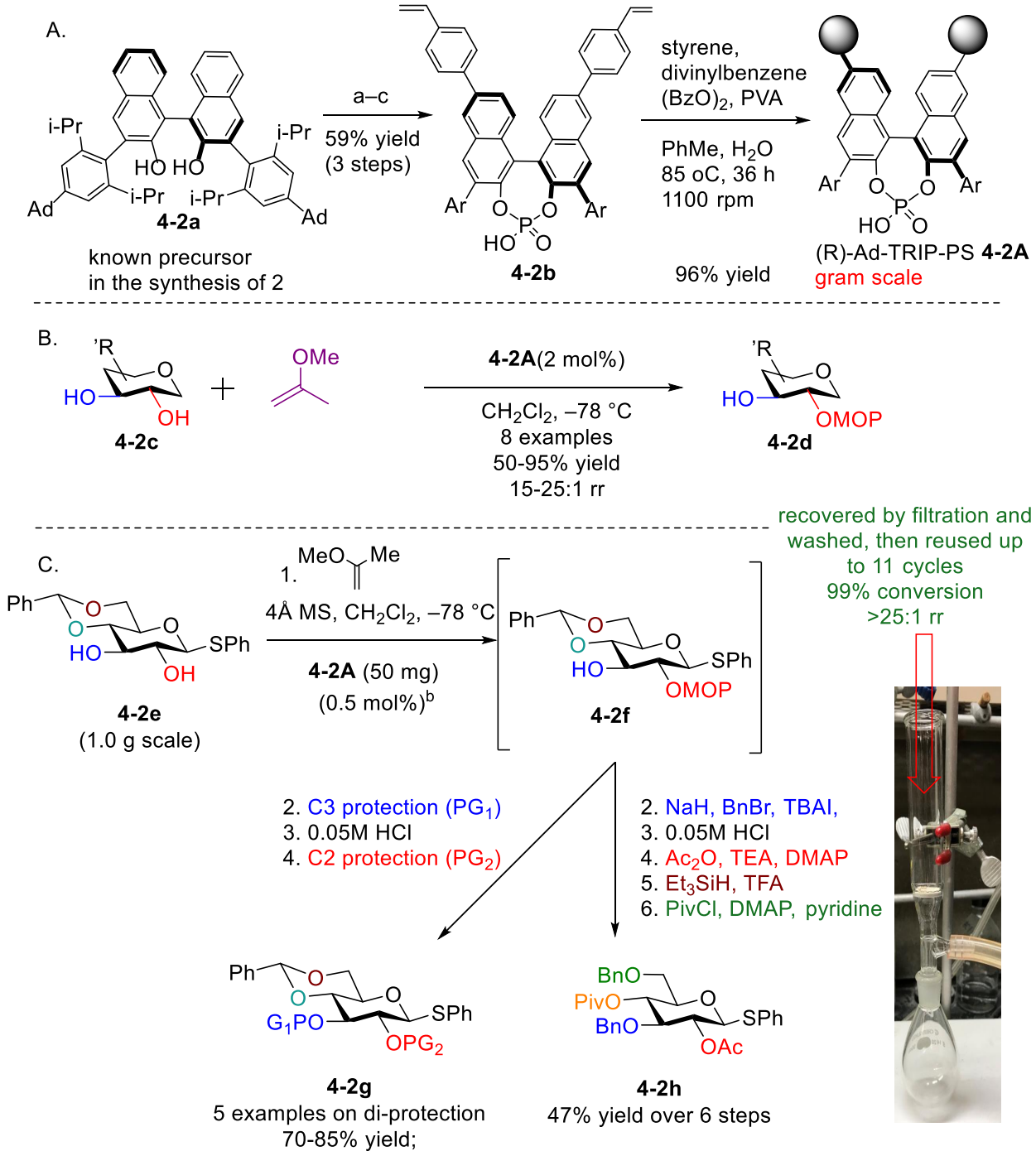

Figure 4.2 (A) Synthesis of PS-CPAs. (B) Applications of PS-CPAs in site-selective acetalizaiton of various *trans*-2,3-diols (C) Applications of PS-CPAs in single-pot functionalization of monosaccharides.

Chapter 3 of this thesis investigates CPAs to address problems associated with the regioselective synthesis of carbohydrates and demonstrates the usage of CPAs for the single-pot

functionalization of monosaccharides leading to differentially protected derivatives. To further improve the practicality of this approach, we developed immobilized chiral phosphoric acids (*R*)-Ad TRIP (**4-2A**) that could be used to accomplish regiodivergent acetal protection of monosaccharide-based diols in good-to-excellent selectivities and conversions. Unlike their achiral counterparts, catalyst **4-2A** allows to differentiate equatorial hydroxy groups at the C2 and C3-positions of pyranoses and selectively produce regioisomeric products. In particular, **4-2A** could be readily recycled by filtration, washed, and reused up to eleven times on 1.0 to 5.0 g scale acetalizations with loadings as low as 0.5 to 0.1 mol% without losing its reactivity and selectivity, which we believe could significantly reduce the catalyst costs. In addition, regioselective one-pot gram scale syntheses of 6 differentially protected *D*-glucose derivatives were accomplished with the same 50 mg batch of catalyst **4-2A**. The computational and mechanistic studies indicated complex temperature-dependent interplay of two reaction mechanisms. The dominant at low temperatures concerted asynchronous mechanism favors the formation of the C2 isomer due to destabilizing the transition state leading to the C3 isomer interactions between the benzylidene acetal moiety of **4-2c** and catalyst **4-2A**. The developed stereochemical models allow expanding the scope of this transformation, and our future studies will focuse on exploring more complex substrates and applying these transformations in continuous flow (Figure 4.3). One of such uses may involve packing the immobilized CPA catalysts **4-2A** into a column, through which enol ether and **4-2c** will be passed through to achieve the site-selective acetalization to occur on the column (Figure 4.3A). With this concept and obtained product **4-2d**, we will further apply the developed method in Figure 4.2 and adapt these conditions to flow systems to synthesize fully functionalized monosaccharides in a single-pot.

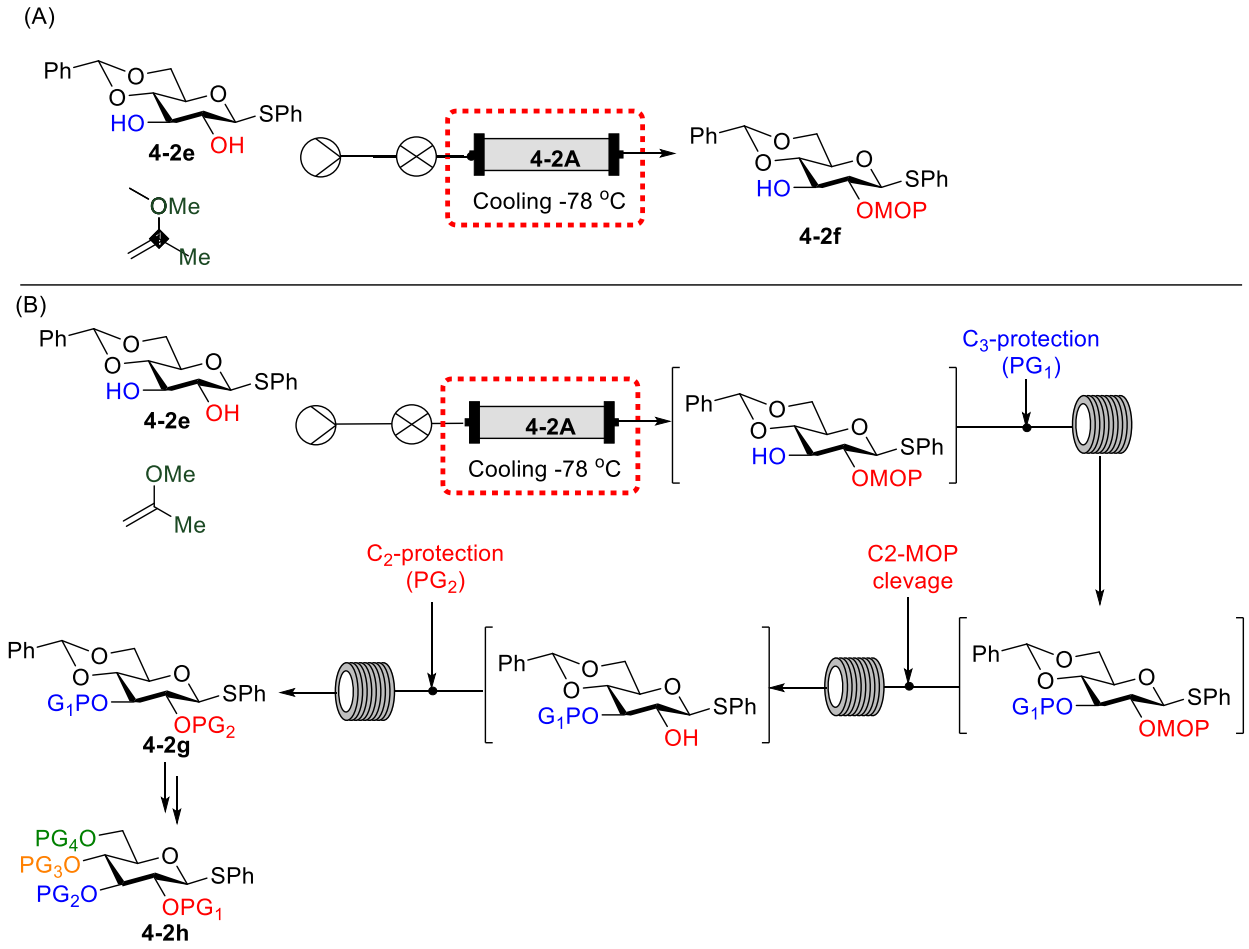

Figure 4.3 Flow set up for (A) site-selective acetalization (B) single-pot functionalization of monosaccharides.